Development and Evaluation of Topical Dasatinib Loaded Lipid Based Nanocarriers for the Treatment of Rheumatoid Arthritis

THESIS

Submitted in partial fulfillment

of the requirements for the degree of

DOCTOR OF PHILOSOPHY

by

MAHIPAL REDDY DONTHI

ID. No. 2019PHXF0054P

Under the Supervision of

Prof. RANENDRA NARAYAN SAHA

Co-supervision of

Prof. GAUTAM SINGHVI
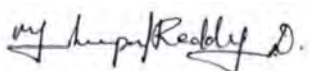
&

Dr. SUNIL KUMAR DUBEY

BITS Pilani

Pilani | Dubai | Goa | Hyderabad | Mumbai

BIRLA INSTITUTE OF TECHNOLOGY AND SCIENCE, PILANI
2024

Declaration

I hereby declare that the work carried out in this thesis titled **"Development and Evaluation of Topical Dasatinib Loaded Lipid Based Nanocarriers for the Treatment of Rheumatoid Arthritis"** is an original piece of research work carried out under the supervision of **Prof. Ranendra Narayan Saha**, with co-supervision of Prof. Gautam Singhvi and Dr. Sunil Kumar Dubey at BITS-Pilani, Pilani Campus, Pilani, India. This thesis has not been submitted by me for the award of any other degree of any other University/Institute.

Mahipal Reddy Donthi

2019PHXF0054P

Research scholar

BITS-Pilani, Pilani Campus

Date:

BIRLA INSTITUTE OF TECHNOLOGY AND SCIENCE, PILANI

CERTIFICATE

This is to certify that the thesis entitled "**Development and Evaluation of Topical Dasatinib Loaded Lipid Based Nanocarriers for the Treatment of Rheumatoid Arthritis"** submitted by **Mahipal Reddy Donthi**, ID. No. **2019PHXF0054P** for award of Ph.D. degree of the institute, embodies original work done by him under my supervision.

Signature of the Supervisor

Co-supervisor

Prof. Ranendra Narayan Saha
Senior Professor,
Department of Pharmacy,
BITS-PILANI, Pilani Campus, Rajasthan,
Former Vice-Chancellor (Acting), BITS-PILANI
Former Director, BITS-Pilani, Dubai Campus, Dubai,
UAE

Prof. Gautam Singhvi
Associate Professor,
Department of Pharmacy,
BITS-Pilani, Pilani Campus, Rajasthan

Co-supervisor
Dr. Sunil Kumar Dubey
General Manager,
R&D Healthcare Division Emami Ltd,
Belgharia, Kolkata

Date:

Acknowledgements

As a mark of respect for my research supervisor, Prof. Ranendra Narayan Saha, Former Vice Chancellor (Acting) of BITS-Pilani, Pilani Campus; Former Director, BITS-Pilani, Dubai Campus, UAE, I would like to express my feelings through humble prayer. I am grateful for his inspiration throughout my dissertation work. Throughout the dissertation, he was helpful, cooperative, and encouraging. His manner of imparting knowledge during critical times is memorable. His moral support always pushed and lifted me to do my best. His creative ideas enabled me to complete work with spontaneity and passion.

I am thankful to Professor V Ramgopal Rao, Vice-Chancellor, BITS-Pilani, Prof. Souvik Bhattacharyya, Former Vice-Chancellor, Prof. Sudhir Kumar Barai, Director, BITS Pilani, Pilani Campus, Soumyabrata Chakraborty, Registrar, BITS Pilani, Pilani Campus, Shamik Chakraborty, Associate Dean, AGSRD, BITS Pilani, Pilani Campus, for providing excellent work facilities and an absorbing research environment. I wish to express sincere thanks to Prof. Anil Gaikawad, Head, Department of Pharmacy, Prof. Hemant Jadhav, Prof. Atish Paul, former Head, Department of Pharmacy, for constant support in providing resources required during my research work.

I would like to express my gratitude to Prof. Gautam Singhvi, Associate professor, BITS-Pilani, Pilani Campus, and Dr. Sunil Kumar Dubey, General Manager, R&D Healthcare Division Emami Ltd., Belgharia, Kolkata, India. I'm very grateful of the help I received while working on my dissertation work. Additionally, I have moral support, which has always pushed and encouraged me to achieve my best.

I am extremely thankful to the members of my Doctoral Advisory Committee (DAC), Prof. Murali Manohar Pandey and Prof. Rajeev Taliyan for reviewing my thesis and providing constructive comments. I would like to express my heartfelt gratitude to Prof. Anil Jindal, Convener, Departmental Research Committee (DRC), for his invaluable assistance in

Abstract

Rheumatoid arthritis (RA) is a chronic inflammatory autoimmune disease that primarily affects joints and causes inflammation, cartilage destruction, and bone resorption. The worldwide prevalence of RA is about 5 per 1000 adults. By 2025, it is anticipated that the number of arthritis patients will reach 67 million. There are multiple treatment options available to manage RA, including nonsteroidal anti-inflammatory drugs (NSAIDs) to alleviate pain and inflammation; corticosteroids for immediate symptom relief; biologic agents that target immune system proteins; disease-modifying antirheumatic drugs (DMARDs) to slow disease progression by targeting the immune system. However, current therapies provide temporary relief and conventional DMARDs may lead to intolerances, drug toxicity, contraindications, or comorbidities. Therefore, there is a need for effective RA treatments, with ongoing research focusing on investigating Tyrosine kinases (TKs) as potential options.

Tyrosine kinases, including receptor tyrosine kinases (RTKs) play a critical role in RA pathogenesis by activating proteins involved in cellular and cytokine responses. Approved small molecule tyrosine kinase inhibitors (TKIs) like tofacitinib, baricitinib, and upadacitinib effectively manage RA symptoms and inflammation by targeting the immune response. Promising alternative therapeutic targets, such as nilotinib, imatinib, fostamatinib, dasatinib (DTB), and bosutinib, inhibit tyrosine kinase receptors (TKR) associated with cellular responses and bone erosion in RA, suggesting TKR inhibition as a potential management strategy for RA.

Dasatinib (DTB) is a second-generation multi-targeting tyrosine kinase inhibitor (TKI) that inhibits the discoidin domain receptors 1 (DDR 1) and 2 (DDR 2), as well as inflammatory cytokines such as tumor necrosis factor alpha (TNF- α) and interleukin 6 (IL-6), which plays critical roles in the progression of RA. Oral administration of DTB causes serious side effects such as pulmonary hypertension and pleural effusions. The topical administration of DTB could be a viable approach for enhancing therapeutic efficacy, local effect, and reducing

systemic side effects. Though, topical preparations are advantageous to achieve localized effects, the conventional formulations also present some disadvantages like unable to deliver hydrophobic drugs effectively and may fail to provide the required therapeutic drug concentration at the intended target site, i.e., the inflammatory region. To address these limitations, lipid-based nanocarriers loaded gel can be used to incorporate DTB and deliver the therapeutic moiety via topical route in RA condition.

In this dissertation, lipid-based nano-emulgel and solid lipid nanoparticles (SLNs) were investigated for the topical delivery of DTB. These lipid nanocarriers have advantages such as high drug loading, stability, and sustained release. The overall objective is to design and characterize two lipid-based nanocarriers, i.e., DTB loaded nano-emulgel and SLNs, to improve the permeation and sustained release at the targeted site through topical delivery.

A simple, accurate, and robust isocratic HPLC method was developed to estimate DTB concentration in different *in-vitro* and *ex-vivo* samples. The developed HPLC method was validated in accordance with regulatory guidelines. The method was linear in the concentration range of 100 to 10000 ng/mL (R^2- 0.9995) at 315 nm. The lower detection and quantification limits for DTB were determined to be 33.12 and 100.4 ng/mL, respectively. The % recovery was within the limits (98.80 ± 0.41 to 101.5 ± 0.21). The relative standard deviation for intraday and interday precision was found to be within 2%. In addition, a bioanalytical method was utilized to estimate DTB levels in rat plasma.

DTB loaded nano emulsion was developed by the quality by design (QbD) approach. The nano emulsion was prepared using hot emulsification, followed by size reduction using hominization. The optimized batch showed, size and entrapment efficiency of 172.53 ± 3.33 nm (0.160 ± 0.014 PDI) and $95.11 \pm 0.16\%$, respectively. The *in-vitro* drug release of DTB-loaded nano emulsion showed extended-release up to 24 h and shown to follow the Hixson Crowell model. *In-vitro* cell line study revealed that the formulation excipients had no effect

on the viability of HaCaT cells as determined by the MTT assay and a dose-dependent reduction in the expression of inflammatory cytokines (TNF-α and IL-6) was observed in RAW 264.7 cell lines. In *ex-vivo* permeation study after 12h, the amount of drug permeated through the skin was found to be 12.52 ± 0.29 $\mu g/cm^2$ and 4.31 ± 1.07 $\mu g/cm^2$ for DTB loaded nano-emulgel and free drug loaded gel, respectively. After 24h, it was found to be 23.59 ± 0.04 $\mu g/cm^2$ and 6.86 ± 1.98 $\mu g/cm^2$. The skin deposition study revealed that the amount drug deposited were found to be 143.62 ± 22.31 and 17.46 ± 3.28 ng/cm^2 for DTB loaded nano-emulgel and free drug loaded gel respectively after 24 hr. The skin deposition was found to be 10 folds higher in the case of the optimized formulation as compared to the free loaded gel. DTB loaded SLNs were developed by the QbD approach.

DTB loaded SLNs were prepared using QBD approach for the optimization of lipid, surfactant concentration and homogenization speed. The SLNs were prepared using hot emulsification, followed by size reduction using homogenization. The optimized batch showed size and entrapment of 147.20 ± 11.01 nm (0.255 ± 0.009 PDI) and $91.19 \pm 0.55\%$, respectively. The *in-vitro* drug release of SLNs dispersion showed extended-release up to 24 h and shown to follow the Korsmeyer-Peppas model. In the HaCaT cell lines, the MTT assay demonstrated that the excipients used in the SLNs had no impact on cell viability. Additionally, in the RAW 267.4 cell lines, the expression of TNF-α and IL-6 has shown dose-dependent inhibitory effect. In *ex-vivo* permeation study, the amount of drug permeated through the skin was found to be 33.72 ± 2.05 $\mu g/cm^2$ and 4.31 ± 1.07 $\mu g/cm^2$ for DTB loaded SLNs gel and free drug loaded gel, respectively after 12h. After 24h, it was found to be 36.17 ± 3.5 $\mu g/cm^2$ and 6.86 ± 1.98 $\mu g/cm^2$.s The skin deposition study revealed that after 24h, the amount drug deposited were found to be 277.50 ± 9.63 ng/cm^2 and 17.49 ± 3.28 ng/cm^2 for DTB loaded SLNs gel and free drug loaded gel formulation respectively. The Deposition was found to be 20 folds higher in the case of the optimized formulation as compared to the free loaded gel.

The *in-vivo* skin irritation studies for the optimized nanoemulgel and SLNs loaded gel were showed non-irritant to the Sprague–Dawley (SD) rats with no signs of erythema, itching and edema after the 72h topical application. In Freund's complete adjuvant (FCA) immunization study, swelling and redness was developed in the hind paw of the rats 24 hours after FCA injection. After induction with FCA, significant weight loss was observed in rats in the initial days of the study. Following 27th day of treatment, significant weight gain in animals treated with diclofenac, DTB loaded nano-emulgel, DTB loaded SLNs gel was observed compared to FCA control group. In the nociceptive threshold examining study, a consistent decrease in paw withdrawal threshold was observed in FCA treated rats compared to normal control animals, and the pain threshold was found to be lowest on day 5. Topical administration of DTB-loaded nano-emulgel, DTB loaded SLNs and diclofenac gel were significantly reduced the withdrawal latency from the day 10 when compared to the FCA-treated control group. In the assessment of motor incoordination study, sub plantar administration of FCA resulted in decrease in fall off time compared to the untreated group. Rats treated with DTB-loaded nano-emulgel, DTB loaded SLNs and diclofenac gel significantly increased the fall off time from day 5 till day 28 as compared to the FCA control group.

The overall study concluded that the designed DTB-loaded lipid nanocarriers (nano-emulgel and SLNs) improved *in-vitro* efficacy and sustained-release compared to conventional topical preparation. The developed formulations are free from the toxic solvents, and all ingredients used are within the inactive ingredient guidelines (IIG) limits. The outcome of the present study emphasizes an industrial feasible process for the development of DTB loaded lipid carriers for topical delivery.

List of Tables

List of Figures

List of Abbreviations and Symbols

%	Percentage
<	Less than
>	More than
≤	Less than equal to
≥	More than equal to
=	Equal to
Å	Amstrong
°C	Degree Celsius
μg	Microgram
μm	Micrometer
μL	Microliter
μM	Micromolar
λmax	Lambda max
α	Alpha
β	Beta
γ	Gamma
σ_0	yield stress
ABL	Abelson
ACPA	Anti-citrullinated protein antibody
AIC	Akaike Information Criteria
AID	Autoimmune Disease
AIA	Adjuvant Induced Arthritis
AQbD	Analytical quality by design
ANOVA	Analysis of variance
API	Active Pharmaceutical Ingredient
ATP	Analytical target profile
ATR-FTIR	Attenuated total reflectance Fourier transform infrared
AUC	Area Under Curve
BBD	Box–Behnken design

BCR	Breakpoint cluster region
BLK	B lymphoid tyrosine kinase
BTK	Bruton tyrosine kinase
CCD	Center Composition Design (CCD)
CD	Cluster of Differentiation
cm	Centimeter
CAA	Critical Analytical Attributes
CMA	Critical material attributes
CML	Chronic myeloid leukemia
C_{max}	Maximum concentration
cGMP	Current Good Manufacturing Process
CCD	Center Composition Design
CFA	Complete Freund's Adjuvant
CP	Chromosome- Positive
CPP	Critical process parameters
CQA	Critical quality attributes
CRP	c-reactive protein
CSF1R	Colony stimulating factor 1 receptor
CT	Column Temperature
CYP	Cytochrome
DDR	Discoidin domain receptor tyrosine kinase
DL	Drug Loading
DLS	Dynamic Light Scattering
DMARD	Disease Modifying Anti-Rheumatic Medications
DMEM	Dulbecco's modified Eagle's medium
DMSO	Dimethyl sulfoxide
DOE	Design of experiments
DSC	Differential scanning calorimetry
DTB	Dasatinib
EBNA2	Epstein-Barr virus infection and RA, as EB nuclear antigen 2
EE	Encapsulation efficiency
ELISA	Enzyme-linked immunosorbent assay

EPHA2	Ephrin receptor tyrosine kinase A2
ERK	Extracellular signal-regulated kinase
FBS	Fetal bovine serum
FDA	Food and Drug Administration
FDG	Free Drug Loaded Gel
FDS	Free Drug Solutions
FESEM	Field Emission Scanning Electron Microscopy
FFD	Fractional Factorial Design
FGF	Fibroblast growth factor
FLS	Fibroblast-like synoviocytes
FMO-3	Flavin-containing monooxygenase 3
FMEA	Failure Mode Evaluation and Analysis
FR	Flow Rate
FRK	Fyn-related kinase
FST	Frequency sweep test
g	Gram
g/mol	Gram per mole
GI	Gastrointestinal
h	Hour
HLA	Human Leukocyte Antigen
HCK	Hemopoietic cell kinase
HPLC	High-pressure liquid chromatography
IAEC	Institutional animal ethical committee
IC50	Inhibitory Concentration
ICH	The International Council for Harmonization
IFN	Interferon
IL	Interleukin
IS	Internal Standard
IV	Injection Volume
J	Flux
Jss	Steady-state flux
K	Consistency index

KDa	Kilo Daltons
Kp	permeability coefficient
kV	Kilo Volt
L	Liter
LCK	Lymphocyte cell-specific protein tyrosine kinase
LOD	Limit of detection
LOQ	Limit of quantification
LVR	Linear Viscoelastic Region
LYN	Lck-related novel protein tyrosine kinase
M	Molar
MA	Material attributes
MP	Mobile phase
mg	milligram
min	Minutes
mL	Milliliter
mm	Millimetre
mM	millimolar
mPa.s	millipascal-second
MPP	Matrix metalloproteinase
MTT	3-(4,5-dimethylthiazol-2-yl)-2,5-diphenyl tetrazolium bromide
MTX	Methotrexate
mV	milli Volts
n	Power index
NLCs	Nanostructured Lipid Carrier
ng	Nanogram
nM	Nanomolar
nm	Nanometer
NF-kB1	Nuclear Factor Signal Pathway
NSAID	Nonsteroidal anti-inflammatory drug
OS	Oscillatory Strain
OSS	Oscillatory Strain Sweep

O/W	Oil-in-water
PB	Phosphate Buffer
PBS	Phosphate Buffer Saline
PDA	Photodiode Array
PDGFR	Platelet-derived growth factor receptor
PDGFR-β	Platelet-derived growth factor receptor beta
PDI	Poly dispersibility index
PGE2	Prostaglandin E2
PI3K	Phosphoinositide 3-kinase
PKA	Protein Kinase A
PP	Process parameters
PS	Particle size
QC	Quality Control
R^2	Coefficient of correlation
RAS	Risk assessment
RE	Regression Equation
REM	Risk Estimation Matrix
RP-HPLC	Reverse phase high performance liquid chromatography
RPN	Risk Priority Number
RSD	Relative Standard Deviation
SC	Subcutaneous
SD	Standard Deviation
SLNs	Solid Lipid Nanoparticles
SLS	Sodium Lauryl Sulfate
QbD	Quality by design
QTPP	Quality target product profile
RA	Rheumatoid arthritis
RANK	Receptor activator of nuclear factor κ B
RANKL	Receptor activator of nuclear factor κ B ligand
REM	Risk Estimation Matrix
RPM	Revolutions Per Minute
RPN	Risk Priority Number

RSD	Relative standard deviation
RSM	Response surface methodology
RT	Retention time
RTK	Receptor tyrosine kinase
s	Seconds
SC	Stratum Corneum
SD	Standard deviation
SF	Synovial fluid
SLNs	Solid Lipid Nanoparticles
SRC	Sarcoma
SYK	Spleen tyrosine kinase
TDDS	Topical drug delivery systems
TF	Tailing factor
Tmax	Time taken to reach maximum concentration
t1/2	Half-life
TNF	Tumor Necrosis Factor
TNF-α	Tumor Necrosis Factor alpha
TLR	Toll-like receptors
TK	Tyrosine Kinase
TKI	Tyrosine kinase inhibitor
TWEL	Trans epidermal water loss
UGT	Uridine diphosphate-glucuronosyltransferase
USFDA	United States Food and Drug Administration
VEGF	Vascular endothelial growth factor
VEGFR	Vascular endothelial growth factor receptor
Vd	Volume of distribution
w/v	Weight per volume
w/w	Weight per weight
ZP	Zeta potential

Table of contents

Content	Page No.

Chapter-1

Introduction

1   Introduction

Rheumatoid arthritis (RA) is a condition that involves inflammation of the joints, leading to the destruction of cartilage and loss of bone tissue. As an immune-mediated disease, it is triggered by the body's immune system attacking its own joint tissue, resulting in synovial joint inflammation and destruction, as illustrated in Figure 1.1. Wrist and metacarpophalangeal joints are the first to show symptoms; later, the knees, ankles, feet, and elbows become involved as the primary sites of cell-mediated responses [1,2].

RA affects a significant portion of the global population, with 0.5-1% of adults worldwide being affected, regardless of ethnicity. Incidence rates vary, with 25-50 new cases per 100,000 people reported in various studies [3]. In certain populations, such as the indigenous population, the prevalence of RA can be particularly high with rates of 5.30% in the Pima, 6.80% in the Chippewa, and 2.40% in the Qom reported [4,5]. The prevalence of RA varies across different regions, with rates ranging from 0.13% in algeria to 0.90% in congo in African countries, 0.6-1% in Asian countries, and 1.90% in Australia, based on self-reported data from the 2017-2018 National Health Survey [6].

1.1   Histopathology in rheumatoid arthritis

The synovium is a sensitive lining that plays a crucial role in normal joints, and it is composed of two layers, the intimal and subintimal layer. In RA, inflammatory cells infiltrate and thicken the intimal layer, which can damage the cartilage and bone. The subintimal layer also undergoes significant changes resulting in hypertrophied synovium called pannus, which invades and erodes surrounding tissues. In RA patients, cartilage undergoes significant changes that reduce its structural integrity, resiliency, and water content due to the excessive production of proteolytic enzymes like collagenase and stromelysin. Inflammatory molecules like Interleukin-1 (IL-1) and

Tumor necrosis factor- alpha (TNF-α) can also degrade the extracellular matrix, leading to decreased cartilage production. RA results in bone loss due to the resorption of type I collagen by osteoclasts, which is activated by cytokines such as TNF, IL-1, and IL-17. These cytokines can also regulate the expression of receptor activators of nuclear factor B ligand (RANKL). Additionally, activated synovial cells can release signaling molecules that promote bone degradation. In RA, the synovial fluid (SF) becomes highly inflammatory, resulting in effusions with high protein content called exudative. Neutrophils are the major cell type in the SF, while lymphocytes and macrophages infiltrate rheumatoid synovial tissue. Increased white blood cells called polymorphonuclear leukocytes are also found in the SF, contributing to tissue destruction [7–9]**.**

Figure 1.1 Differentiation of joint in healthy and rheumatoid arthritis condition.

1.2   Pathophysiology of the rheumatoid arthritis

RA typically initiates with the production of rheumatoid factor (RF) and anti-citrullinated protein antibody (ACPA). From there, it progresses to the clinical manifestations, such as synovitis, joint inflammation, and angiogenesis, which ultimately leads to the destruction of the articular cartilage

and adjacent bones. This clinical manifestation is generally observed in genetically predisposed individuals who have been exposed to one or more environmental triggers [1,10,11].

RA is characterized by the infiltration of T lymphocytes, B cells, and monocytes into the synovial membrane of multiple joints. This condition is associated with synovitis, which is marked by endothelial cell activation prior to neovascularization. The synovial lining can experience hyperplasia as a result of the expansion of cells resembling fibroblasts and macrophages, leading to the enlargement of the synovial membrane known as the pannus. This pannus can infiltrate the junction between cartilage and bone, causing damage to the cartilage and erosion of the bone (Figure 1.2). Inflammatory cytokines such as TNF α and IL-6 activate molecules like RANKL, prostaglandins (Pg), and matrix metalloproteinases (MMP), which contribute to the symptoms of pain, swelling, and the breakdown of both cartilage and bone. RANKL, TNF, and IL-6 also activate osteoclasts in the synovial membrane, which can lead to further destruction of bone tissue [12,13]. These cellular and molecular processes are crucial to the progression of the disease and the resulting joint deterioration caused by swelling [14].

The exact origin of RA is still under clinical investigation, but both genetic and environmental factors triggered the RA conditions. RA is associated with multiple gene loci, with certain Human Leukocyte Antigen (HLA) class II antigens, such as HLA-DRB1*01 and HLA-DRB1*04, being closely linked to the condition due to the presence of a "shared epitope" responsible for presenting antigens to T lymphocytes [14–16].

Various factors such as tobacco use, periodontitis, viral infections, and the appearance of the microbiome in the gut and lungs have been identified as potential risk factors for the development of RA. In particular, certain species of prevotella and porphyromonas gingivalis bacteria in the

microbiome may contribute to the development of RA by triggering an autoimmune response [17,18].

Epigenetic modifications like DNA methylation and histone acetylation can promote inflammation. Citrullination of arginine and carbamylation of lysine can break immunological tolerance by creating neoepitopes of autologous proteins [19]**,** resulting in autoantibodies against ACPAs, RF, nuclear antigens, or cross-reactive autoantigens. These autoantibodies can form immunological complexes that activate complements and cause inflammation [20–22]**.** ACPAs alone cause mild inflammation, but with RFs, the inflammation gets severe. Synovium inflammation in pre-RA patients is usually asymptomatic. Early RA symptoms include mild arthritis to severe polyarticular disease and the generation of numerous positive autoantibodies. Later stages can show erosive disease or joint space narrowing due to cartilage deterioration. [23,24]**.**
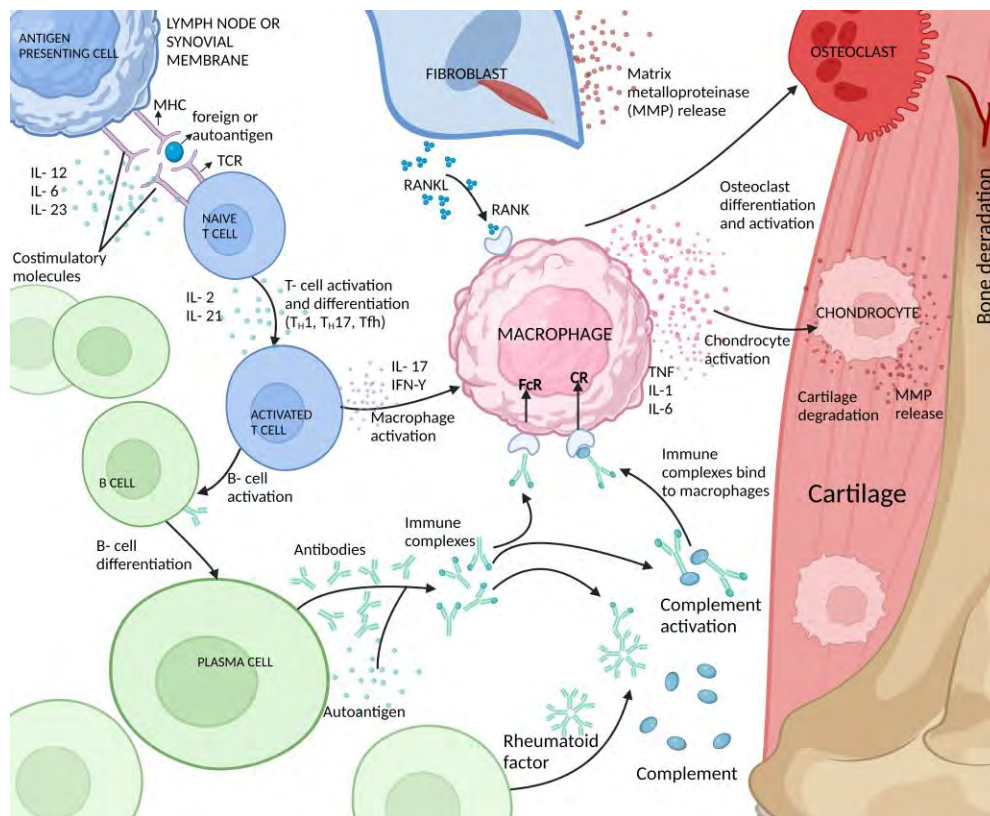
Figure 1.2 Pathophysiology of rheumatoid arthritis [14].

1.3   Different approaches for the management of rheumatoid arthritis

There is a range of treatments available that can help in controlling the symptoms and decreasing the disease's progression. Also, it is crucial to remember that each person will respond better to different treatments for RA.

Here are some examples of the numerous RA management approaches:

1. Nonsteroidal anti-inflammatory drugs (NSAIDs): NSAIDs are frequently used in RA to reduce pain and inflammation. They function by lowering prostaglandin synthesis, which are bodily substances responsible for inflammation and pain.

2. Disease-modifying antirheumatic drugs (DMARDs): These work by inhibiting the immune system to slow down the progression of RA. These medications may have side effects and may take weeks or months to start working.

3. Corticosteroids: These are potent anti-inflammatory medications that can quickly relieve RA symptoms. However, concerning the possibility of side effects, they are normally administered in small doses and for a short period.

4. Biologic agents: A more recent class of drugs known as biologic agents that target particular immune system proteins involved in RA inflammation. These medications, which are often given by injection or infusion, have a high potential for symptom relief and slowing down the disease progression.

5. Physical therapy: For patients with RA, physical therapy can enhance strength, lessen pain, and improve joint mobility. Each person with RA can have a customized exercise program made by a physical therapist to suit their particular demands.

6. Surgery: To replace damaged joints or to repair torn tendons and ligaments, surgery may be required in severe RA patients. For many persons with RA, joint replacement surgery can significantly reduce symptoms and enhance overall quality of life [25,26].

1.4   Current treatment for rheumatoid arthritis

Drugs can be classified into two groups for the management of RA. The first group consists of Nonsteroidal Anti-Inflammatory Drugs (NSAIDs) and Corticosteroids. The second group includes Disease Modifying Anti-Rheumatic Drugs (DMARDs) such as methotrexate, hydroxychloroquine, leflunomide, tofacitinib, and sulfasalazine. These medications slow down joint degeneration and disease activity [27,28].

European League Against Rheumatism (EULAR) RA treatment recommendations include three phases [29], comprising of the following:

Phase I therapy

RA patients are encouraged to start DMARDs immediately after diagnosis. The recommended initial treatment is methotrexate. If this is not well tolerated, other synthetic DMARDs such as leflunomide, sulfasalazine, or injectable gold can be considered. Patients who have not previously taken DMARDs are generally advised to begin with monotherapy rather than a combination of synthetic DMARDs. However, a low or medium-dose glucocorticoid may be added (typically 5-10 mg/day of prednisone). Patients should move to phase II if clinical remission or low disease activity is not obtained within 3-6 months [29].

Phase II Therapy

In the second phase, patients may switch to another synthetic DMARD, either alone or in combination with others. Glucocorticoids can be added if required. Adding a biological drug like a TNF-α antagonist is recommended as an alternative escalation of therapy if the desired clinical

outcome of low disease activity or clinical remission is not achieved within 3-6 months. In case of failure in achieving the desired clinical outcome with biological drugs, patients should move on to the third phase of treatment.

Phase III Therapy

In phase III, it may be advisable to switch to an alternative TNF-α antagonist along with a synthetic DMARD or opt for a cell-targeted therapy or cytokine antagonist instead of the biologic treatment. In case the desired clinical reduction or low disease activity is not attained in three to six months of treatment, modifications or additions to the current therapy may be necessary [29].

To this end, researchers are constantly looking for novel therapeutic targets, such as small-molecule inhibitors and gene therapies, to improve patient outcomes as well as life quality. Remission can be difficult to achieve for various reasons, and one major factor is the inability to continuously use conventional DMARDs due to intolerances, drug toxicity, contraindications, or comorbidities [30,31]. As a result, there is still a need for effective treatments for RA. Consequently, there is a pressing need for new RA treatments to address this gap. The recent investigation is extensively focusing on the Tyrosine kinases (TKs) [32].

1.5 Role of tyrosine kinase inhibitors in rheumatoid arthritis

TKs are the superheroes of the enzyme world, responsible for initiating the signal transduction cascade. These incredible enzymes are divided into two categories: receptor tyrosine kinases (RTKs) and non-RTKs [33]. Their ability to activate multiple proteins has been linked to the onset of RA [34]. The kinases play a critical role in cellular and cytokine responses in RA pathogenesis [35,36]. The use of small molecules TKIs, such as janus kinase inhibitors tofacitinib, baricitinib, and upadacitinib, has been approved for treating moderate-to-severe active RA patients who have an inadequate response or intolerance to at least one DMARD. These TKIs have shown significant

potential in managing the symptoms of RA by targeting the immune response that causes inflammation and joint damage. Preclinical studies have shown that nilotinib and imatinib exhibit better therapeutic activity on collagen-induced arthritis in mice model [37,38]. Other drugs such as fostamatinib, imatinib, nilotinib, Dasatinib (DTB), and bosutinib have emerged as promising alternative therapeutic targets for treating RA [37–41]. In RA pathogenesis, the cellular responses, including the proliferation and migration of fibroblast-like synoviocytes, angiogenesis, T cell, B cell, mast cell activation, and osteoclast formation leading to bone erosion is controlled by the tyrosine kinase receptors (TKR) (Figure 1.3) [35]. TKR inhibition could thus be the better option for the management of RA.
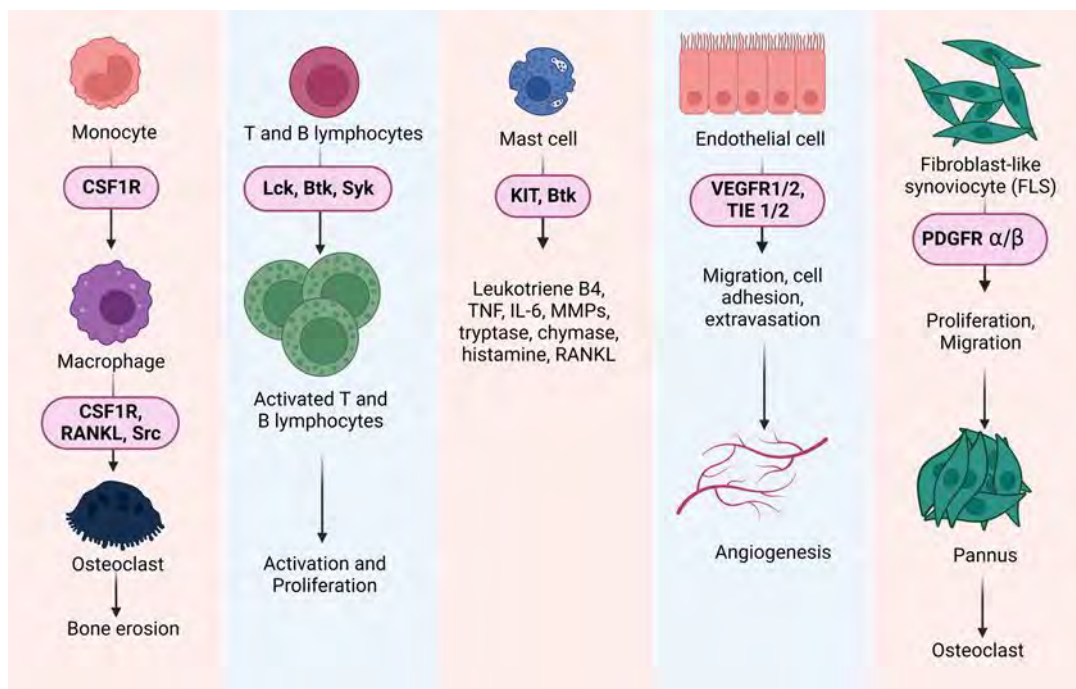
Figure 1.3 Cellular responses mediated by tyrosine kinases that contribute to the pathogenesis of rheumatoid arthritis. [35].

1.6   Role of dasatinib in rheumatoid arthritis

Dasatinib is a multitargeted inhibitor that exhibits better inhibitory effects on collagen receptor tyrosine kinases Discoidin domain receptor 1(DDR1) and DDR2 and is more potent than imatinib

and nilotinib [42]**.** Also, DTB inhibits several targets that are potent for treating RA, such as SRC family kinases, c-KIT, BCR/ABL, platelet derived growth factor receptor (PDGFR), TNF-α, IL6, PI3K, and ERK [43]**.** A recent study demonstrated the therapeutic efficacy of DTB in the CIA mice model and its result on FLS in RA patients [44–46]. Based on this evidence, it was suggested that DTB could be a viable therapy for RA. The reported literature disclosed that oral DTB (SPRYCEL tablet) exhibits severe side effects in patients treated with SPRYCEL used as single-agent therapy in clinical studies and post-marketing experience. The side effects includes blood and lymphatic system disorder (anemia, neutropenia, and thrombocytopenia), cardiac disorders (cardiac dysfunction, pericardial effusion, and arrhythmia), respiratory and thoracic disorders (pleural effusion, dyspnea, pulmonary edema, and pulmonary hypertension), gastrointestinal (GI) disorders (GI bleeding, colitis, gastritis, mucosal inflammation, and diarrhea), psychiatric disorders (depression, insomnia, anxiety, and confusional state) (Figure 1.4) [47–51]**.** To avoid the above-mentioned side effects, topical administration of DTB could be a viable approach, that can improve the therapeutic efficacy, and local effect, increase penetration into underlying layers of skin, and decrease oral-associated side effects [52].
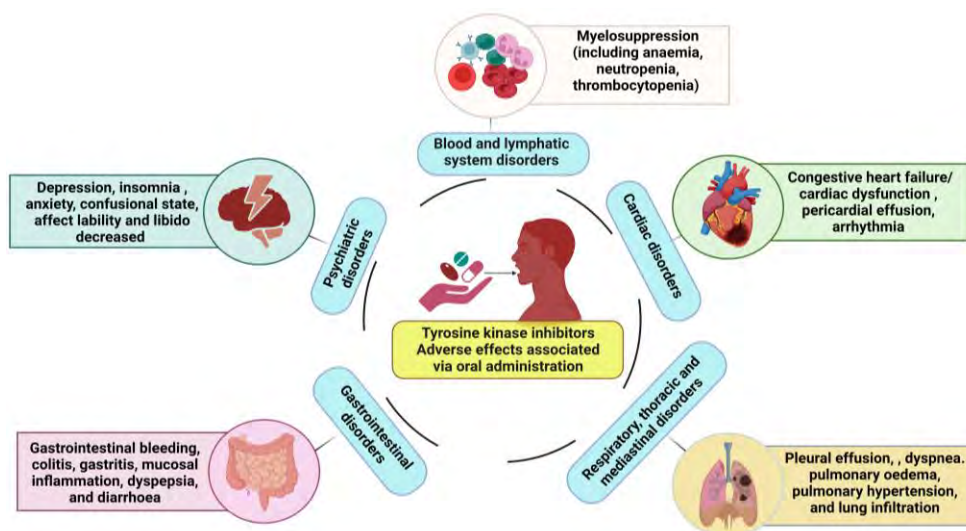
Figure 1.4 Adverse effect of oral administration of dasatinib.

1.7   Topical drug delivery system (TDDS)

The practice of administering medications through the skin to generate localized or systemic effects is known as topical drug delivery. Even though the skin acts as a barrier that inhibits drug penetration, TDDS has been developed to circumvent this issue [53]. TDDS can be formulated as creams, gels, ointments, lotions, patches, sprays, and foams, among other forms. They can deliver drugs to the site of action with minimal systemic absorption via topical administration [54]. TDDS has several merits; it is non-invasive, has lower chances of overdose, avoids GI tract entry and first-pass metabolism, improves patient compliance, and provides very less systemic side effects and targeted drug delivery to specific areas of the body. However, challenges in designing TDDS includes skin variability, drug stability, and achieving appropriate drug release rates [54,55]. Dermatological disorders such as eczema, psoriasis, and acne, as well as pain management and hormone replacement therapy, are commonly treated with TDDS. The potential applications of TDDS are expected to expand as research and development in this field persist [56]. Moreover, the conventional topical formulations have certain limitations, such as poor drug solubility, moisture entrapment in powders, cake formation in suspensions, coalescence of oil globules, poor adherence, reduced spreadability, limited drug penetration, skin irritation, and dose variability. To overcome these limitations, novel topical formulations have been developed, which offer improved drug delivery, enhanced therapeutic efficacy, and reduced side effects. Advanced drug delivery technologies such as liposomes, solid lipid nanoparticles, nanostructured lipid carriers, and nano-emulsions can be utilized to design novel topical formulations that enhance drug penetration [57].

1.7.1   Factors affecting topical drug delivery system

1.7.1.1   Physiological condition of the skin

Race

Due to increased lipid and electrical skin resistance, drugs diffuse at a faster rate in blacks than White.

Skin barrier properties in neonates and aged

SC hydration and stabilization is seen nearly three months after birth; newborn skin is relatively rough, dry, and slightly hydrophobic in nature. As the aging, the moisture content of the skin decreases, and also ruination of the epidermal junction happens, thereby leading to very less availability of area for transmission into the dermis.

Skin temperature

Skin remains at a temperature range of 32-37°C. Consequently, when the temperature rises diffusion also improves, but an increase in temperature also causes discomfort [54,58,59].

1.7.1.2 Physicochemical Properties of the active moiety

Partition coefficient (log P)

The partition coefficient is used to measure the relative solubility between water and lipid. For intermediate transdermal delivery, log P is between 1-3, lipophilic drug (log P>3) follows the intracellular route, and hydrophilic drug (log P <1) follows the intercellular route.

Molecular size

The flux of a drug molecule is inversely related to its molecular size. An optimal drug molecule for topical delivery requires a size of approximately 500 KDa or less.

Solubility/Melting point

Typically, organic solutes exhibit low solubility at normal ambient conditions (temperature and pressure) and show high melting points. Lipophilic drugs tend to permeate more rapidly than hydrophilic substances, but it is also important for them to possess aqueous solubility, which is required in many topical formulations.

Diffusion coefficient

The ability of a drug to penetrate through the skin depends on its diffusion coefficient. At a constant temperature, the diffusion coefficient of a drug is influenced by its properties, diffusion medium, and the interaction between them [54,59]**.**

1.8 Challenges in topical delivery

While topical delivery can be an effective way to deliver drugs and other substances to specific areas of the body, the major challenge is permeability through the skin barrier. The skin is a natural barrier that can be difficult to penetrate. To be effective, topical drugs must be able to penetrate the skin and reach the underlying tissues or bloodstream. To optimize the effectiveness of the medication, it is essential to have a thorough understanding of the anatomy and physiology of the skin during the selection and design of a formulation. The skin is a multifaceted organ comprising three layers: the (outermost layer), dermis (middle), and hypodermis (innermost layer). Each cm^2 contains 100 sweat glands, 15 sebaceous glands, 40-70 hair follicles, and 12 nerves. The skin protects from external and is also involved in Vitamin D metabolism, touch sensing, and topical drug delivery (Figure 1.5).
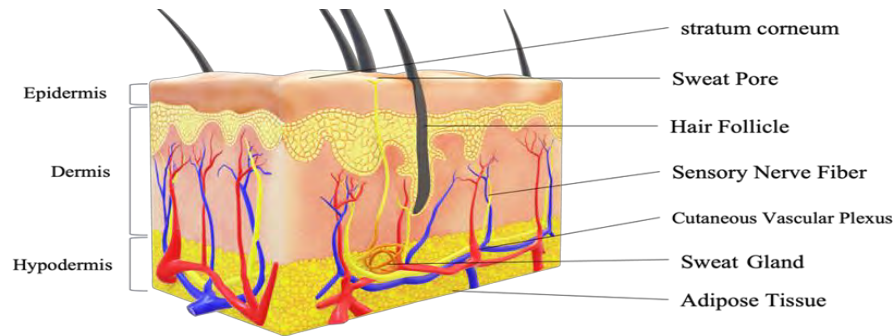
Figure 1.5 Skin morphology.

The epidermis is the skin's outermost layer and a crucial part of the body's defense against the environment. It includes different cell types, such as keratinocytes, Merkel cells, Langerhans cells, and melanocytes. Keratinocytes form the majority of the epidermis and create the skin's barrier, controlling water levels and absorbing certain substances. The epidermis comprises proteins and lipids that form a barrier against water loss and hazardous chemicals, with the basal, squamous, granular, and cornified layers. The cornified layer forms a physical shield to the underlying epidermis and prevents water loss and the passage of hazardous substances into the skin. Despite lacking nuclei, these large flat cells play a crucial role in promoting the shedding of dead skin cells. The basal layer consists of keratinocytes that migrate from the basal layer to the cornified layer over a minimum of 28 days [60–62]. Located just next to the epidermis, the dermis provides support and nutrition to the skin and includes two layers: the papillary and reticular dermis. The papillary dermis, a thin layer of collagen fibers, lies below the dermo-epidermal junction, while the reticular dermis is a thicker layer composed of collagen bundles parallel to the skin surface. The dermis contains stromal cells, structural cells of blood and lymph vessels, and immune cells [63]. The hypodermis is the innermost layer of the skin and consists mainly of adipocytes, blood vessels, lymphatic vessels, and nerves. It serves several functions, such as acting as an energy reserve, protecting the skin, and allowing for mobility. Fat cells begin to form in this layer during fetal development around the fifth month of gestation [64,65]

1.9   Drug permeation pathway

1.9.1   Transcellular through SC

This is likely the primary way that substances can pass through the skin. Also referred to as "bulk diffusion." Initially, lipid-soluble substances pass through the skin's lipid-rich cell membrane. Afterward, they move into the cell through the lipid-rich matrix that is nonpolar and non-aqueous, which lies between tonofilaments. Small water-soluble molecules enter the protein part of the cell membrane and then pass-through small pores between the protein subunits, crossing the lipid barrier. The diffusion then continues through channels within the skin lined by keratin molecules. These channels are sometimes referred to as "pores" and are around 10ºA in size. When hydrated, these channels widen, speeding up the process of diffusion.

1.9.2   Trans appendageal permeation

The process of diffusion that occurs through the sweat glands and pilosebaceous units is called "shunt diffusion." These appendages are covered only by the superficial parts of the SC. Although the surface area of these openings is very small compared to the total body surface area, they can rapidly absorb a limited number of diffusing molecules, which may be significant in the first few minutes of transport before a steady state is established. After that, the transcellular pathway is more dominant.

1.9.3   Paracellular SC

The Paracellular pathway could potentially play a role in the transportation of electrolytes through the skin, as these substances are highly insoluble in lipid membranes. Shunt diffusion may also be used as an alternative method of absorption. It is considered to be the most common pathway in drug absorption [55] **(**Figure 1.6).
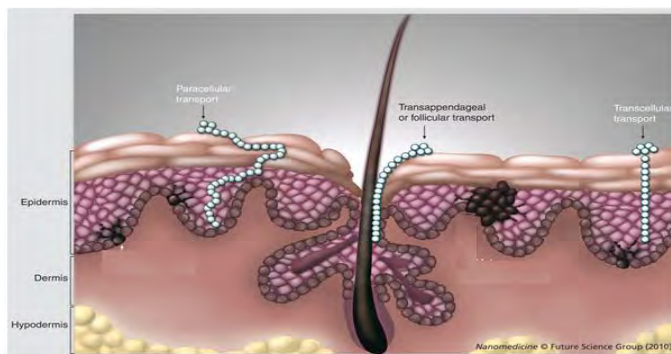
Figure 1.6 Illustration of entry of nanoparticle into skin [66].

1.10 Approaches for permeation enhancement

Topical delivery systems have many benefits, such as the ability to control and maintain the release of drug candidates that have a short biological half-life and need to be given often. Few drugs have physiochemical properties that make it hard for them to pass through the skin. Permeation enhancement is an important consideration in topical delivery, as it can help increase the absorption of drugs through the skin and improve their therapeutic effectiveness. The different permeation enhancement techniques such as chemical (alcohols, fatty acids, simple hydration, azones, transcutol solvents, and sulphoxides), physical penetration enhancers (iontophoresis, electroporation, and ultrasound), microneedles, nanoparticles (nanoemulsions, polymeric nanoparticles, liposomes, Solid lipid Nanoparticles (SLNs) and combination approaches (chemical enhancer can be used in conjunction with a physical enhancer or a penetration enhancer-containing vesicle to improve drug permeation) can be used to improve the permeability across the skin [58,59,65,67].

1.10.1 Nano-emulgel

Nanoemulgel is a type of drug delivery system that combines a nanotechnology-based emulsion with a gel base. This combination allows for increased absorption and penetration of the drug through the skin. When applied to the skin, the emulsion droplets in the nanoemulgel penetrate the

outermost layer of the skin SC. The small droplet size (usually less than 200 nm) of the emulsion facilitates increased surface area and transport of the drug through the skin's barrier layer and reaching the target site through transcellular and paracellular routes and, thus increasing its permeation, efficacy and meanwhile reducing side effects. The gel base of the nanoemulgel provides a sustained-release effect by forming a matrix and thin film on the skin surface. It is non-greasy with increased viscosity and spreadability leading to more patient compliance. Use of low or less chemical enhancers owning to increase safety and toxicity, and low production cost as it can be prepared by using either high or low energy techniques [68–70]. Verma and Easwari developed leflunomide loaded nano-emulgel preparation with particle size (PS) of 113.55 ± 1.73 nm, zeta potential (ZP) of 26.12mV with drug release of 98.13 ± 1.20%, showed leflunomide nano-emulgel, may be potential alternative drug therapy in topical treatment for arthritis [71]. Chandra et al. developed ginger extract-loaded nano-emulgel preparation with PS of 60.14±1.03 nm, ZP of -22.2mV and drug release of 93.53 ± 2.09%, resulting in improved transdermal permeation [72]. M.K Jeengar et al. prepared curcumin-loaded emu oil-based nano emulgel for the treatment of RA, the results revealed that the Curcumin emu oil-based nano-emulgel has shown better activity in Complete Freund's Adjuvant (CFA) induced arthritic rat model compared to free curcumin drug gel [73].

1.10.2 Solid lipid nanoparticles (SLNs)

Solid lipid nanoparticles (SLNs) are nanocarriers consisting of a solid core made of biocompatible lipids that can effectively encapsulate both hydrophilic and hydrophobic drugs.

SLNs increase the stability of drugs and provide controlled release and high drug loading capacity. Compared to liposome preparation, the lipids used in SLN preparation are cost-effective. SLN's small size allows it to form a thin layer on the SC, which reduces transepidermal water loss (TWEL)

and increases moisture levels, resulting in hydrated skin. Hydrated skin creates gaps in the corneocytes, allowing for SLNs accumulation in the SC. By embedding in the stratum layers, the particles enhance skin retention, gradually release the drug, and provide prolonged action without significant systemic absorption [74–76]. Few works for increased efficacy and suitability are reported. Bhalekar and his co-workers formulated chloroquine SLN gel as a topical delivery system for the treatment of RA. The developed SLNs preparation showed PS of 113.75 nm with % EE of 97.23%, showed chloroquine SLN gel has maximum retention (79.33%) in the skin than chloroquine phosphate gel (47.47%), resulting in reduced bone and cartilage degradation when compared to chloroquine phosphate gel [77]. Kesharwani et al. developed etoricoxib SLN gel with PS of <150 nm with ZP of -25.6mV indicating the stability of the formulation, % EE was found to be 70.766%. The study showed Carbopol containing SLN gel has better anti-inflammatory activity [78]**.**

1.11 Quality by design (QbD) significance in formulation development

The process of preparing nanocarriers is lengthy, requiring a wide variety of resources and individual steps. Nanocarrier physicochemical properties, biological parameters, and pharmacological behavior are highly sensitive to even small changes in the process. The changes can have an effect on the major characteristic parameters such as size, PDI, drug release, loading, and entrapment. Nano-formulations have demonstrated assurance in preclinical studies, but regulatory issues and a lack of data on scale-up prevent their commercialization. Poor reproducibility of the current process makes it difficult to accomplish consistent outcomes in the scale-up and manufacturing capability of nanocarriers. There are many challenges that must be overcome in order to develop nanocarriers that meet the necessary standards for safety, efficacy, and stability.

To prepare nanocarriers, it's crucial to comprehend how the different components interact with each other and how slight changes in their concentrations due to process parameters can affect the final outcome. A thorough understanding of the interaction between slight changes in each component and process parameters (PP) is critical for the large-scale manufacture of nanoformulations with programmed quality. The QbD method is a precisely defined strategy that focuses on scientific evidence and quality risk management, with the aim of ensuring a thorough understanding of the product and maintaining control over its production process. The FDA's risk-based approach presented in 2004 clearly described cGMP-based pharma companies.

In order to speed up the approval process for nanocarrier-based formulations, it is important to develop robust formulations, and QbD can help by providing insight into the factors that control the formulation constraints and manufacturing variables. The QbD-based method is beneficial for investigating various factors affecting the finished product using the DOE technique. DOE is a method that allows for the study of the interplay between 2 material attributes (MA), process parameters (PP), and the interplay between the PP and MA, thus allowing for the acquisition of comprehensive and detailed information about the formulation. This method is useful for addressing issues that arise during production and scaling up, and it is essential for maintaining a constant process because final product testing is insufficient in establishing quality. Quantitative risk analysis and quantitative control of risks are represented graphically by QbD.

Developing evocative product quality specifications based on safety and effective clinical outcomes is the goal of quality-based drug development. It aids in the study of material and process factors, which improves process efficiency with reduced product variation. QbD provides a technical framework for the main root cause investigation, formulation development, and efficiency of the manufacturing process. Formulation optimization was carried out in this study by identifying

quality target product profiles, critical quality attributes, critical material attributes, and critical process parameters.

1.12 Gaps and objective of the current research work

Rheumatoid Arthritis (RA), being an autoimmune disorder, majorly involves angiogenesis, osteoclast and bone erosion. Among different group of drugs used, tyrosine kinase inhibitors play a crucial role in cellular and cytokine responses involved in the pathogenesis of RA. Amongst all the tyrosine kinase inhibitors, Dasatinib exhibits inhibitory activity against multiple targets involved in RA, including SRC family kinases, c-KIT, BCR/ABL, PDGFR, TNF-α, IL-6, PI3K, and ERK. Additionally, DTB effectively regulates the proliferation of FLS in RA conditions. Presently, DTB is administered orally, which can result in several side effects, including myelosuppression, gastrointestinal bleeding, pulmonary hypertension, and pleural effusions. To address these side effects, topical administration of DTB could be a viable approach. However, conventional topical formulations have some limitations in delivering the hydrophobic drugs to the joint region due to their poor solubility in water and limited permeability through the stratum corneum, require frequent application to achieve the desired therapeutic concentration. These formulations, primarily water-based, struggle to effectively dissolve hydrophobic drugs and facilitate their penetration into deeper skin layers for therapeutic effects. Moreover, conventional topical formulations may cause discomfort to patients due to greasiness, and staining or discoloration.

The development of topical nanocarriers are alternative strategies for the delivery of hydrophobic drugs to enhance skin penetration, availability at disease site and provide better therapeutic outcomes with minimal systemic side effects. In addition to this, nanocarriers offer a protective effect against drug degradation and provide sustained drug release. Among the various types of

lipid nanoparticles, we have decided to explore nano-emulgel and solid lipid nanoparticles (SLNs) due to the lipids used in the formulations are high biocompatible, low toxicity, and biodegradability. Moreover, compared to microparticles, both nano-emulgel and SLNs gel exhibit high permeation capacity owing to their nano size. Furthermore, they enable efficient drug loading and controlled drug release, thereby enhancing the therapeutic potential of the delivered drug. Moreover, after application, nanocarriers offer an elegant appearance and can be easily wiped off from the skin.

In light of above advantages, in our current investigation, we aim to enhance permeability and therapeutic activity of the DTB by delivering through topical nano-emulgel and SLNs gel formulations. To achieve this, we have employed Quality by Design (QbD) approach for formulation development and optimization. Firstly, for quantification of DTB in various sample matrix, we have developed and validated analytical method and utilized for the estimation of DTB in both bulk drug and lipid nano formulations. For the formulation development, we screened lipids and surfactants based on solubility, stability and compatibility. Further, based on quality risk assessment, critical material attributes and process parameters were selected for the Design of Experiments (DOE). The DOE based optimized formulations were carried out for the evaluation of entrapment efficiency, particle size, in vitro drug release, in vitro cell lines (cytotoxicity, and expression of IL-6 and TNF-α levels). Further, the formulations were evaluated for ex vivo skin permeation, skin deposition, and bio adhesion strength. In-vivo investigation of optimized formulations were performed in Sprague Dawley (SD) using Freund's complete adjuvant (FCA)-induced arthritis model. Both the formulations i.e DTB loaded nanoemulgel and SLNs were evaluated for their improved therapeutic efficacy.

References

1. Cooles, F.A.H. and Isaacs, J.D. (2011) Pathophysiology of rheumatoid arthritis. *Curr Opin Rheumatol* 23, 233–240

2. Firestein, G.S. and McInnes, I.B. (2017) Immunopathogenesis of Rheumatoid Arthritis. *Immunity* 46, 183–196

3. Uhlig, T. *et al.* (2014) The Burden of Disease in Rheumatoid Arthritis. *Pharmacoeconomics* 32, 841–851

4. Cross, M. *et al.* (2014) The global burden of rheumatoid arthritis: estimates from the Global Burden of Disease 2010 study. *Ann Rheum Dis* 73, 1316–1322

5. Peláez-Ballestas, I. *et al.* (2018) Epidemiology and socioeconomic impact of the rheumatic diseases on indigenous people: an invisible syndemic public health problem. *Ann Rheum Dis* 77, 1397–1404

6. Almutairi, K. *et al.* (2022) The prevalence of rheumatoid arthritis in Western Australia. *BMC Rheumatol* 6, 1–8

7. Strand, V. *et al.* (2007) Biologic therapies in rheumatology: lessons learned, future directions. *Nature Reviews Drug Discovery 2007 6:1* 6, 75–92

8. Choy, E.H.S. and Panayi, G.S. (2001) Cytokine pathways and joint inflammation in rheumatoid arthritis. *N. Engl. J. Med.* 344, 907–916

9. Johns Hopkins (2023) RA Pathophysiology • Johns Hopkins Arthritis Center. *2023*. [Online]. Available: https://www.hopkinsarthritis.org/arthritis-info/rheumatoid-arthritis/ra-pathophysiology-2/. [Accessed: 14-Mar-2023]

10. McInnes, I.B. and Schett, G. (2011) The pathogenesis of rheumatoid arthritis. *N Engl J Med* 365, 2205–2219

11. McInnes, I.B. and Schett, G. (2017) Pathogenetic insights from the treatment of rheumatoid arthritis. *The Lancet* 389, 2328–2337

12. Redlich, K. and Smolen, J.S. (2012) Inflammatory bone loss: pathogenesis and therapeutic intervention. *Nat Rev Drug Discov* 11, 234–250

13. Ramiro, S. *et al.* (2017) Safety of synthetic and biological DMARDs: a systematic literature review informing the 2016 update of the EULAR recommendations for management of rheumatoid arthritis. *Ann Rheum Dis* 76, 1093–1101

14. Aletaha, D. and Smolen, J.S. (2018) Diagnosis and Management of Rheumatoid Arthritis: A Review.*JAMA - Journal of the American Medical Association*, 320American Medical Association, 1360–1372

15. Viatte, S. and Barton, A. (2017) Genetics of rheumatoid arthritis susceptibility, severity, and treatment response. *Seminars in Immunopathology 2017 39:4* 39, 395–408

16. Gregersen, P.K. *et al.* (1987) The shared epitope hypothesis. an approach to understanding the molecular genetics of susceptibility to rheumatoid arthritis. *Arthritis Rheum* 30, 1205–1213

17. Wegner, N. *et al.* (2010) Peptidylarginine deiminase from Porphyromonas gingivalis citrullinates human fibrinogen and α-enolase: Implications for autoimmunity in rheumatoid arthritis. *Arthritis Rheum* 62, 2662

18. Manfredo Vieira, S. *et al.* (2018) Translocation of a gut pathobiont drives autoimmunity in mice and humans. *Science* 359, 1156–1161

19. Ospelt, C. *et al.* (2017) Epigenetics in the pathogenesis of RA. *Seminars in Immunopathology 2017 39:4* 39, 409–419

20. Tan, E.M. and Smolen, J.S. (2016) Historical observations contributing insights on etiopathogenesis of rheumatoid arthritis and role of rheumatoid factor. *Journal of Experimental Medicine* 213, 1937–1950

21. Aletaha, D. *et al.* (2015) Rheumatoid factor, not antibodies against citrullinated proteins, is associated with baseline disease activity in rheumatoid arthritis clinical trials. *Arthritis Res Ther* 17, 1–10

22. Sokolove, J. *et al.* (2014) Rheumatoid factor as a potentiator of anti-citrullinated protein antibody-mediated inflammation in rheumatoid arthritis. *Arthritis and Rheumatology* 66, 813–821

23. Nielen, M.M.J. *et al.* (2004) Specific autoantibodies precede the symptoms of rheumatoid arthritis: A study of serial measurements in blood donors. *Arthritis Rheum* 50, 380–386

24. H de Hair, M.J. *et al.* (2014) Features of the Synovium of Individuals at Risk of Developing Rheumatoid Arthritis Implications for Understanding Preclinical Rheumatoid Arthritis. *Arthritis and Rheumatology* 66, 513–522

25. Tayar, J.H. and Suarez-Almazor, M.E. (2010) New understanding and approaches to treatment in rheumatoid arthritis. *Br Med Bull* 94, 201–214

26. Köhler, B.M. *et al.* (2019) Current therapeutic options in the treatment of rheumatoid arthritis. *J Clin Med* 8, 1–15

27. Davis, J.M. and Matteson, E.L. (2012) My Treatment Approach to Rheumatoid Arthritis. *Mayo Clin Proc* 87, 659–673

28. Nogueira, E. *et al.* (2016) Update on Therapeutic Approaches for Rheumatoid Arthritis. *Curr Med Chem* 23, 2190–2203

29. Smolen, J.S. *et al.* (2017) EULAR recommendations for the management of rheumatoid arthritis with synthetic and biological disease-modifying antirheumatic drugs: 2016 update. *Ann Rheum Dis* 76, 960–977

30. Caporali, R. and Zavaglia, D. (2019) Real-world experience with tofacitinib for the treatment of rheumatoid arthritis. *Clin Exp Rheumatol* 37, 485–495

31. Yu, C. *et al.* (2019) Remission rate and predictors of remission in patients with rheumatoid arthritis under treat-to-target strategy in real-world studies: a systematic review and meta-analysis. *Clin Rheumatol* 38, 727–738

32. Wu, J. *et al.* (2019) Tyrosine kinase inhibitors for the treatment of rheumatoid arthritis: phase I to II clinical trials. *Expert Opin Investig Drugs* 28, 1113–1123

33. Hubbard, S.R. and Miller, W.T. (2007) Receptor tyrosine kinases: mechanisms of activation and signaling. *Curr Opin Cell Biol* 19, 117–123

34. Bullock, J. *et al.* (2019) Rheumatoid Arthritis: A Brief Overview of the Treatment. *Medical Principles and Practice* 27, 507

35. Swanson, C.D.A. *et al.* (2009) Tyrosine kinases as targets for the treatment of rheumatoid arthritis*Nature Reviews Rheumatology*, 5Nature Publishing Group, 317–324

36. Okamoto, H. and Kobayashi, A. (2011) Tyrosine kinases in rheumatoid arthritis. *J Inflamm* 8, 21

37. Koyama, K. *et al.* (2007) Imatinib mesylate both prevents and treats the arthritis induced by type II collagen antibody in mice. *Mod Rheumatol* 17, 306–310

38. Akashi, N. *et al.* (2011) Comparative suppressive effects of tyrosine kinase inhibitors imatinib and nilotinib in models of autoimmune arthritis. *Mod Rheumatol* 21, 267–275

39. Kang, Y. *et al.* (2019) Efficacy and safety of multiple dosages of fostamatinib in adult patients with rheumatoid arthritis: A systematic review and meta-Analysis. *Front Pharmacol* 10, 897

40. Ozanne, J. *et al.* (2015) The clinically approved drugs dasatinib and bosutinib induce anti-inflammatory macrophages by inhibiting the salt-inducible kinases. *Biochem J* 465, 271–279

41. Dohse, M. *et al.* (2010) Comparison of ATP-binding cassette transporter interactions with the tyrosine kinase inhibitors imatinib, nilotinib, and dasatinib. *Drug Metab Dispos* 38, 1371–1380

42. Day, E. *et al.* (2008) Inhibition of collagen-induced discoidin domain receptor 1 and 2 activation by imatinib, nilotinib and dasatinib. *Eur J Pharmacol* 599, 44–53

43. Korashy, H.M. *et al.* (2014) Dasatinib. *Profiles Drug Subst Excip Relat Methodol* 39, 205–237

44. Guo, K. *et al.* (2019) Treatment Effects of the Second-Generation Tyrosine Kinase Inhibitor Dasatinib on Autoimmune Arthritis. *Front Immunol* 9

45.   Bottini, N. and Firestein, G.S. (2013) Duality of fibroblast-like synoviocytes in RA: passive responders and imprinted aggressors. *Nat Rev Rheumatol* 9, 24

46.   Collison, J. (2016) Features of synovium in RA remission revealed. *Nature Reviews Rheumatology 2016 12:6* 12, 316–316

47.   Fox, L.C. *et al.* (2017) The incidence and natural history of dasatinib complications in the treatment of chronic myeloid leukemia. *Blood Adv* 1, 802

48.   Krauth, M.T. *et al.* (2011) Extensive pleural and pericardial effusion in chronic myeloid leukemia during treatment with dasatinib at 100 mg or 50 mg daily. *Haematologica* 96, 163–166

49.   Rasheed, W. *et al.* (2009) Reversible severe pulmonary hypertension secondary to dasatinib in a patient with chronic myeloid leukemia. *Leuk Res* 33, 861–864

50.   Quintás-Cardama, A. *et al.* (2009) Bleeding Diathesis in Patients With Chronic Myelogenous Leukemia Receiving Dasatinib Therapy. *Cancer* 115, 2482

51.   Sprycel, F. (2006) SPRYCEL® FDA pill

52.   DR, L. and MJ, B. (2010) Topical nonsteroidal anti-inflammatory drugs for the treatment of pain due to soft tissue injury: diclofenac epolamine topical patch. *J Pain Res* 3, 223

53.   Touitou, E. (2002) Drug delivery across the skin. *Expert Opin Biol Ther* 2, 723–733

54.   Marwah, H. *et al.* (2016) Permeation enhancer strategies in transdermal drug delivery. *Drug Deliv* 23, 564–578

55.   Marwah, H. *et al.* (2014) Permeation enhancer strategies in transdermal drug delivery. *Drug Deliv* 23, 564–578

56.   KOO, J. and LEBWOHL, A. (2001) Psychodermatology: The Mind and Skin Connection. *Am Fam Physician* 64, 1873–1879

57.   Gorain, B. *et al.* (2016) Comparative biodistribution and safety profiling of olmesartan medoxomil oil-in-water oral nanoemulsion. *Regul Toxicol Pharmacol* 82, 20–31

58.   Mota, A.H. *et al.* (2021) Therapeutic Implications of Nanopharmaceuticals in Skin Delivery. In *Nanopharmaceuticals: Principles and Applications* 1, pp. 205–272

59.   Park, C.W. *et al.* (2012) Investigation of formulation factors affecting in vitro and in vivo characteristics of a galantamine transdermal system. *Int J Pharm* 436, 32–40

60.   Matoltsy, A.G. (1976) Keratinization. *Journal of Investigative Dermatology* 67, 20–25

61.   David H. Chu (2018) Development and Structure of Skin. *Fitzpatrick's Dermatology in General Medicine*

62.   UCLA, R.O.T. (2009) *Skin cancer skin cancer*, 74

63. Zeng, Q. *et al.* (2017) 6.20.Skin Tissue Engineering. *Comprehensive Biomaterials II* 6, 334–382

64. Kolarsick, P.A.J. *et al.* (2011) Anatomy and Physiology of the Skin. *J Dermatol Nurses Assoc* 3, 203–213

65. William D. James, T.G.B. (2006) *Andrews' diseases of the skin : clinical dermatology | WorldCat.org*, ((10th edn)), 306(2)

66. Donthi, M.R. *et al.* (2023) Nanoemulgel: A Novel Nano Carrier as a Tool for Topical Drug Delivery. *Pharmaceutics* 15

67. Harrison, J.E. *et al.* (1996) The relative effect of azone® and transcutol® on permeant diffusivity and solubility in human stratum corneum. *Pharm Res* 13, 542–546

68. Sengupta, P. and Chatterjee, B. (2017) Potential and future scope of nanoemulgel formulation for topical delivery of lipophilic drugs. *Int J Pharm* 526, 353–365

69. Ojha, B. *et al.* (2021) Nanoemulgel: a promising novel formulation for treatment of skin ailments. *Polymer Bulletin* 79(7), 4441–4465

70. Sultana, F. *et al.* (2013) An Overview of Nanogel Drug Delivery System. *J Appl Pharm Sci* 3, S95–S105

71. Verma, V. and Easwari, T.S. (2022) A Novel Approach of Leflunomide Nanoemulgel for Topical Drug Delivery System. *Int J Pharm Investig* 12, 199–204

72. Chandra, A. *et al.* (2019) Formulation and Evaluation of Ginger Extract Loaded Nanoemulgel for the Treatment of Rheumatoid Arthritis. *Journal of Drug Delivery and Therapeutics* 9, 559–570

73. Jeengar, M.K. *et al.* (2016) Emu oil based nano-emulgel for topical delivery of curcumin. *Int J Pharm* 506, 222–236

74. Rapalli, V.K. *et al.* (2021) Solid lipid nanocarriers embedded hydrogel for topical delivery of apremilast: In-vitro, ex-vivo, dermatopharmacokinetic and anti-psoriatic evaluation. *J Drug Deliv Sci Technol* 63, 102442

75. Rapalli, V.K. *et al.* (2020) Psoriasis: pathological mechanisms, current pharmacological therapies, and emerging drug delivery systems. *Drug Discov Today* 25, 2212–2226

76. Rapalli, V.K. *et al.* (2020) Curcumin loaded nanostructured lipid carriers for enhanced skin retained topical delivery: optimization, scale-up, in-vitro characterization and assessment of ex-vivo skin deposition. *European Journal of Pharmaceutical Sciences* 152, 105438

77. Bhalekar, M.R. *et al.* (2015) Anti-rheumatic activity of chloroquine-SLN gel on wistar rats using complete freund's adjuvant (CFA) model. *Indian J Rheumatol* 10, 58–64

78. Kesharwani, R. *et al.* (2016) Formulation and Evaluation of Solid Lipid Nanoparticle (SLN) Based Topical Gel of Etoricoxib. *J Appl Pharm Sci* 6, 124–131

Chapter-2
Drug Profile
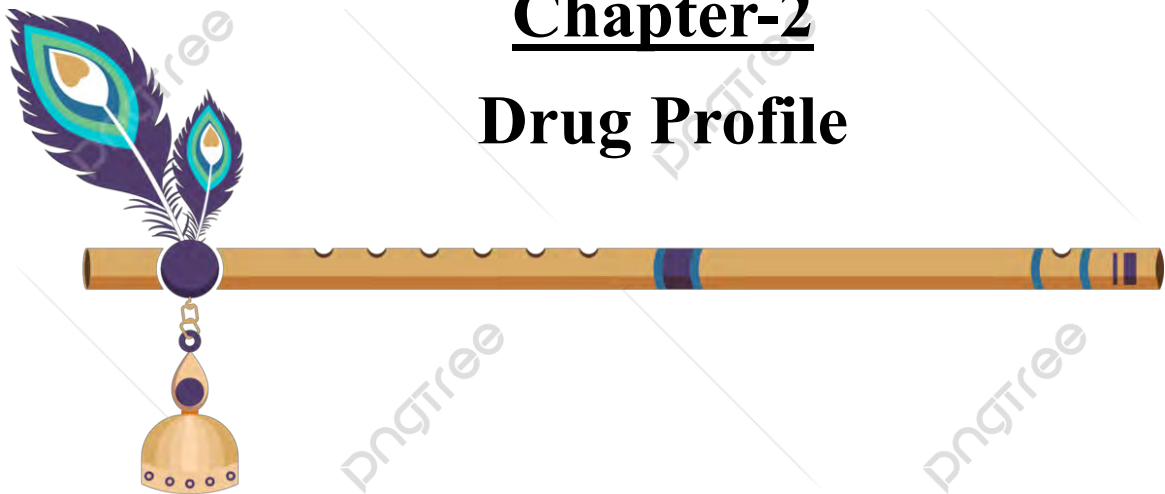
2 Introduction

DTB is chemically known as N-(2-chloro-6-methylphenyl)-2-[[6-[4-(2-hydroxyethyl)-piperazin-1-yl]-2-methylpyrimidin-4-yl] amino]-1,3-thiazole-5-carboxamide shown in Figure 2.1 [1]. Dasatinib (DTB) was developed through a collaboration between Otsuka Pharmaceutical Co., Ltd and Bristol-Myers Squibb [2–4]. DTB was approved by the United States Food and Drug Administration (USFDA) in 2006 for treating adults with Philadelphia chromosome-positive chronic myeloid leukemia in the chronic phase (CP-CML). DTB is a second-generation tyrosine kinase inhibitor (TKI) that selectively targets Breakpoint cluster region- Abelson (BCR-ABL) kinase, a fusion protein resulting from the chromosomal translocation known as the Philadelphia chromosome (9;22) [5]. This fusion protein is present in 95% of patients with chronic myeloid leukemia (CML).
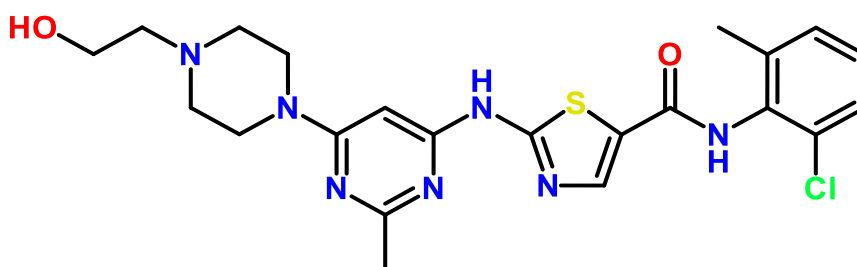
Figure 2.1 Structure of dasatinib.

It also inhibits SRC-family tyrosine kinases such as BLK, FRK, FYN, HCK, LCK, LYN, and YES. Other potential DTB targets include PDGFR, VEGFR1/2, TIE1/2, Lck, SYK, KYT, BTK, and CSF1R. DTB aids in inhibiting inflammatory cytokines such as TNF-α, IL-1, and IL-6. These potential targets and inflammatory cytokines play a significant role in the pathogenesis of rheumatoid arthritis [6–11]

2.1 Drug properties

Table 2.1 Drug properties of dasatinib.

Name	Dasatinib
Molecular formula	$C_{22}H_{26}ClN_7O_2S$
Molecular weight	488.01 g/mol
BCS class	II
Melting point	280-286 °C [12]
Log P	1.80 [12]
pKa (Basic)	7.18
Solubility in various solvents	Freely soluble in DMSO and slightly soluble in acetonitrile, ethanol, methanol, and acetone. [13,14]
Water Solubility	0.013 mg/mL [12]
Half-life	3-5 h [15]
Metabolism	CYP3A4 [15]
Pharmacological class	Tyrosine kinase inhibitors
Role in RA	Inhibits matrix metalloproteinase (MMP), fibroblast-like synoviocytes (FLS), Vascular endothelial growth factor (VEGF), TNF-α, IL6, and IL-1β.
Proprietary names	Sprycel, Dasamyl, Beedan, Nextki, Dasamaps, Dsatinib ML, Dasapan, Dasanat, Dasatrue, Leu Kinib
Available strengths	20mg- 140 mg

2.2 Clinical pharmacology

DTB exerts its therapeutic effects through multiple mechanisms of action. Its primary mode of

action involves inhibiting various kinases, such as BCR-ABL, c-KIT, PDGFRβ, EPHA2, and

SRC (LCK, FYN, YES, SRC) [16]. By engaging in intricate interactions at a molecular level, DTB binds to the ABL kinase in multiple ways, as demonstrated by insightful modeling studies. DTB demonstrates remarkable effectiveness against different types of leukemic cells, including both imatinib mesylate-sensitive and -resistant cells, while effectively inhibiting the growth of chronic myeloid leukemia cells and counteracting imatinib resistance caused by genetic mutations in the BCR-ABL kinase. It accomplishes this by activating alternative signalling pathways, such as the SRC family kinases, thereby surpassing the constraints imposed by these genetic alterations.

Apart from its primary mode of action, DTB exerts its therapeutic influence through a secondary mechanism. This involves the modulation of inflammatory mediators and immune responses. DTB has been found to suppress the production of pro-inflammatory cytokines such as IL-1β, TNF-α, and IL-6 while simultaneously promoting the production of the anti-inflammatory cytokine IL-10 [17]. These immunomodulatory effects contribute to the overall therapeutic potential of DTB in various disease contexts.

DTB demonstrates promising efficacy in preclinical models for autoimmune diseases. In mice with collagen-induced arthritis (CIA), DTB administration effectively inhibits the production of collagen type II (CII) antibodies, including subclasses of immunoglobulin G (IgG) such as IgG1, IgG2, and IgG2b. This inhibition of the autoimmune response by DTB slows down the progression of arthritis in these mice [18]. Additionally, DTB exerts inhibitory effects on fibroblast-like synoviocytes (FLS), specialized cells involved in the development of autoimmune arthritis. Moreover, DTB reduces the expression of various factors involved in joint inflammation and destruction, including VEGF, DKK1, MMP13, and FGF, thereby mitigating the pathological processes associated with autoimmune arthritis [18]. FLS represents a critical target in the treatment of autoimmune arthritis, and the effectiveness of DTB in CIA models further highlights its potential therapeutic value in arthritis [19].

Furthermore, DTB exhibits an intriguing inhibitory effect on collagen receptor tyrosine kinases DDR1 and DDR2 [20].

2.3 Pharmacokinetics

The pharmacokinetic study of DTB was performed on 229 healthy individuals and 137 leukemia patients in another group.

Absorption

Oral administration of DTB exhibited a biological half-life of 3-5 h and a Tmax of 0.5-6 h. The linear elimination character and AUC of DTB showed a direct correlation with dose, ranging from 15 to 240 mg/day. In a study of 54 healthy subjects, the consumption of high-fat meals following the administration of 100 mg of DTB resulted in a 14% increase in AUC [21].

Distribution

In individuals, it has been observed that dasatinib exhibits a substantial apparent volume of distribution (2,505 L) with a coefficient of variation (CV% 93%). These findings indicate that DTB is widely distributed in the extravascular space. Through in vitro experiments, it has been determined that dasatinib binds to plasma proteins at a rate of around 96% when considering clinically significant concentrations [21].

Metabolism

DTB undergoes significant metabolism in humans, mainly through the action of the cytochrome P450 (CYP) 3A4, which is primarily responsible for forming its active metabolite. Other enzymes, such as uridine diphosphate-glucuronosyltransferase (UGT) and flavin-containing monooxygenase 3 (FMO-3), also play a significant role in the metabolism of DBT. [21].

Elimination

DTB is primarily eliminated through the fecal route, mostly as metabolites. Administration of a single dose of [14C]-labeled DTB revealed that 4% of the radioactivity was excreted in urine and 85% in feces within ten days. Unchanged DTB accounted for 0.1% of the radioactivity observed in urine and 19% in feces, with the remaining radioactivity corresponding to metabolites [21].

2.4 Population Pharmacokinetics

Pharmacokinetics data shows that age and gender do not significantly impact the clinical effectiveness of DTB. However, no studies have been conducted on pediatric patients [21].

2.5 Drugs that alter the plasma concentrations of DTB

A study showed that co-administration of 200 mg of ketoconazole BID with a single dose of 20 mg of DTB QD increased the C_{max} by four-fold and AUC by five-fold in a group of 18 patients with solid tumors. A few examples of CYP3A4 inhibitors include ketoconazole, clarithromycin, itraconazole, erythromycin, nefazodone, nelfinavir, saquinavir, atazanavir, ritonavir, indinavir, and telithromycin. This CYP3A4 inhibitor decreases the metabolism of DTB and increases the plasma concentration [21].

Rifampicin

 A single dose of DTB administered after continuous administration of 600 mg rifampicin showed decreased AUC by 82% and C_{max} of DBT by 81%. This study was observed in a group consisting of 20 healthy subjects [21].

Antacids

Based on nonclinical data, DTB has pH-dependent solubility. A dose of 50 mg of DTB administered after 2 h of administration of antacids such as magnesium or aluminum hydroxide showed an increase in C_{max} by 26% but no deliberate change in AUC. The same test conducted

by co-administration of 30mL of aluminum or magnesium hydroxide and a 50mg dose of DTB showed a reduction of AUC by 55% and C_{max} by 58%. This study is conducted on 24 healthy subjects [21].

Famotidine

In a study with 24 healthy subjects, the single dose of 50 mg of DTB co-administered after 10 h of famotidine showed a decrease in AUC of DBT by 61% and C_{max} by 63%[21].

CYP3A4 Substrates

In a study with 54 healthy subjects, 100 mg DTB co-administrated with simvastatin showed an increase of mean C_{max} of simvastatin by 37% and AUC by 20%, respectively [21].

2.6 Adverse effects

Most of the negative effects linked to DTB treatment are typically mild to moderate in severity, and with appropriate intervention, they are usually reversible and manageable. Some common side effects include hypertension, cardiac failure, and coronary artery disease [10]. It is important to use caution when administering DTB to patients with hypokalaemia or hypomagnesemia because it can potentially prolong the QT interval. Pleural effusion is another typical side effect of DTB, but it can be effectively managed with a change in strength and supportive care. Additionally, DTB may cause internal bleeding and thrombocytopenia, which may be compounded with antiplatelet and anticoagulant drugs [12,22]

2.7 Overdose

Clinical studies have reported only a few cases of DTB overdose, and the maximum reported dosage of 280 mg/day for seven days resulted in severe myelosuppression and bleeding in patients. In animals, acute overdose resulted in cardiotoxicity, with ventricular hemorrhage and necrosis at a dose greater than 100 mg/kg (600 g/m^2) in rodents. In monkeys, a single dose greater than 10 mg/kg (120 mg/m^2) tended to increase systolic and diastolic blood pressure [23]

2.8 Type of dosage form and available strength

The tablets of DTB come in various strengths ranging from 20 mg to 140 mg (50, 70, 80, and 100 mg). These tablets are biconvex and film-coated, with a white to off-white color [23].

References:

1. Lakka, N.S. *et al.* (2020) Separation and Characterization of New Forced Degradation Products of Dasatinib in Tablet Dosage Formulation Using LC–MS and Stability-Indicating HPLC Methods. *Chromatographia* 83, 947–962

2. Bristol-Myers (2009) Otsuka and Bristol-Myers Squibb Announce a Change in Contract Regarding Collaboration in Japan in the Oncology Therapy Area | News Releases | Otsuka Pharmaceutical Co., Ltd. *Otsuka and Bristol-Myers Squibb Announce a Change in Contract Regarding Collaboration in Japan in the Oncology Therapy Area*

3. Bristol-Myers Squibb (2013) Bristol Myers Squibb - FDA Approves U.S. Product Labeling Update for Sprycel® (dasatinib) to Include Three-Year First-Line and Five-Year Second-Line Efficacy and Safety Data in Chronic Myeloid Leukemia in Chronic Phase. *Bristol-Myers Squibb Company*

4. BMS (2009) Bristol Myers Squibb - Bristol-Myers Squibb Announces Extension of U.S. Agreement for ABILIFY® and Establishment of an Oncology Collaboration with Otsuka

5. Lindauer, M. and Hochhaus, A. (2018) Dasatinib. *Recent Results in Cancer Research* 212, 29–68

6. Ntari, L. *et al.* (2021) Combination of subtherapeutic anti-TNF dose with dasatinib restores clinical and molecular arthritogenic profiles better than standard anti-TNF treatment. *J Transl Med* 19, 165

7. Swanson, C.D.A. *et al.* (2009) Tyrosine kinases as targets for the treatment of rheumatoid arthritis *Nature Reviews Rheumatology*, 5Nature Publishing Group, 317–324

8. Guo, K. *et al.* (2019) Treatment Effects of the Second-Generation Tyrosine Kinase Inhibitor Dasatinib on Autoimmune Arthritis. *Front Immunol* 9

9. Montero, J.C. *et al.* (2011) Inhibition of SRC family kinases and receptor tyrosine kinases by dasatinib: possible combinations in solid tumors. *Clin Cancer Res* 17, 5546–5552

10. Hantschel, O. *et al.* (2007) The Btk tyrosine kinase is a major target of the Bcr-Abl inhibitor dasatinib. *Proc Natl Acad Sci U S A* 104, 13283

11. Day, E. *et al.* (2008) Inhibition of collagen-induced discoidin domain receptor 1 and 2 activation by imatinib, nilotinib and dasatinib. *Eur J Pharmacol* 599, 44–53

12. Korashy, H.M. *et al.* (2014) Dasatinib. *Profiles Drug Subst Excip Relat Methodol* 39, 205–237

13. Annapurna, T. *et al.* (2022) Dastinib nasosponges-formulation development and evaluation. *Journal of Innovations in Applied Pharmaceutical Science (JIAPS)* DOI: 10.37022/JIAPS.V7I1.259

14. Sodeifian, G. *et al.* (2022) Solubility of Dasatinib monohydrate (anticancer drug) in supercritical CO2: Experimental and thermodynamic modeling. *J Mol Liq* 346, 117899

15. M, M. *et al.* (2016) Antioxidant Effect of Silymarin During Non-Enzymatic Peroxidation of Rat Kidney Microsomes and Mitochondria. *Biochemistry & Molecular Biology Letters* 2, 102

16. Guo, K. *et al.* (2018) Treatment Effects of the Second-Generation Tyrosine Kinase Inhibitor Dasatinib on Autoimmune Arthritis. *Front Immunol* 9

17. Ntari, L. *et al.* (2021) Combination of subtherapeutic anti-TNF dose with dasatinib restores clinical and molecular arthritogenic profiles better than standard anti-TNF treatment. *J Transl Med* 19

18. Juarez, M. *et al.* (2016) DKK1 expression by synovial fibroblasts in very early rheumatoid arthritis associates with lymphocyte adhesion in an in vitro flow co-culture system. *Arthritis Res Ther* 18

19. Guo, K. *et al.* (2019) Treatment Effects of the Second-Generation Tyrosine Kinase Inhibitor Dasatinib on Autoimmune Arthritis. *Front Immunol* 9

20. Day, E. *et al.* (2008) Inhibition of collagen-induced discoidin domain receptor 1 and 2 activation by imatinib, nilotinib and dasatinib. *Eur J Pharmacol* 599, 44–53

21. SPRYCEL^{TM} (2006) SPRYCEL^{TM} Rx only (dasatinib) Tablets. *United states food and drugs administration*

22.   McIntyre, J.A. *et al.* (2006) Dasatinib. Treatment of leukemia treatment of solid tumors Bcr-Abl and Src kinase inhibitor. *Drugs Future* 31, 291–303

Chapter- 3
Analytical Method Development
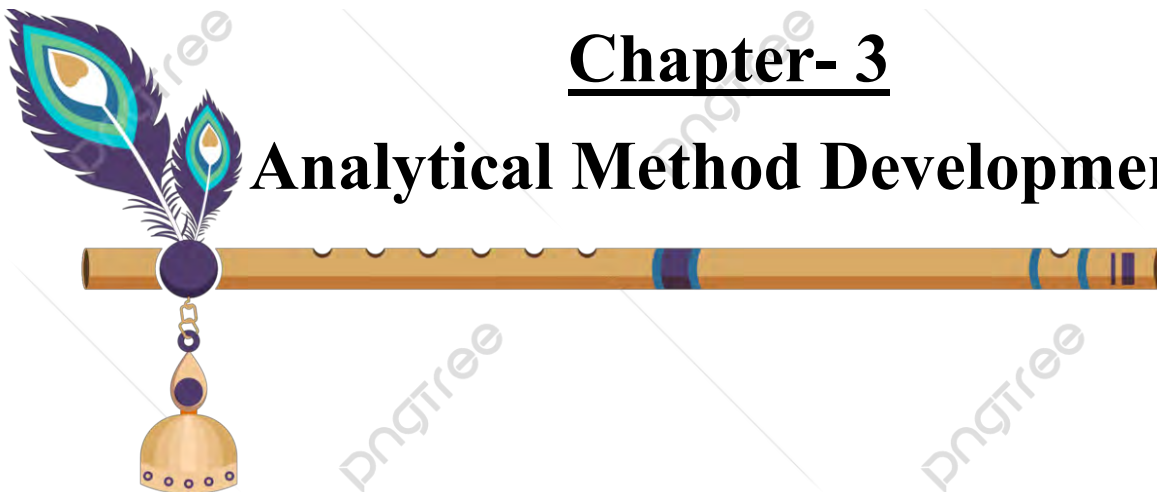
3 Introduction

Analysis and a highly sensitive analytical method are very crucial and play a key role in the development of formulations because those methods are the tools for the evaluation of the designed formulations. The evaluation covers entrapment efficiency (EE), *in-vitro* drug release, percentage purity of drug by assay, *ex-vivo* drug release, and *in-vivo* studies [1]. To define the desired criteria of the formulation like safety, quality, and performance, we require an accurate, sensitive, reproducible, and reliable method that should be compliance with standard validation criteria as described by the US Food and Drug Administration (USFDA) and the International Council for Harmonisation of Technical Requirements for Pharmaceuticals for Human use (ICH) [2].

3.1 Chemicals and reagents

HPLC-grade methanol and acetonitrile were purchased from Merck Limited, Mumbai (India). Analytical grade potassium dihydrogen phosphate (KH_2PO_4), sodium hydroxide (NaOH), and ethylenediamine tetraacetic acid (EDTA) were purchased from Himedia Pvt ltd Mumbai (India). Orthophosphoric acid and hydrochloric acid (HCl) were purchased from Molychem Mumbai (India). The milli-Q water used for the experiment was obtained from the in-house unit of BITS-Pilani, Pilani campus.

3.2 Analytical method development of DTB by Reverse Phase-High Performance Liquid Chromatography (RP-HPLC)

RP-HPLC is a reliable and widely used analytical technique for determining active pharmaceutical ingredients (API) in analytical samples. A systematic literature review was conducted for the development of an RP-HPLC method for DTB analysis and estimation [3–5]. The methods that were reported have been found to have poor sensitivity (as measured by LOD and LOQ), a limited range of linearity, and involve the use of a mobile phase consisting

of acetonitrile alone or in combination with methanol using larger columns as stationary phase. This may result in making the analysis costly [6–8].To overcome the above-stated issues, we developed an eco-friendly analytical method with methanol as an organic solvent in the mobile phase and C18 with a 50 mm length column as the stationary phase. A Quality by design (QbD) approach was employed for the systematic development of the RP-HPLC method to study the impact of each variable that affects the quality of the analytical method.

The Analytical Quality by Design (AQbD) approach has been successfully applied in several scientific studies to develop efficient, inexpensive, and reliable chromatographic methods for the quantitative determination of analytes from pharmaceutical preparations. The AQbD is a paradigm for the development of analytical methods that aims to understand the predefined objectives and associated interactions, where risk assessment (RAS) studies were conducted to identify potential Critical Analytical Attributes (CAA). A factor screening study was conducted to find the independent variables. Next, the method was optimized to create the desired chromatographic conditions [9,10].

3.2.1 Instruments and chromatographic conditions

For the development of the dasatinib (DTB) analytical method, chromatographic conditions were optimized using Shimadzu HPLC of the SPD-M20A photodiode array (PDA) detector. The Waters X-bridge™ C18 column (4.6*50mm), with 5µm particle size (PS) and mobile phase consisting of methanol and phosphate buffer, was used for the separation of DTB. The pH of the mobile phase was adjusted with ortho-phosphoric acid and NaOH. The analysis of DTB was carried out at a detection wavelength of 315 nm with a run time of 10 min. The Column Temperature was kept constant at 25 °C. LC solution software version 1.24 SP1 was used for the method development and data acquisition.

3.2.2 Stock, standard preparation, and buffer preparation

The primary stock solution was prepared by dissolving 1mg of DTB in 1 mL of methanol to obtain a concentration of 1mg/mL. The secondary stock solution of 100μg/mL was prepared from the primary stock solution. From the secondary stock solution, calibration standard solutions in the range of 100-10000 ng/mL were prepared by serial dilution using methanol. The Quality control (QC) solutions were prepared from the standard stock (1mg/mL) at LQC, MQC, and HQC levels representing the concentrations of 300 ng/mL, 2000 ng/mL, and 8000 ng/mL, respectively.

3.3 Application of QbD for the optimization of RP-HPLC analytical method

Before applying the QbD, preliminary trials were carried out for the identification of critical, independent variables affecting the analysis of DTB. Initially, the effect of mobile phase composition, such as the type of organic solvents (acetonitrile and methanol) and concentration of buffer salts (phosphate buffer and ammonium acetate buffer, were screened. Based on the peak asymmetry, methanol and phosphate buffer were selected for further optimization of the analytical method.

3.3.1 Analytical target profile and critical analytical attributes

In the QbD approach, determining the appropriate analytical target profile (ATP) is a preliminary enactment step to achieve the intended criteria for the development of the analytical method. Table 3.1 enumerates the various components of ATP to be achieved for the development of the DTB analytical method. The ATP should define appropriate constituents of CAAs that further controls the quality of the analytical method. Based on the reported data and preliminary trials, the potential CAAs were identified for this analytical method as Retention Time (RT) and Tailing Factor (TF) [11,12].

Table 3.1 Analytical Target Profile for the analytical method development of dasatinib.

ATP	Objective	Explanation
Sample	Active molecule/ Degradation product	Development of analytical method and estimation of Active Pharmaceutical Ingredient (API) in nanoformulation
Type of Chromatography	Reverse Phase Chromatography	Non-polar stationary phase improves the retention of molecules
Instrument	HPLC with a quaternary pump	Provides high resolution of molecules
Nature of the sample	Liquid	Analyte must be in a liquid phase to ensure complete miscibility
Standard Preparation	Linear dilution method	Standard dilution of drug solution to ensure its proper elution
Sample Preparation	Manual handling	Preparation of sample is carried out by manual weighting followed by mixing with methanol.
Method application	Estimation of DTB	The method is applicable to detect DTB in Nano formulations

3.3.2 Risk Assessment (RAS)

Initial RAS was carried out to understand the impact of various factors affecting the ATP that can execute an impact on the efficiency of the developed RP-HPLC. A fishbone diagram was conceptualized for evaluating the relationship between CAAs to achieve desired ATP. A risk estimation matrix (REM) was established to evaluate the plausible risk factors, and effects of them were marked as low, moderate, and high-risk. Further, Risk priority number (RPN) scores were calculated using the below-mentioned formula.

Severity(S)* Detectability (D) * Occurrence (O) = RPN

3.3.3 Factors screening study (2-level fractional factorial design)

For screening independent variables that affect ATP, a 2-level fractional factorial design with 8 runs and 5 factors was used. Table 3.3 depicts the experimental design, which shows the effect of five factors, namely, the percentage of organic solvent (methanol), the pH of the buffer, the flow Rate (FR) of the mobile phase, the Injection Volume (IV), and the Column temperature at two levels, high (+1) and low (-1). For the statistical analysis, Design- expert (DoE) software version 7.0.0 was used, with a linear polynomial model to evaluate the effect of independent variables and their interaction terms. Using Pareto charts, the critical,l independent variables influencing the CAAs were finally identified [13].

3.3.4 Factor optimization study using Box-Behnken Design (BBD)

Based on the factor screening study and RAS, three major factors showing significant impact on the dependent variables were optimized using BBD surface response design at 3 levels with 3 factors. Table 3.4 displays the matrix design containing optimized factors. Methanol (X_1), pH (X_2), and FR (X_3) at their low (-1), medium (0), and high (+1) levels suggesting 17 runs [14]. A 10000 ng/mL concentration of DTB was used for the experimental runs to investigate the impact of % methanol, pH, and FR on the designated CAAs, i.e., TF and RT.

3.3.5 Optimization data analysis and model validation

Design Expert® ver.7.0.0 software was used for optimization data analysis and model validation to fit the experimental data into quadratic polynomial models for estimating various studied responses as well as the inspected variables. The coefficient of correlation (R^2) and lack of fit analysis were chosen as model evaluation parameters from a variety of options. The coefficients with $p < 0.001$ were then taken into account when assessing the analysis of variance (ANOVA) model. The factor-response relationship was also examined graphically using 3-D response and 2-D contour plots [9].

3.4 Method validation

The developed method was further validated for system suitability, specificity, linearity, range, accuracy, precision, Limit of Quantification (LOQ), Limit of Detection (LOD), and robustness as per the ICH Q2 (R1) guidelines [15].

3.4.1 System suitability

System suitability was performed by injecting six replicates of 10000 ng/mL concentration. The standard deviation (SD) and % relative standard deviation (RSD) was evaluated further to assess whether the reproducible results are produced with the system for the developed method. [16].

3.4.2 Linearity and range

The linearity and range of the developed analytical method were evaluated using standard calibration solutions in the range of 100-10000 ng/mL with triplicates of each sample. The calibration curve (CC) was constructed by plotting the concentration of DTB on the X-axis and the peak area on the Y-axis. The obtained model was further analyzed using linear regression analysis. The regression coefficient and regression equation (RE) were determined.

3.4.3 Limit of detection (LOD) and limit of quantification (LOQ)

The sensitivity of the analytical procedure is represented by LOD and LOQ. The LOD is defined as the lowest concentration of analyte measured and distinguished from the noise level. A LOQ is defined as the lowest concentration of analyte that can be quantified with accuracy and precision within the approved range. The LOD and LOQ were determined from the following formula [18].

$$LOD = 3.3 \times \frac{\sigma}{S}$$

$$LOQ = 10 \times \frac{\sigma}{S}$$

Here, σ represents the "standard deviation of the intercept"

S represents the "slope" of the calibration curve

3.4.4 Accuracy and precision

The accuracy and precision of the developed method were evaluated for QC samples at LQC (300 ng/mL), MQC (2000 ng/mL), and HQC (8000 ng/mL) with triplicate of each sample. The accuracy and precision of the developed analytical method for DTB were represented as percentage recovery and % RSD respectively, for both intra-day and inter-day samples [19,20].

3.4.5 Robustness

Based on ICH guidelines, robustness is the fitness of analytical practice which is not exaggerated by tiny variations but by significant changes in the experimental factors. Here, the developed method was screened by slight changes in the operating conditions, i.e., Column temperature (20 to 30 ℃), the ratio of mobile phase mixture (±1.5%), and pH of the buffer (4.7 to 5.3) [21].

3.5 Forced degradation studies

Forced degradation studies of DTB were conducted to check whether the developed method was stability indicative such that it should differentiate the active ingredient from its degradant products without any interference. DTB standard solution of 100 µg/mL was prepared and exposed to different stress conditions such as acidic, alkali, oxidative, thermally induced, and photolytic degradation. The study was conducted for 24 h at 60 ℃. Before analysis, the base samples were treated with acid to neutralize, while acidic samples were neutralized with a base. After neutralization, the samples were diluted with methanol to prevent damage to the column. The prepared samples were filtered through a 0.22µ membrane filter and injected into HPLC for analysis [22].

3.5.1 Acidic and alkali degradation

The concentration of 100µg/mL was prepared in acid/base and kept at 60 ºC. 1 mL of the sample was taken and diluted with respective acid (1 N HCl) and base (1 N NaOH). To assess the acidic and alkali degradation, the sample was further diluted with methanol to get a final concentration of 10000 ng/mL and analyzed by HPLC.

3.5.2 Oxidative degradation

The concentration of 100µg/mL was prepared in 30% hydrogen peroxide (H_20_2) and kept at 60 ºC. To evaluate the oxidative degradation of DTB, 1 mL of sample was taken and diluted with methanol to get a final concentration of 10000 ng/mL and further analyzed by HPLC

3.5.3 Thermal degradation

Thermal degradation was carried out by taking 100µg/mL of DTB in diluent and kept at 60 ºC for 24 h. A 10000 ng/mL was prepared by diluting with methanol from the above solution and analyzed by HPLC.

3.5.4 Photolytic degradation

A standard working solution of 100µg/mL in diluent was exposed to UV conditions at 200 wh/m^2 for 24 h. A further sample was diluted and analyzed by HPLC.

3.6 Results and discussion

3.6.1 Development and optimization of the method using QbD

A thorough literature review was used to conduct preliminary research for the development of the DTB RP-HPLC method, and initial trials were carried out using various mobile phase compositions. Methanol and 10 mM phosphate buffer combination produced good peak properties, and further trials were carried out using 50:50 methanol and phosphate buffer ratios to identify the CAAs that impact the ATP.

3.6.1.1 Identification of analytical target profile and critical analytical attributes

The exploration of ATP incited the QbD method to analytical development. The ATP chosen

for analytical method development is shown in Table 3.1. The CAAs from the ATP were opted

for because they were explored for their ability to influence the final characteristics. RT and

TF were identified as CAAs of analytical method development that has a significant impact on

quality.

3.6.1.2 Risk identification and risk assessment

The RAS was conducted, and the Ishikawa diagram shown in Figure 3.1 was used to identify

ATP and CAA. The methanol ratios, pH of the buffer, FR, IV, and Column temperature were

all considered potential risk factors against RT and TF, according to the REM. Failure mode

effects analysis (FMEA) was used to assign RPN scores based on risk potentiality; the scores

were given based on reported studies. The REM and RPN scores of the CMAs and CPPs are

shown in Table 3.2. RPN scores of more than 50 are regarded as critical for optimizing critical

attributes.

Table 3.2 Risk estimation matrix (REM).

CMAs and CPPs	CQAs		FMEA			
	Retention time	Tailing factor	Severity	Detectability	Occurrence	RPN score
Methanol	High	High	9	8	8	576
pH	High	Medium	8	7	6	336
Injection volume	Low	Medium	3	5	4	60
Column temperature	Medium	Low	7	3	4	84
Flow rate	High	Medium	9	7	8	504
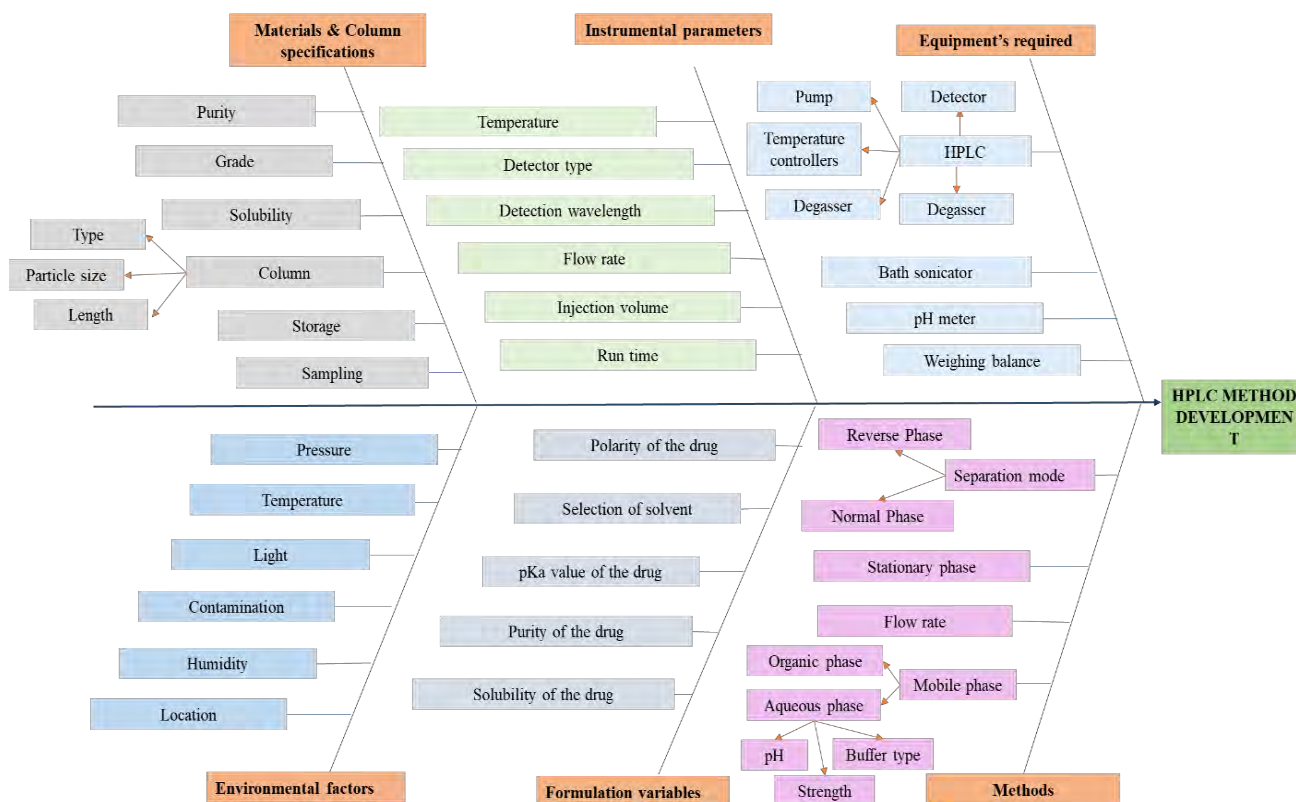
Figure 3.1 Fishbone diagram.

3.6.1.3 Factors screening studies

The screening studies used CMA from RAS to analyze the interaction between factors and responses. A two-level factorial design (Design-Expert 7.0.0) with eight trials with five factors at low and high-level concentrations was used for screening. The suggested % methanol, pH of the buffer, FR, IV, and CT were investigated. As shown in Table 3.3, eight trials were carried out by the design. All suggested conditions were carried out by varying independent variables while holding all other parameters constant. As dependent variables, RT and TF were studied. Table 3.3 displays the response values obtained following the implementation of a two-level factorial design with five factors and two levels. The interaction and efficiency of the factors against the responses were depicted in Pareto charts. From Pareto charts, the factors present above the Bonferroni limit (6.58) are considered critical facts. From Figure 3.2, methanol, pH, and FR were considered critical factors affecting both RT and TF.

Table 3.3 Experimental design 2-level factorial design- runs and responses.

Run	Factor 1 A: Methanol (%)	Factor 2 B: pH (Numbers)	Factor 3 C: Injection volume (µL)	Factor 4 Column temperature (℃)	Factor 5 Flow rate (mL/min)	Response 1 Tailing factor (Numbers)	Response 2 Retention time (min)
T1	40.00	4.00	15.00	30.00	1.20	1.60	1.91
T2	60.00	4.00	15.00	20.00	0.80	1.07	1.65
T3	40.00	6.00	15.00	20.00	1.20	1.22	9.80
T4	60.00	6.00	15.00	30.00	0.80	1.31	3.20
T5	40.00	4.00	25.00	30.00	0.80	0.81	8.21
T6	60.00	4.00	25.00	20.00	1.20	1.80	1.17
T7	40.00	6.00	25.00	20.00	0.80	1.06	3.40
T8	50.00	5.00	20.00	25.00	1.00	1.18	2.74
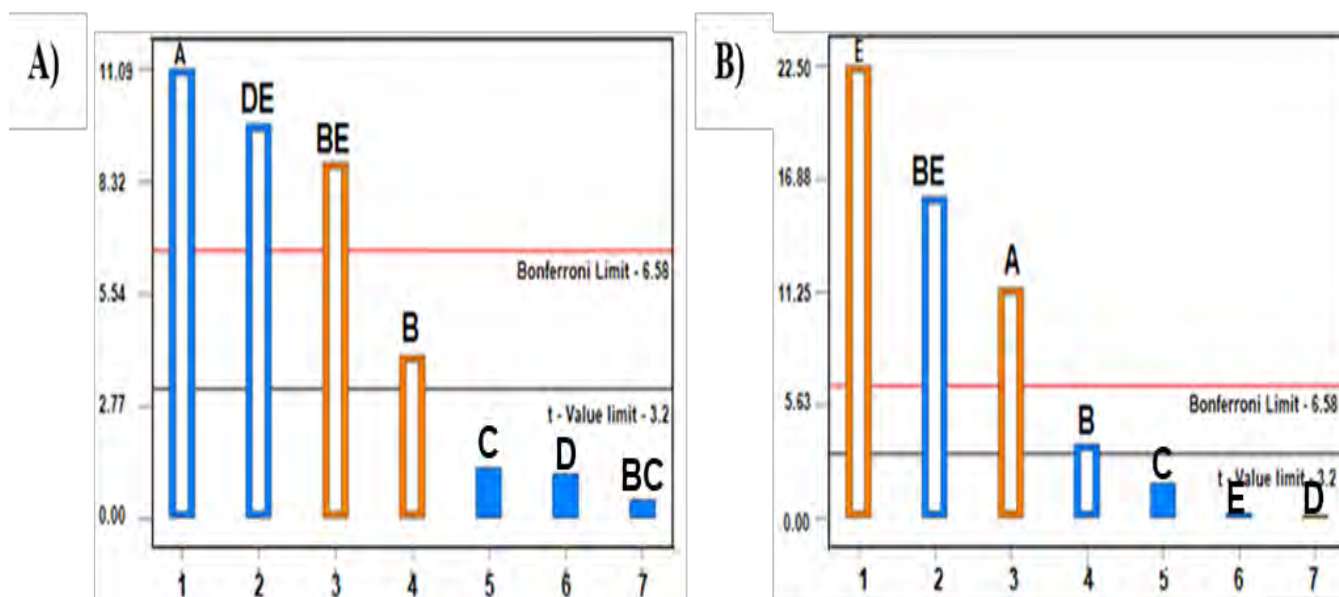
Figure 3.2 Half-normal plots and Pareto charts for factor screening study. (A) Pareto charts for retention time; (B) Pareto charts for tailing factor.

*Note; A= Methanol, B= pH, C= Injection volume, D= Column temperature & E= Flow rate.

3.6.1.4 Factors optimizing studies

Based on the RAS report, the screening study report finalized various factors such as methanol (%), pH of the buffer, and FR. In the responses, RT and TF are regarded as CAAs. A BBD with 17 trials was keyed with three factors and three levels using Design-Expert 7.0.0 software

for method optimization. The suggested methanol percentage, buffer pH, and FR (independent variables) were investigated at three levels: low, medium, and high. As shown in Table 3.4, 17 runs were carried out by the design. The runs were carried out by varying the independent variables while keeping all other parameters constant, and the RT and TF were investigated as response variables. The IV (20μL) and Column temperature (25 ºC) used in all trials were constant. ANOVA was used to assess the model efficiency and the significance of the selected input variables. The BBD with three components and three levels was used, and the response values obtained after the design was executed shown in Table 3.4.

Table 3.4 Experimental design 3-level *3-factor Box Behnken design runs and responses.

Run	Factor 1 A: Methanol (%)	Factor 2 B: pH (Numbers)	Factor 3 Flow rate (mL/min)	Response 1: Tailing factor (Numbers)	Response 2: Retention time (min)
1	60.00	5.00	1.20	1.34	1.86
2	40.00	6.00	1.00	1.00	8.30
3	60.00	5.00	0.80	1.63	2.05
4	50.00	5.00	1.00	1.19	3.03
5	60.00	6.00	1.00	1.80	3.51
6	50.00	5.00	1.00	1.20	3.03
7	40.00	5.00	0.80	1.27	80
8	50.00	6.00	0.80	1.70	6.50
9	50.00	6.00	1.20	1.82	1.68
10	50.00	5.00	1.00	1.20	3.03
11	60.00	4.00	1.00	1.40	2.30
12	40.00	4.00	1.00	1.80	5.21
13	50.00	4.00	0.80	1.96	1.58
14	50.00	4.00	1.20	1.93	1.705
15	40.00	5.00	1.20	1.52	3.6
16	50.00	5.00	1.00	1.19	3.01
17	40.00	5.00	1.20	1.51	3.61

3.6.1.5 Effect of independent variables on tailing factor

The TF after 17 trials was found to be in the range of 1.00 - 1.96, as shown in Table 3.4. The Quadratic model has an F-value of 95.95, suggesting its significance. Figures 3.3A & 3.3B represent contour and 3D plots of the TF. With an F-value of 3, the lack of fit has shown to be insignificant compared to pure error. The coded values of chosen factors are represented in regression equation (RE) 1.

$$TF = 1.20 + 0.072A - 0.095B + 0.00613C + 0.30AB - 0.14AC + 0.038BC - 0.055\,A^2 + 0.36\,B^2 + 0.30\,C^2 \qquad \text{(Eq. 1)}$$

The collusive effect is represented by the positive symbol in the RE, which indicates an increase in response value with the respective input variable. The hostile effect, represented by the negative symbol in the RE, indicates a decrease in response value with the respective input variable. The lack of fit indicates dissimilarity in the data of the best-fit model and allows competent model fitting of the experimental. An insignificant lack of fit in the experimental data specifies the model's best fit. TF increases as methanol and pH decrease, as represented by the RE (Eq. 1). The FR had no effect on the TF.
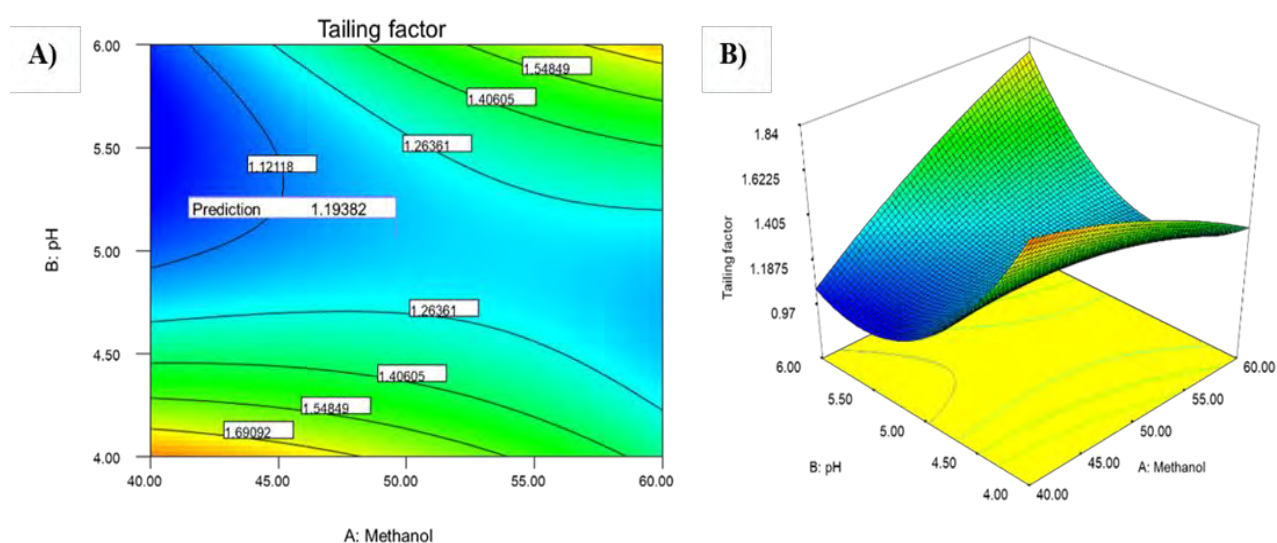
Figure 3.3 Box–Behnken optimization graphs illustrating the effect of independent variables tailing factor. (A) The contour plot graph of factors effecting tailing factor; (B) The three-dimensional graph of factors effecting tailing factor.

3.6.1.6 Effect of independent variables on retention time

The RT after 17 trials was found to be in the range of 1.58 - 8.3 min, as shown in Table 3.4. The F-value of 867.37 for the Quadratic model indicates the model's significance. The contour and 3D plot of the RT are shown in Figures 3.4A and 3.4B. The lack of fit has been shown insignificant, with an F-value of 3 compared to the pure error. The coded values of chosen responses are described in the RE (Eq. 2)

$$RT \text{ (min)} = 1.20 + 0.072A - 0.095B + 0.006125C + 0.30AB - 0.14AC + 0.038BC - 0.055 A^2 + 0.36 B^2 + 0.30 C^2 \quad \text{(Eq. 2)}$$

The RE (Eq. 2) represents the decrease in RT as methanol and FR increase. The increased RT was observed as the pH increased
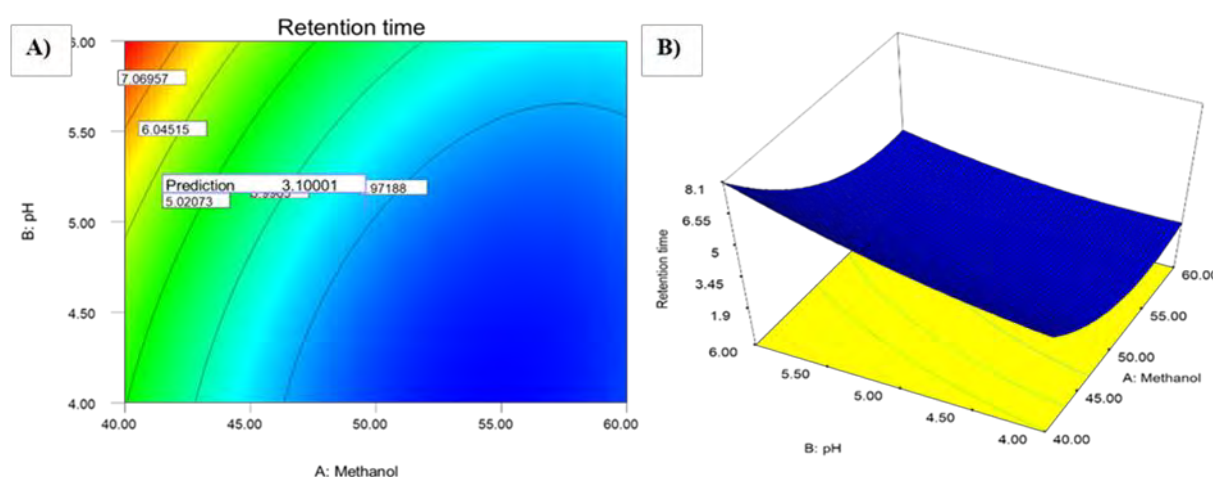
Figure 3.4 Box–Behnken optimization graphs illustrating the effect of independent variables retention time. (A) The contour plot graph of factors effecting retention time; (B) The three-dimensional graph of factors effecting retention time.

3.6.1.7 Validation of the design to select optimized method

The numerical and desirability methods were used to optimize the method. The goal was to find the analytical method with better TF and RT. Table 3.5 illustrates a summary of the required criteria that must be met in order to attain the desired response. The design expert software produced 20 solutions, with a higher desirability close to 1 was picked for method run

(Coded as Run-18). The design was validated using the following run with methanol (50%), pH 5, and FR (1 mL/min). The TF was 1.19 and the RT of the optimized method run was found to be 3.09 min. The selected run percent deviation with RT was 0.02 min and TF was less than 0.01, indicating that the predicted value was close to the actual value, indicating the desirability of the design. Figure 3.5A and 3.5B depicts the counter and 3D surface graphs of RT and TF for optimized run and same method run was carried out for method validation and drug loaded emulsion analysis.
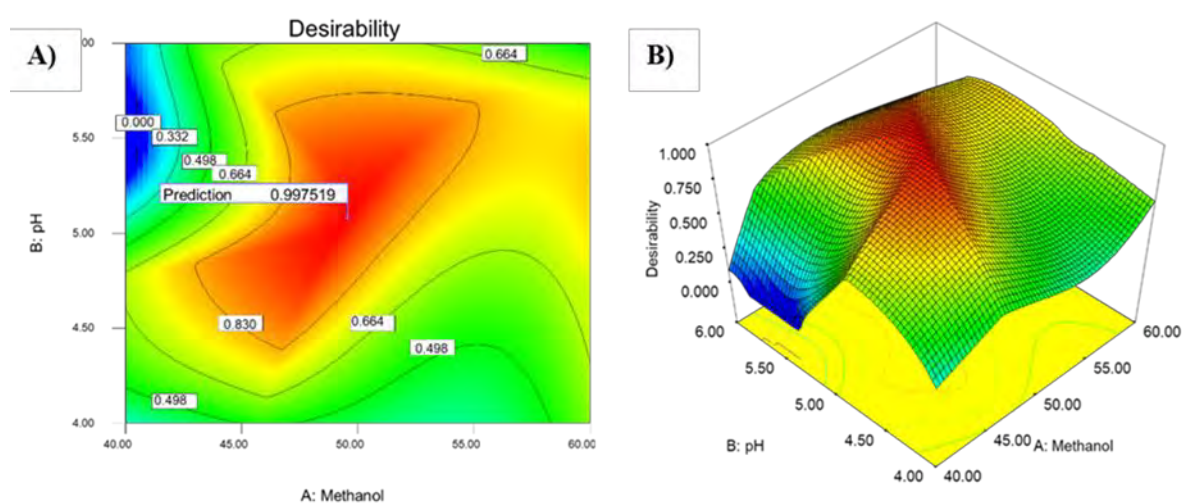
Figure 3.5 Box–Behnken optimization graphs illustrating the effect of independent variables desirability. (A) The contour plot graph of factors effecting desirability; (B) The three-dimensional graph of factors effecting desirability.

Table 3.5 Summary of the requirement criteria.

Name	Lower Limit	Upper Limit	Low Level	High level
Methanol	40	60	-1	+1
pH	4.0	6.0	-1	+1
FR	0.80	1.20	-1	+1
TF	1.00	1.96	-1	+1
RT	1.58	8.30	-1	+1

3.6.2 Method validation

3.6.2.1 System suitability

System suitability of the developed analytical method was performed and the % RSD for the six injections were found to be < 2% indicates the acceptability of the method. Different parameters also evaluated for system suitability include RT (3.09 min), and TF (1.19). The results indicate that there is no significant difference between the six injections for various parameters confirms the suitability of the developed method. The overlay of the chromatogram was shown in the Figure 3.6.
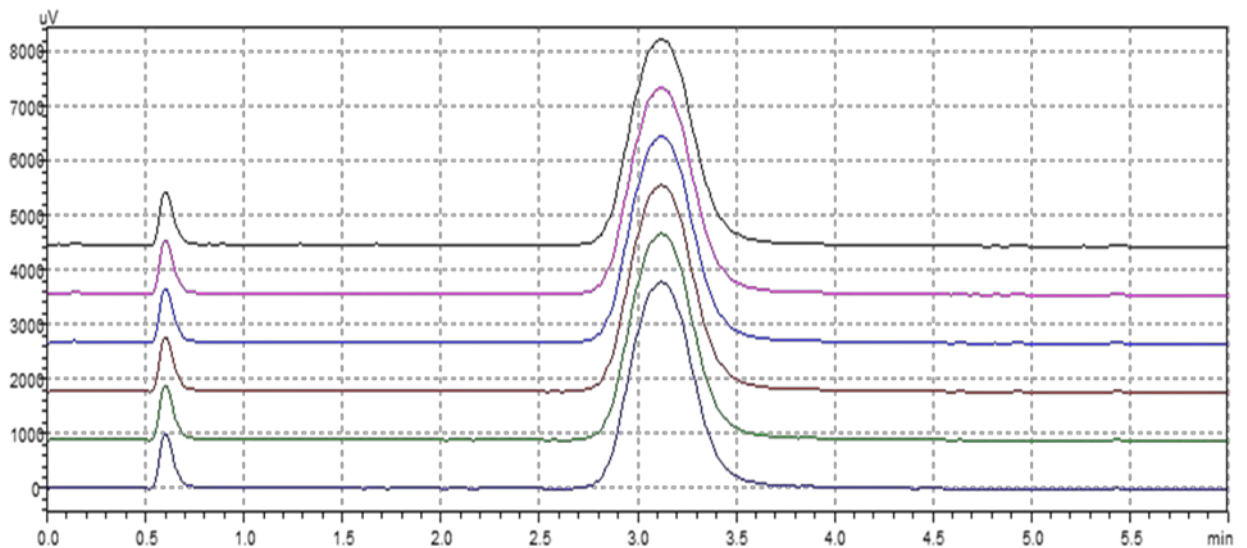
Figure 3.6 Overlay of dasatinib chromatograms for system suitability.

3.6.2.2 Specificity

To evaluate the specificity, the standard drug solution (10000 ng/mL) was compared against blank and the representative chromatographs were mentioned in Figure 3.7. The DTB chromatogram showed the major peak at RT at 3.09 min where the peak was absent in the blank chromatogram indicating the specificity of the method.
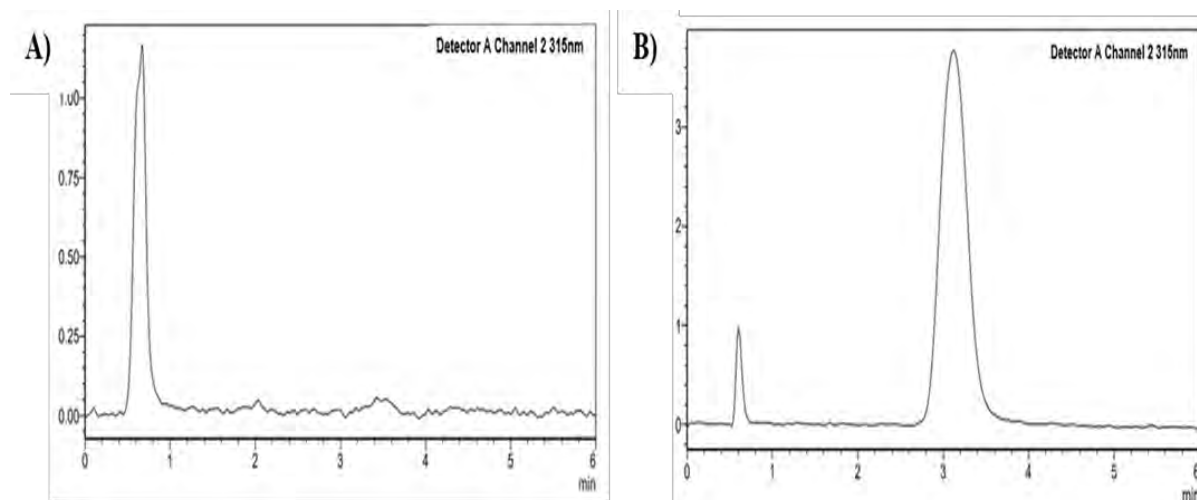
Figure 3.7 Chromatogram of (A) Blank; (B) Dasatinib.

3.6.2.3 Linearity, range, limit of detection, and limit of quantification

The CC was constructed for the DTB and which is shown in Figure 3.8. The regression analysis revealed the linearity of the method with a 0.9995 R^2 value for a concentration range of 100-10000 ng/mL. The linear regression equation was determined to be y = 75.888x-5979.1. The LOD and LOQ were calculated from the slope of CC and SD of the intercept and it was determined to be 33.12 ng/mL and 100. 4 ng/mL respectively.
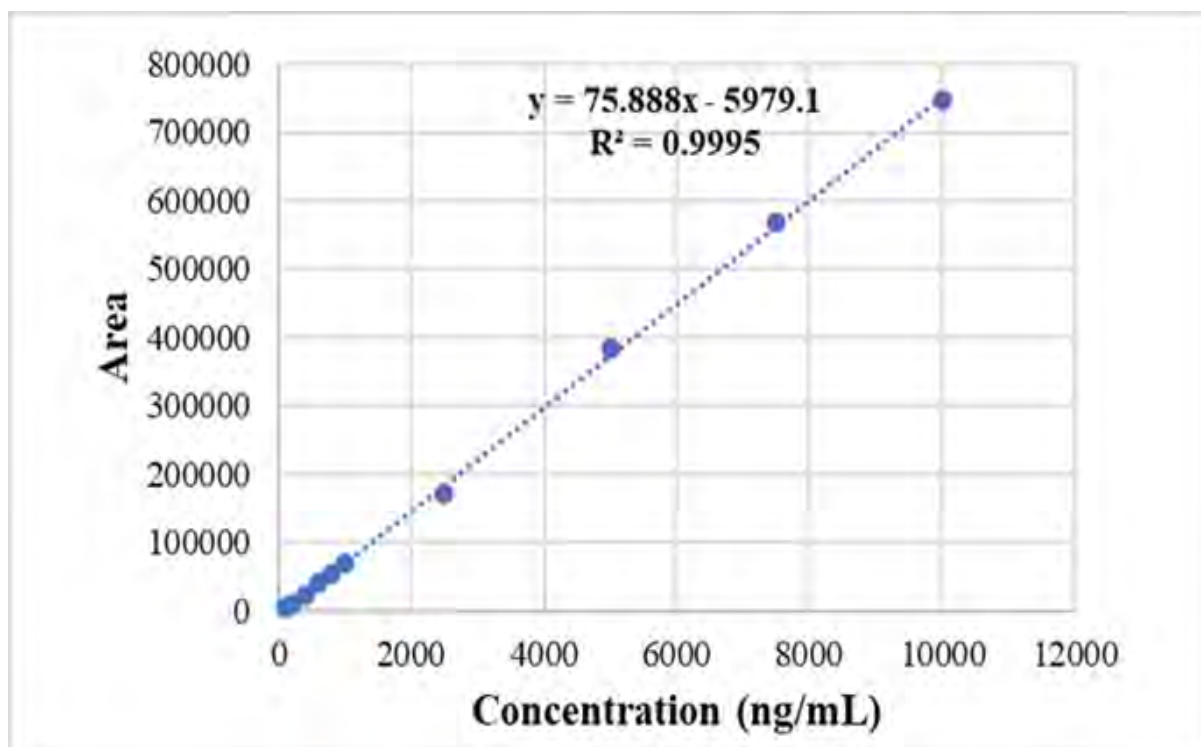
Figure 3.8 Calibration curve for dasatinib.

3.6.2.4 Accuracy and Precision

The accuracy and precision of the QC samples at LQC (300 ng/mL), MQC (2000 ng/mL), and HQC (8000 ng/mL) levels were determined and the data was mentioned in Table 3.6. The intra-day and inter-day percentage recovery were within the acceptable limits with a range of 98-102% according to ICH guidelines. For the intra-day and inter-day precision the % RSD were found to be < 2% representing the developed method was highly accurate and precise.

Table 3.6 Accuracy and Precision.

Control	Conc. (ng/mL)	Precision (% RSD)		Accuracy (%) (Mean ± SD)	
		Intra-day	Inter-day	Intra-day	Inter-day
LQC	300	0.664	0.64	101.5 ± 0.21	98.80 ± 0.41
MQC	2000	1.75	1.67	98.89 ± 1.03	99.65 ± 0.35
HQC	8000	1.80	0.180	99.12 ± 1.2	99.1 ± 0.87

3.6.2.5 Robustness

For evaluating the robustness of the method, deliberate changes in the intrinsic method parameters were done such as mobile phase ratio (50 ±3: 50 ±3 ratio of phosphate buffer and methanol), pH (5 ± 0.3), and column temperature (25 ±5 ^{0}C). No significant changes were observed in the peak area, RT, theoretical plates and TF indicating the method was not affected by small changes in any one the above-mentioned parameters.

3.6.3 Forced Degradation Studies

The percentage degradation of DTB was mentioned in Table 3.7. The data revealed that the percentage degradation of the drug was very less (< 6 %) under thermal and photolytic degradation till 24 h. For acidic, alkali and oxidative degradation studies were conducted till 10% degradation appeared. DTB contains amine, amide, and hydroxyl functional groups, which are susceptible to degradation under hot acid, alkaline and oxidative stress conditions. The respective chromatograms of forced degradation study at each condition were mentioned in Figure 3.7. The acid degradation (3.188 min), alkali degradation (3.33 min), oxidative degradation (3.9 min), thermal degradation (2.90 min), and photolytic degradation (3.53 min) studies showed a peak of DTB. So, the data revealed that the developed analytical method was not able to detect any degradant peaks at 315 nm. The possible reason for this outcome is that the hydrophilic degradation products eluted early with the solvent front. Moreover, as the degradants did not absorb around 315 nm and may have appeared at a lower wavelength, they were not identifiable, and their existence was only indicated by a decline in the peak area.

Table 3.7 Forced degradation studies of dasatinib.

Condition	Time (h)	% Degradation
1 N HCl	1	11.28
1 N NaOH	2	10.94
30 % H_2O_2	1	11.
Thermal	24	5.20
UV	24	4.50
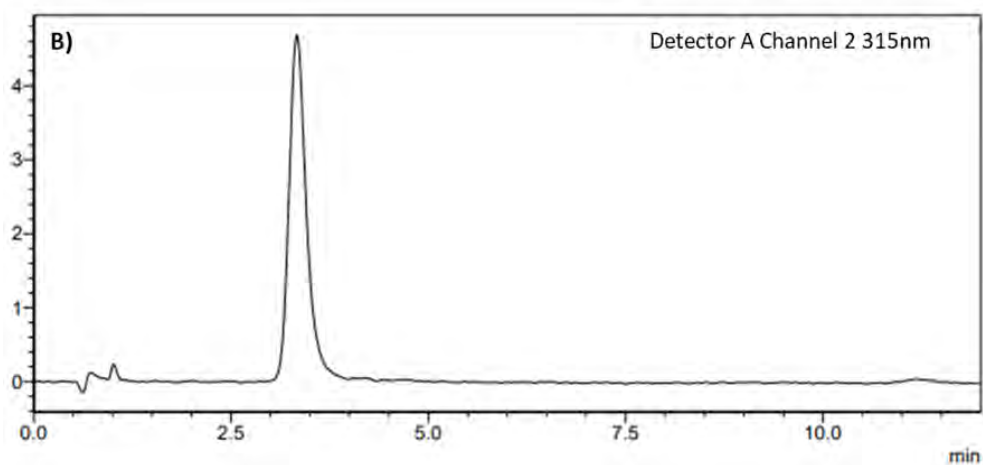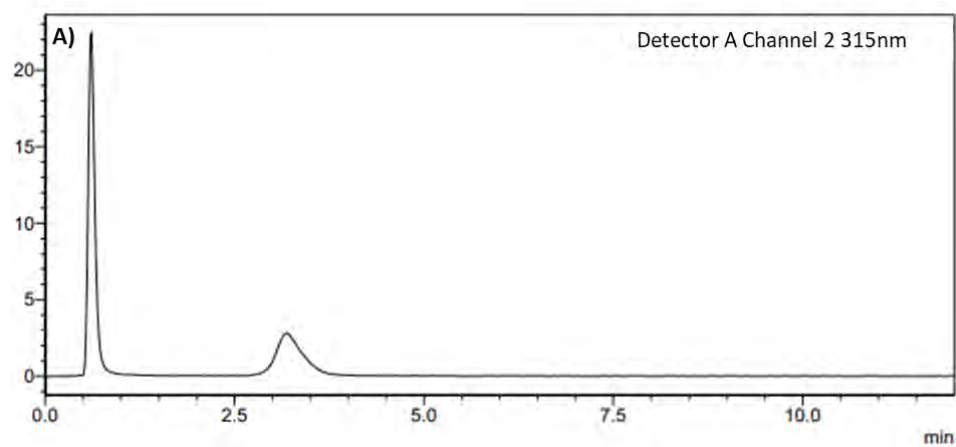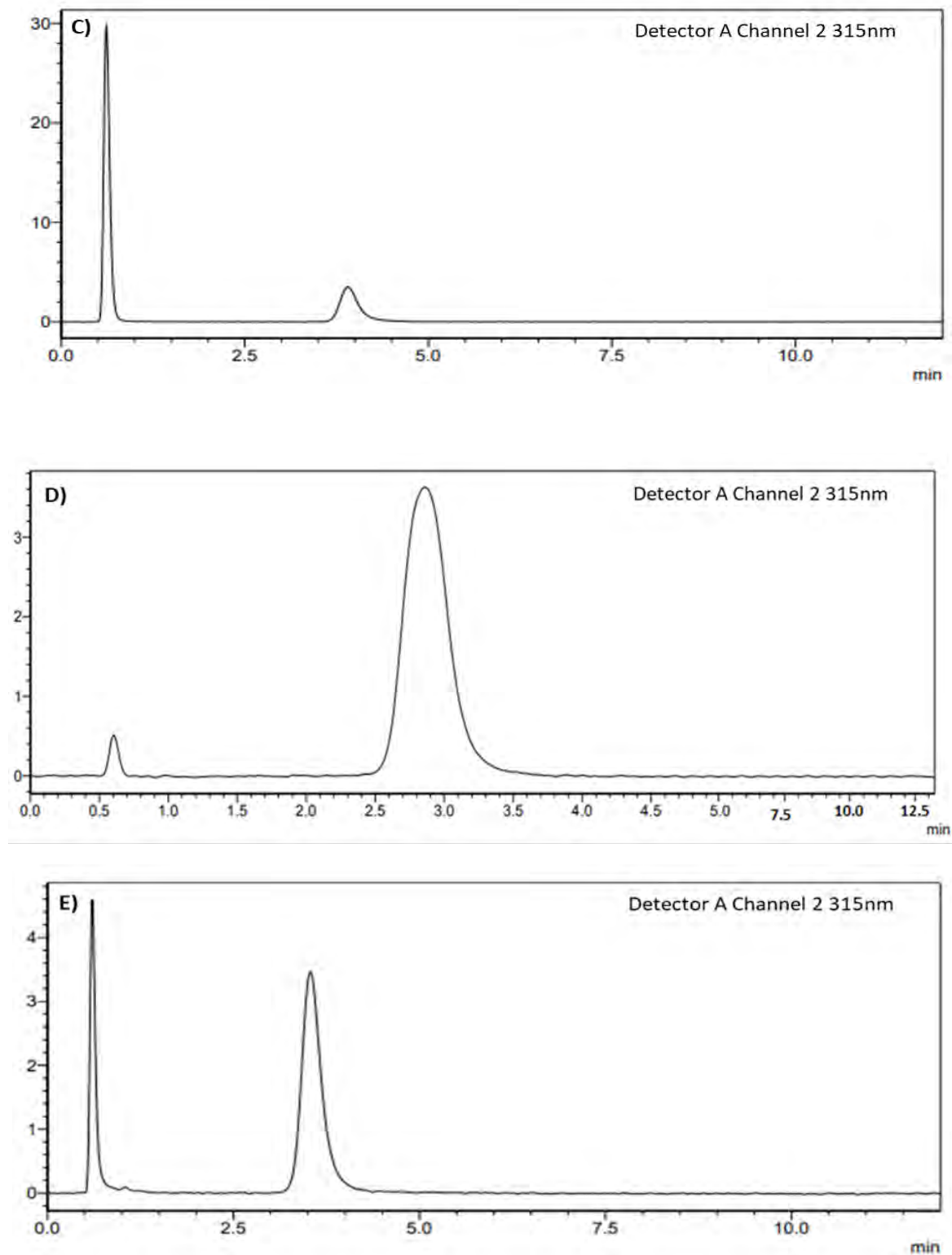
Figure 3.9. Forced degradation peaks of dasatinib in different buffers. (A) 1 N HCl; (B) 1N NaOH; (C) H$_2$O$_2$; (D) Thermal; (E) UV.

3.7 Applicability of the developed method

The validated analytical method was used to analyze the developed nanoformulation, including assay, encapsulation efficiency, in-vitro drug release, and ex-vivo skin permeability studies, which are discussed in detail in chapter 5 and 6. Also, no excipient interference was observed during the analysis. Henceforth, the developed method can only identify DTB drug, and the degradant products of DTB are not interfering with this method**.**

3.8 RP-HPLC Method for Quantification of dasatinib in Rat Plasma

3.8.1 Instrumentation and chromatic chromatographic conditions

The chromatographic condition has mentioned in section 3.2.1. The Waters X-bridge™ C18 column (4.6*50mm), with 5μm particle size and mobile phase consisting of methanol and phosphate buffer was used for the DTB quantification. The pH of the mobile phase was adjusted to 5 with ortho-phosphoric acid and NaOH. The analysis of DTB was carried out at a detection wavelength of 315 nm with a RT of 10 min. The column temperature was kept constant at 25 °C.

3.8.2 Collection of rat plasma

The blood collection procedure was approved by the institutional animal ethical committee (IAEC) BITS-Pilani, Pilani Campus (Protocol No. IAEC/RES/31/04). The Healthy Sprague Dawley rats were taken from the central animal facility (CAF), BITS-Pilani, Pilani Campus, Rajasthan, India. The obtained animals were caged in the standard conditions (23 ± 2 °C, 60 ±5% RH and 12 h dark & light cycle) with a standard pellets diet and water ad libitum. The respective blood sample was collected from the retro-orbital sinus of Sprague Dawley rats into 10% w/v EDTA solution containing eppendorf. Further, collected samples was allowed for the centrifugation for 8000 rpm for 30 min at 4 °C. The supernatant was separated in to the fresh Eppendorf and stored at -20 °C till further usage.

3.8.3 Sample clean-up

A single-step protein precipitation method was carried out for the extraction of DTB from the plasma. In brief, 192 µL of plasma, 4uL of the analyte, and 4µL of IS, i.e., Atorvastatin, was taken in a 2 mL Eppendorf, further 600 µL of methanol of extraction solvent was added to analytic containing plasma sample, vortexed for 7 min and centrifuged for 10 min at 15000 rpm. The obtained supernatant was filtered through a syringe filter (0.22 µm) into HPLC vials and analyzed.

3.8.4 System Suitability and Selectivity

To assess the performance of the system, a system suitability test was conducted by injecting the sample repeatedly 6 times with identical concentration to evaluate column performance, reproducibility, and resolution. Selectivity was performed using six different plasma samples. After sample processing, samples were injected into RP-HPLC.

3.8.5 Linearity

To assess linearity, seven calibration standards covering a range of 150 ng.mL^{-1} to 5000 ng. mL^{-1} concentration was utilized. DTB to IS ratio was plotted against nominal plasma concentrations to prepare CC. The obtained data were fitted using a linear RE.

3.8.6 Limit of detection and Lower limit of quantification (LLOQ)

The lower concentration of analytes that can be identified from the noise level is referred to as the LOD, while the lower concentration of samples that can be accurately and precisely quantified without exceeding ± 20% recommendations is known as the limit of quantification (LOQ). The LOD and LLOQ were calculated using the formula mentioned in section number 3.4.3.

3.8.7 Recovery

The evaluation of percentage recovery involved the analysis of plasma samples spiked with DTB at LQC, MQC, and HQC levels (n=3). The spiked DTB concentration in the mobile phase was used as a reference point for comparison.

3.8.8 Results and Discussion

3.8.8.1 Method Development

3.8.8.1.1 Optimization of chromatographic parameters and sample preparation technique

The method development process involved employing various strategies to achieve simple and cost-effective parameters. A methodological approach was taken to select the mobile phase (pH, polarity), stationary phase, FR, column temperature, and IV to obtain peak symmetry, consistent recovery, and optimal resolution between the DTB and IS. After validating the analytical method, minor modifications were made to the mobile phase composition, and the remaining chromatographic conditions were used similarly to the analytical method. The selected analytical column was a Waters X-bridge C18 (4.6 x 50 mm, 5µm), and the mobile phase consisted of methanol- phosphate buffer (pH: 5; 10 mM) in a 48:52 % v/v ratio, with a flow rate of 1 mL/min. The injection volume was 20 µL, and the RT for DTB and atorvastatin calcium (IS) were optimized to 3.54 and 5.95 min, respectively. The wavelength was set to 315 nm, and the total run time was 10 min. To obtain a clean sample without interference from endogenous substances, plasma sample preparation involved experimenting with using protein precipitation with methanol gave good and consistent recovery.

3.8.8.1.2 System Suitability and Selectivity

The system was assessed for suitability, and it demonstrated proper resolution and reproducibility. The sample clean-up process was highly selective, as indicated by the absence of significant plasma matrix interference at analyte RT. Figure 3.10 shows the chromatograms

of blank plasma, plasma with an HQC of analyte (DTB) with RT of 3.549 min, and IS with RT of 5.943 min.
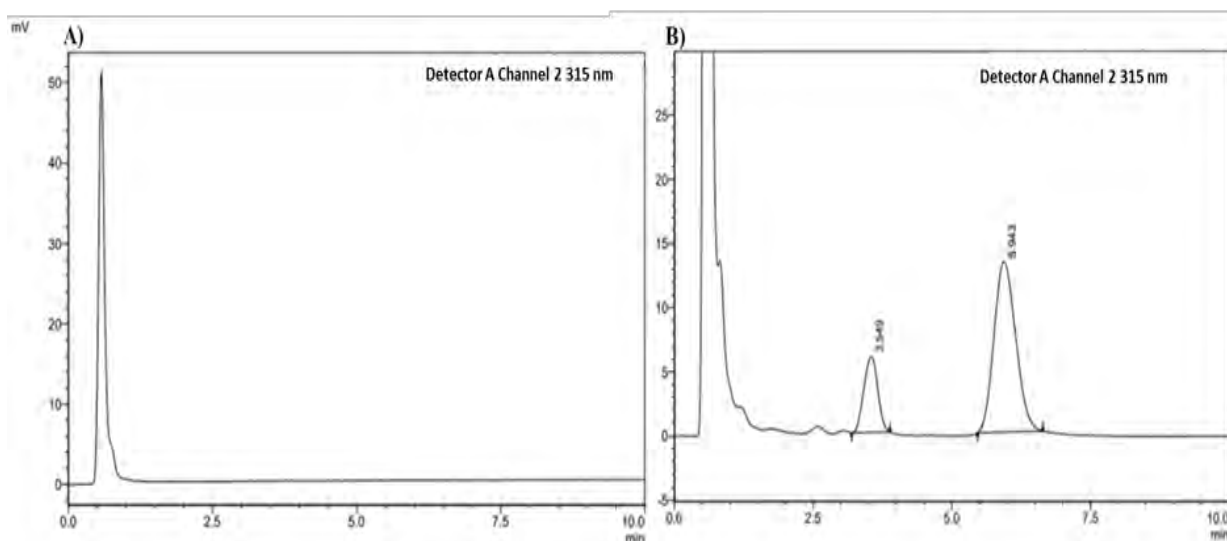
Fig 3.10 Bioanalytical chromatograms of A) Blank; B) Dasatinib (3.549 RT).

3.8.8.1.3 Linearity, LOD, and LLOQ

The CC exhibited reproducibility in the concentration range of 150-5000 ng.mL^{-1}, with an R^2 value of 0.9984. The linear regression equation was determined to be y = 0.006x-0.0143. The intercept and slope for the calculation were selected from CC. The LOD for DTB in this method was determined to be 50 ng/mL. The LLOQ for the method was set at 150 ng/mL. The LLOQ was quantifiable within a margin of ± 20%.

3.8.8.1.4 Recovery

The percent recoveries of DTB were performed under optimized conditions. The mean % recovery of DTB at the QC levels was found to be 88.5 ± 1.55%.

3.9 Conclusion

The QbD methodology used to develop an RP-HPLC method for measuring DTB in bulk drugs and emulsion is a great approach to ensure the quality of the method. Multivariate analysis is also an excellent way to evaluate the impact of various variables on the quality attributes of the

method. The validation of the method with excellent linearity, accuracy, precision, sensitivity, system suitability, and robustness is a critical step in ensuring the method's reliability and accuracy. Additionally, establishing the LOD and LOQ of DTB and demonstrating higher sensitivity than other reported methods is noteworthy. The force degradation studies of DTB under acidic and basic conditions further demonstrate the method's robustness and suitability for the quantification of DTB in emulsion formulation. Overall, it seems like this method is highly feasible and reliable for measuring DTB, and the study provides a strong basis for its use in pharmaceutical research and development. Further, in the developed method, slight changes were made in mobile phase composition and used for the bioanalytical method. The developed bioanalytical method was utilized for the analysis of the drug in rat plasma samples after topical administration of nano formulations.

References

1.   Singh, G. and Pai, R.S. (2014) Optimization (central composite design) and validation of HPLC method for investigation of emtricitabine loaded poly(lactic-co-glycolic acid) nanoparticles: in vitro drug release and in vivo pharmacokinetic studies. *ScientificWorldJournal* 2014, 1–12

2.   Peraman, R. *et al.* (2015) Analytical Quality by Design: A Tool for Regulatory Flexibility and Robust Analytics. *Int J Anal Chem* 2015, 1–9

3.   A. Sreedevi et all. (2013) Development and validation of novel HPLC method for the estimation of dasatinib in bulk and pharmaceutical dosage forms. *international journal of research in pharmacy and chemistry* 03, 724–729

4.   isara (2022) Development and Validation of Stability Indicating RP-HPLC Method for the Estimation of Dasatinib from Bulk and Tablet. *International Research Journal Commerce arts science.1-8*

5.   Rao KNV et all. (2013) Analytical Method development and Validation of Dasatinib in its Pharmaceutical dosage form by UPLC with Forced Degradation Studies. *International Journal for Pharmaceutical Research Scholars* 02, 221–227

6.   Bandi Ramachandra et all. (2014) Validation of RP-HPLC method for estimation of dasatinib in bulk and its pharmaceutical dosage forms. *Int J Pharm Biol Sci* 04, 61–68

7.   Bayas, J.P. and Sumithra, M. (2021) Analytical Method Development and Validation of Dasatinib in Bulk and Pharmaceutical Formulation using Quality by Design. *Res J Pharm Technol* 14, 1591–1596

8.   P. R. Sankar et all. (2019) Development and validation of rp-hplc method for the determination of dasatinib in tablet dosage form | international journal of pharmaceutical sciences and research. *Int J Pharm Sci Res* 13, 4531–4537

9.   Jain, A. *et al.* (2019) QbD-Driven Analytical Method Development and Validation for Raloxifene Hydrochloride in Pure Drug and Solid Oral Dosage Form. *https://doi.org/10.1080/22297928.2019.1624193* 9, 463–477

10.   Patel, K.Y. *et al.* (2021) QbD approach to HPLC method development and validation of ceftriaxone sodium. *Future Journal of Pharmaceutical Sciences 2021 7:1* 7, 1–10

11.   Hashem, H. and El-Sayed, H.M. (2018) Quality by design approach for development and validation of a RP-HPLC method for simultaneous determination of co-administered levetiracetam and pyridoxine HCl in prepared tablets. *Microchemical Journal* 143, 55–63

12.   Saini, S. *et al.* (2020) QbD-steered development and validation of an RP-HPLC method for quantification of ferulic acid: Rational application of chemometric tools. *Journal of Chromatography B* 1155, 122300

13.   Singh, B. *et al.* (2005) Optimizing Drug Delivery Systems Using Systematic "Design of Experiments." Part I: Fundamental Aspects. *Critical Reviews™ in Therapeutic Drug Carrier Systems* 22, 27–105

14.   Politis, S.N. *et al.* (2017) Design of experiments (DoE) in pharmaceutical development. *Drug Dev Ind Pharm* 43, 889–901

15.   FDA (2023) FDA Guidance for Industry: Q2B Validation of Analytical Procedures: Methodology - ECA Academy[Online]. Available: https://www.gmp-compliance.org/guidelines/gmp-guideline/fda-guidance-for-industry-q2b-validation-of-analytical-procedures-methodology. [Accessed: 28-Mar-2023]

16.   Pradhan, R. *et al.* (2020) QbD-driven development and validation of HPLC method for determination of Bisphenol A and Bis-sulphone in environmental samples. *Int J Environ Anal Chem* 100, 42–54

17.   Rapalli, V.K. *et al.* (2019) Stability indicating liquid chromatographic method for simultaneous quantification of betamethasone valerate and tazarotene in in vitro and ex vivo studies of complex nanoformulation. *J Sep Sci* 42, 3413–3420

18.   Italiya, K.S. *et al.* (2017) Simultaneous estimation of lisofylline and pentoxifylline in rat plasma by high performance liquid chromatography-photodiode array detector and its application to pharmacokinetics in rat. *J Chromatogr B Analyt Technol Biomed Life Sci* 1061–1062, 49–56

19.   Bhatt, D. *et al.* (2018) Analytical Method Development and Validation for the Estimation of Canagliflozin in Bulk and Formulation by RP- HPLC. *International Journal of Pharmaceutical Sciences and Drug Research* 10, 139-143

20. Kumar, P.A. *et al.* (2017) Simultanious determination of related organic impurities of Ibuprofen and Paracetamol in combination solid dosage form by Rp-HPLC with Qbd approach. *Oriental Journal of Chemistry* 33, 1461–1468

21. Rignall, A. (2017) ICHQ1A(R2) Stability Testing of New Drug Substance and Product and ICHQ1C Stability Testing of New Dosage Forms. *ICH Quality Guidelines* DOI: 10.1002/9781118971147.CH1. 3-44

22. Iram, F. *et al.* (2016) Forced Degradation Studies. *J Anal Pharm Res* Volume 3(6), 73
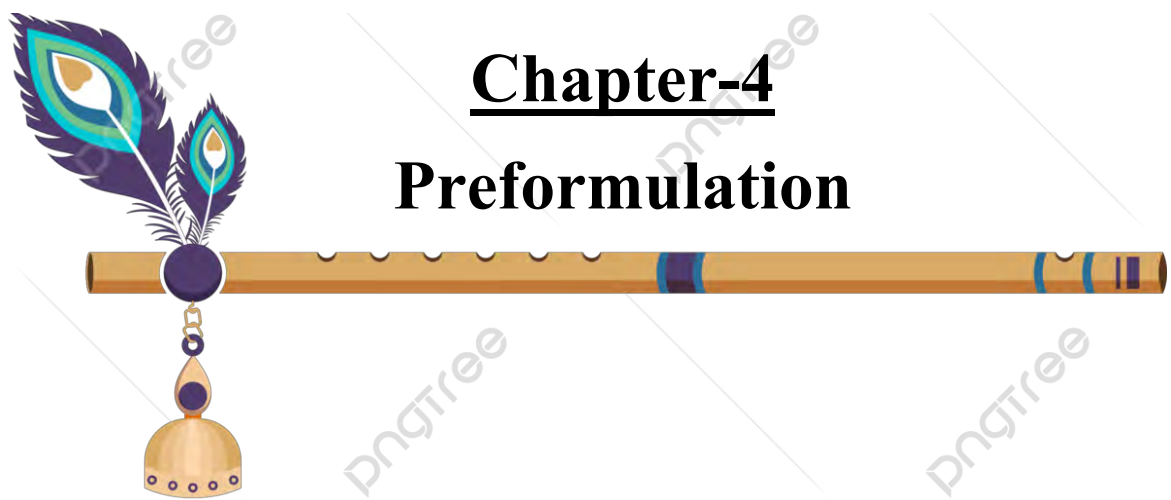
Chapter-4

Preformulation

4 Introduction

Developing a new drug is a costly endeavour that requires a rigorous evaluation and characterization of the drug molecule to ensure that it possesses the desired safety, efficacy, and quality. To achieve this, pre-formulation studies play a critical role in determining the physicochemical properties of the drug candidate and its interactions with various excipients and salts. This information is vital in selecting suitable and effective excipients to prepare a stable, safe, and effective formulation of consistent quality and performance, which helps reduce in development time and costs. Preformulation studies involve analyzing the powder characteristics of the drug, including particle size, crystallinity, and polymorphism, as well as determining its solubility in different solvents, buffers, and pKa. Stability in both solid and solution states and its compatibility with excipients [1–3]. Our research focuses on the development of nano-emulgel and solid lipid nanoparticles (SLNs) necessitates the undertaking of appropriate studies to obtain crucial information about the drug's characteristics and aid in the design of the suitable nanoparticulate formulation.

4.1 Instruments/Equipment

Wenser HD touch screen analytical weighing balance (Labman scientific instruments, Delhi, India) and electronic weighing balance (Shimadzu, Kyoto, Japan) were used to determine weights, and a waterproof pocket pH meter was used to determine pH values (Eutech Instruments Pvt Ltd., Singapur, Singapore). Attenuated total reflection infrared spectroscopy (ATR- IR, Bruker's, Ettlingen, Germany) was used for drug-excipient compatibility study and as purity tests for DTB API identification. Differential scanning calorimetry (DSC) Shimadzu DSC-60 plus was used for thermal analysis. A bath sonicator (Labman scientific instruments, Chennai, India) was used for solubilizing the API and buffer salts. Reverse Phase High-

performance liquid chromatography (RP-HPLC Shimadzu, Kyoto, Japan) for quantitative sample analysis.

4.2 Materials

Peceol, geleol, labrasol, capryol 90, compritol 888 pellets, precerol, monosteol, and gelot 64 and gelucire 44/16 were obtained as gift samples from Gattefosse, India (Mumbai, India). Palmitic acid and stearic acid were bought from SD Fine Chem (Mumbai, India). Potassium dihydrogen phosphate (KH_2PO_4), sodium hydroxide (NaOH), methanol, acetonitrile, acetone, methylparaben, and propylparaben were purchased from Merck Ltd (Mumbai, India). The remaining laboratory chemicals were acquired from HiMedia (Mumbai, India) and Sisco research laboratory Pvt. Ltd. (Maharashtra, India).

4.3 Experimentation

4.3.1 Bulk characterization

The physical characteristics of DTB, such as its color, were assessed through visual observation. To identify DTB, Bruker's ATR-IR with a resolution of 0.5 cm^{-1} and a range of 4000 to 600 cm^{-1} was utilized. Additionally, a DSC thermogram was generated.

4.3.2 Solubility studies

I. Solubility in oils and surfactants

 The solubility of DTB in various oils and surfactants was determined using the saturation solubility method. Excess DTB was added to 1g of the vehicle in a screw-capped vial, and the mixture was vortexed for 5 min using a cyclomixer. The mixture was placed for 48 h at 180 rpm and 25 ± 1 ºC on a rotating shaker [4]. Further, the mixtures were centrifuged at 5000 rpm for 20 min, and the supernatants were filtered through a 0.22-micron syringe filter and diluted with methanol. The solubilized amount of DTB in each vehicle was analyzed using RP-HPLC (Shimadzu LC-20AD, Japan) as described in Chapter 3 [5].

II. Solubility in solid lipids

The solubility of DTB in solid lipids is also performed. But equilibrium solubility is not possible in the case of solid lipids. As a result, a modified solubility method was used to ensure the DTB solubility in solid lipids. For lipid screening, stearic acid, compritol 888 pellets, precerol, monosteol, and palmitic acid were used. In a screw-capped vial, 500 mg of lipid was heated above its melting point. A known amount of DTB was added incrementally to a molten lipid with an adequate vertex. The amount of DTB that had become soluble in the molten lipid was visually recorded at this time. The culmination of the molten lipidic appeared transparent and pale yellowish color [6]

III. Solubility in various pH buffers

The saturation solubility method was selected, and it was conducted in different pH buffer media, including water. In this method, a mechanical shaker was used for shaking at 200 rpm for 24 h at 25 ± 1 ºC. After 24 h, the drug solution was centrifuged at 5000 rpm for 20 min. Then the supernatant solution was separated and diluted with suitable media [7,8]. The solubilized amount of DTB in each vehicle was analyzed using RP-HPLC (Shimadzu LC-20AD, Japan).

4.3.3 Stability studies

I. Solution state stability

The solution state stability of DTB was evaluated in various buffer solutions in the pH range of 4.5 to 7.4. A known concentration of DTB standard (10 µg. mL^{-1}) was prepared in different pH buffers, and the solutions were kept at 25.0 ± 2 ºC in 10mL volumetric flasks. The study was conducted for 72 h period. Samples were collected in predefined intervals and analyzed using the developed HPLC method. The % of drugs remaining to be degraded plotted against time

II. Drug-excipient compatibility studies by DSC and ATR-IR

DSC thermogram of pure DTB, individual solid excipients (Sodium meta bisulfite, methylparaben, propylparaben, and carbopol ETD 2020), and physical mixture were obtained using Shimadzu DSC 60 model. About 4 mg of the sample was taken in an aluminum crucible using dry nitrogen as the inert gas. The heating range was programmed to 20-300 º C with a heating rate of 10 ºC/min for analyzing each sample [9].

Further, the same excipients were characterized for ATR-IR, ranging from 4000 to 600 cm−1 with a resolution of 0.5 cm−1, to confirm the distinctive absorption bands corresponding to the specific functional groups present in those excipients [10].

4.3.4 Optimization of thickener content in oil

In the emulgel formulation, there is a possibility of the oil seeping out from the gel matrix. To prevent this, the thickness of the oil was increased by adding the thickener (general) to the oil phase. The procedure was mentioned briefly,

The oil: thickener (90:10, 80:20, 70:30, and 60:40) ratios were prepared for 1g. Each ratio was heated to a temperature of 70 ± 5 ºC to get a homogeneous mixture. The mixtures were then allowed to cool down to room temperature, and their ability to achieve a semi-solid consistency was evaluated. This investigation aimed to identify the optimal oil: thickener ratio that would effectively prevent oil seepage from the gel matrix in the emulgel formulation.

4.3.5 Pseudoternary phase diagrams

Oil [peceol and geleol (70:30)], surfactant (labrasol), and co-surfactant (capryol 90) were screened based on data obtained from the solubility. Furthermore, the water titration method was used to generate the pseudoternary phase diagram to determine the micro-emulsion area [11]. Surfactant and cosurfactant mixture (S_{mix}) were prepared in 1:1 and 2:1 ratios. After that, the 1:9 to 9:1 ratio of oil and S_{mix} mixtures were prepared for 1g. All of the prepared ratios

were thoroughly mixed and titrated with water while continuously mixing, and any turbidity was inspected. The pseudoternary phase diagrams were plotted using Triplot 4.1.2 software based on the obtained percentage components.

4.4 Results and discussion

4.4.1   Bulk characterization

The DTB was visually observed as off-white color. In ATR-IR, characteristic absorption bands were found to be 1501.97 cm^{-1}, 1573.66 cm^{-1}, 1624 cm^{-1}, 3229.9 cm^{-1}, and 3402.12 cm^{-1} for C–H, C–C, C=O, O–H, and N–H (secondary amine N-H stretch), respectively Figure 4.1 [12]. The DSC thermogram of pure DTB showed a sharp endothermic peak at a temperature of 282 ºC which follows the reported value (280-286 ºC) in Figure 4.2 [13]. This demonstrates the drug's purity.
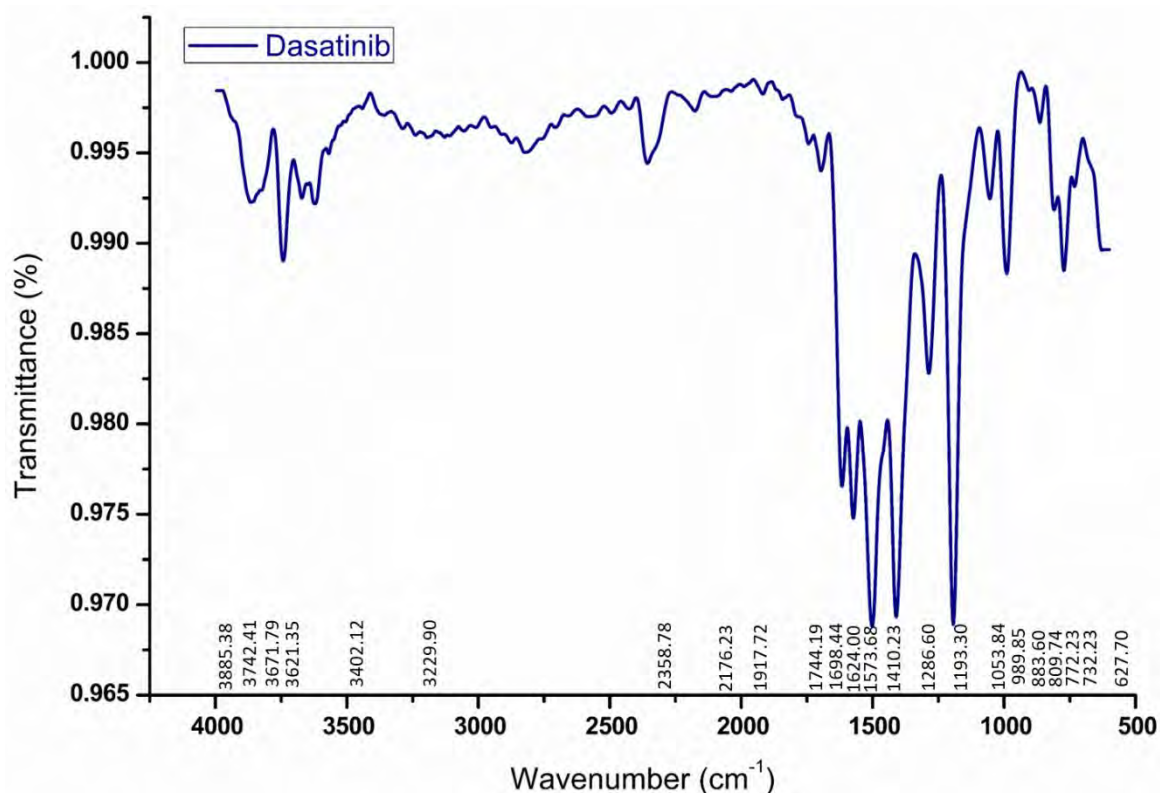
Figure 4.1 ATR-IR spectra of pure dasatinib.
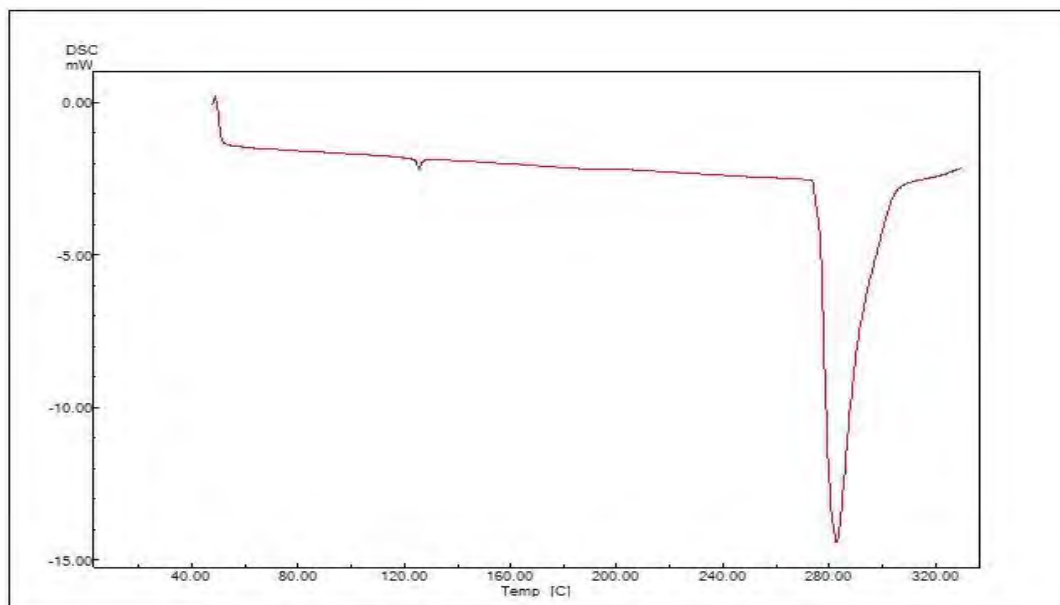
Figure 4.2 DSC thermogram of pure dasatinib.

4.4.2 Solubility studies

I. Solubility in oils and surfactants

The solubility of DTB was determined in various vehicles, as depicted in Figure 4.3. Oils, such as labrafac lipophile, misine CC, labrafac PG, and peceol were evaluated. Surfactants, such as capryol 90, labrasol, labrafil M2125, labrafil 1944, and labrasol ALF, were included and based on the maximum solubility of the drug. Peceol as the oily vehicle, labrasol as the surfactant, and capryol 90 as the cosurfactant was selected for further studies. In peceol, DTB was found to have maximum solubility of 3.06 ± 0.06 mg/g. In labrasol, DTB had a solubility of 10.61 ± 0.03 mg/g. Further, in capryol 90 solubility was found to be 8.76 ± 0.07 mg/g.

II. Solubility in solid lipids

The solubility of DTB was determined in various vehicles, as depicted in Figure 4.4. Lipids, such as stearic acid, compritol 888 pellets, precerol, monosteol, and palmitic acid, were evaluated. In palmitic acid, DTB was found to have maximum solubility of 20.52 ± 0.06 mg/g and which was used as the lipid vehicle in the formulation.
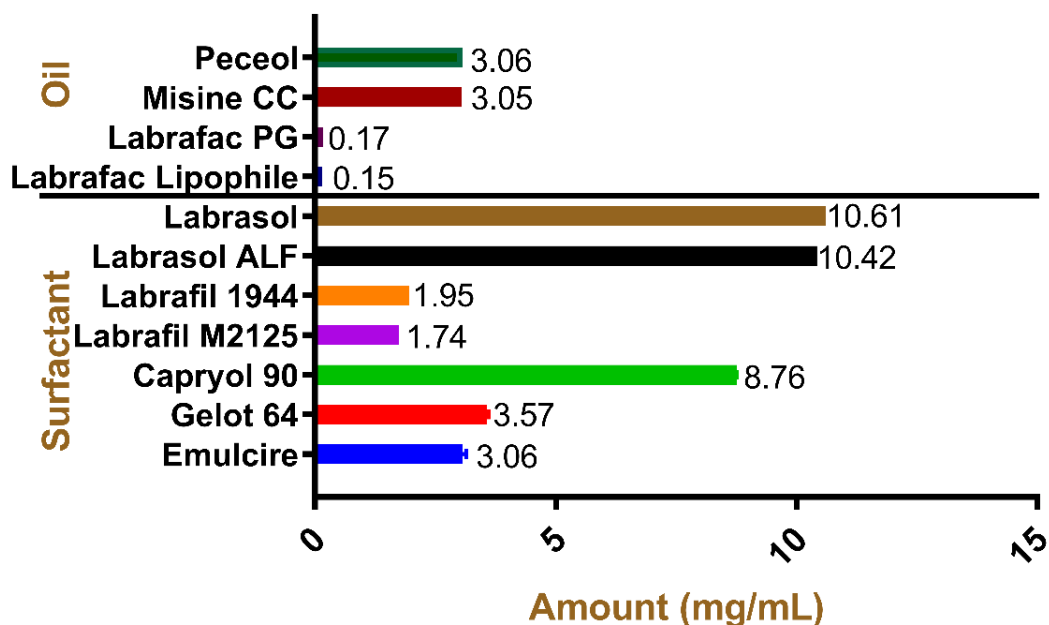
Figure 4.3 Solubility of dasatinib in different oils and surfactants.
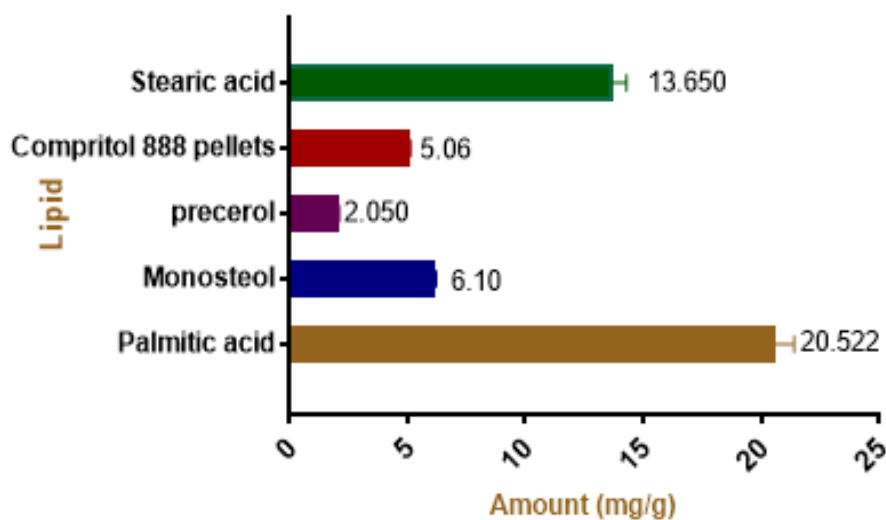
Figure 4.4 Solubility of dasatinib in different solid lipids.

III. Solubility in various pH buffers

Solubility studies of DTB were performed in different pH buffers, and results are shown in Figure 4.5; DTB was found to have pH-dependent solubility. Hence, the solubility study was performed at different pH of the media. From the results, it can be observed that as the pH

increased towards alkaline, the solubility decreased. The highest solubility of DTB was found to be 0.48 ± 0.001 mg/mL in pH 5.5 phosphate buffer containing 1% triton X100; this media was used as drug release media for the dissolution study. The DTB has less solubility in water, i.e., 0.05 ± 0.001 mg/mL.
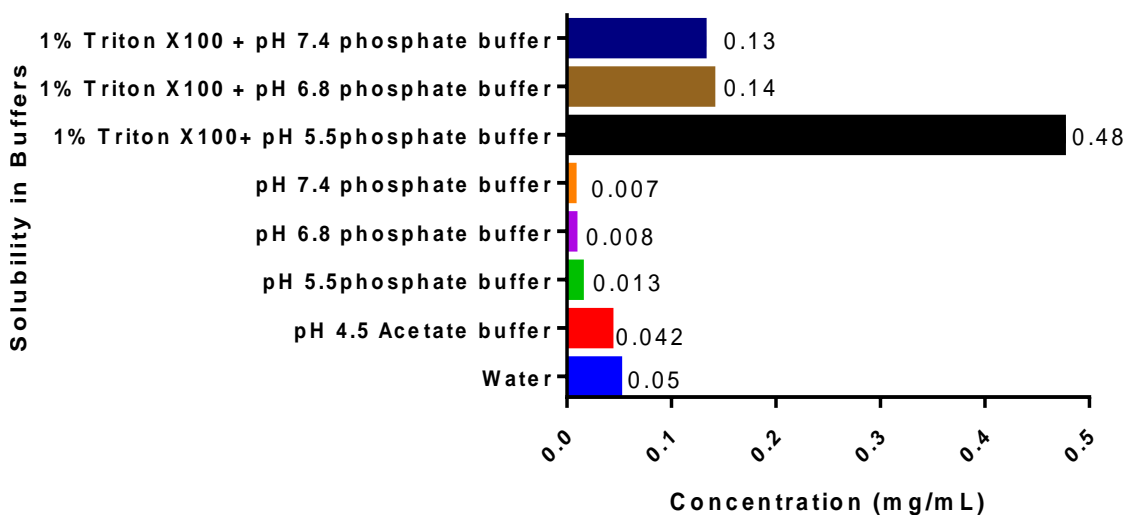
Figure 4.5 Solubility of dasatinib in different pH buffers.

4.4.3   Stability studies

I. Solution state stability

The solution state stability of DTB as a function of time was assessed in different buffer solutions with pH ranging from 4.5 to 7.4 using a concentration of 10 µg. mL^{-1}. Figure 4.6 shows that the degradation of DTB was slow and slight, which is less than 3%. Overall, these findings demonstrated that DTB remained stable in all the pH buffers.
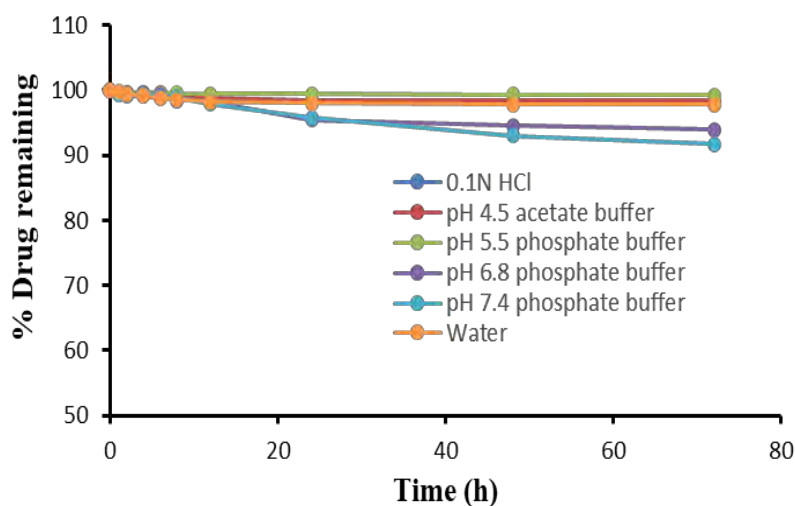
Figure 4.6 Solution stability studies in different pH buffers.

II. Drug-excipient compatibility studies by DSC and ATR-IR

DSC thermogram of the pure drug, excipients, and physical mixture is represented in Figure 4.7. DTB pure drug showed a sharp endothermic peak at 282.4 °C. Sodium metabisulfite and methylparaben, and propylparaben excipients showed sharp endothermic peaks at 154.1 °C, 124 °C, and 96.2 °C, respectively. Additionally, carbopol ETD 2020 showed an endothermic glass transition peak at 113.1 °C. In the physical mixture, the melting point of DTB was found to be 283.1 °C. Thus, there was no interaction between drugs and excipients. Further, the excipients were used in the formulation development.

The ATR-IR spectra revealed the characteristic absorption bands of DTB at 1498.59 cm^{-1}, 1581.11 cm^{-1}, 1624 cm^{-1}, 3229.9 cm^{-1}, and 3402.12 cm^{-1} for C–H, C–C, C=O, O–H, and N–H (secondary amine N-H stretch), respectively and these bands correspond to the reported peaks [12]. In the physical mixture, the absorption occurred at 1497.15 cm^{-1}, 1582.73 cm^{-1}, 1620 cm^{-1}, 3200 cm^{-1}, and 3418 cm^{-1} for C–H, C–C, C=O, O–H, and N–H (secondary amine N-H stretch), respectively. These results demonstrated that the presence of all solid excipients (physical mixture) did not alter the absorption bands, suggesting that there is no incompatibility between the drug and excipients Figure 4.8.
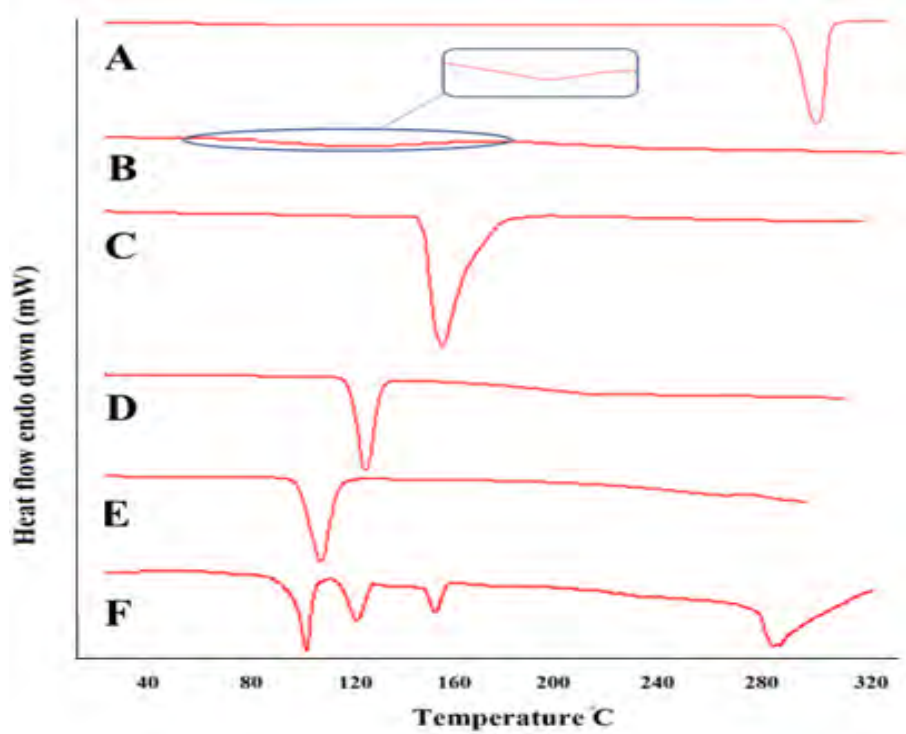
Figure 4.7 DSC thermogram of (A) DTB; (B) Carbopol ETD 2020; (C) Sodium meta bisulfite; (D) Methylparaben; (E) Propylparaben; (F) Physical mixture.
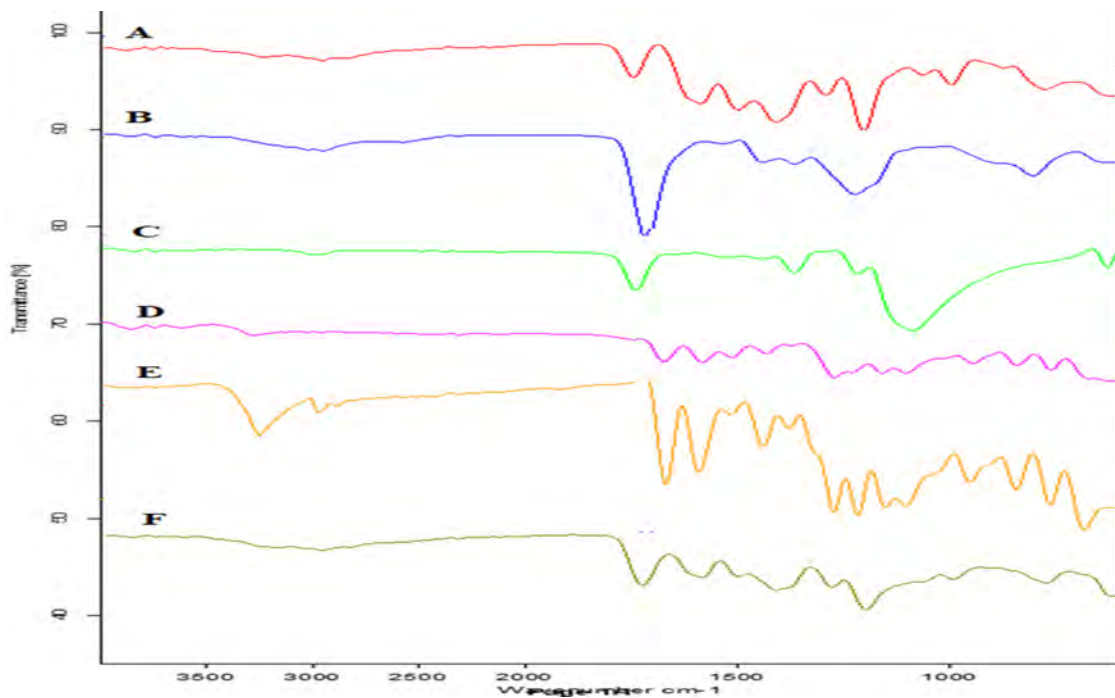
Figure 4.8 ATR-IR Peaks of (A) Dasatinib; (B) Carbopol; (C) Sodium Meta bisulfate; (D) Methylparaben; (E) Propylparaben; (F) Physical mixture.

4.4.4 Optimization of thickener content in oil

Different ratios of peceol and geleol were selected, i.e., 9:1, 8:2, 7:3, and 6:4. Initially, the oil was heated to 70 ± 5 °C using a heating magnetic stirrer; after that, the geleol was added, and thoroughly mixed. Once the mixture was uniformly combined with the oil, it was allowed to cool down. The 9:1 and 8:2 ratios remained as flowable liquids at 35 ± 5 °C, while the 7:3 ratio had a semisolid form, and the 6:4 ratio existed as a wax form. The desired semi-solid consistency was attained using the 7:3 ratio of peceol: geleol. This ratio was selected as the oil phase in the emulgel formulation

4.4.5 Pseudoternary Phase Diagrams

The pseudoternary diagrams were plotted to spot the emulsion area, Figure 4.9. Here, oil [peceol and geleol (70:30)], surfactant (labrasol), and cosurfactant (capryol 90) were selected. Ratios of 1:1 and 2:1 surfactant mixtures were prepared, as well as oil and Smix ratios of 1:9 to 9:1. Mixtures were prepared and titrated with water until turbidity was seen. In both ratios, a 2:1 ratio of Smix had more emulsion area. Hence, a 2:1 ratio of Smix was used for designing the emulsion formulation.
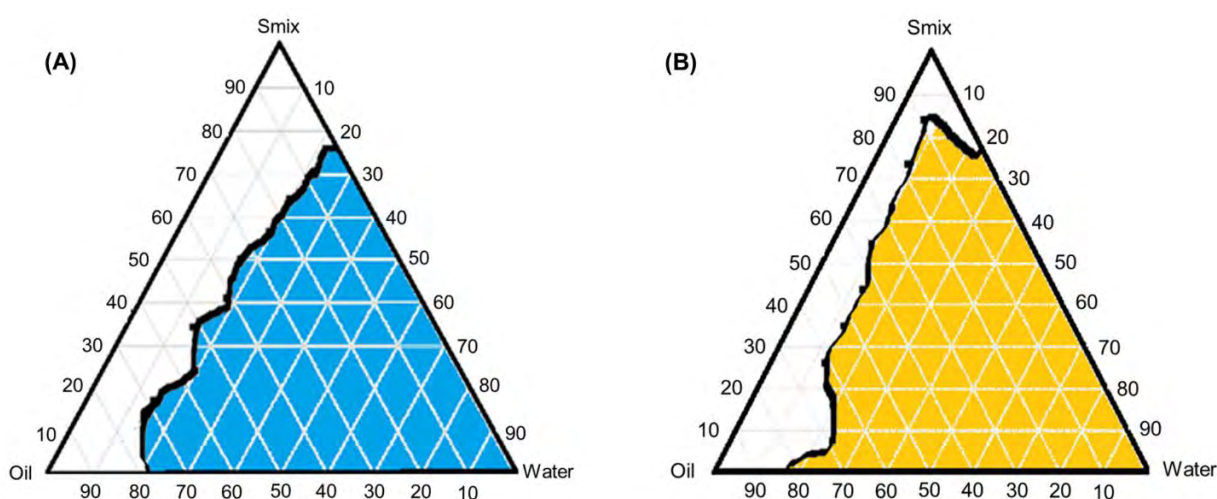
Figure 4.9 Pseudoternary phase diagrams series. (A) Containing oil and Smix ratios of 1:1; (B) Containing oil and Smix ratios of 2:1, blue and orange color (emulsion zone), white color (non-emulsion zone).

4.5 Conclusion

The DTB sample successfully passed all identification tests, demonstrating its quality. Solubility studies revealed its high solubility in specific oils, surfactants, co-surfactants, solid lipids, and pH 5.5 phosphate buffer containing 1% triton X 100. Stability tests across various pH buffers and water indicated no significant degradation, while compatibility studies confirmed the absence of any drug or excipient incompatibility. The optimized surfactant and co-surfactant ratio (2:1) from the ternary phase diagram showed a high emulsion zone. These findings led to the selection of appropriate excipients for further formulation development. For the emulgel formulation, peceol: geleol mono and diglycerides (70:30) and labrasol: capryol 90 (2:1) were selected as the oily vehicle and surfactant, respectively. For the SLNs formulation, palmitic acid (solid lipid) and emulsion (o/w stabilizer) were selected.

References

1. Gibson, M. (2016) Pharmaceutical Preformulation and Formulation. *CRC Press* 1, 443–467

2. Nyqvist, H. (1986) Preformulation Studies of Drug Substances for Solid Dosage Forms. *Drug Dev Ind Pharm* 12, 953–968

3. Dave, V.S. *et al.* (2015) Drug-Excipient Compatibility Studies in Formulation Development: Current Trends and Techniques. *American Association of Pharmaceutical Scientists (AAPS) Formulation Design and Development (FDD) Section Newsletter*

4. Madhav, K.V. and Kishan, V. (2017) Self micro emulsifying particles of loratadine for improved oral bioavailability: preparation, characterization and in vivo evaluation. *J Pharm Investig* 48, 497–508

5. Jakki, R. *et al.* (2013) Development of a self-microemulsifying drug delivery system of domperidone: In vitro and in vivo characterization. *Acta Pharm* 63, 241–251

6. Shah, K.A. *et al.* (2007) Solid lipid nanoparticles (SLN) of tretinoin: potential in topical delivery. *Int J Pharm* 345, 163–171

7.   Maheshwari, R.K. and Indurkhya, A. (2010) Formulation and Evaluation of Aceclofenac Injection Made by Mixed Hydrotropic Solubilization Technique. *Iran J Pharm Res* 9, 233

8.   Jagdale, S.K. *et al.* (2019) Enhancement of Dissolution of Fenofibrate Using Complexation with Hydroxy Propyl β-Cyclodextrin. *Turk J Pharm Sci* 16, 48

9.   Donthi, M.R. *et al.* (2015) Preparation and Evaluation of Fixed Combination of Ketoprofen Enteric Coated and Famotidine Floating Mini Tablets by Single Unit Encapsulation System. *J Bioequivalence Bioavailab* 07, 1–5

10.   Donthi, M.R. *et al.* (2022) Formulating Ternary Inclusion Complex of Sorafenib Tosylate Using β-Cyclodextrin and Hydrophilic Polymers: Physicochemical Characterization and In Vitro Assessment. *AAPS PharmSciTech* 23, 1–15

11.   Patel, A.R. and Vavia, P.R. (2007) Preparation and in vivo evaluation of SMEDDS (self-microemulsifying drug delivery system) containing fenofibrate. *AAPS J* 9, E344–E352

12.   Korashy, H.M. *et al.* (2014) Dasatinib. *Profiles Drug Subst Excip Relat Methodol* 39, 205–237

13.   SPRYCEL^{TM} (2006) SPRYCEL^{TM} Rx only (dasatinib) Tablets. *United states food and drugs administration*

Chapter-5

Formulation and Characterization of Dasatinib-loaded Nanoemulgel
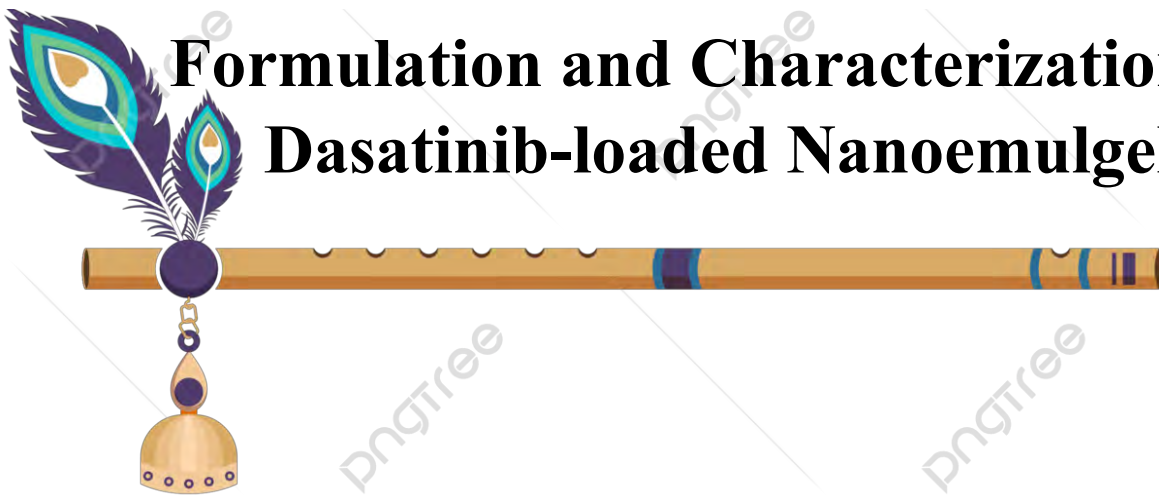
5 Introduction

Oral administration of dasatinib (DTB) exhibits few side effects [1]. To avoid the side effects and improve the efficacy, topical administration of DTB could be a viable approach. Though topical preparations offer advantages in achieving localized effects and enhancing penetration into deeper layers of the skin. However, conventional topical formulations have certain drawbacks like unable to deliver hydrophobic drugs effectively and may fail to provide the required therapeutic drug concentration at the intended target site, i.e., the joint region. Moreover, these formulations exhibit greasiness and excessive stickiness, which ultimately contributes to low patient adherence [2,3]. To overcome the limitations associated with conventional delivery systems and improve therapeutic efficacy, it is imperative to enhance solubility and permeability. Nano lipid-based delivery systems have emerged as a novel approach that not only enhances permeability but also addresses stability concerns [4–6]. Among the various nano lipoidal delivery systems, like liposomes, transferosomes, microemulsions, and nanostructured lipid carriers (NLCs), etc., nanoemulsion is one of the remarkable success in delivering lipophilic and poorly permeable drugs via the topical route. Nanoemulsions have garnered considerable scientific attention due to their enhanced stability, improved solubility enhancement capacity, and high drug-loading efficiency. Nanoemulsion combined with a gelling agent is commonly referred to as nanoemulgel, where the gel matrix can convert the nanoemulsion into a stable nanoemulgel. In nanoemulgel, the emulsion shows similarities with other nano-carriers in terms of reducing enzymatic degradation, enhancing hydrolysis, and improving drug permeation. Additionally, besides enhancing drug penetration through the skin, it is equally important to maintain therapeutic drug concentrations for a sufficient period of time. The gel component of nanoemulgel plays a crucial role in improving viscosity and spreadability, thereby resulting in an enhanced retention time. Furthermore, nanoemulgel exhibits exceptional properties, including easy spreadability, thixotropic

behaviour, non-greasy texture, and ease of removal [6–8]. By leveraging the advantages of nanoemulgel, it becomes possible to achieve efficient and effective delivery of therapeutic agents through the skin [9,10].

In the present study, formulation variables were investigated using a quality by design (QbD) based approach. The QbD model emphasizes a systemic approach in the development of pharmaceutical products. This article aims to provide insight into the selection of formulation ingredients of a nanoemulgel, method of preparation and its characteristics, pharmacokinetics and pharmacodynamics, and safety of the same.

5.1 Materials

Peceol, geleol, labrasol, capryol 90 and transcutol P from were obtained as gift samples from Gattefosse, India (Mumbai, India). Isopropyl myristate (IPM), membrane filters (0.45 μm) were purchased from (Hi-Media Mumbai, India). Acetonitrile, methanol (HPLC grade), propyl paraben, methyl paraben, orthophosphoric acid, potassium dihydrogen phosphate and dialysis membrane (molecular weight cut off 12,000–14,000) were procured from Merck, (Mumbai, India). Triton X 100 was purchased from Himedia (Mumbai, India). Other than that, only analytical-grade reagents, solvents, and chemicals were employed.

5.2 Study design

The experimental design offers a systematic, structured framework of the product process, as well as process knowledge and reliable information about the factors and their relative responses. Therefore, systematized execution is more crucial than ever. A representative study design is depicted as a route map in Figure 5.1.
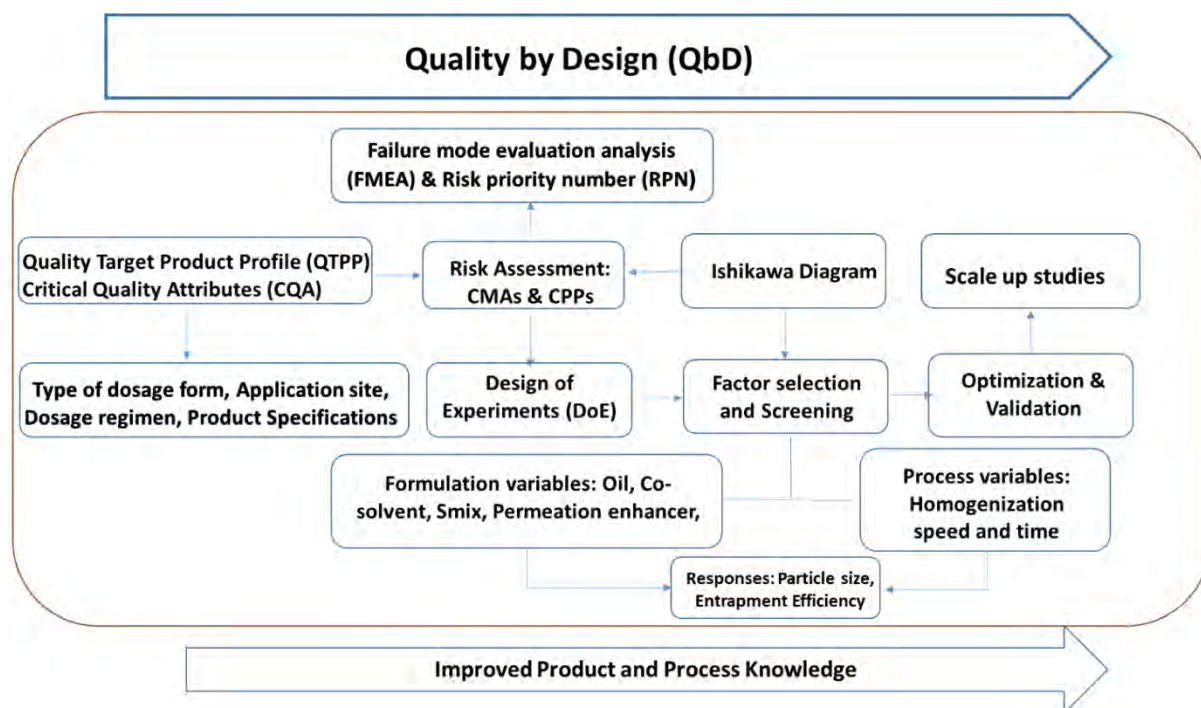
Figure 5.1 Representative image for steps involved in the QbD approach for nanoemulgel.

5.2.1 Quality target product profile (QTPP) and critical quality attributes (CQAs)

QbD plays a vital role in designing high-quality formulations. Achieving high quality in manufactured products requires a thorough understanding of the material type, involved processes, and quality attributes. The quality target product profile (QTPP) provides a comprehensive description of the product's safety and efficacy standards. CQAs were chosen to regulate the required features of the desired finished product in order to meet QTPP. The patient should be considered as the first priority while deciding the CQAs of the formulation. QTPP and CQAs were chosen based on research and knowledge of topical lipidic formulations before optimizing DTB-loaded nanoemulgel [11].

5.2.2 Quality risk assessment

During the development of nanoemulgel formulation, critical formulation and process variables can alter the formulation's CQAs and cause formulation failure. In order to develop action plans for critical material attributes (CMAs) and critical process parameters (CPPs), the probability and potential severity of these risk factors, as well as the resulting failure modes, should be determined. Ishikawa diagram was used to estimate the risk factors for process and

formulation variables of nanoemulgel. In light of the potential factors that could affect the properties of the formulation, a risk matrix evaluation (REM) was carried out. The CMAs and CPPs were established by utilizing the REM to analyze the variables with low, medium, and high-risk potential. Failure mode effects analysis (FMEA) was assessed for each factor's severity, probability, and occurrence. The risk priority number (RPN) was determined using equation 1, with a 0–10 ranking. The RPN score was used to identify CMAs and CPPs [12,13]

Severity(S)* Detectability (D) * Occurrence (O) = RPN   (eq.1)

5.2.3 Factor screening studies

The effect of oil, co-solvent (isopropyl myristate), S_{mix} (Surfactant mixture), and permeation enhancer (transcutol P) on the size, entrapment, and drug release of the proposed emulsion was studied using a fractional factorial design (FFD) 2^{4-1} and the factors were selected based on the risk assessment report. The concentration of components keyed into two levels (low and high) i.e., oil concentrations of 5 and 20 % w/w, S_{mix} concentrations of 3 and 10 % w/w, transcutol P concentrations of 2.5 and 10 % w/w, and isopropyl myristate concentrations of 2.5 and 10 % w/w were used. The Design-Expert software (version 7.0.0) was used to produce 8 runs at random as shown in Table 5.1, which served as the foundation for this study. Based on obtained data, the interaction and severity of the factors against the responses were depicted using graphical 3D response surface representations and pareto charts. The formulation with the best screening findings was subsequently evaluated for *ex-vivo* permeability on rat skin by loading it into a 0.5% carbopol gel base to observe the effect the permeation enhancer. Further, the screened factors were carried out for the optimization studies.

Table 5.1 Experimental trails performed using two-level factorial design.

Ingredients (g)	DF1	DF2	DF3	DF4	DF5	DF6	DF7	DF8
Dasatinib (DTB)	0.01	0.01	0.01	0.01	0.01	0.01	0.01	0.01
Peceol +Geleol (7:3)	1.00	1.00	4.00	4.00	1.00	1.00	4.00	4.00
Labrasol + capryol (2:1)	2.00	0.60	0.60	2.00	0.60	2.00	0.6	2.00
Transcutol P	2.00	2.00	2.00	0.50	0.50	0.50	0.50	2.00
Isopropyl myristate	0.50	2.00	0.50	0.50	0.50	2.00	2.00	2.00
Methyl paraben	0.10	0.10	0.10	0.10	0.10	0.10	0.10	0.10
Propyl paraben	0.01	0.01	0.01	0.01	0.01	0.01	0.01	0.01
Sodium metabisulfite	0.04	0.04	0.04	0.04	0.04	0.04	0.04	0.04
Aqueous phase	14.50	14.40	12.90	13.00	17.40	14.50	12.90	10.00
Total weight (g)	20.00	20.00	20.00	20.00	20.00	20.00	20.00	20.00

5.2.4 Factor optimizing studies

Based on FFD data, oil and S_{mix} were selected as the formulation variables, and the remaining two components (transcutol P and isopropyl myristate) were kept in constant concentration in the formulation. In addition, the CPP selected from the ishikawa diagram i.e., homogenization speed and time. The selected formulation and process variables on the responses of size and entrapment were evaluated using a face-centered center composition design (CCD) without axil points. The factors were keyed into two levels i.e., low (-1) and high (+1). The design matrix suggested 17 experimental runs containing center points of each selected variable. Further, the prepared batches were evaluated for general characterization studies like phase separation, dilution test and microscopy for crystal growth observation.

5.2.5 Optimization data analysis and model validation

Design of experiment software was used for the optimization, data analysis, and model validation to fit the experimental data into quadratic polynomial models for estimating the

examined responses, as well as the inspected variables. The coefficient of correlation (R^2) and lack of fit analysis was chosen to serve as model assessment parameters from a variety of metrics. After that, the coefficients with $p < 0.001$ were considered when testing the analysis of variance (ANOVA) model. Furthermore, both 3-D response and 2-D counter plots were utilized in order to explore the factor response relationship. Based on the numerical optimization and desirability function, the best compositional solution was chosen. This is accomplished by switching the different CQA i.e., desirable size, and maximizing the percentage entrapment of the drug in the formulation.

5.3 Formulation of DTB loaded nanoemulsion

5.3.1 Method of preparation

The compositions for the optimized formulation using QbD approach was shown in the results section. Each formulation was prepared as a single batch of 20 g. The formulation was fabricated using the O/W hot homogenization method and the method of preparation is explained briefly, in two steps 1-3 [14].

Step 1: Oil phase preparation; The oil phase was prepared by dissolving the S_{mix} in the oil phase and isopropyl myristate mixture. Further, DTB, methyl paraben and propyl paraben were added to the oil base, mixed well, and kept in a bath sonicator at 60 ºC till the components get dissolved.

Step 2: Aqueous phase preparation; The aqueous phase was prepared by dissolving the transcutol p and sodium meta bisulphite and kept under stirring at 40 ºC.

Step 3: O/W nanoemulsion preparation; The oil phase was added dropwise to the aqueous phase under continuous homogenization at 40 ºC. The mix was finally, cooled down to room temperature.

5.3.2 Scale-up studies

The volume of the batch was increased to 50 mL and 100 mL based on validation parameters. The quantities needed for formulation development were correspondingly increased with scale-up. The diameter of the batch vessel and the homogenizer were changed in the 50 and 100 mL size batches. The homogenizer with a 6 mm probe diameter (capacity 5–30 mL) was used to fabricate a batch of 20 mL, and the beaker.

5.3.3 Characterization of nanoemulsion

5.3.3.1 Attenuated total reflection-infrared spectroscopy (ATR-IR)

The IR spectrum of DTB, optimized nanoemulsion and placebo nanoemulsion were analyzed to gain insights into the molecular arrangement and characteristics of the formulation using Bruker's ATR-IR at 4000 to 600 cm^{-1} with 0.5 cm^{-1} resolution.

5.3.3.2 Measurement of size, polydispersity index (PDI), and zeta potential (ZP)

Size, PDI, and ZP were measured using the dynamic light scattering (DLS) technique by Malvern zeta sizer (Nano ZS, Malvern Instruments, UK) with a 173-degree angle of detection at 25 ºC. About 100 µL of the emulsion was taken and diluted to 1mL (1:10 dilution) and analyzed for size, PDI, and ZP [15].

5.3.3.3 Entrapment efficiency (EE)

The encapsulation efficiency (EE) was determined using an indirect method, which involved separating the free drug present in the nanoemulsion using the dialysis technique. To do this, 1g of DTB-loaded emulsion was placed inside a dialysis tube (molecular weight cutoff of 3.5 kDa) and both ends of the tube were tied carefully. The dialysis bag was placed in 30 mL of distilled water at 37±0.5 °C under stirring at 200 rpm. After an hour 1 mL of the aqueous sample was removed and analyzed using RP-HPLC. The EE of DTB in the emulsion was measured by using the following equation 2 [16].

$$\% \text{ EE } = \frac{W \text{ total} - W \text{free}}{Wtotal} \times 100 \qquad \text{(eq.2)}$$

Where, W_{total} - weight of drug added in the system, W_{free} - free drug in the formulation

5.3.3.4 Thermodynamic stability studies

The optimized emulsion was subjected to allow various thermodynamic studies such as a centrifugation test, freeze-thaw study, and heat-cooling cycle [17]. In the centrifugation test, the optimized emulsion 1g was diluted to 10 mL with water and allowed to undergo centrifugation at 5000 rpm for 15 min (REMI CPR-24) and assessed for instability. For the freeze-thaw study, the temperatures were maintained between -21 ºC for 24 h followed by +25 ºC for three cycles and recorded the instability. During the heating cooling cycle, the formulation was subjected to three heating-cooling cycles. The temperature for the cooling cycle was applied at 4 ºC in the refrigerator and 45 ºC for more than 48h designed for the heating cycle and recorded the instability.

5.3.3.5 Microscopy for evaluating crystal growth

The presence of crystals in the nanoemulsion was observed using a Zeiss AX10 Microscope at 1 h period. A drop of sample was placed on a glass slide, and images were captured at a resolution of 40x.

5.3.3.6 Morphology by field-emission scanning electron microscopy (FESEM)

Field-emission scanning electron microscopy (AURIGA® Carl Zeiss, Oberkochen, Germany) was used to investigate the morphology of nanoemulsion. A drop of optimized emulsion was appropriately diluted with distilled water and placed on the surface of the coverslip and dried well. Before FESEM analysis, samples containing coverslips were coated with a thin layer of gold (10 nm). Images were captured at a 2 kV accelerating voltage [18].

5.3.3.7 *In-vitro* drug release study

The dialysis bag (M.W. cut off 12,000 KDa) method was used to conduct comparative *in-vitro* drug release for selected emulsions and free drug solutions (FDS). In the dialysis bag, separate samples of nano emulsion and FDS equivalent to 500 µg each were taken in individual dialysis bags and both ends of the bag were tied carefully. The bag was placed in release media containing pH 5.5 phosphate buffer (PB) + 1% triton X100. The temperature was carefully maintained at 37± 0.5 °C, and the samples were continuously stirred at 400 rpm for a duration of 24 h. 1 mL sample was withdrawn at each predetermined time point and replaced with an equal amount of fresh medium to maintain sink condition. The sample was analyzed by HPLC at 315 nm after suitable dilution. The drug release kinetics and mechanisms of optimized formulation was analyzed using DD solver dissolution kinetic modelling software. The best fit was selected based on the obtained R^2 values from each of the models [19].

5.4 Formulation of dasatinib-loaded nanoemulgel

5.4.1 Method of Preparation

The emulgel was prepared using optimized emulsion formula with slight modifications in the aqueous portion for gelling agent addition and the preparation process was briefly explained below.

The oil phase was prepared by dissolving the S_{mix} in a peceol and isopropyl myristate mixture. Further, DTB, methyl paraben, and propylparaben were added to the oil base mixed well and kept in a bath sonicator at 60 ºC till the components get dissolved. In the aqueous phase, 40 % milli-Q water was taken from the total water content designed in the formula and added to transcutol P and sodium meta bisulphite, heated at 40 ºC and it was added dropwise to the oil phase to form the nanoemulsion under continuous stirring. The formed nanoemulsion was homogenized at 15,000 rpm for 7 min and cooled down to room temperature. 0.5 % carbopol ETD 2020 was added to the rest 60% milli-Q water and it was neutralized to pH 5.5 with 1%

NaOH Solution to form a gel at room temperature under continuous homogenization. The fabricated emulsion was added dropwise to the gel base under continuous stirring at room temperature to form the nanoemulsion loaded gel known as nanoemulgel [20].

5.4.2 Evaluation of nanoemulgel

5.4.2.1 Physical appearance and pH determination

The prepared DTB-loaded nanoemulgel was visually inspected for color, consistency, and homogeneity [21]. The selected nanoemulgel pH was determined using calibrated hand pH meter. 10% emulgel dispersion was prepared with milli-Q water and the measurement was recorded at ambient temperature [22].

5.4.2.2 Spreadability study

The spreadability of the optimized nanoemulgel was performed using the graph paper method. Two known-weight glass slides were placed over the graph paper. X and y axis were displayed and a square was drawn on chart paper. 0.5 g of gel was placed on the glass slide within the square. Then the second glass slide was kept over the first slide and the weights were added incrementally. The incremental diameter of the spread gel was noted. The following equation was used for the calculation [23] [24].

$$Ei = d^2 \frac{\pi}{4}$$

where: E_i = spreadability of the sample weight for a given i (mm^2); d = diameter (mm).

Spreadability factor (Sf) was calculated using the following equation

$$Sf = \frac{A}{w}$$

where: Sf = spreadability factor; A = total area (mm^2); W = total weight (g)

5.4.2.3 Drug content determination

The drug content in the formulation was evaluated by dissolving a known amount of selected nanoemulgel in methanol using sonication. After suitable dilution, the sample was analyzed at 315 nm using HPLC.

5.4.2.4 Particle integrity of lipid emulsion-loaded gel

The fabricated nanoemulgel formulation was dispersed in milli-Q water and changed to attain a clear, uniform dispersion. As aforementioned, the PS of the obtained dispersion was evaluated using a Malvern zeta sizer.

5.4.2.5 Rheology study

Viscosity

The optimized nanoemulgel was evaluated for viscosity using an Anton Paar MCR 92 and a flat-faced spindle with a constant shear rate of 10 s^{-1} at 25 ºC. The viscosity average of twenty points was noted.

Shear flow

The selected formulation's flow tendency was determined using a technique that examines the relationship between viscosity and shear rate or shear stress. Specifically, it aids in determining the dependence of viscosity on shear rate or shear stress. The continuous ramp step was selected with a shear rate range of 0 to 10s^{-1} for 50 points at 25 °C. The results obtained were recorded as the shear rate, shear stress, and viscosity of each point [25].

Strain sweep test

In this test, the formulation was characterized by increasing oscillatory strain (OS) at a constant frequency. The results are expressed in terms of the formulation's storage (G') and loss (G") moduli as the strain range increases, which also provides information about the Newtonian behaviour or linear viscoelastic region (LVR) of the formulation. Strain sweep measurements were taken at 32 ºC in the range of 0.01 to 100%, with a constant angular frequency of 10 s^{-1}.

Frequency sweep test (FST)

The FST is used to determine the relationship between testing frequency and a formulation's storage (G') and loss (G") moduli. Furthermore, it provides information about a material's viscoelastic properties and state by comparing the two G' and G" values over a frequency range.

5.5 *In-vitro* cell line study

5.5.1 Cytotoxicity Studies

The cytotoxicity of DTB and DTB-loaded nanoemulgel was investigated using HaCaT (Human Keratinocyte) cell lines. This analysis aimed to assess whether the presence of excipients in the formulation, along with DTB, had any cytotoxicity on the HaCaT cells. Here, the MTT [(3-(4, 5-dimethyl thiazolyl-2)-2, 5-diphenyltetrazolium bromide)] test was used to investigate cell cytotoxicity. The cell growth medium was composed of 90 % Dulbecco's modified eagle's medium (DMEM) and 10 % fetal bovine serum (FBS). The number of viable cells in the cell suspension was determined using a hemocytometer and the trypan blue exclusion method. For the test, 5×10^3 cells/ well seeded in a 96-well plate for 24 h in a CO_2 incubator at 37 °C with 5% CO_2 saturated humidity. The following day, treatment was given with free DTB and optimized nanoemulgel at different concentrations 50, 100, 150, 250, 500, 750, 1000, 1500, 2500, and 5000 nM. After 48 h, the medium was discarded, followed by a PBS wash and an MTT test. To assess the vitality of the cells, the absorbance was measured at 570 nm with a reference wavelength of 630 nm using an Enzyme-linked immunosorbent assay (ELISA) microplate reader (Biotek, Winooski, VT). The experiments were carried out in triplicate, and the results were expressed as the mean ± SD [26].

5.5.2 Effect on the production of TNF-α and IL-6

The role TNF-α and IL-6 have been reported for proinflammatory effect in RA [27]. This study examined how optimized nanoemulgel affected RAW 264.7 (isolated macrophages from mouse blood) cells ability to produce TNF-α and IL-6. DMEM + 2 mM Glutamine + 10 %

FBS used as cell supplement media. RAW264.7 cells were pre-incubated for 2 h with DTB, optimized nanoemulgel, and diclofenac sodium (DCS) after being seeded at a density of 2 x 10^5 cells per well in 24 well plate. Lipopolysaccharide (1μg/mL) was used to stimulate the cells for 24 h. A sandwich ELISA kit was used to determine the amount of TNF-α and IL-6 produced in cell supernatants according to the manufacturer's recommended experimental procedures. The absorbance at 450 nm was measured using an ELISA microplate reader (Biotek, Winooski, VT). The studies were performed in triplicate, and the data were presented as a mean ± SD.

5.6 *Ex-vivo* studies

5.6.1 *Ex-vivo* permeation study

Optimized nanoemulgel formulation and the Free drug loaded gel (FDG) comparative permeation studies were conducted. The study was carried out in fabricated Franz diffusion cells (2.27 cm^2 area and volume 40 mL), using rat skin. The skin was isolated and placed between the donor and acceptor compartment of Franz diffusion cells. Further, a gel containing 200mg equivalent of DTB from the 0.05% formulation was applied to the dorsal side of the skin. Phosphate buffer pH 5.5 contain 1% triton X100 as release medium at 37 ±0.5 °C under continuous stirring at 200 rpm throughout 24 h. 1 mL sample was withdrawn at each predetermined time point and replaced with an equal amount of fresh medium. The sample was analyzed by RP-HPLC at 315 nm after suitable dilution [28].

5.6.2 Skin deposition study

The optimized nanoemulgel formulation was applied to the dermal surface of the skin. After 24 h, the skin was cut into small pieces and treated with extraction solvent (methanol) followed by homogenization for 20 min to extract the deposited drug embedded in the skin. Further, the extraction solvent was centrifuged at 5000 rpm for 10 min. The supernatant was collected and the deposited drug content was analyzed using RP-HPLC [23,29].

5.6.3 Bio adhesion study

Rat skin freshly isolated was sectioned into pieces and washed in PBS. Separately, the rat skin was tied to two slides. One slide was fixed to the top of the wooden platform, while another slide was tethered to the right side of the balance. After that, the left and right-side pans were balanced by the addition of extra weights to the left-side pan. Approximately 1g of selected nano emulsion-loaded placebo gel, optimized DTB loaded nanoemulgel, and 0.5% carbopol gel formulations were placed in between two glass slides containing hairless rat skin, and the excess weight was removed from the left side pan to sandwich the two slides containing skin and remove the entrapped air between them by applying pressure and then it was kept in the same position for 5min, then water was added slowly to the left pan until the slides separated. The weight (gram force) of the added water was calculated and noted as bio adhesive strength. It was calculated using the below equation 3 [30].

$$\text{Bioadhesive strength} = \text{Weight required (g)} / \text{Area (cm}^2) \qquad \text{(eq.3)}$$

5.7 *In- vivo* studies

5.7.1 Skin irritation study

The experiment was conducted after obtaining prior approval from the Institutional Animal Ethical Committee (IAEC) under Protocol No. IAEC/RES/31/04. The Healthy Sprague-Dawley rats were taken from central animal facility (CAF), BITS-Pilani, Pilani Campus, Rajasthan, India. One day before the beginning of this experiment, the hair on the rat's dorsal side of the skin was removed with a shaver. The rats were divided into five groups (n=3). Group I; Untreated group, Group II; Free DTB loaded gel- FDG (200mg from 0.05% gel), Group III; optimized DTB loaded nanoemulgel (200mg from 0.05% gel), Group IV; Placebo emulgel (200mg from 0.05% gel), Group V; received 5% SLS gel. Finally, application areas were visually examined for erythema. Erythema severity was measured using the following scale, with scores ranging from 0 to 4. 0; no erythema, 1; Mild (barely perceptible light pink), 2;

Severe (dark pink), 3; Mild to severe (light red), 4; Severe (extreme redness), and the images were taken at 0, 6, 12, 24, 48, and 72 h intervals [31,32]

At the end of the 24 h, all of the animals were sacrificed. The skin biopsy (1 cm^2) samples were stored in a 10% formalin solution for 48 h before being processed for histopathology studies. The specimens were prepared according to the Bancroft developed protocol [33].

5.7.2 Assessment of the anti-inflammatory effect

The adjuvant-induced arthritis (AIA) model in rats was used to assess the optimized nanoemulgel therapeutic effect for RA. Rats weighing 150-250 g were divided into six groups at random. The following details were provided for each group: Group I; AIA (Positive control), Group II; received marketed formulation diclofenac -MFD (0.5 g/kg), Group III; received optimized nanoemulgel (200 mg containing 100µg dose), Group IV; received an Placebo emulgel, Group V; received FDG (200 mg containing 100µg dose), Group VI; normal group (Negative control) and 0.1 mL of Complete Freund's Adjuvant (CFA) was injected to hind paw of rats except group VI. The volume of hind paw was measured using a water plethysmometer at 0, 0.5, 1, 2, 3, 6, 9, 12, 15, 18, 21, 24, and 27 days after CFA injection, at the pinnacle of the swelling region of the joint was treated with respective formulations (from the day 5). The effectiveness of the anti-inflammatory treatment was evaluated by swelling degree using the following equation 4 [34].

$$\text{Swelling degree (\%)} = (V_t - V_n) / V_n * 100 \qquad \text{(eq.4)}$$

Where, V_n - paw volume before the injection of CFA; V_t - paw volume at the t day

5.7.3 Assessment of arthritis from physical parameters

During the test period, between 0 and 27 days, the rats body weight (% increase in body weight) and arthritis scores (based on visual inspection were recorded every 3 days were noted [35].

5.7.3.1 Nociceptive threshold

The nociceptive threshold was determined using Eddy's hot plate method [34]. The rats were acclimatized 3 days before the experiment. For all animals, the pain threshold was determined by the paw withdrawal latency to radiant heat stimuli (paw withdrawal) with a maximum cut-off time of 15s.

5.7.3.2 Motor incoordination test

The motor co-ordination test was performed on arthritis rats treated with topical optimized nanoemulgel formulation using an accelerating rota rod [36]. Rats were positioned on the rotating rod of the apparatus, and the time it took for each rat to fall from the roller was noted. Prior to the data collection day, all the animals were acclimatized to the accelerating rota rod over three training sessions. The test was conducted on the 0, 0.5, 1, 2, 3, 6, 9, 12, 15, 18, 21, 24, and 27 days of the arthritis study. Each animal in each group had three trials at 10 min time intervals, and the fall time was recorded.

5.7.3.3 Storage stability

The formulations are studied to determine physical and chemical characteristics. Formulated emulgel of DTB is kept at 25° c for span of 15days, 1 month and 2month. PS integrity and assay is determined by Zetasizer and validated HPLC method.

5.7.3.4 Statistical analysis

Each experiment was repeated three times, and the results are provided as the mean ± SD. Statistical analysis was executed using two-way ANOVA followed by sidak's multiple comparison tests estimated using GraphPad prism (v 7.0), p values <0.05.

5.8 Results and Discussion

5.8.1 Formulation optimization by QbD

5.8.1.1 Identification of quality target product profile and critical quality attributes

After identifying the QTPP, the QbD method for nanoemulgel preparation was developed. Table 5.2 shows the QTPP was selected for DTB-loaded nanoemulgel. The CQAs were preferred over the QTPP because they were explored to affect the final product characteristics. Table 5.3 shows that PS, EE, and drug release were identified as CQAs of DTB-loaded nanoemulgel and have more impact on product quality.

Table 5.2 The quality target product profile of dasatinib loaded nanoemulgel.

Quality target product profile	Target	Critical quality attributes	Justification
Dosage form	Nanoemulgel	NA	To enhance the permeation of dasatinib
Route of administration	Topical	NA	Enhance the DTB concentration at targeted site without systemic side impacts
Dosage strength	0.05%	NA	To select the minimum effective dose
Stability	At least 3 months stability at room temperature	Yes	Effect the product quality
Particle size (nm)	< 200	Yes	Enhance the drug permeation through skin barriers
Polydispersity index (PDI)	< 0.3	Yes	perfectly uniform size distribution leads to uniform release, permeation, and drug loading in nanoparticles
% Entrapment efficiency (% EE)	>90	Yes	Greater entrapment leading to higher drug loading with less lipid concentration
***In-vitro* drug Release profile**	Sustained	Yes	Increased activity time without systemic exposure
pH	5.5	Yes	Affect the physiochemical stability and mimic with physiological pH leads to reduce the skin irritation
Solubility	Maximum	Yes	Impact the drug permeation
Note: NA- Not applicable			

Table 5.3 Critical quality attributes of dasatinib loaded nanoemulgel.

Critical Quality Attributes	Related to critical material attributes	Related to critical process parameters	Failure mode	Justification
Particle size (PS)	Concentration of S_{mix} and lipid	Change in homogenization speed and time	Entrapment, loading efficiency, drug release and skin permeation of the drug	• Increase in concentration of lipid increases size resulting in decrease in release and permeation. • Increase in speed and time of homogenization and concentration of S_{mix} decreases size, entrapment and loading efficiency
Entrapment efficiency (EE)	Concentration of S_{mix} and lipid	Change in homogenization speed and time	Loading efficiency, size, drug release and skin permeation	• Increase in concentration of lipid and S_{mix} increases entrapment resulting in decrease in drug release and permeation (due to lipid portion effect) • Increase in speed and time of homogenization decreases entrapment, loading efficiency
Drug release	Concentration of S_{mix} and lipid	Change in homogenization speed and time	Poor therapeutic effect	• Increase in concentration of lipid and S_{mix} increases size and lipid matrix resulting in decrease in drug release and permeation. • Increase in speed and time of homogenization increases release due to the decreased size (indirect effect)

5.8.1.2 Risk identification and risk assessment

The risk assessment was conducted, and CPPs and CMAs were identified using the ishikawa

diagram shown in Figure 5.2. Based on reported studies and preliminary results, REM was

formulated. The RPN scores were assigned in FMEA based on the risk potentiality; the scores

were given based on reported studies. Table 5.4 shows the risk estimation matrix and RPN scores of the CMAs and CPPs. RPN scores > 125 are considered as vital for optimizing critical attributes. The lipid and S_{mix} concentrations can influence the drug loading and PS of emulsion, which can affect the drug permeation and efficacy of the formulation, and are hence considered as high-risk parameters. Further, homogenization speed and time were considered as potential risk factors, as they may affect PS and uniformity of particle distribution.
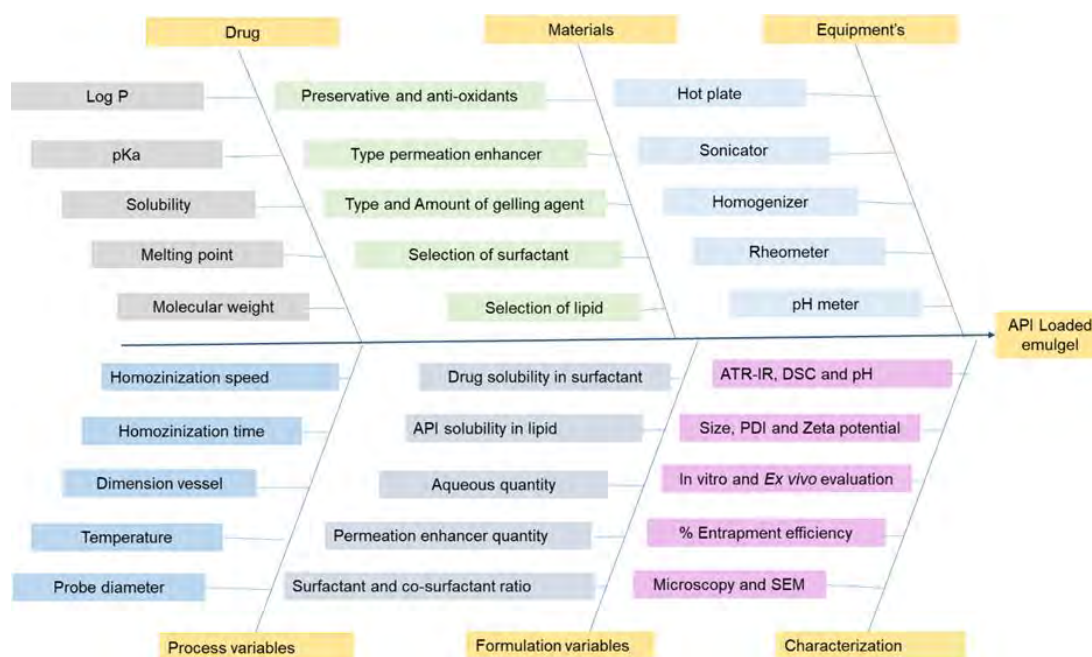
Figure 5.2 Ishikawa diagram illustrated the potential critical material attributes and critical process parameters that effect the critical quality attributes of dasatinib-loaded nanoemulgel formulation.

Table 5.4 Risk estimation matrix for initial risk assessment and failure mode effects analysis score based on qualitative analysis of different material attributes and process parameters.

Critical material attributes and critical process parameters	Critical quality attributes			Failure mode effects analysis			
	PS	EE	Drug Release	Severity	Detectability	Occurrence	RPN Score
Amount of Lipid	High	High	High	8	6	6	288
S$_{mix}$ concentration	High	High	High	8	5	6	240
Co-solvent	Medium	Medium	Medium	5	3	4	60
Permeation enhancer	Medium	Medium	Medium	5	3	4	60
Homogenization Time	High	High	Low	6	5	5	150
Homogenization speed	High	High	Low	7	5	5	175
Process temperature	Low	Medium	Low	4	3	2	24

5.8.1.3 Factor screening studies

CMAs from risk assessment were used in the screening studies to analyze the interaction between factors and responses. For formulation screening, a two-level factorial design (Design-Expert 7.0.0) with eight formulations was used with four factors at low- and high-level concentrations. The suggested amounts of lipid, co-solvent, permeation enhancer, and S_{mix} concentration were investigated. Eight batches were carried out in accordance with the design, as shown in Table 5.1. Formulations were designed by varying independent variables while carrying all other parameters constant (process and formulation parameters). PS, EE, and drug release were investigated as dependent variables. The concentrations of the preservatives such as methyl paraben and propyl paraben used were 0.5% and 0.05% (w/w), respectively, and the anti-oxidant sodium metabisulphate (0.2%) remained constant across all formulation trials. Table 5.5 shows the response values obtained after implementing a two-level factorial design with four factors and two levels. The interaction and efficiency of the factors against the responses were represented in the form of a pareto chart, as seen in Figure 5.3.

Table 5.5 Responses of experimental trails performed using two-level factorial design.

Formulation code	Size (nm)	% Entrapment	% Drug release (24h)	PDI
DF1	546.97 ± 48.9	96.25 ± 0.5	69.80 ± 3.30	0.401 ± 0.02
DF2	311.70 ± 19	88.44 ± 0.21	86.30 ± 1.80	0.280 ± 0.01
DF3	2055.00 ± 19	92.70 ± 0.23	55.10 ± 3.60	0.380 ± 0.07
DF4	559.00 ± 80	93.32 ± 0.11	46.97 ± 2.50	0.655 ± 0.03
DF5	223.00 ± 15.13	89.97 ± 0.18	90.58 ± 3.30	0.141 ± 0.07
DF6	620.00 ± 21.35	92.28 ± 0.23	84.00 ± 3.00	0.883 ± 0.16
DF7	3054.00 ± 40	91.50 ± 0.32	49.10 ± 6.50	0.412 ± 0.05
DF8	1345.00 ± 380	91.28 ± 0.53	57.20 ± 5.80	0.724 ± 0.06
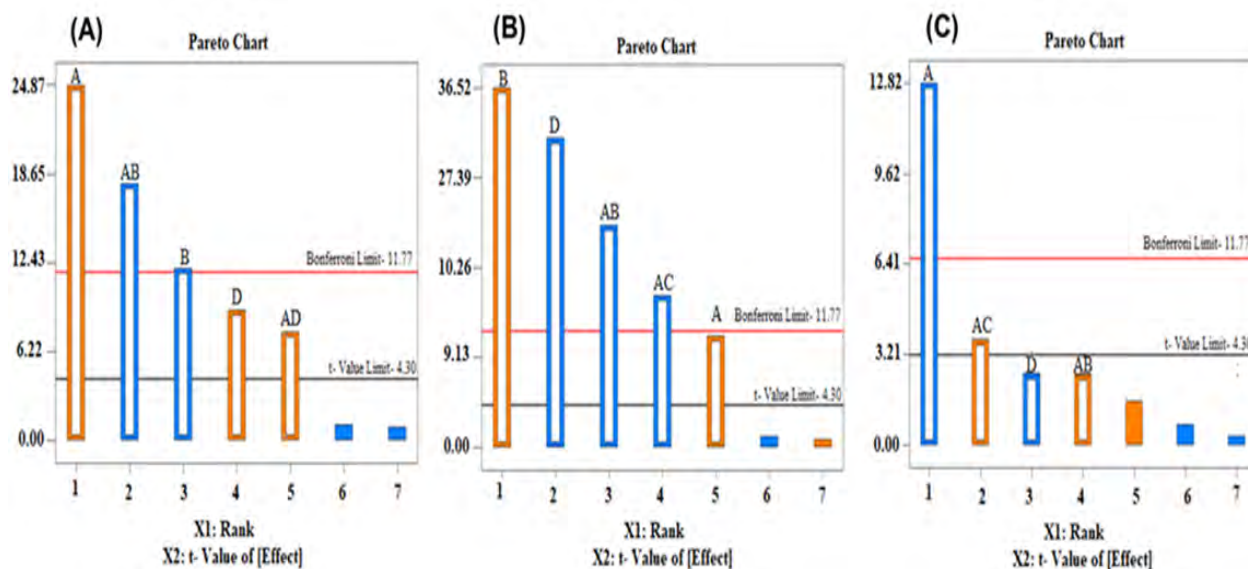
Figure 5.3 Pareto chart representation for two-level factorial design depicting the interaction and efficiency of the factors against the responses. (A) Size; (B) Entrapment; (C) Drug release.

*Note: A=Lipid, B=Surfactant, C= Isopropyl myristate, D= Transcutol P.

5.8.1.4 Factor optimizing studies

The report resulting from the screening studies finalized various CMAs, such as lipid and S_{mix}, as well as CPPs, such as homogenization time and speed, based on the risk assessment report. PS and EE are considered as CQAs in the responses. For formulation optimization, a CCD with 17 formulations was keyed with four factors and three levels using DoE. This suggested quantity of lipid, S_{mix} concentration, homogenization speed, and time were investigated at three levels: low, medium, and high. In accordance with the design, 17 formulations were prepared. The runs and response values obtained after the design was shown in Table 5.6. Formulations were developed by varying independent variables while carrying all other parameters constant (process and formulation parameters), PS and EE were studied as response variables. The concentrations of co-solvents, permeation enhancers, preservatives, and antioxidants used in all formulations were constant. ANOVA was used to assess the model efficiency and the significance of the selected input variables. The general characterization studies for the 17 trails were represented in Table 5.7. The respective microscopy images were shown in the Figure 5.4.

Table 5.6 Experimental trails executed using CCD with respective results.

Formulation Code	Factor1 A: Lipid Base (%)	Factor 2 B: S_{mix} (%)	Factor 3C: Homogenization Speed (RPM)	Factor 4D: Homogenization Time (min)	Response 1 Size (nm)	Response 2 EE (%)	PDI
CF1	5	3	10,000	15	186.03 ± 1.70	87.87 ± 0.16	0.157 ± 0.009
CF2	6	4	15,000	5	310.70 ± 3.63	84.31 ± 0.25	0.358 ± 0.033
CF3	5	4	10,000	10	312.27 ± 2.84	86.30 ± 0.13	0.304 ± 0.010
CF4	4	4	5000	15	222.47 ± 5.48	86.95 ± 0.10	0.294 ± 0.021
CF5	6	2	5000	15	181.30 ± 10.54	84.53 ± 0.13	0.292 ± 0.050
CF6	6	2	15,000	15	193.53 ± 8.0	84.92 ± 0.63	0.343 ± 0.023
CF7	4	4	15,000	15	163.77 ± 3.93	91.21 ± 0.10	0.231 ± 0.012
CF8	4	2	5000	5	271.23 ± 47.89	88.64 ± 0.44	0.416 ± 0.114
CF9	6	4	5000	5	1782.53± 770.61	95.23 ± 0.24	0.952 ± 0.083
CF10	6	3	10,000	10	445.13 ± 147.90	90.09 ± 0.05	0.549 ± 0.135
CF11	5	3	5000	10	374.37 ± 2.87	91.02 ± 0.06	0.348 ± 0.032
CF12	5	3	10,000	10	308.77 ± 2.15	89.81 ± 0.18	0.284 ± 0.033
CF13	5	3	15,000	10	275.77 ± 4.44	89.71 ± 0.31	0.282 ± 0.027
CF14	5	3	10,000	5	322.90 ± 1.35	91.85 ± 0.42	0.273 ± 0.029
CF15	4	2	15,000	5	300.37 ± 1.50	86.53 ± 0.21	0.244 ± 0.011
CF16	5	2	10,000	10	314.67 ± 2.24	84.38 ± 0.61	0.317 ± 0.023
CF17	4	3	10,000	10	297.40 ± 3.48	93.30 ± 0.40	0.313 ± 0.045
CF18	4	3	15,000	7	172.53 ± 3.33	95.11 ± 0.16	0.160 ± 0.014

Table 5.7 General characterization of prepared formulation.

| Code	Viscosity (mPaS)	Phase separation	Dilution test	Microscopy For crystal growth
CF1	10.77 ± 0.76	No	No Phase separation	No
CF2	30.65 ± 5.20	Yes	Phase separation	No
CF3	31.15 ± 4.69	Yes	Phase separation	No
CF4	9.86 ± 4.32	No	No Phase separation	No
CF5	52 ± 6.51	No	No Phase separation	No
CF6	70 ± 5.65	Yes	Phase separation	Yes
CF7	8 ± 0.60	No	No Phase separation	No
CF8	9.56 ± 3.21	Yes	Phase separation	No
CF9	8.29 ± 2.85	Yes	Phase separation	No
CF10	9.05 ± 2.45	Yes	Phase separation	No
CF11	10.69 ± 1.99	No	No Phase separation	No
CF12	7.7 ± 2.88	No	No Phase separation	No
CF13	10.13 ± 3.05	No	No Phase separation	No
CF14	11.14 ± 0.74	No	No Phase separation	No
CF15	11.52 ± 1.02	No	Phase separation	Yes
CF16	11.31 ± 1.12	No	Phase separation	Yes
CF17	14 ± 3.74	Yes	No Phase separation	Yes
CF18	10.77 ± 0.76	No	No Phase separation	No
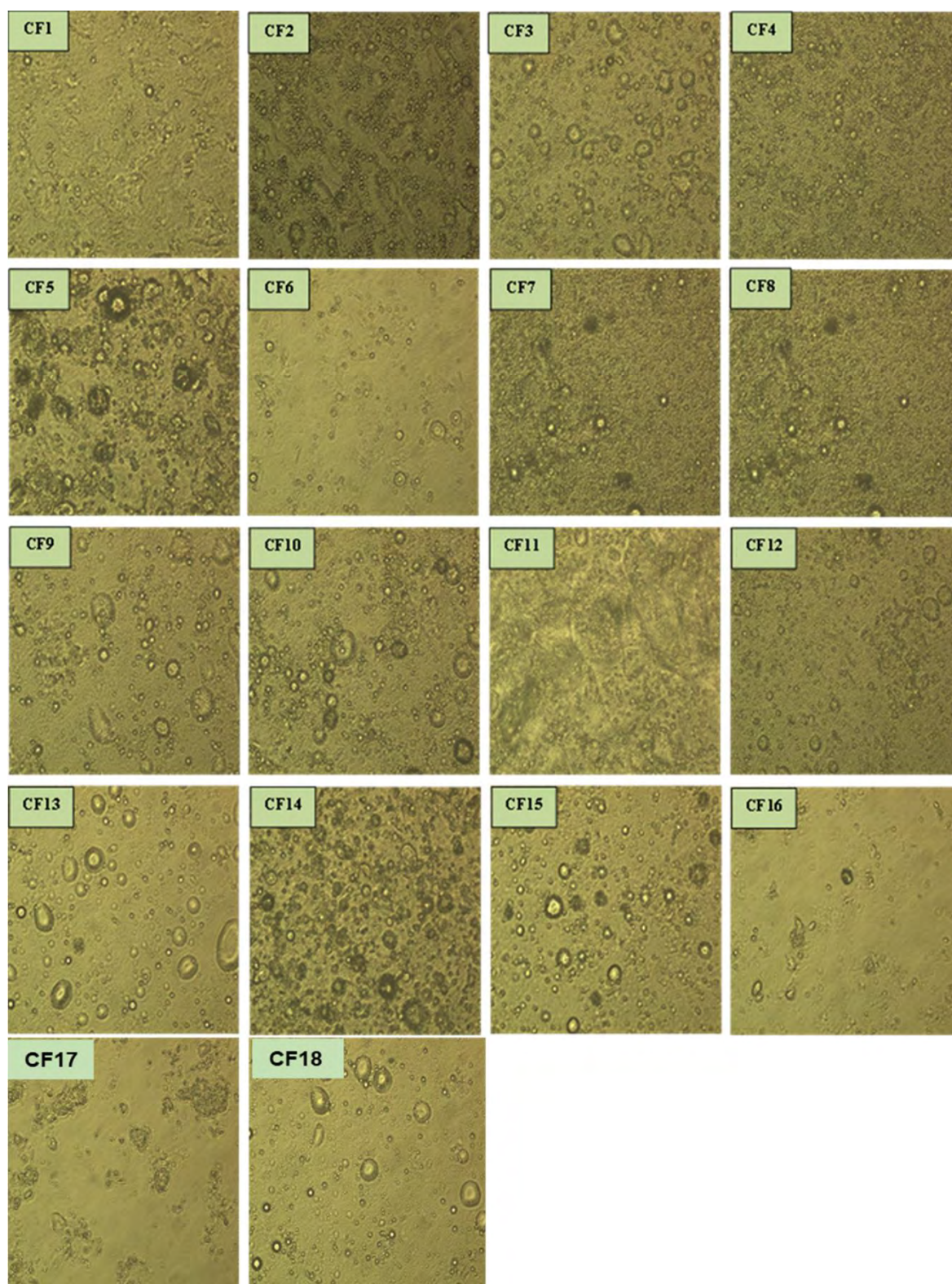
Figure 5.4 Microscopy images of different emulsion formulations for crystal growth observation (40x).

5.8.1.5 Independent variables effect on particle size

The PS of the DTB-loaded nanoemulsion after 17 trials were in the range of 163.77–1782.53 nm, as shown in Table 5.6. The quadratic model has a 229.45 F-value, indicating its significance. Figure 5.5 A, & 5.5 B demonstrate the contour plots and three-dimensional plots of the response variable, PS. When compared to the pure error, the lack of fit was found to have a F-value of 2, which indicates its insignificance. The coded values of chosen independent variables are depicted in RE (5).

Size $= 271.12 + 145.00$ A $- 1.20$ B $- 40.33$C $- 68.43$D $+ 21.48$AB $- 30.70$AC $- 44.77$AD $- 344.55$ BC $- 191.84$BD $+ 322.59$ CD $+ 205.15$A^2 $+ 48.62$B^2 $+ 60.22$C^2 $- 10.38$D^2 $\qquad$ (eq.5)

The collusive effect is represented by the positive symbol in the regression equation, which denotes an increase in response value with respect to the corresponding input variable. The hostile effect is represented by the negative symbol in the RE, which indicates a decrease in response value with the corresponding input variable. The lack of fit suggests dissimilarity in the best fit model's data and allows the model fitting of experimental results to be competent. The model's best fit is indicated by an insignificant lack of fit in the experimental results. The RE (5), represents the increase in PS as lipid concentration increases. The PS was reduced with an increase in % S$_{mix}$ concentration, homogenization time, and speed. The S$_{mix}$ has the potential to reduce surface tension at the oil–water interface and improve particle stabilization, resulting in smaller particles. The increased speed and time of homogenization, reduces the PS of the formulation, breaking the large particles into smaller size particles.

Figure 5.5 Central composite design optimization graphs illustrating the effect of independent variables on particle size. (A) The contour plot graph of factors effecting particle size; (B) The three-dimensional graph of factors effecting particle size.

5.8.1.6 Effect of independent variables on entrapment efficiency

The average EE of the DTB-loaded emulsion after 17 formulations was in the 84.31–95.23% range, as shown in Table 5.6. The quadratic model's F-value of 711.82 indicates the model's significance. Figure 5.5 C & 5.5 D revealed the contour plot and three-dimensional graph of the response variable EE. The lack of fit was insignificant, with a 2.21 F-value compared to the pure error. The RE (6), depicts the coded values of chosen independent variables.

Entrapment $= 89.89 - 1.60A + 0.96B - 0.77C - 1.99D - 0.86AB - 1.84AC - 0.42AD - 0.37BC - 1.31BD + 2.46CD + 1.80A^2 - 4.56B^2 + 0.46C^2 - 0.037D^2$ (eq.6)

The eq. (6) represents the increase in entrapment with an increase in concentration of lipid and S_{mix}. The reduced EE was observed as the homogenization time and speed increased. The lipid and S_{mix} concentrations increase drug solubility, which leads to an increase in EE. Increased homogenization time and speed decreases the entrapment, as expected due to drug expulsion during the formulation's breakage of micro particulates into nano size particles.
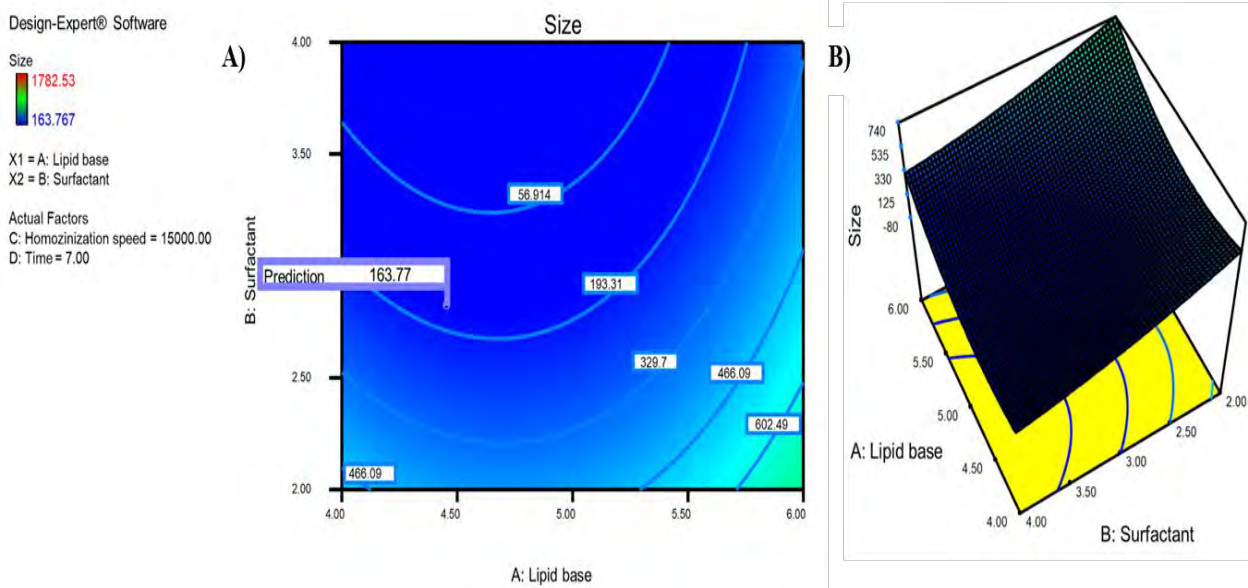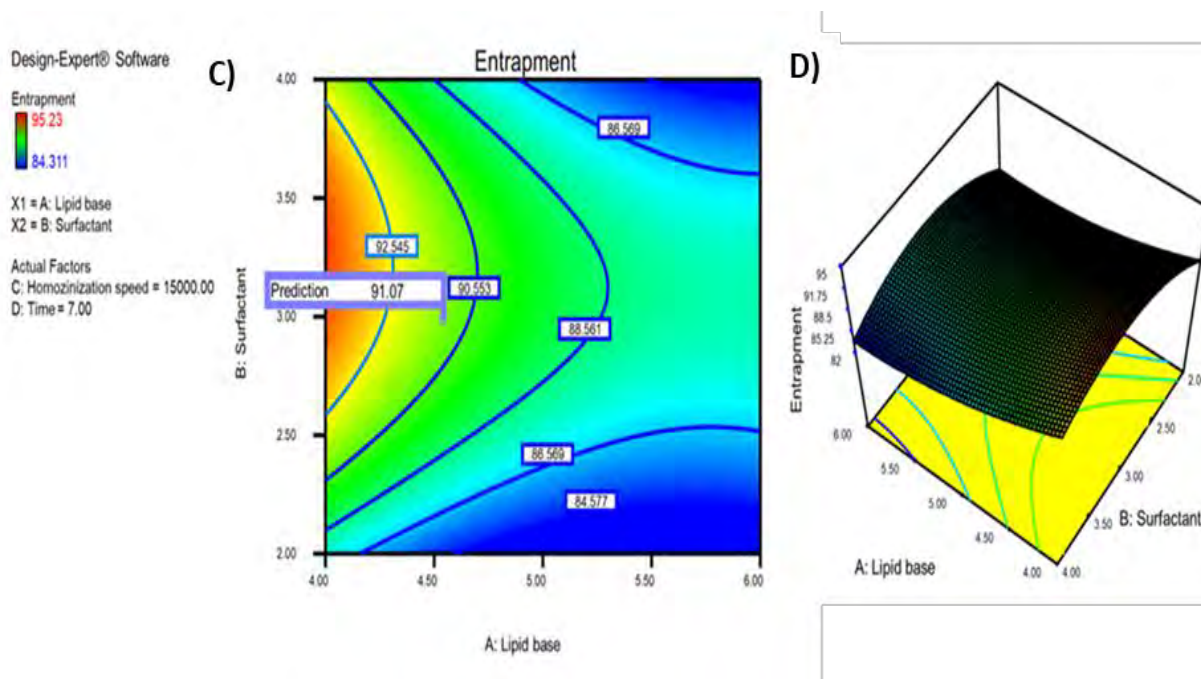
Figure 5.5 Central composite design optimization graphs illustrating the effect of independent variables on entrapment efficiency. (C) The contour plot graph of factors effecting on encapsulation efficiency; (D) The three-dimensional graph of factors on effecting encapsulation efficiency.

5.8.1.7 Validation of the design to select optimized batch

The numerical and desirability methods were used to optimize the DTB-loaded emulsion. The goal was to find the formulation with the best EE and smallest PS. Table 5.6 illustrates a summary of the requirement criteria that must be met in order to attain the anticipated response. The Design-Expert software produced 27 solutions, and the one with higher desirability close to 1 was picked for preparing the DTB loaded nanoemulsion (CF18 emulsion) as shown in the Table 5.8. The design was validated using the following formulation with lipid content (4%), S_{mix} concentration (3%), homogenization speed (15,000 rpm), and time (7 min). The formulation's mean PS was 172.53 ± 3.33 nm, with a PDI of 0.160 ± 0.014. The EE of the optimized formulation was found to be 95.11 ± 0.16 percent. The formulation's percent drug release was greater than 89.90 ± 6.25 in 12 h, which represents a sustained release profile. The predicted values of EE and PS were close to the actual value, indicating the desirability of the design. Figure 5.6 A & 5.6 B depicts the desirability graphs and three-dimensional surface

graphs of PS and EE for optimized formulation, and this same formulation was carried out for the scale-up studies.

Table 5.8 Optimized emulsion formulation (CF18 emulsion).

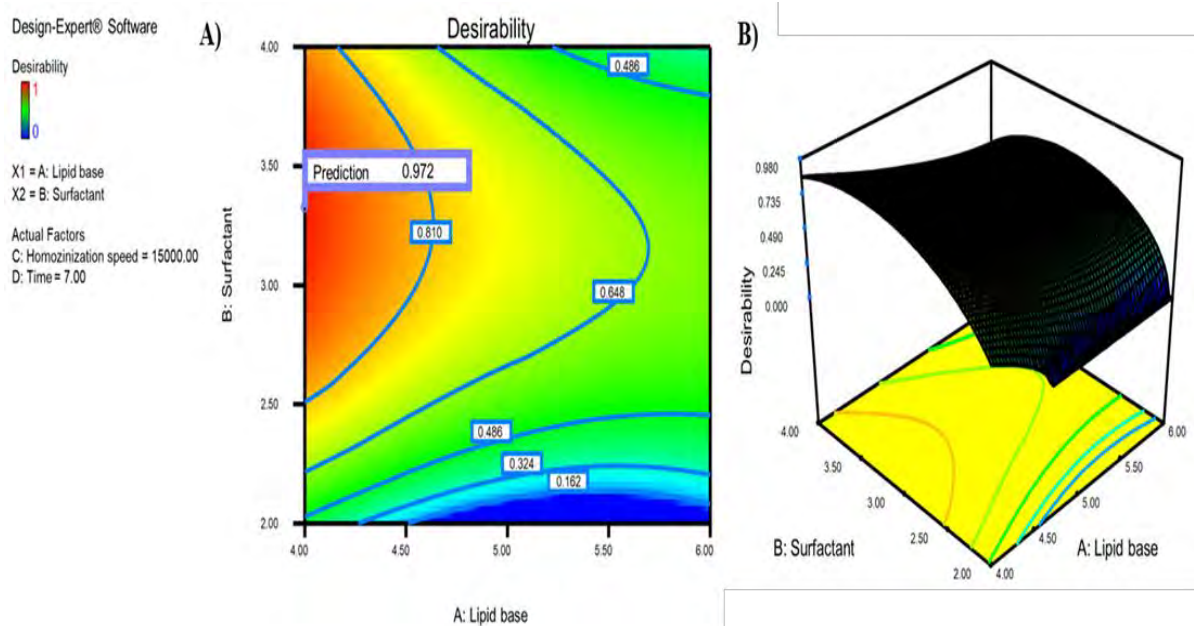| Ingredients	CF18
Dasatinib	0.01
Peceol + geleol (7:3)	1.00
Labrasol + capryol (2:1)	0.60
Transcutol P	0.50
Isopropyl myristate	0.50
Methyl paraben	0.10
Propyl paraben	0.01
Sodium metabisulfite	0.04
Aqueous phase	17.20
Total weight (g)	20.00
Homogenization speed (RPM)	15000
Homogenization time (min)	7

Figure 5.6 Central composite design desirability graphs illustrating factors against desirability value. (A) The contour plot graph; (B) The three-dimensional graph.

5.8.2 Scale-up studies

The optimized nano emulsion (CF18 emulsion) was selected for the scale up studies. The batch sizes of 20, 50, and 100 mL were formulated using the design space suggested parameters. The

formulation compositions remained unchanged, but the amount of lipid and S_{mix} concentrations were increased with respect to batch size. In the process parameters, the homogenization speed was constant for three batches, but the processing time was increased by 2 min (total 9 min) for 100 mL batch formulation. The 20 mL and 50 mL batch sizes were prepared, as per the design space suggested time (7 min). Additionally, the vessel diameter played a vital role in the size reduction process during homogenization. Thus, the homogenization time was adjusted according to the batch size, and also a suitable vessel size was selected with respect to the individual bath size.

5.8.3 Characterization of emulsion

5.8.3.1 Attenuated total reflection infrared spectroscopy (ATR-IR)

The IR spectra of DTB, optimized placebo nanoemulsion (CF18P emulsion), and CF18 emulsion are shown in Figure 5.7. The characteristic peaks of DTB were found to be 1498.59 cm^{-1}, 1581.11 cm^{-1}, 1624 cm^{-1}, 3229.9 cm^{-1}, and 3402.12 cm^{-1} for C–H, C–C, C=O, O–H, and N–H (secondary amine N-H stretch), respectively. The distinct DTB peaks vanished in the CF18 emulsion, and the peaks that remained matched the CF18P emulsion. This indicates that the pure drug was entrapped within the lipid matrix, resulting in the loss of drug characteristic peaks.
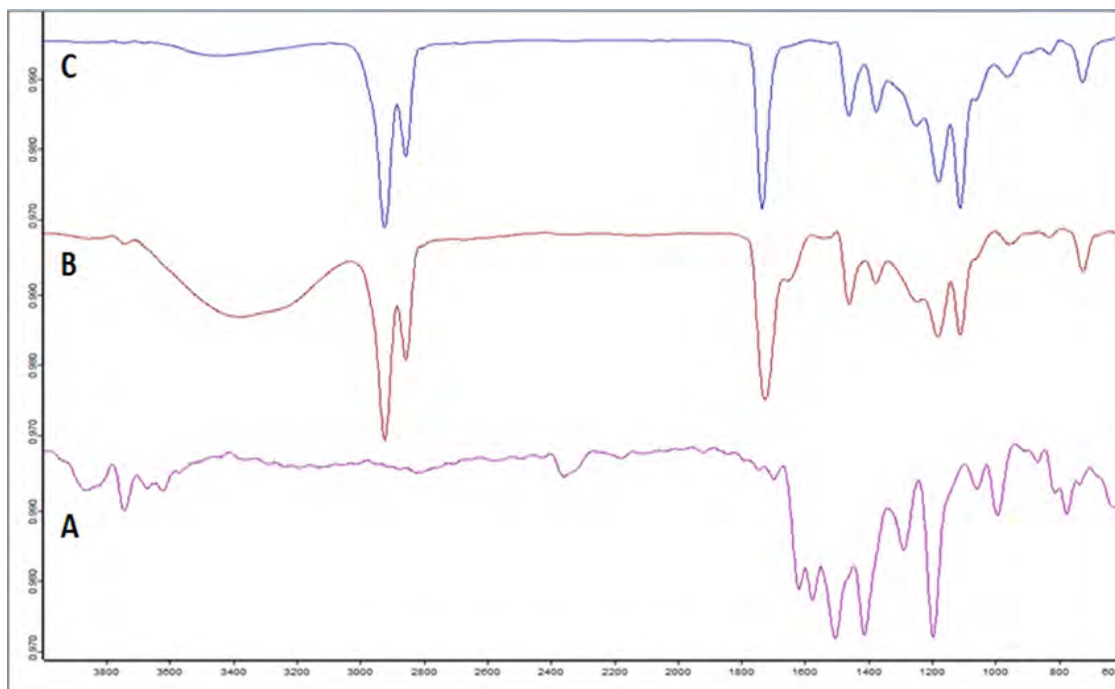
Figure 5.7 ATR-IR peaks of (A) Dasatinib; (B) CF18placebo emulsion; (C) CF18 emulsion.

5.8.3.2 Measurement of size, polydispersity index (PDI), and zeta potential (ZP)

The PS of the three formulations were 172.53 ± 3.33 nm (0.160 ± 0.014 PDI), 167.90 ± 10.68 nm (0.225 ± 0.121 PDI), and 154.90 ± 11.09 nm (0.30 ± 0.07 PDI), respectively, for batches of 20, 50, and 100 mL. The average ZP of the optimized formulation was -57.233 ± 4.97 mV, and the ZP ranging from 40 to 60 mV is considered to be stable. ZP was 40–60mV, which reduces particle coalescence/aggregation [37]. For 20, 50, and 100mL batches, EE was $95.11 \pm 0.16\%$, $95.25 \pm 0.245\%$, and $95.42 \pm 0.18\%$, respectively. According to the findings, all batches were found to have similar characteristics. The reported studies suggest that the PS of nano formulation less than 200 nm exhibit improved permeation [38]. A PDI less than 0.300 indicates that the formulation is uniform.

5.8.3.3 Morphology by field–emission scanning electron microscopy (FESEM)

The particles were found to be evenly distributed and of uniform size in the morphological study. The formulation morphology was observed to be spherical and in the 140–200 nm range Figure 5.8. Additionally, they were non-aggregated, spherical, and had a smooth, flexible

boundary, demonstrating their stability against ostwald ripening due to specific collapse particles.
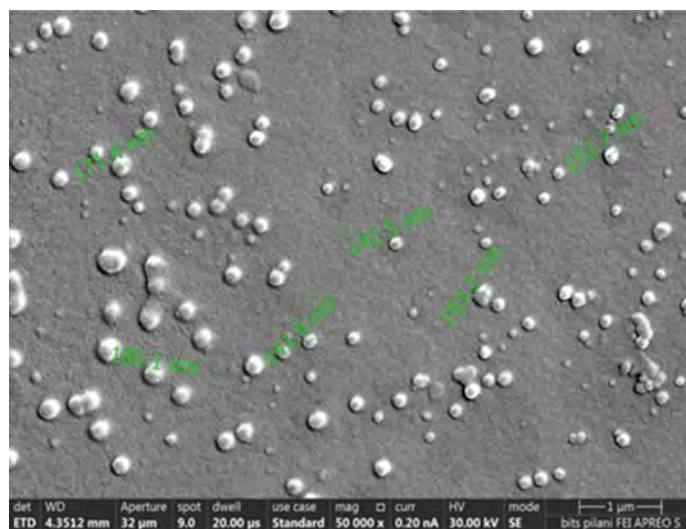
Figure 5.9 FESEM image of optimized emulsion (CF18 emulsion).

5.8.3.4 Thermodynamic stability study

The prepared emulsion was evaluated for thermodynamic stability and found to be stable when subjected to centrifugation and a freeze–thaw cycle. As a result of centrifugation and a freeze–thaw cycle, the nanoemulsion showed no signs of drug precipitation or creaming/cracking. Thus, this indicated its stability.

5.8.3.5 *In-vitro* drug release studies

The *in-vitro* release study of all three batches of 20, 50, and 100 mL CF18 emulsion and FDS were performed for up to 24 h, represented in Figure 5.9. Within 4 h, the FDS was found to show 100% drug release. The drug-loaded emulsion has shown drug release for up to 24 h. The drug release for 20, 50, and 100mL batches after 6 h were around 56.78 ± 4.71%, 42.63 ± 4.27%, and 51.50 ± 5.30%. After 12 h, the release was 93.50 ± 6.25%, 87.64 ± 1.22%, and 88.71 ± 2.62%; after 24 h, the release was 103.40 ± 0.98%, 95.31± 0.39%, and 95.93 ± 1.73%, respectively. All CF18 emulsion batches illustrated sustained release patterns with no significant variation. The *in-vitro* release profiles of the drug from all three batches (20, 50, and 100 mL) followed the Hixson Crowell model because the plots seemed to have the highest

R^2 values, i.e., 0.9912, 0.9710, and 0.9809, respectively. The obtained values were shown in Table 5.9. The model assumed that the rate of drug release is limited by dissolution and not diffusion, which indicates that the drug dissolved in the lipid might be responsible for the sustained release [39].
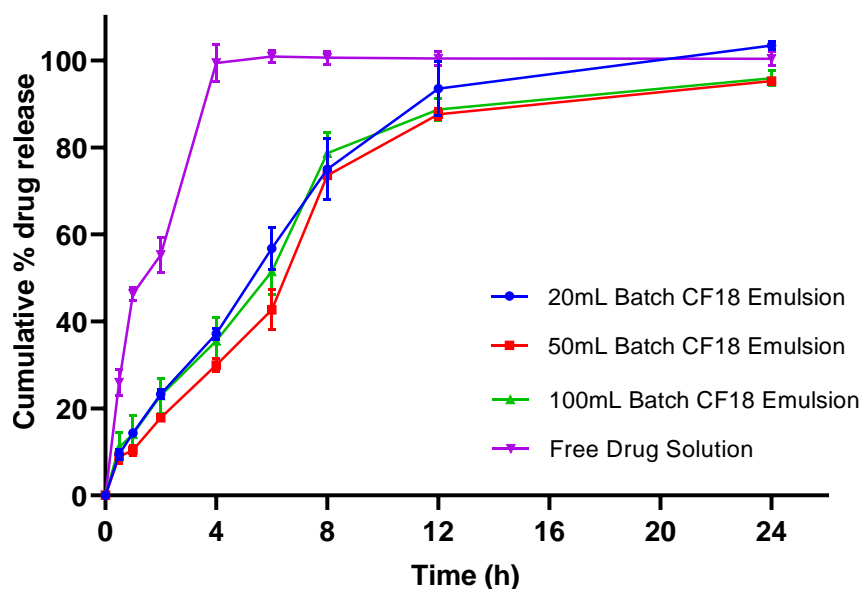
Figure 5.9 *In-vitro* comparative drug release profile of CF18 emulsion (20, 50 and 100 mL) and free drug.

Table 5.9. Release kinetics data of dasatinib loaded emulsion.

Batch Size (Ml)		Zero Order	First Order	Higuchi	Korsmeyer Peppas	Hixson Crowell
20	R^2	0.6900	0.9790	0.9430	0.9454	0.9912
20	AIC	75.6555	51.4332	60.4207	62.0220	43.5941
50	R^2	0.7266	0.9595	0.9064	0.9163	0.9710
50	AIC	73.6516	56.4597	64.0006	64.9945	53.4487
100	R^2	0.6329	0.9733	0.9239	0.9243	0.9809
100	AIC	76.2149	52.6162	62.0542	64.0076	49.5992

5.8.4 Nanoemulgel Characterization

5.8.4.1 Physical appearance, pH determination, spreadability, and drug content determination

The optimized DTB loaded nanoemulgel (CF18 emulgel) formulation had a milky white creamy appearance with a smooth homogeneous texture and excellent consistency Figure 5.10. Topical formulations should have a pH that is compatible with skin pH. A change in pH can irritate or disrupt the skin. Thus, pH of the formulation was adjusted to 5.5 ± 0.1 with 1% NaOH solution. The spreadability of the optimized nanoemulgel formulation and placebo was found to be 1.20 ± 0.003 cm^2.g^{-1} and 1.26 ± 0.05 cm^2.g^{-1}, respectively. No significant change was observed in drug-loaded formulation compared to the placebo gel. The drug content was found to be $98.25 \pm 1.2\%$.

Figure 5.10 CF18 emulsion and CF18 emulgel formulation.

5.8.4.2 Particle integrity in hydrogel matrix

The prepared CF18 emulgel was characterized for PS, and it was found to be similar to that of the emulsion, i.e., 170.01 ± 30.26 nm. Morphological analysis of the emulgel by using FESEM also showed similarity with that of the CF18 emulsion, as seen in Figure 5.11. Henceforth, the data revealed that the nanocarriers remain intact after being loaded into the carbopol ETD 2020 hydrogel matrix.
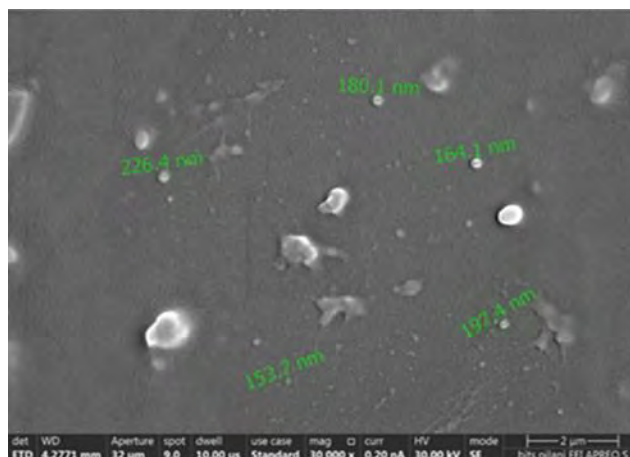
Figure 5.11 The FESEM image of CF18 emulgel.

5.8.4.3 Rheological behaviour

Viscosity

The average viscosity of the optimized formulation was determined to be 4580.13 ± 103.0232 mPa.S at a constant shear rate and at increasing time showing no significant change in viscosity. Hence, Newtonian behaviour of the gel is demonstrated, as shown in Figure 5.12.

Shear flow

The flow characteristics of the CF18 emulgel was conducted, and the results were shown in Figure 5.13. Here, the viscosity and shear stress varied with the function of shear rate. As a result, the formulation demonstrated non-Newtonian behaviour that corresponded to the Herschel-Bulkley model, equation (7).

$$\sigma = \sigma_0 + K \cdot \gamma \, n \qquad\qquad (eq.7)$$

where 'σ_0' represents yield stress, 'K' represents consistency index, and 'n' represents power index; $n < 1$. The viscosity decreased as the shear rate increased, indicating shear thinning and pseudoplastic behaviour of the CF18 emulgel.
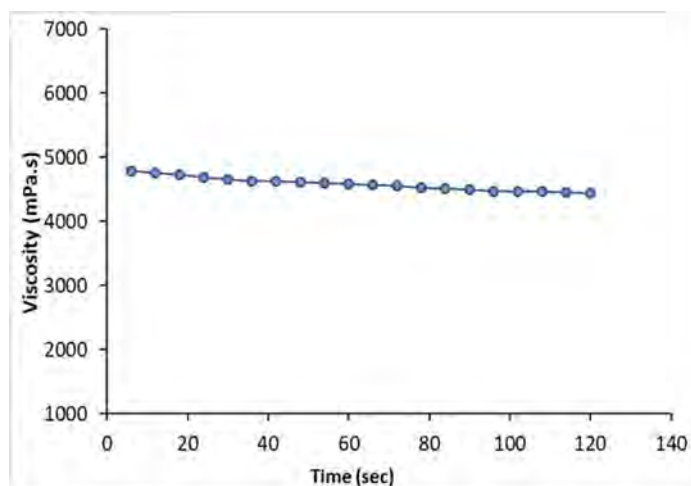
Figure 5.12 Viscosity of CF18 emulgel.
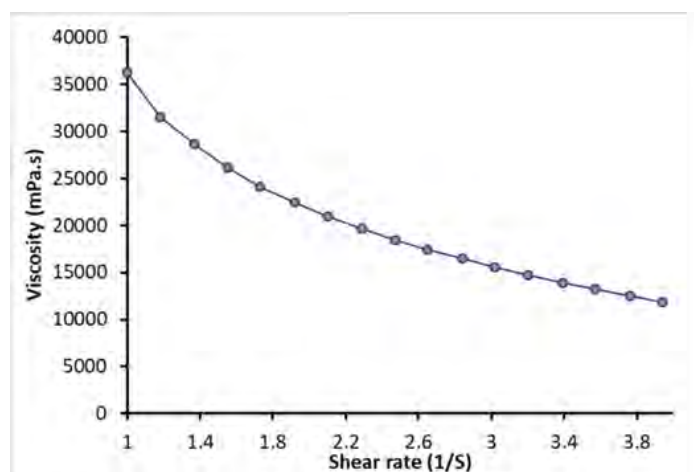
Figure 5.13 Shear flow of CF18 emulgel.

Strain sweep test

An oscillation strain sweep (OSS) test was used to find the LVR, in which the viscoelastic moduli change with time or frequency. The LVR ended with a 10% decrease (1.65%) in the storage modulus (G′) plateau value. Subsequently, the loss modulus (G″) started to go up. This meant that the viscoelastic properties might not extensively be independent of the strain amplitude, which indicates that the sample lost its original structure upon the function of oscillation strain (OS). The flexible long straight chain of polymers may form some coiling, which could lead to some degree of interlocking to reach a state with the least amount of energy. Furthermore, hydrogen bonding can also develop an infinite number of bridges between

neighbouring molecules, resulting in complete cross-linking. When OS was applied, polymeric chains uncoiled and aligned with the flow.

The polymeric chain state changed from disorderly to orderly, arranged during oscillation, and the transformation was reversible. In Figure 5.14, the values of log G′ and log G″ versus the logarithm of % strain showed that the LVR had a predominant elastic behaviour, indicating the strongest gel structure.
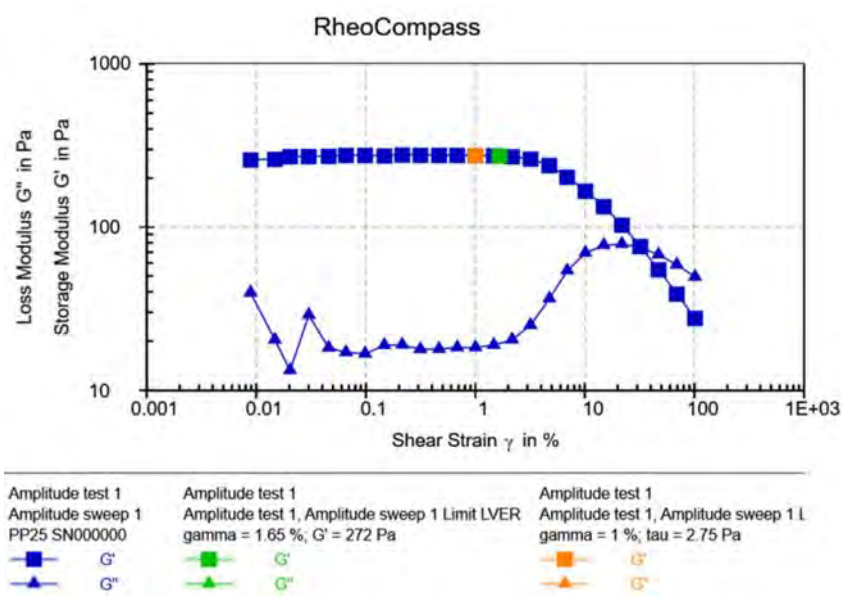
Figure 5.14 Amplitude sweep test of formulation employing angular frequency.

Frequency sweep test

When the gel's structural integrity is intact, frequency changes do not affect G′ and G″ [40]. Figure 5.15 A & B depicts the frequency distribution versus frequency logarithm. Elastic and viscous modulus were frequency independent in CF18 emulgel. G′ was greater than G″ across the frequency range, indicating strong gel structure.

To summarize the rheology, the viscosity study demonstrated an independent effect upon an incremental shear time at constant shear stress, indicating that the gel has an excellent consistency. The prepared emulgel showed a storage modulus greater than loss modulus G″ in frequency strain and frequency sweep tests, indicating a strong gel structure. The structural integrity of the gel formulation was indicated by the viscosity, frequency strain and frequency

sweep tests. In addition, increasing shear stress with time transformed the solid gel state to a flowable state (shear thinning behaviour), indicating spreadability. During topical application, the desired spreadability forms a thin layer on the skin's surface with improved bio-adhesive properties, resulting in sustained release with an enhanced therapeutic effect. Hence, it can be concluded that DTB nanoemulgel would be a viable option for the patient [41,42].
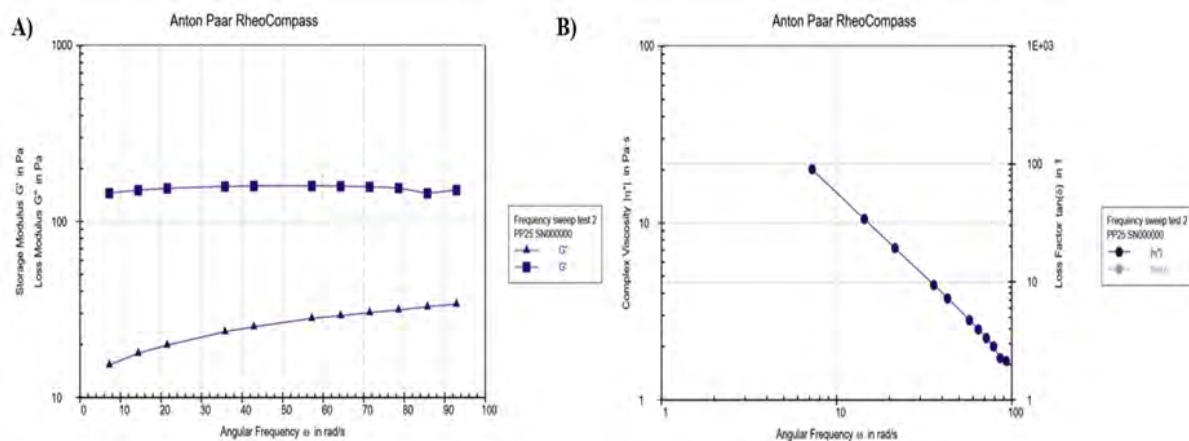
Figure 5.15 A) FST of CF18 emulgel (loss modulus and storage modulus); B) FST of CF18 emulgel (complex viscosity).

5.8.5 *In-vitro* cell line study

5.8.5.1 Cytotoxicity studies

The cytotoxicity test for free DTB and CF18 emulgel was performed on HaCaT cell lines. Keratinocytes were chosen because they account for 95% of epidermal skin cells. The cytotoxic effects of free DTB and CF18 emulgel dispersion on HaCaT cell lines are shown in Figure 5.16. DTB had no significant effect on keratinocyte cells. More than 50% cell viability was observed at a treatment of 1000 nM concentration of free DTB and CF18 emulgel. The findings demonstrated that different excipients used in formulations are not produce toxicity to keratinocyte cells.
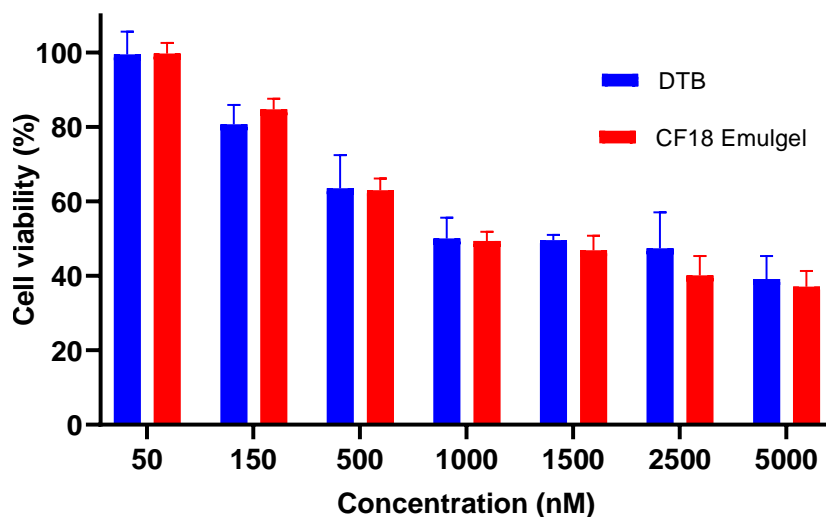
Figure 5.16 Cell viability study in HaCaT cell lines.

5.8.5.2 Effect on the production of TNF-α and IL-6

TNF-α and IL-6 plays a crucial role in the growth of fibroblasts and the induction of pro-inflammatory mediators including PGE2 and IL-1 during the pathogenesis of RA. As a result, it encourages synovitis and drives the destruction of bone and cartilage. As compared to free DTB, CF18 emulgel treatment significantly decreased the LPS-induced TNF-α production from RAW 264.7 cells, as depicted in Figure 5.17. The results suggested that the anti-arthritic properties of the CF18 emulgel may inhibit inflammatory cytokines such as TNF-α. Inhibiting TNF-α production is associated with decreased inflammation and cartilage deterioration, which can halt the progression of arthritis. Similarly, CF18 emulgel treatment resulting in the reduction of IL-6 compared free DTB as shown in the Figure 5.18.
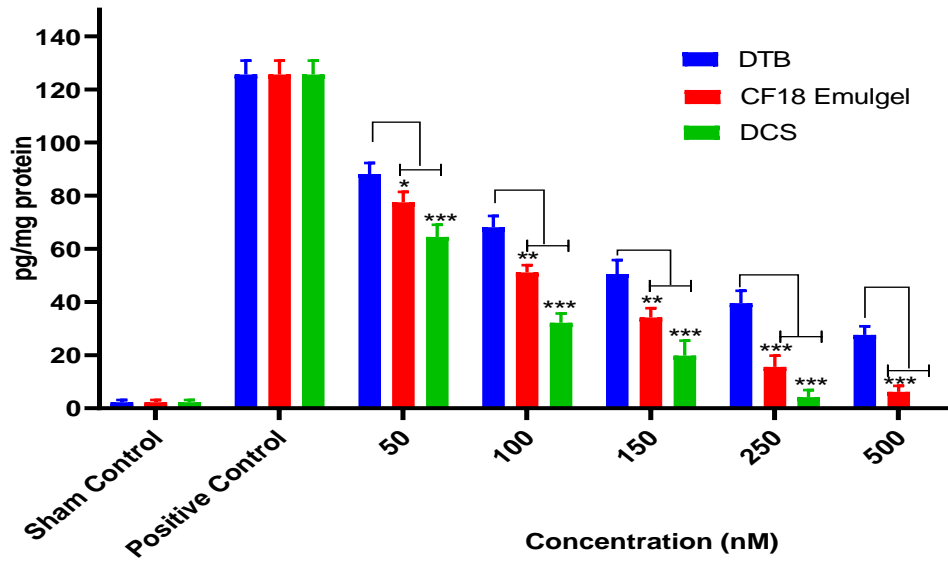
Figure 5.17 Effect on production of TNF-α expression level of dasatinib (DTB), CF18 emulgel and diclofenac gel (DCS).
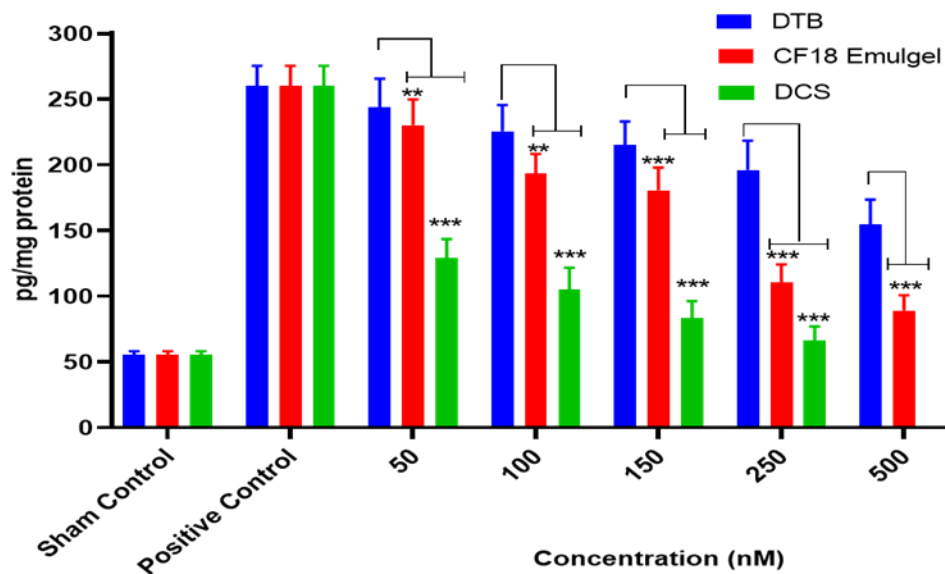
Figure 5.18 Effect on production of IL-6 expression level of dasatinib (DTB), CF18 emulgel and diclofenac gel (DCS).

5.8.6 *Ex-vivo* studies

5.8.6.1 *Ex-vivo* skin permeation study

The optimized CF18 emulgel and FDG formulations were used for *ex-vivo* permeation studies on rat abdominal skin using a pH 5.5 PB containing 1% Triton X100 as release media, and the total amount of permeation over a 24 h period is shown in Figure 5.19. After 12 h, the amount

of drug permeated through the skin was found to be 12.52 ± 0.29 µg/cm^2 and 4.31 ± 1.07 µg/cm^2 for CF18 emulgel and FDG formulations, respectively. After 24 h, it was found to be 23.59 ± 0.04 µg/cm^2 and $6.86.57 \pm 1.98$ µg/cm^2. The flux across skin was found to be 0.38 ± 0.04 µg /cm^2 /h for CF18 emulgel and 0.1 ± 0.03 µg/cm^2/h for FDG formulations. CF18 emulgel has greater drug permeation ($p < 0.001$) and flux across the skin than FDG. Hence, the study concluded that the permeation of the topical nanoemulgel compared to the free drug loaded gel, attributed to several factors. The smaller droplet sizes of the nanoemulgel enhanced the surface area and improved skin contact, facilitating better drug-skin interaction and overall permeation. Also, surfactants and penetration enhancer present in the nanoemulgel modify the skin's barrier properties, promoting drug penetration by disrupting the lipid structure, increasing hydration, and creating pathways for drug molecules to pass through the skin.
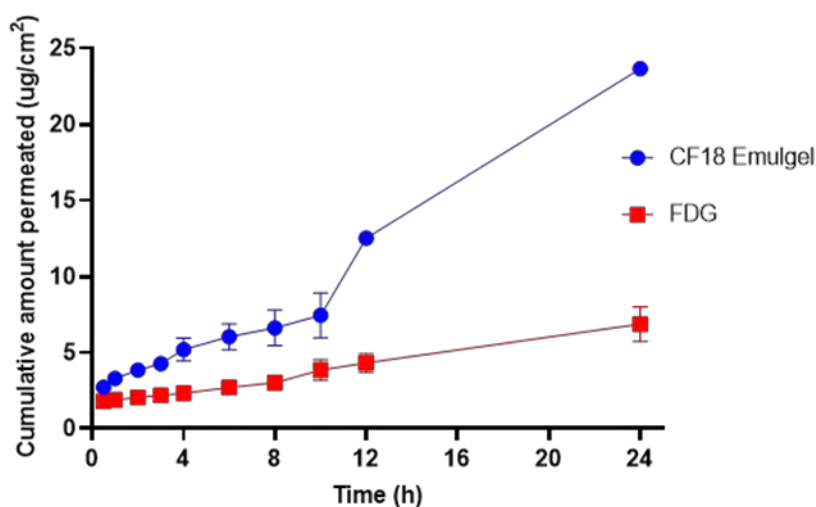
Figure 5.19 *Ex-vivo* permeation study of CF18 emulgel and free drug loaded gel (FDG).

5.8.6.2 Skin deposition study

After 24 h, the amount of drug deposited was found to be 143.62 ± 22.01 ng/cm^2 and 17.45 ± 3.28 ng/cm^2 for CF18 emulgel and FDG formulation, respectively, as shown in Figure 5.20. The deposition was found to be 10-fold higher ($p < 0.05$) in the case of the CF18 emulgel as

compared to the FDG. As a result, the study concluded that the CF18 emulgel has better deposition capacity and will deliver the drug to deeper layers in a sustained manner.
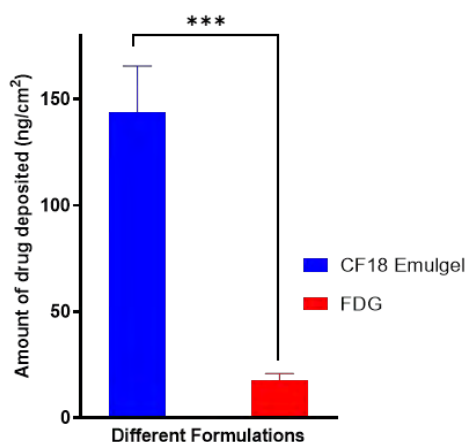
Figure 5.20 Skin deposition study for CF18 emulgel and free drug loaded gel (FDG). *** p <0.001 vs. FDG.

5.8.6.3 Bio adhesion studies

The adhesive strength of CF18 nanoemulgel, optimized placebo nanoemulgel (CF18P emulgel), and 0.5% carbopol plain gel was determined to be 6.1 ± 0.14, 6.35 ± 0.25, and 6.65 ± 0.05, respectively, Figure 5.21. The adhesiveness of the CF18 emulgel was shown to have similar results to the placebo gel, but a slight variation (non-significant) was observed with 0.5% carbopol gel, indicating that the lipid nanoparticles dispersed uniformly in the aqueous gel base did not interfere with the swelling mechanism of the carbopol gel [23].
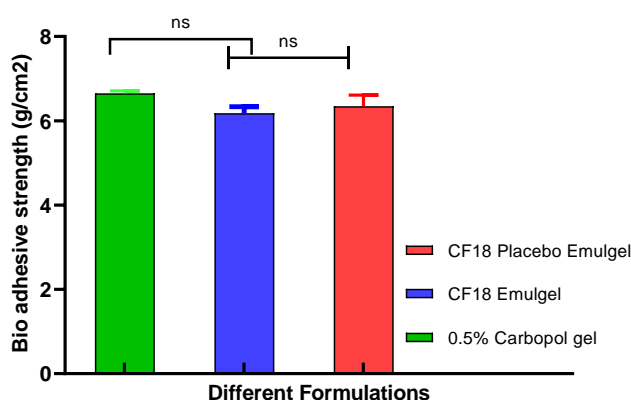
Figure 5.21 Comparative bio-adhesion strength CF18 placebo emulgel, CF18 emulgel and 0.5% Carbopol gel.

5.8.7 *In-vivo* studies

5.8.7.1 Skin irritation studies

After 72 h of observations, the scores for erythema, atonia, and fissuring of the five groups were represented in Table 5.10

Except 5% SLS gel, all other formulations behaved similarly to the non-treated (negative control group). Therefore, the developed topical formulation is safe for the skin, and the study images were represented in Figure 5.22. After 72 h, the animals were sacrificed, and the treated skin patches were examined for histopathology, as shown in Figure 5.23. The epidermis layer of the untreated skin was thin, and no necrosis was observed. It also appeared similarly in CF18 nanoemulgel, CF18P emulgel, and FDG. Increased thickness (hyperkeratosis) of the epidermis layer with necrosis was observed in the case of 5% SLS gel when compared to other formulation treated skin. Because of the binding of the SLS-loaded gel to the keratin in the subcutaneous, ionic and hydrophobic interactions cause the subcutaneous to swell.

Lipid removal from the subcutaneous exposes more keratin binding sites, causing protein denaturation. Surfactants also interact with horny layer proteins to cause reversible skin damage [32]. Lipid removal irreversibly destroys subcutaneous structure. CF18 emulgel used non-ionic lipids and surfactants. They do not interact ionically with skin ionic proteins, reducing irritancy. Thus, topical CF18 emulgel is a non-irritant.

Table 5.10 Comparative *in-vivo* skin irritation studies between CF18P emulgel, CF18 nanoemulgel, FDG & 5% SLS Gel.

Erythema and Oedema					
Time (h)	CF18P Emulgel	CF18 emulgel	FDG	5% SLS GEL	Normal group
0	0	0	0	0	0
1	0	0	0	0	0
6	0	0	0	0	0
12	0	0	0	1	0
24	0	0	0	2	0
48	0	0	0	3	0
72	0	0	1	3	0
Atonia- A decrease in normal elasticity of the skin					
0	1	1	1	1	1
1	1	1	1	1	1
6	1	1	1	2	1
12	1	1	1	2	1
24	1	1	1	3	1
48	1	1	1	3	1
72	1	1	2	3	1
Fissuring- Cracks on skin					
0	1	1	1	1	1
1	1	1	1	1	1
6	1	1	1	1	1
12	1	1	1	1	1
24	1	1	1	2	1
48	1	1	1	2	1
72	1	1	1	2	1

Note: Grading for skin reaction for Erythema and Oedema (0- None, 1- Slight, 2- Moderate, 3- Severe), Atonia - A decrease in normal elasticity of the skin 1- Slight (slight impairment of elasticity), 2- Moderate (slow return to normal), 3- Marked (No elasticity), Fissuring - Cracks on skin 1- Slight (Definite cracks in epidermis), 2- Moderate (Cracks on dermis), 3- Marked (Cracks and bleeding).

Figure 5.22 *In-vivo* skin irritation study.

Note*(A) Group I-Untreated group; (B) Group II-FDG (200 mg from 0.05% gel); (C) Group III- CF18 emulgel (200 mg from 0.05% gel); (D) Group IV-CF18P emulgel (200 mg from 0.05% gel); (E) Group V-received 5% SLS gel.

*Note

(→) Hyperkeratosis

(→) Necrosis
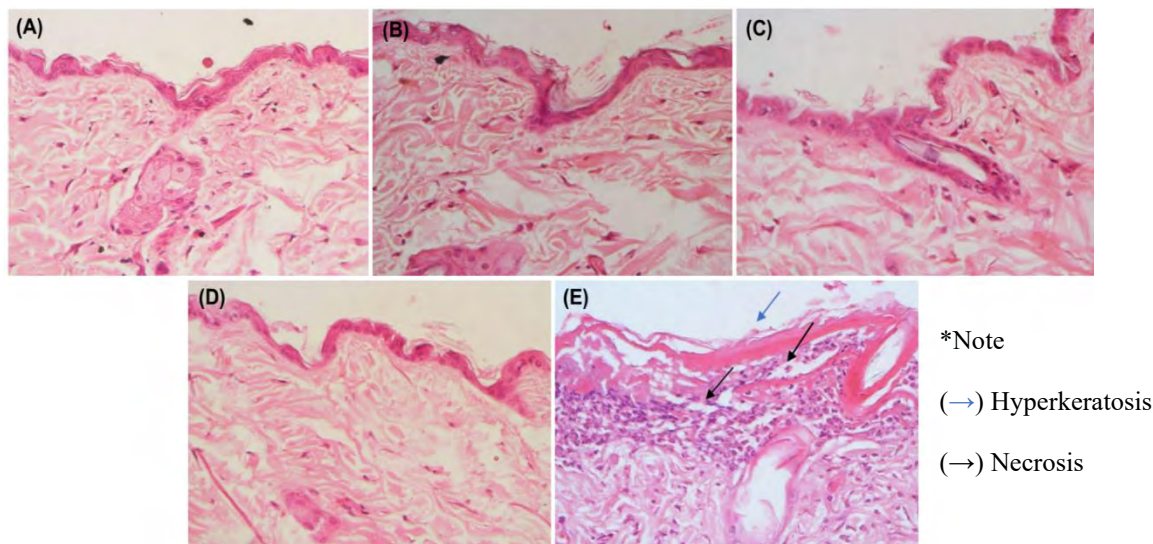
Figure 5.23 Histopathology of skin sample after skin irritation studies.
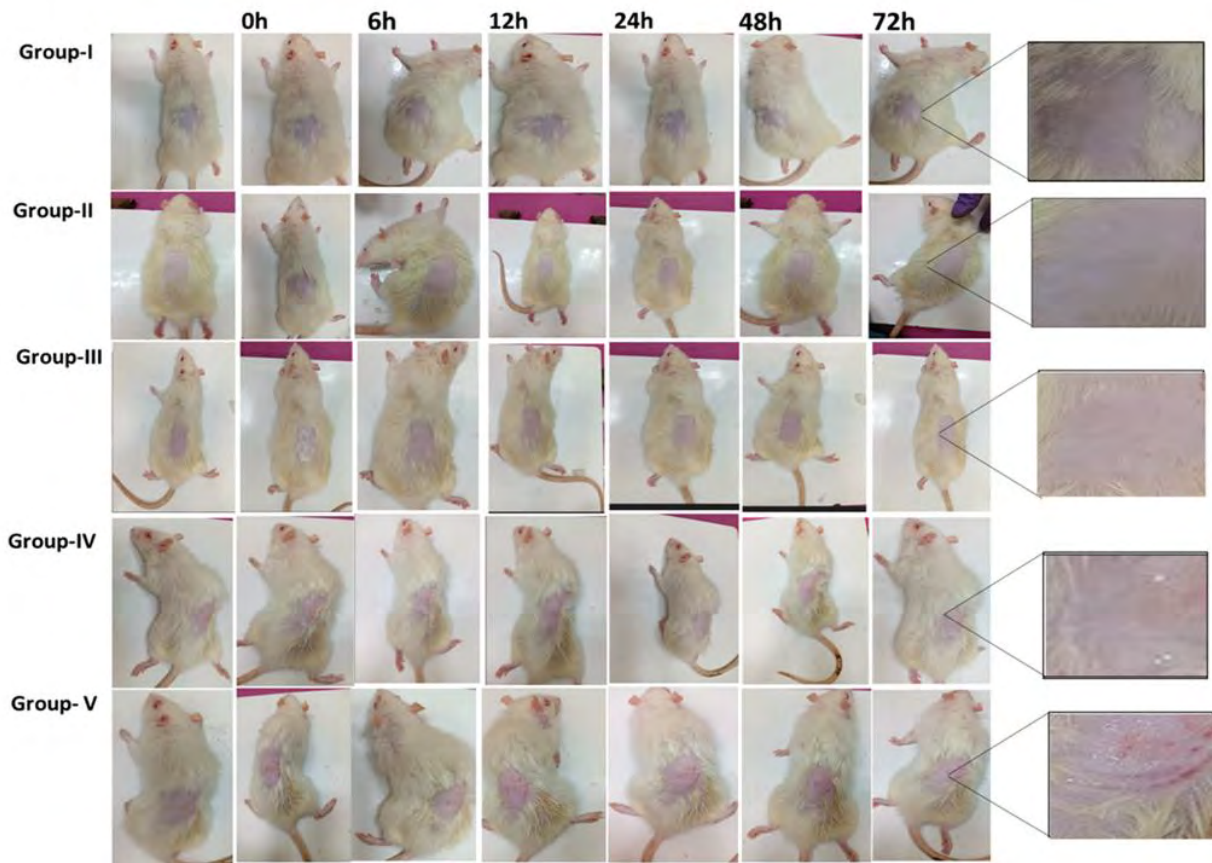
Note*(A) Group I-Untreated group; (B) Group II-FDG (200 mg from 0.05% gel); (C) Group III- CF18 emulgel (200 mg from 0.05% gel); (D) Group IV-CF18P emulgel (200 mg from 0.05% gel); (E) Group V-received 5% SLS gel.

5.8.7.2 FCA-induced arthritis model (chronic inflammatory model)

5.8.7.2.1 Assessment of arthritis from physical parameters

During the FCA immunization experiment period, rats lost significant weight ($p < 0.05$–$p < 0.001$), as depicted in Figure 5.24. Meanwhile, significant weight gains ($p < 0.001$) were observed in animals treated with MFD, CF18 nanoemulgel, and FDG after the 27th day. The CF18 emulgel resulted in a significant ($p < 0.5$) improvement in body weights when compared to topical FDG administration; however, a similar difference was observed in the MFD-treated group. The results showed that the CF18 emulgel formulation was more effective, with a significant weight gain beginning on the 12th day ($p < 0.05$). On the fifth day, FCA-injected hind paws swelled to maximum and converted to red (first phase). After that, the swelling subsided until the 10th day. Disseminated arthritis caused the paw to swell again (second phase), worse than before (first phase). Topical CF18 emulgel and MFD from the 5th day of arthritis induction suppressed ($p < 0.01$) the second phase Figure 5.25 and reduced hind paw edema /redness in the arthritis groups (Figure 5.27). As depicted in Figure 5.26 & 5.26, the arthritic clinical score decreased significantly from day 15–27 ($p < 0.05$), indicating anti-arthritic activity. Compared to the AIA control group, the blank formulation did not affect body weight change, paw swelling, or arthritic score.

Figure 5.24 Effect of different formulations on Body weight of the rat for CF18 placebo emulgel; CF18 emulgel, free drug loaded gel (FDG); adjuvant induced arthritis (AIA); marketed formulation diclofenac (MFD); normal groups.

*** $p < 0.001$. ** $p < 0.01$, *$p<0.5$ vs. normal group; +++ $p < 0.001$. ++ $p < 0.01$, + $p < 0.5$ vs. AIA control.
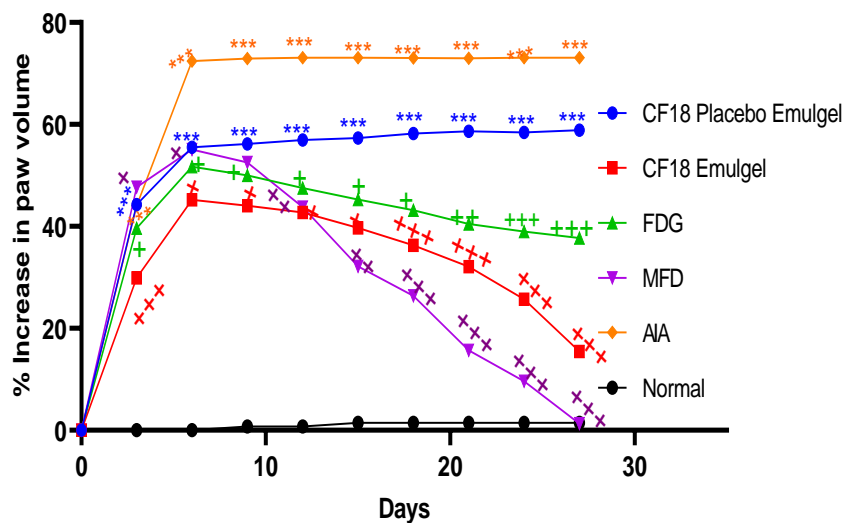
Figure 5.25 Effect of different formulations on Paw volume of the rat for CF18 placebo emulgel; CF18 emulgel, free drug loaded gel (FDG); adjuvant induced arthritis (AIA); marketed formulation diclofenac (MFD); normal groups.

 *** $p < 0.001$. ** $p < 0.01$, *$p<0.5$ vs. normal group; +++ $p < 0.001$. ++ $p < 0.01$, + $p < 0.5$ vs. AIA control.
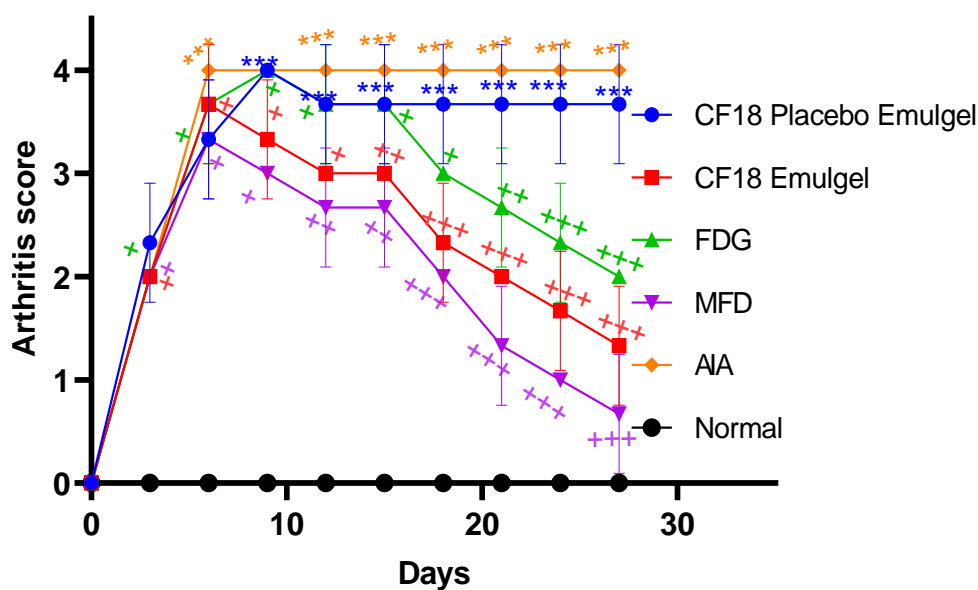
Figure 5.26 Effect of different formulations on Arthritis score for CF18 placebo emulgel; CF18 emulgel; free drug loaded gel (FDG); adjuvant induced arthritis (AIA); marketed formulation diclofenac (MFD) and normal groups.

*** $p < 0.001$. ** $p < 0.01$, *$p<0.5$ vs. normal group; +++ $p < 0.001$. ++ $p < 0.01$, + $p < 0.5$ vs. AIA control.

Figure 5.27 Representative images of FCA injected hind paws after 28 days of treatment with various formulations.
*Note; (A) Normal; (B) AIA; (C) CF18P emulgel; (D) FDG; (E) CF18 emulgel; (F) MFD.

5.8.7.2.2 Nociceptive threshold

FCA-induced arthritis, which causes chronic hypersensitivity to nociceptive stimulation, is a good model for the assessment of chronic pain in rats [43]. FCA-treated rodents had lower paw withdrawal thresholds than normal control group animals, and the pain threshold was lowest on day 5, as shown in Figure 5.28. Compared to FCA-treated control group animals, CF18 emulgel and MFD reduced withdrawal latency from 1st to 5th day and increased paw withdrawal threshold from the 10th day. As per the results of the hot plate test, which showed an increased reaction time, CF18 emulgel appears to have an anti-nociceptive effect.
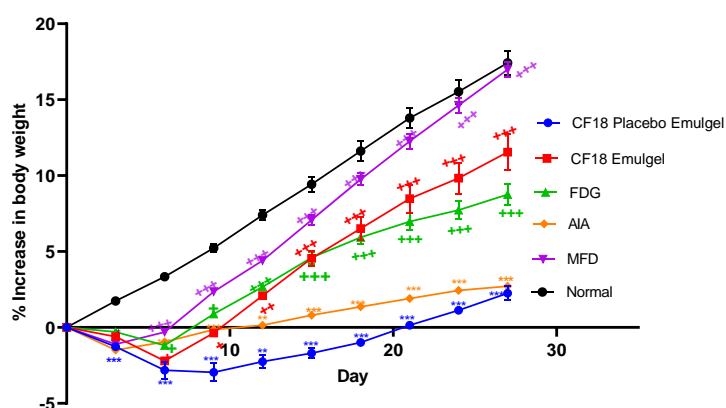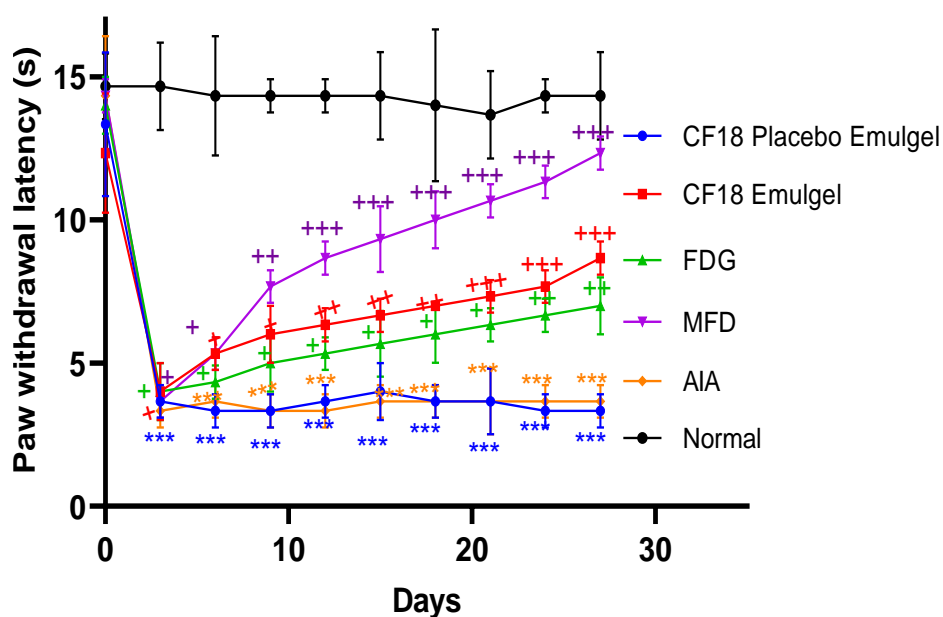
Figure 5.28 Effect of different formulations on paw withdrawal threshold for CF18 placebo emulgel, CF18 emulgel, free drug loaded gel (FDG), adjuvant induced arthritis (AIA), marketed formulation diclofenac (MFD) and normal groups.

*** $p < 0.001$. ** $p < 0.01$, *$p<0.5$ vs. normal group; +++ $p < 0.001$. ++ $p < 0.01$, + $p < 0.5$ vs. AIA control.

5.8.7.2.3 Motor incoordination test

The AIA model causes both pain and motor dysfunction, which ultimately results in hyperalgesia [44]. Motor incoordination is a sign of functional impairment and nervous system inflammation [45]. Motor incoordination was assessed by the mean fall-off time in the rota rod test. FCA sub-plantar injection diminished fall-off time compared to the normal control group. Compared to the FCA control group, rats treated with CF18 emulgel and MFD had a significantly longer fall off time from day 5 to day 28 Figure 5.29. These findings suggest that DTB-induced counter regulation of spinal glial activation improved motor coordination in CF18 nanoemulgel. Therefore, DTB loaded nanoemulgel applied topically may treat arthritis induced motor incoordination.
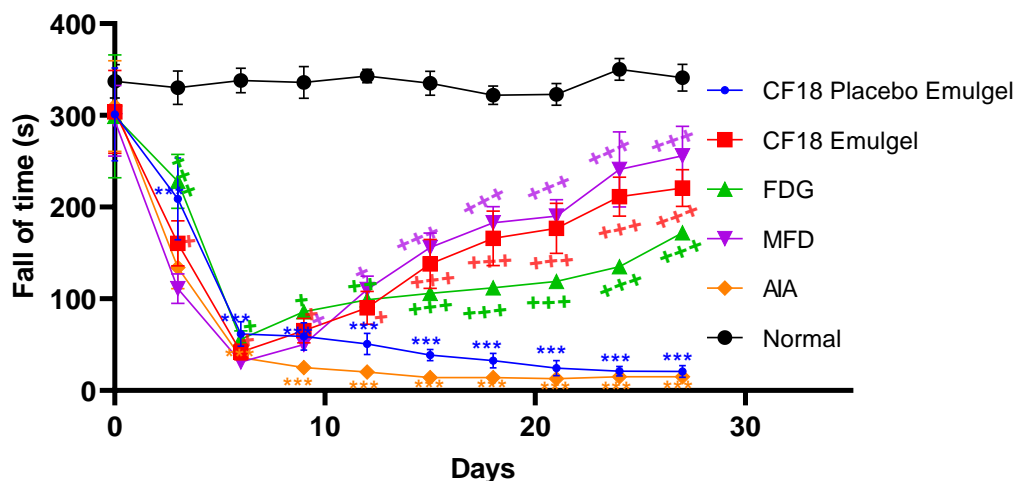
Figure 5.29 Effect of different formulations on motor incoordination for CF18 placebo emulgel; CF18 emulgel, free drug loaded gel (FDG); adjuvant induced arthritis (AIA); marketed formulation diclofenac (MFD); normal groups.

*** p < 0.001. ** p < 0.01, *p<0.5 vs. normal group; +++ p < 0.001. ++ p < 0.01, + p < 0.5 vs. AIA control.

5.8.8 Storage stability of DTB loaded emulgel

The DTB loaded emulgel depicted particles integrity using Malvern zeta sizer without any aggregation. The assay results depicted no substantial change (< 2%) as represented in Table 5.11, indicating the stability of DTB loaded emulgel.

Table 5.11. Stability data of dasatinib loaded emulgel.

Stability data of DTB loaded emulgel at 25°C				
Parameter	**0 Month**	**15 days**	**1st Month**	**2nd Month**
Assay of gel (%)	101.00 ± 0.560	98.95 ± 0.735	98.92 ± 0.305	98.01 ± 0.62
Size (nm)	170.27 ± 30.26	176.25 ± 14.31	183.96 ± 17.78	194.62 ± 22.14
PDI	0.187 ± 0.064	0.285 ± 0.00	0.155 ± 0.015	0.258 ± 0.05

5.9 Outcomes of the research

In this research, emulgel was used to improve permeation while minimizing the systemic absorption of DTB, resulting in enhanced efficacy in RA treatment. The QbD method was used to examine the effect of different factors and their interactions in order to achieve the desired product. The higher drug solubility in lipid increased the % EE while decreasing drug leakage

from the formulation. The optimal concentration of S_{mix} in the formulation favoured low PS with even distribution by stabilizing the oil-in-water interface. Carbopol ETD 2020 exhibited excellent spreadability and consistency during storage. The prepared CF18 emulgel spread as a thin layer on the skin's surface, hydrating it by reducing trans-epidermal water loss. This hydration promotes skin lipid swelling and helps to improve permeation. *Ex-vivo* studies revealed that the CF18 emulgel had better permeation than FDG. Further, *in-vivo* studies revealed that the CF18 emulgel exhibited better efficacy in FCA induced rat model. The study demonstrated the ease of developing nanoemulgel formulations from a wide range of materials, with improved safety and efficacy.

5.10 Conclusion

In this study, the improvement in skin permeation and deposition of a DTB-loaded nanoemulgel was determined using a QbD-based approach. Using a CCD, the effect of lipid, S_{mix} concentration, and homogenization time on PS and % EE was investigated. The results revealed that topical DTB-loaded nanoemulgel increased skin permeation and deposition, as expected, due to the occlusive effect of forming a very thin layer on the skin's surface. The emulsion's *in-vitro* drug release demonstrated sustained release. The cell culture results illustrated the safety of the excipients, and the decrease in TNF-α and IL-6 levels expressed the efficacy of the CF18 emulgel formulation. As a result, we conclude that topical delivery of DTD-loaded nanoemulgel is a viable approach for the treatment of RA. However, more studies are required to improve the DTB loading to simulate the clinical dose for humans in the treatment of RA.

References

1. Fox, L.C. *et al.* (2017) The incidence and natural history of dasatinib complications in the treatment of chronic myeloid leukemia. *Blood Adv* 1, 802

2. Rapalli, V.K. *et al.* (2021) Revisiting techniques to evaluate drug permeation through skin. *Expert Opin Drug Deliv* 18, 1829–1842

3. Begum, S.G. *et al.* (2019) a review on emulgels-a novel approach for topical drug delivery. *Asian Journal of Pharmaceutical Research and Development* 7, 70–77

4. Tamjidi, F. *et al.* (2013) Nanostructured lipid carriers (NLC): A potential delivery system for bioactive food molecules. *Innovative Food Science & Emerging Technologies* 19, 29–43

5. Rahman, M. *et al.* (2016) Emergence of liposome as targeted magic bullet for inflammatory disorders: current state of the art. *Artif Cells Nanomed Biotechnol* 44, 1597–1608

6. Anand, K. *et al.* (2019) Nanoemulgel: Emerging as a Smarter Topical Lipidic Emulsion-based Nanocarrier for Skin Healthcare Applications. *Recent Pat Antiinfect Drug Discov* 14, 16–35

7. Abd, E. *et al.* (2018) Minoxidil Skin Delivery from Nanoemulsion Formulations Containing Eucalyptol or Oleic Acid: Enhanced Diffusivity and Follicular Targeting. *Pharmaceutics 2018, Vol. 10, Page 19* 10, 19

8. Schroeter, A. *et al.* (2010) New nanosized technologies for dermal and transdermal drug delivery. A review. *J Biomed Nanotechnol* 6, 511–528

9.   Anand, K. *et al.* (2019) Nanoemulgel: Emerging as a Smarter Topical Lipidic Emulsion-based Nanocarrier for Skin Healthcare Applications. *Recent Pat Antiinfect Drug Discov* 14, 16–35

10.   Nagaraja, S. *et al.* (2021) Topical Nanoemulgel for the Treatment of Skin Cancer: Proof-of-Technology. *Pharmaceutics* 13, 902–902

11.   Namjoshi, S. *et al.* (2020) Quality by design: Development of the quality target product profile (QTPP) for semisolid topical products. *Pharmaceutics* 12, 287

12.   Sivaraman, A. and Banga, A.K. (2015) Quality by design approaches for topical dermatological dosage forms. *Res. Rep. Transdermal Drug Deliv* 4, 9–21

13.   Rapalli, V.K. *et al.* (2021) QbD-driven formulation development and evaluation of topical hydrogel containing ketoconazole loaded cubosomes. *Materials Science and Engineering: C* 119, 111548

14.   Dong, L. *et al.* (2015) The effect of rheological behavior and microstructure of the emulgels on the release and permeation profiles of Terpinen-4-ol. *Eur J Pharm Sci* 78, 140–150

15.   Dudhipala, N. and Veerabrahma, K. (2016) Candesartan cilexetil loaded solid lipid nanoparticles for oral delivery: characterization, pharmacokinetic and pharmacodynamic evaluation. *Drug Deliv* 23, 395–404

16.   Krishna, K.V. *et al.* (2019) Design and Biological Evaluation of Lipoprotein-Based Donepezil Nanocarrier for Enhanced Brain Uptake through Oral Delivery. *ACS Chem Neurosci* 10, 4124–4135

17. Rashid, S.A. *et al.* (2021) Olive Oil Based Methotrexate Loaded Topical Nanoemulsion Gel for the Treatment of Imiquimod Induced Psoriasis-like Skin Inflammation in an Animal Model. *Biology (Basel)* 10, 1121

18. Khosa, A. *et al.* (2020) Lipid Nanocarriers for Enhanced Delivery of Temozolomide to the Brain. *Methods Mol Biol* 2059, 285–298

19. Mwangi, A.N. *et al.* (2021) Meloxicam emulgels for topical management of rheumatism: Formulation development, in vitro and in vivo characterization. *Saudi Pharmaceutical Journal* 29, 351–360

20. Sharma, V. *et al.* (2018) Emulgels. *Polymeric Gels* DOI: 10.1016/B978-0-08-102179-8.00009-0

21. Thakur, V. *et al.* (2012) Formulation and in vitro Evaluation of Gel for Topical Delivery of Antifungal Agent Fluconazole Using Different Penetration Enhancers. *Drug invention today*

22. Nikumbh, K. V. *et al.* (2015) Formulation development, in vitro and in vivo evaluation of microemulsion-based gel loaded with ketoprofen. *Drug Deliv* 22, 509–515

23. Pal, R.R. *et al.* (2019) Tamanu oil potentiated novel sericin emulgel of levocetirizine: repurposing for topical delivery against DNCB-induced atopic dermatitis, QbD based development and in vivo evaluation. *J Microencapsul* 36, 432–446

24. Deuschle, V.C.K.N. *et al.* (2015) Physical chemistry evaluation of stability, spreadability, *in vitro* antioxidant, and photo-protective capacities of topical formulations containing *Calendula officinalis* L. leaf extract. *Brazilian Journal of Pharmaceutical Sciences* 51, 63–75

25. Stojkov, G. *et al.* (2021) Relationship between Structure and Rheology of Hydrogels for Various Applications. *Gels* 7

26. Guichard, A. *et al.* (2015) Effects of topical corticosteroids on cell proliferation, cell cycle progression and apoptosis: in vitro comparison on HaCaT. *Int J Pharm* 479, 422–429

27. Wei, S.T. *et al.* (2015) Serum Levels of IL-6 and TNF-α May Correlate with Activity and Severity of Rheumatoid Arthritis. *Med Sci Monit* 21, 4030

28. Schreier, H. and Bouwstra, J. (1994) Liposomes and niosomes as topical drug carriers: dermal and transdermal drug delivery. *Journal of Controlled Release* 30, 1–15

29. Wavikar, P. and Vavia, P. (2013) Nanolipidgel for enhanced skin deposition and improved antifungal activity. *AAPS PharmSciTech* 14, 222–233

30. Khullar, R. *et al.* (2012) Formulation and evaluation of mefenamic acid emulgel for topical delivery. *Saudi Pharmaceutical Journal* 20, 63–67

31. ElMeshad, A.N. and Tadros, M.I. (2011) Transdermal delivery of an anti-cancer drug via w/o emulsions based on alkyl polyglycosides and lecithin: design, characterization, and in vivo evaluation of the possible irritation potential in rats. *AAPS PharmSciTech* 12, 1–9

32. Jibry, N. and Murdan, S. (2004) In vivo investigation, in mice and in man, into the irritation potential of novel amphiphilogels being studied as transdermal drug carriers. *European journal of pharmaceutics and biopharmaceutics* 58, 107–119

33. Bancroft, J.D. and Gamble, M. (2008) Theory and Practice of Histological Techniques. 6th Edition, Churchill Livingstone, Elsevier, China. - References - Scientific Research Publishing[Online]. Available:

https://www.scirp.org/(S(vtj3fa45qm1ean45vvffcz55))/reference/ReferencesPapers.aspx?ReferenceID=1582193. [Accessed: 29-Mar-2023]

34. Patil, M.V.K. *et al.* (2012) Anti-arthritic and anti-inflammatory activity of Xanthium srtumarium L. ethanolic extract in Freund's complete adjuvant induced arthritis. *Biomedicine & Aging Pathology* 2, 6–15

35. Jeengar, M.K. *et al.* (2016) Emu oil based nanoemulgel for topical delivery of curcumin. *Int J Pharm* 506, 222–236

36. Jones, B.J. and Roberts, D.J. (1968) The quantitative measurement of motor inco-ordination in naive mice using an accelerating rotarod. *Journal of Pharmacy and Pharmacology* 20, 302–304

37. Waghule, T. *et al.* (2019) Voriconazole loaded nanostructured lipid carriers based topical delivery system: QbD based designing, characterization, in-vitro and ex-vivo evaluation. *J Drug Deliv Sci Technol* 52, 303–315

38. Waghule, T. *et al.* (2020) Nanostructured Lipid Carriers as Potential Drug Delivery Systems for Skin Disorders. *Curr Pharm Des* 26, 4569–4579

39. Mohamed Rizwan, I. and Damodharan, N. (2020) Mathematical Modelling of Dissolution Kinetics in Dosage forms. *Res J Pharm Technol* 13, 1339–1345

40. Carlfors, J. *et al.* (1998) Rheological evaluation of Gelrite® in situ gels for ophthalmic use. *European Journal of Pharmaceutical Sciences* 6, 113–119

41. Dantas, M.G.B. *et al.* (2016) Development and Evaluation of Stability of a Gel Formulation Containing the Monoterpene Borneol. *Scientific World Journal* 2016, 1–4

42. Rapalli, V.K. *et al.* (2020) Curcumin loaded nanostructured lipid carriers for enhanced skin retained topical delivery: optimization, scale-up, in-vitro characterization and

assessment of ex-vivo skin deposition. *European Journal of Pharmaceutical Sciences* 152, 105438

43.   Larson, A.A. *et al.* (1986) Pain threshold changes in adjuvant-induced inflammation: a possible model of chronic pain in the mouse. *Pharmacol Biochem Behav* 24, 49–53

44.   Schaible, H.G. *et al.* (2005) Neurogenic aspects of inflammation. *Rheum Dis Clin North Am* 31, 77–101

45.   Levine, J.D. *et al.* (2006) Neurogenic Inflammation and Arthritis. *Ann N Y Acad Sci* 1069, 155–167

Chapter-6

Formulation and Characterization of Dasatinib loaded Solid Lipid Nanoparticles

6 Introduction

Oral administration of Dasatinib (DTB) is associated with several side effects, as mentioned in section 1.7. However, topical administration presents a potential solution to circumvent these clinical complications. Despite this, the skin poses a formidable obstacle, impeding the absorption of active pharmaceutical ingredients (APIs) when using conventional topical formulations such as creams, ointments, lotions, and solutions. Consequently, this leads to lower drug concentrations at the intended target site[1,2]. To overcome this limitation, nanocarriers, including nanoemulsions, Solid Lipid Nanoparticles (SLNs), liposomes, and polymeric nanoparticles, have emerged as promising options. These nanocarriers offer the ability to surpass the skin barrier without causing harm and employ intracellular and intercellular transport mechanisms for enhanced drug penetration or the formation of depots in deeper skin layers[3,4]. This enables sustained release, ultimately maximizing therapeutic efficacy. Among the all-nano carriers, our current investigation revolves around exploring the potential of SLNs in topical drug delivery[5].

SLNs are the first generation colloidal lipidic nanostructures comprising of solid lipid which is stabilized by the emulsifier [6]. SLNs offer several advantages in comparison to conventional topical formulations. They exhibit simple scalability, ensuring ease of production on a larger scale. Moreover, SLNs contribute to high patient compliance due to their improved stability and ease of application. The lipids utilized in SLNs formulation possess remarkable biocompatibility and biodegradability properties, enhancing their safety profile. Furthermore, SLNs enable increased drug solubility, addressing the challenge of delivering hydrophobic drugs effectively to the deeper layers i.e., joint region [7] [8] As per our knowledge topical delivery of DTB loaded SLNs has not been reported for the treatment RA.

The Quality by Design (QbD) approach can provide qualitative products with a clear understanding of the formulation and process variable effect on their characteristic responses. In the present research, the dependent and independent variables of SLNs formulation were investigated using the QbD approach. The purpose of this study is to provide an overview of the future and rationale for the topical delivery of DTB-loaded SLNs.

6.1   Materials

Palmitic acid was bought from SD Fine Chem (Mumbai, India). Gelot 64 and Gelucire 48/16 samples as gifts from Gattefosse (Mumbai, India). Dialysis bag with a molecular weight cutoff of 12,000–14,000 kDa, membrane filters (0.22 µm), propyl paraben (PP) and methyl paraben (MP) were procured from Merck (India). Triton X 100 was purchased from Himedia (Mumbai, India). The remaining laboratory chemicals were acquired from HiMedia (Mumbai, India) and Sisco research laboratory Pvt. Ltd. (Maharashtra, India)

6.2   Study design

QbD is a systemic approach that facilitates product, process understanding and control, based on sound science and quality risk management. The various setup steps involved in the QbD approach was mentioned as road map in Figure 6.1. In QbD, Quality target product profile (QTPP) specifies the desired product quality, ideal product characteristics, safety and efficacy of the final drug product. Initially, the QTPP was established with a variety of variables that could affect the formulation permeation of finished SLNs. For that formulation, critical quality attributes (CQAs) were selected, which govern the desired characteristics of the targeted formulation. The CQAs should ensure that the product meets the needs of the patients. The critical material attributes (CMAs) and critical process parameters (CPPs) were selected as major influencing factors on the CQAs based on the literature and the ishikawa diagram. The criticality of the factors was

determined using the Risk estimation matrix (REM), with potential criticality graded as low, medium and high. Subsequently, failure mode evaluation and analysis (FMEA) was used to assess the severity, probability, and occurrence of each individual factor. The risk priority number (RPN) score was calculated using equation 1 and the ranking number was assigned (0-10). The CMAs and CPPs were fixed based on the RPN number (Rapalli et al., 2021; Sivaraman & Banga, 2015).

Severity(S)* Detectability (D) * Occurrence (O) = RPN   (eq.1)

6.2.1   Box Behnken design (BBD) for optimization

Based on the preformulation studies, as mentioned in the section 4.3.2 the excipients were selected for the formulation development using BBD. The lipid concentration, surfactant concentration and homogenization time were investigated against particle size (PS) and entrapment efficiency (EE) at three levels: low, medium, and high, while other process and formulation parameters were kept constant. The design matrix suggested 17 experimental runs containing centre points of each selected variable. The interaction of the factors with the desired characteristic responses was evaluated, and the formulation was optimized with the minimum trials. The Design-Expert 7.0.0 software was used for the optimization, data analysis, and model validation as mentioned in the section number 5.2.5. [9]**.**

6.3   Formulation of dasatinib loaded SLNs

6.3.1   Method of preparation

The formulations were prepared in a single batch size of 10 g using hot homogenization method. The compositions of different formulations were mentioned in Table 6.4. The method involves preparing the lipid phase by mixing gelot 64 into the selective lipid in a beaker at 70 ± 5 °C on a laboratory hot plate. Then, DTB, methyl paraben, and propyl paraben were added to the lipid phase, ensuring thorough mixing to dissolve all components. Simultaneously, the aqueous phase

was prepared by dissolving gelucire 48/16 and sodium meta bisulphite and stirring the mixture constantly at 40 °C. The aqueous phase was then added dropwise to the lipid phase under continuous homogenization at 40 °C, followed by cooling the mixture to room temperature for the resulting in SLNs dispersion.
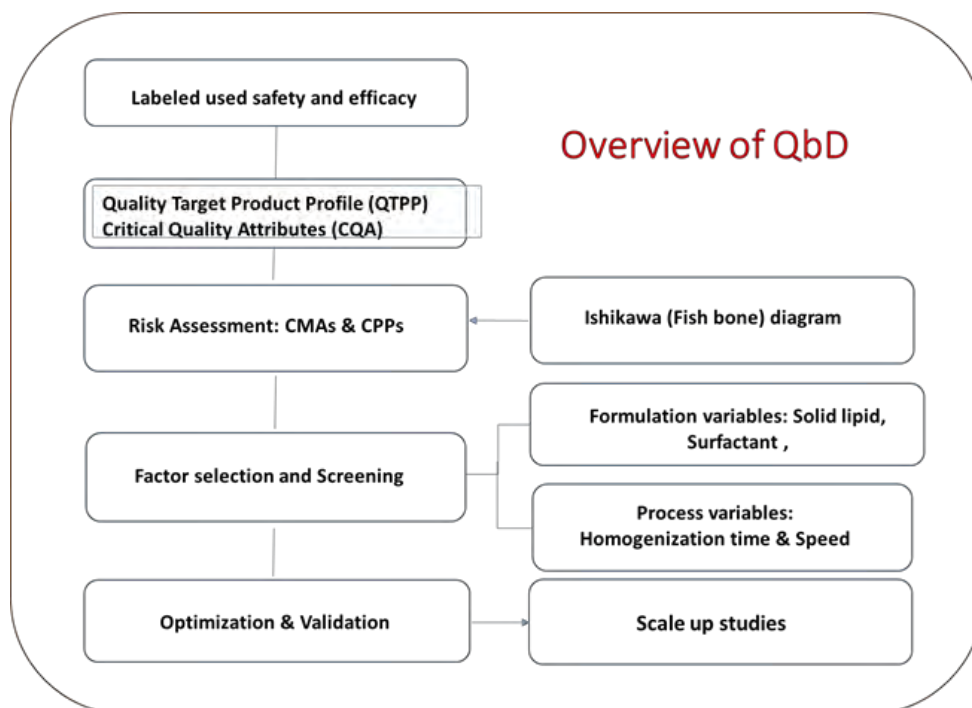
Figure 6.1. Representative image for steps involved in the QbD approach for SLNs.

6.3.2   Scale-up studies

After optimizing the formulation through QbD, and the most effective formulation was chosen to be scaled up to batch sizes of 50 and 100 mL. The quantities of ingredients required for the larger batches were adjusted accordingly. In order to accommodate the larger batch sizes, adjustments were made to the diameter of the batch vessel and the homogenizer used. Specifically, a homogenizer with a 6 mm probe diameter was utilized to produce a 10 mL batch, which had a four

times larger beaker surface area. For the 50 mL and 100 mL batches, a homogenizer with a 20 mm probe diameter was used, which had a capacity range of 30-250 mL.

6.3.3 Characterization of SLNs

Attenuated Total Reflection-Infrared Spectroscopy (ATR-IR), Particle Size (PS), Polydispersity Index (PDI), Zeta Potential (ZP), Morphology by Field-Emission Scanning Electron Microscopy (FESEM) studies were characterized as mentioned in the section 5.3.3. The in-vitro drug release study was performed for SLNs (batch size of 10mL. 50 mL and 100 mL) and free drug loaded solution (FDS) by dialysis bag method, the detailed procedure was mentioned in the section 5.3.3.7

Entrapment efficiency (EE)

The centrifugation method was used to separate the free drug (unentrapped) from the SLNs. Specifically, a centrisart tube containing 1 g of selected formulation was subjected to centrifugation at 15000 rpm for 30 min. The resulting ultrafiltered aqueous phase, which contained the free drug, was then analyzed using RP-HPLC. Finally, the amount was calculated using equation 2 [7]**.**

$$EE = \frac{Wtotal - Wfree}{Wtotal} \times 100 \qquad \text{(eq.2)}$$

Where, W_{total} - weight of drug added in the system, W_{free} - free drug in the formulation

6.4   Formulation of SLNs loaded gel

6.4.1 Method of preparation

The SLNs loaded gel was prepared using the optimised SLNs formulation and carbopol ETD 2020 as the gel base. Initially, the carbopol was passed through a #60 sieve to break up any aggregates or lumps, and then it was added to the SLNs dispersion and thoroughly mixed. Finally, the

dispersion was neutralized using a 1% NaOH solution to form a gel. The fabricated gel was subjected to further characterization.

6.4.2 Evaluation of SLNs loaded gel

The selected gel was visually inspected for color, consistency, and homogeneity. pH, spreadability, particle integrity of SLNs loaded gel, rheological studies (viscosity, shear flow, strain sweep test, frequency sweep test) were performed as mentioned in the section 5.4.2

6.5   *In-vitro* cell line study

The cytotoxicity study in HaCaT cell lines for free DTB & optimized SLNs gel and the effct on production of TNF-α and IL-6 in RAW 264.7 cells for free DTB, optimized SLNs gel and diclofenac sodium (DCS) were performed as mentioned in the section 5.5

6.6   *Ex-vivo* studies

Ex-vivo permeation study, skin deposition study, bio-adhesion study for selected SLNs gel formulation and the free drug-loaded gel (FDG) was carried out as mentioned in the section 5.6

6.7   *In-vivo* studies

6.7.1   Skin irritation study

The rats were divided into five groups of three: Group I was untreated, Group II received FDG-free DTB loaded gel (200 mg from 0.05% gel), Group III received optimized SLNs gel (200 mg from 0.05% gel), Group IV received SLNs placebo gel (200 mg gel), and Group V received 5% SLS gel. The skin irritation study was performed as mentioned in the section 5.7.1

6.7.2   Assessment of the anti-inflammatory effect

In order to evaluate the efficacy of optimized SLNs gel for RA treatment, the adjuvant induced arthritis (AIA) model was employed in rats. Rats weighing between 150-250 g were randomly

assigned to six groups. These groups were as follows: Group I was the positive control, induced with AIA-adjuvant arthritis; Group II received MFD, a commercially available diclofenac formulation (0.5 g/kg); Group III received optimized SLNs gel (200 mg containing a 100 µg dose); Group IV received SLNs placebo gel; Group V received FDG (200 mg containing a 100 µg dose); and Group VI was the negative control (normal group) where 0.1 mL of FCA was injected into the hind paws of the rats, except for Group VI. The volume of the hind paw was measured using a water plethysmometer at various time points (0, 0.5, 1, 2, 3, 6, 9, 12, 15, 18, 21, 24, and 27 days) after Complete Freund's Adjuvant (CFA) injection, and at the peak of joint swelling, the respective formulations were administered (starting from day 5). Swelling degree, % increase in body weight, arthritis scores, nociceptive threshold, motor incoordination tests were performed as mentioned in the section 5.7.3

6.7.3   Storage stability

The formulation is studied to determine physical and chemical characteristics. Formulated SLNs of DTB is kept at 25° C for span of 15days, followed by 1 and 2 months. PS integrity and assay is determined by Zeta sizer and validated HPLC method.

6.7.4   Statistical analysis

The experiments were repeated three times, and the results are presented as the mean ± SD. Statistical analysis was performed using two-way analysis of variance (ANOVA), followed by Sidak's multiple comparison tests, which were calculated using GraphPad Prism (v 7.0) and showed p values < 0.05.

6.8   Results and discussion

6.8.1   Optimization by QbD

6.8.1.1 Identification of quality target product profile and critical quality attributes

Once the QTPP was established, the QbD approach was employed to develop a method for

preparing SLNs. Table 6.1 displays the selected QTPP for SLNs. The CQAs were prioritized

over the QTPP because they were found to influence the ultimate product features. Table 6.2

outlines the identification of PS, EE, and drug release as CQAs for SLNs, which have a greater

impact on product quality.

Table 6.1 Quality target product profile of dasatinib loaded SLNs gel.

Quality Target Product profile	Target	critical quality attributes	Justification
Dosage form	SLNs loaded gel	NA	To enhance the permeation of DTB to the target site
Route of administration	Topical	NA	Enhance the DTB concentration at targeted site for reducing the oral and systemic associated toxicity
Dosage strength	0.05%	NA	To select the minimum effective dose
Particle size (nm)	< 200	Yes	Enhance the drug permeation through the different skin barriers
Polydispersity index (PDI)	< 0.3	Yes	perfectly uniform size distribution leads to uniform release and permeation,
% Entrapment efficiency (% EE)	>90	Yes	Greater entrapment leading to higher drug loading with less lipid concentration
In vitro drug Release profile	Sustained	Yes	Longer duration of action without systemic exposure
pH	5.5	Yes	Affect the physiochemical stability and mimic with physiological pH leads to reduce the skin irritation

Table 6.2 Critical quality attributes of dasatinib loaded SLNs gel.

Critical Quality Attributes	Related to critical material attributes	Related to critical process parameters	Failure mode	Justification
Particle size (PS)	Concentration of Gelucire 48/16 and Solid lipid	Change in homogenization time	Entrapment, drug release and skin permeation of the drug	Increase in concentration of lipid increases size resulting in decrease in release and permeation. Increase in time of homogenization and concentration of Gelucire 48/16 decreases size, entrapment
Entrapment efficiency (EE)	Concentration of Gelucire 48/16 and Solid lipid	Change in homogenization time	Size, drug release and skin permeation	Increase in concentration of lipid increases entrapment resulting in decrease in drug release and permeation Increase in time of homogenization decreases size and entrapment, Increase in concentration of Gelucire 48/16 size and decreases entrapment
Drug release	Concentration of Gelucire 48/16 and lipid	Change in homogenization time	Poor therapeutic effect	Increase in concentration of lipid increases size and lipid matrix resulting in decrease in drug release and permeation Increase in time of homogenization increases release due to the decreased size (indirect effect)

6.8.1.2 Risk identification and risk assessment

The risk assessment was conducted and the ishikawa diagram was used to identify CPPs and CMAs. The ishikawa diagram was depicted in Figure 6.2. Based on the published research and preliminary findings, a REM was formulated. The RPN scores were allocated in FMEA according to the potential risk; these scores were based on previously reported research. Table 6.3 displays the REM and RPN scores for the CMAs and CPPs. RPN scores exceeding 125 were deemed

critical for optimizing critical attributes. The concentrations of lipid and surfactant (Gelucire 48/16) were identified as high-risk parameters since they can influence the drug EP and PS of SLNs, which can affect the drug permeation and efficacy of the formulation. Additionally, homogenization time was regarded as a potential risk factor since it may impact PS and uniformity of particle distribution
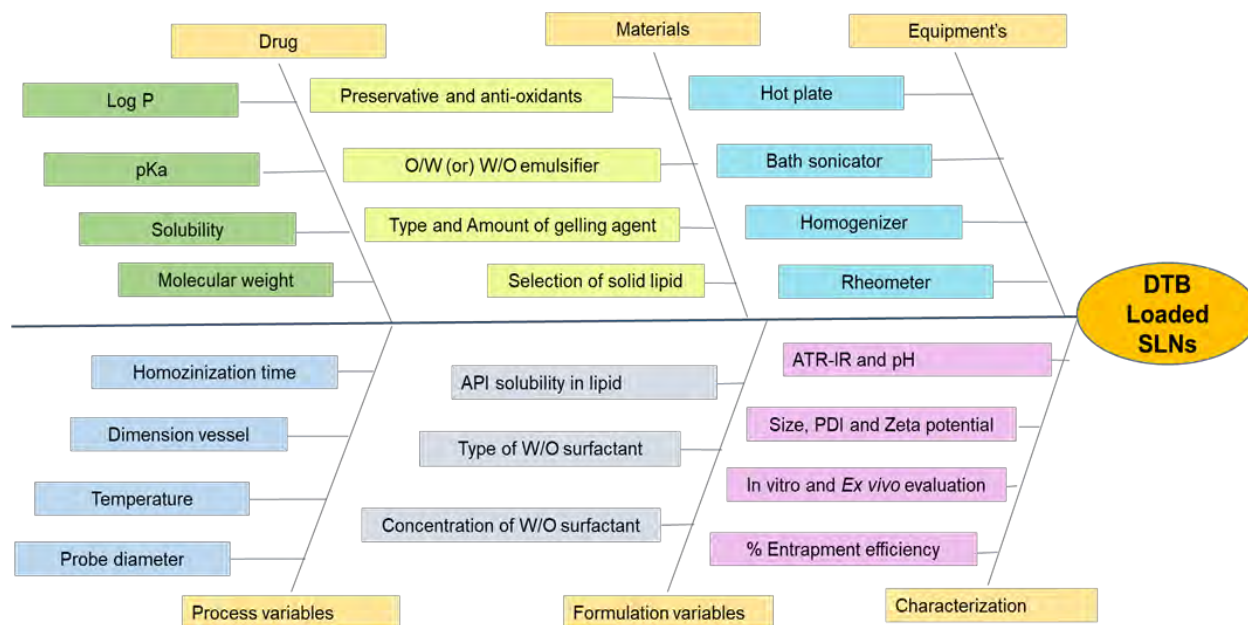

Figure 6.2 Ishikawa diagram illustrated the potential critical material attributes and critical process parameters that effect the critical quality attributes of dasatinib-loaded SLNs gel formulation.

Table 6.3 Risk estimation matrix for initial risk assessment and FMEA score based on qualitative analysis of different material attributes and process parameters.

Times	Critical quality attributes			FMEA			
	PS	% EE	Drug Release	Severity	Detectability	Occurrence	RPN Score
Lipid (Palmitic acid)	High	High	High	9	6	6	324
Surfactant (Gelucire 48/16)	High	High	High	9	5	6	270
Homogenization Time (min)	High	High	Low	7	6	6	252
Homogenization speed (rpm)	Medium	Medium	Low	6	5	4	120
Process temperature (^{0}C)	Low	Medium	Low	5	3	2	30

6.8.1.3 Factor optimizing studies

Based on the risk assessment report, various CMAs, including lipid and gelucire 48/16, and a major CPP, homogenization time, were identified. PS and EE were considered as CQAs in the responses. To optimize the formulation, a BBD with 17 trials was designed, with three factors and three levels, using DoE. The quantity of palmitic acid, gelucire 48/16 concentration, and homogenization time were investigated at three levels: low, medium, and high. Seventeen formulations were prepared in accordance with the design, as depicted in Table 6.4. Independent variables were varied in the formulations, while all other parameters (process and formulation parameters) were kept constant, the PS and EE were examined as response variables. The concentrations of gelot 64 (O/W surfactant), preservatives, and antioxidants used in all trials remained constant. ANOVA was used to evaluate the model efficiency and the significance of the chosen input variables. The BBD with three components and three levels was employed, and the response values obtained after the design was executed are presented in Table 6.4.

6.8.1.4 Independent variables effect on PS

The PS of the dasatinib-loaded SLNs ranged from 97.31 to 329.20 nm after conducting 17 trials, depicted in Table 6.4. The significance of the quadratic model is demonstrated by the F-value of 30.13. Contour and three-dimensional plots of the PS response variable are presented in Figure 6.3 A & B. The lack of fit had a F-value of 2.45, indicating insignificance. Regression equation (RE) 5 displays the coded values of the chosen independent variables.

$$Size = 138.82 + 62.45A - 56.60B - 23.34C - 35.37AB - 2.77AC + 23.14BC + 19.77\,A^2 + 19.30B^2 +$$

$$15.24C^2 \hspace{8cm} eq.(5)$$

Equation depicting the collusive effect as a positive symbol, indicating an increase in response value with the corresponding input variable. Conversely, the hostile effect is represented by a

negative symbol, indicating a decrease in response value with the corresponding input variable. The insignificant lack of fit in the experimental results suggests that the model fitting of experimental results is competent. RE (5) indicates that the PS increases as the lipid concentration increases. Moreover, an increase in the percent gelucire 48/16 concentration and homogenization time resulted in a reduction in PS. Gelucire 48/16 has the potential to reduce surface tension at the lipid-water interface, thereby improving particle stabilization, resulting in smaller particles. Furthermore, increasing the homogenization time reduces the PS of the formulation by breaking down the larger particles into smaller ones.
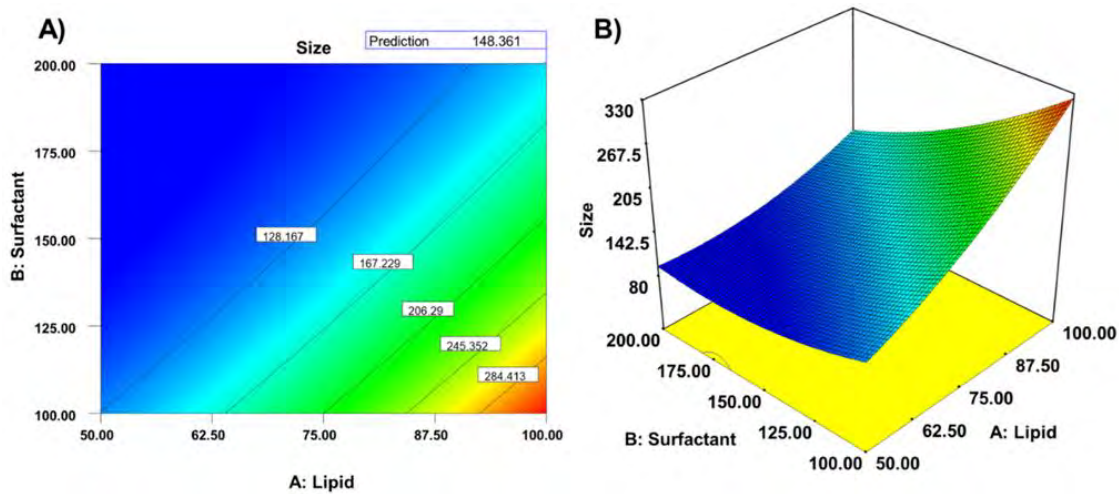

Figure 6.3 BBD optimization graphs illustrating the effect of independent variables particle size. (A) The contour plot graph of factors effecting on particle size; (B) Three-dimensional graph of factors effecting on particle size.

Table 6.4 Experimental trails executed using CCD with respective results for SLNs.

Code	Factor1 A: Lipid Base (mg)	Factor 2 B: Surfactant (mg)	Factor 4 D: Homogenization Time (min)	Response 1 Size (nm)	Response 2 EE (%)	PDI
BBD1	75	200	12	101.05 ± 7.70	85.79 ± 0.20	0.195± 0.01
BBD2	50	100	10	132.26 ± 4.60	86.99 ± 0.13	0.253± 0.02
BBD3	75	100	8	291.93 ± 56.90	86.72 ± 0.30	0.805± 0.05
BBD4	75	100	12	175.47 ± 3.25	85.82 ± 0.05	0.445± 0.08
BBD5	100	200	10	152.77 ± 6.05	91.19 ± 0.10	0.346±0.028
BBD6	50	150	12	103.20 ± 0.72	84.73 ± 0.18	0.136±0.010
BBD7	50	200	10	97.31 ± 1.090	80.62 ± 0.06	0.336±0.013
BBD8	75	150	10	147.67 ± 24.63	84.68 ± 0.20	0.448±0.028
BBD9	75	200	8	124.97 ± 1.81	86.22 ± 2.75	0.418±0.011
BBD10	75	150	10	121.8 ± 4.67	84.02 ± 1.04	0.239±0.005
BBD11	75	150	10	130.37 ± 1.51	84.04 ± 0.27	0.256±0.002
BBD12	50	150	8	120.83 ± 11.83	83.94 ± 0.18	0.303±0.045
BBD13	100	150	12	221.27 ± 8.40	88.56 ± 0.23	0.345±0.018
BBD14	100	100	10	329.2 ± 34.83	87.15 ± 0. 2	0.375±0.040
BBD15	100	150	8	250 ± 20.42	89.24 ± 0.52	0.451±0.005
BBD16	75	150	10	153.73 ± 3.23	84.59 ± 0.02	0.351±0.011
BBD17	75	150	10	140.53 ± 1.19	84.05 ± 0.75	0.330±0.032

*Note; Lipid- palmitic acid; surfactant- gelucire 48/16

6.8.1.5 Effect of independent variables on entrapment efficiency

After 17 trials, Table 6.4 showed that the average EE of the dasatinib-loaded SLNs fell within the

80.62- 91.20 range. The quadratic model's F-value of 51.96 indicates the model's significance. The

response variable EE is depicted in Figure 6.4 A& B as a contour plot and three-dimensional graph.

The lack of fit was found to be insignificant with a 3.11 F-value compared to the pure error.

Equation (6) represents the coded values of the chosen independent variables

$EE = 84.28+ 2.48A- 0.36B- 0.15C+ 2.60AB- 0.37AC+ 0.12BC+1.34A^2+ 0.87B^2 +1.00C^2$ eq.(6)

This regression demonstrates that entrapment increases with an increase in the concentration of lipid and surfactant. Furthermore, an increase in palmitic acid and gelucire 48/16 concentrations improves drug solubility, resulting in an increase in EE. However, as the homogenization time increased, reduced EE was observed due to drug expulsion during the formulation's breakage of micro-particulates into nano-size particles.
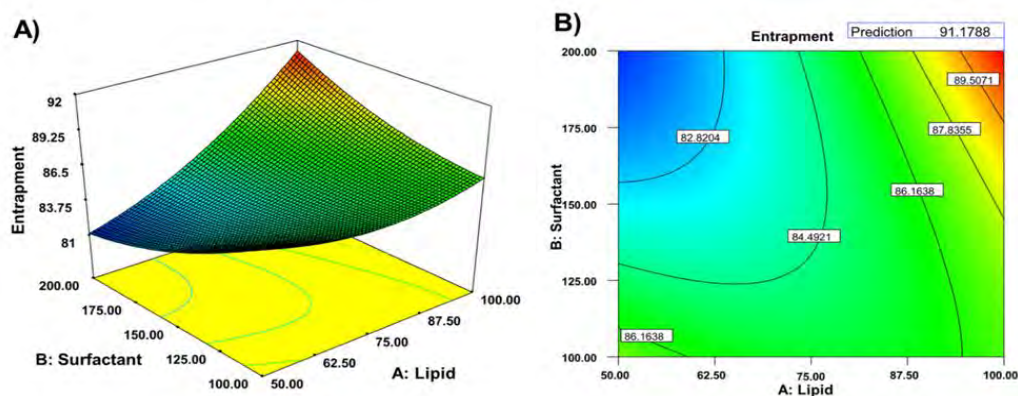

Figure 6.4 BBD optimization graphs illustrating the effect of independent variables entrapment efficiency. (A) Three-dimensional graph of factors on effecting entrapment efficiency; (B) The contour plot graph of factors effecting on entrapment efficiency.

6.8.1.6 Validation of the design to select optimized batch

The dasatinib-loaded SLNs were optimized using both numerical and desirability methods, aiming to identify the formulation with the highest EE and lowest PS. Table 6.4 outlines the criteria required to achieve the expected response. The Design-Expert software generated 27 solutions, and the one with the highest desirability value close to 1 was selected to prepare the dasatinib-loaded SLNs (BBD18 SLNs). The design was validated using a formulation consisting of 100mg lipid content, 200mg gelucire 48/16 concentration, homogenization speed of 15,000 rpm, and time of 10 min, the formulation details mentioned in Table 6.5. The resulting mean PS was 147.20 ± 11.01 nm, with a PDI of 0.255 ± 0.092, and the EE was 91.19 ± 0.55 percent. The optimized formulation exhibited sustained release, with drug release exceeding 90.57 ± 4.31 percent within

12 h. The predicted values for EE and PS were close to the actual values, indicating the effectiveness of the design. The desirability graphs and three-dimensional surface graphs of PS and EE for the optimized formulation are shown in Figure 6.5 A & B. This same formulation was used for scale-up studies.
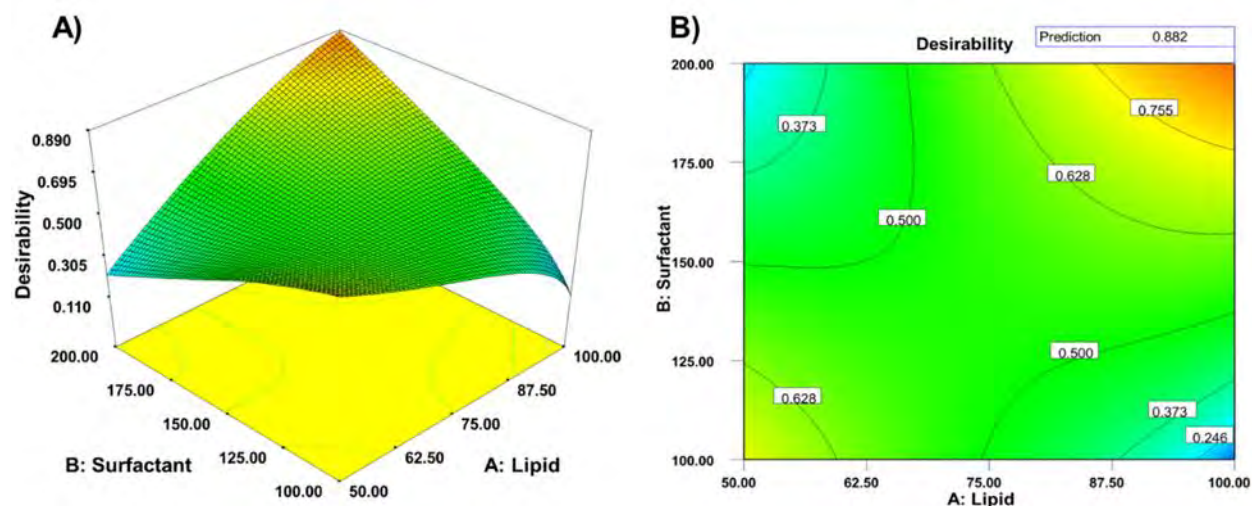

Figure 6.5 BBD desirability graphs illustrating factors against desirability value. (A) The three-dimensional graph; (B) The contour plot graph.

6.8.2 Scale-up studies

The optimized BBD18 SLNs were chosen for scale-up studies, and batch sizes of 10, 50, and 100 mL were formulated using the suggested parameters from the design space. The composition of the formulation remained unchanged, but the amount of lipid and gelucire 48/16 concentrations were increased in proportion to the batch size. The homogenization speed was kept constant for all three batches, but the processing time was increased to 15 min for the 100 mL batch, while the 10 and 50 mL batches were processed for the suggested time of 10 min. The vessel diameter also played a crucial role in the size reduction process during homogenization, and therefore, the homogenization time was adjusted based on the batch size, and a suitable vessel size was chosen for each batch.

Table 6.5 Optimized SLNs formulation (BBD18 SLNs).

Ingredients	BBD18
Dasatinib (mg)	5
Palmitic acid (mg)	100
Gelot 64 (mg)	50
Gelucire 48/16 (mg)	200
Methyl paraben (mg)	50
Propyl paraben (mg)	5
Sodium meta bisulfate (mg)	10
Water (g)	9.60
Total weight (g)	10
Homogenization speed (RPM)	15,000
Homogenization time (min)	10

6.8.3   Characterization of SLNs

6.8.3.1 Attenuated total reflection infrared spectroscopy (ATR-IR)

The IR spectra of DTB, BBD18 SLNs, and BBD18 Placebo SLNs are presented in Figure 6.6, where the characteristic peaks of DTB at 1498.59 cm^{-1}, 1581.11 cm^{-1}, 1624 cm^{-1}, 3229.9 cm^{-1}, and 3402.12 cm^{-1} for C–H, C–C, C=O, O–H, and N–H (secondary amine N-H stretch), respectively, were identified. However, the BBD18 SLNs showed the absence of the distinct DTB peaks, with the remaining peaks matching those of BBD18Placebo SLNs, indicating the entrapment of the pure drug within the lipid matrix, resulting in the loss of its characteristic peaks.
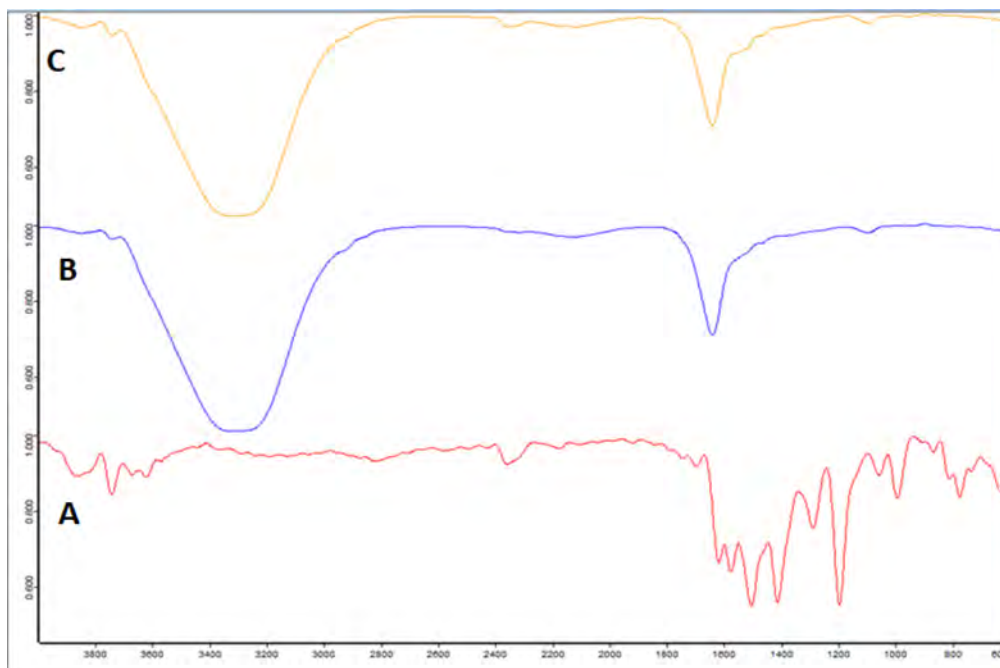
Figure 6.6 ATR-IR Peaks of (A) Dasatinib; (B) BBD18 Placebo SLNs; (C) BBD18 SLNs.

6.8.3.2 Measurement of particle size, poly dispersity index, zeta potential, and encapsulation efficiency

The three formulations exhibited PS values of 147.20 ± 11.01 nm (0.255 ± 0.092 PDI), 166.90 ± 22.30 nm (0.280 ± 0.121 PDI), and 154.23 ± 15.56 nm (0.24 ± 0.13 PDI), respectively, for 10, 50, and 100 mL batches. The optimized formulation had an average ZP of -28.50 ± 4.72 mV, which is considered stable as ZP ranging from ±25 mV reduces particle coalescence/ aggregation [10]. EE was 91.19 ± 0.55%, 92.1 ± 0.1%, and 92.20 ± 0.14% for 10, 50, and 100 mL batches respectively, indicating similar characteristics for all batches. Spherical morphology in the 120-180 nm range was observed in Figure 6.7. It is suggested that nano-formulations with PS less than 200 nm exhibit improved permeation [11],and a PDI value less than 0.300 indicates uniformity of the formulation.
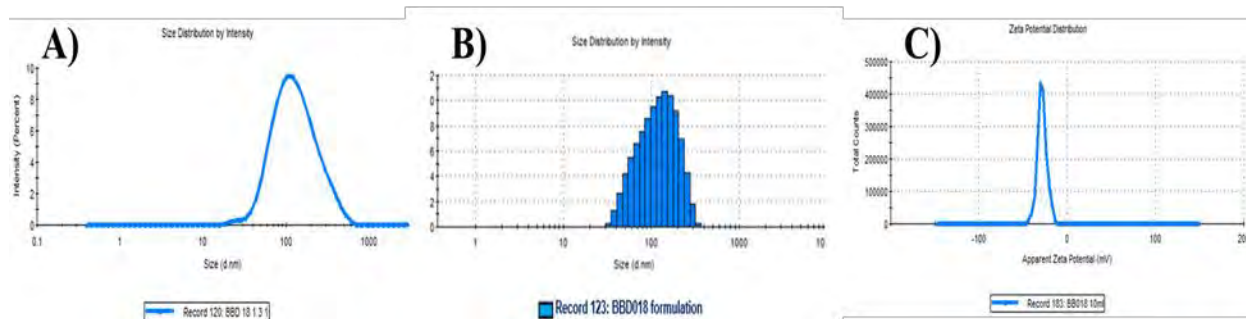
Figure 6.7 Measurement of BBD18 SLNs. (A) Particle size; (B) particle size distribution; (C) apparent zeta potential.

6.8.3.3 Morphology by field–emission scanning electron microscopy (FESEM)

In the morphological analysis, the particles were observed to be uniformly distributed with an average size of 146.8 ± 15.12 nm, (Figure 6.8). The particles exhibited a non-aggregated, spherical shape with a smooth and flexible surface, indicating their resistance to ostwald ripening caused by particle coalescence.
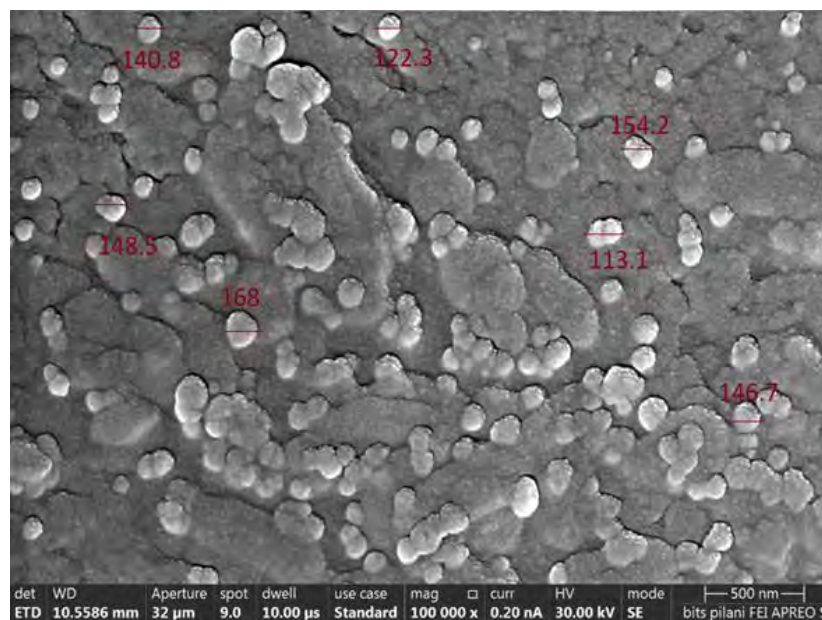

Figure 6.8 FESEM image of BBD18 SLNs formulation.

6.8.3.4 *In-Vitro* drug release studies

The *in-vitro* release study of BBD18 SLNs and FDS was conducted for 24 h on all three batches (10, 50, and 100 mL), as illustrated in Figure 6.9. While FDS exhibited complete drug release within 4 h, the drug-loaded SLNs displayed sustained drug release over 24 h. After 6 h, the drug release percentages for 10, 50, and100 mL batches were approximately 76.95 ± 0.28%, 77.45 ± 2.28%, and 71.32 ± 0.93%, respectively, while after 12 h, the release was 95.47 ± 2.22%, 88.90 ± 4.32%, and 87.34 ± 4.32%, respectively. After 24 h, the release was 99.98 ± 2.12%, 99.88 ± 2.46%, and 99.43 ± 1.12%, respectively, and all BBD18 SLNs batches exhibited similar sustained-release patterns. The drug release profiles for all three batches (10, 50, and 100 mL) were consistent with the Korsmeyer-Peppas model, as the plots exhibited high R^2 values of 0.987, 0.989, and 0.991, respectively, and the n values were less than 0.45, indicating Fickian diffusion. These results are summarized in Table 6.6, suggesting that the slower and sustained drug release is due to its dissolution within the lipid [12].
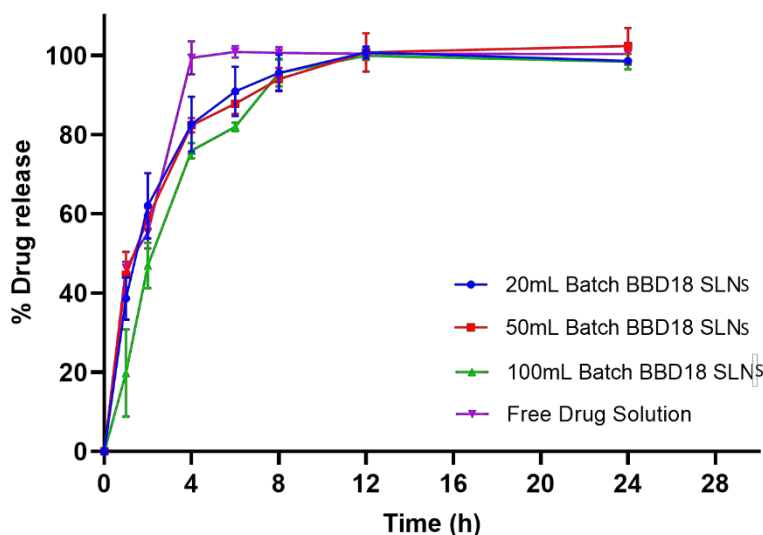

Figure 6.9 *In-vitro* comparative release profile of pure dasatinib solution with different batch sizes of BBD18 SLNs formulation.

Table 6.6 Release kinetics data of dasatinib-loaded SLNs.

		10ML	50ML	100ML
Zero order	R^2 Value	0.756	0.769	0.806
	AIC	76.327	75.602	74.033
Higuchi	R^2 Value	0.9235	0.9305	0.9501
	AIC	62.8551	61.7378	58.5390
Korsmeyer Peppas	R^2 Value	0.9874	0.9892	0.9913
	AIC	47.0635	47.1180	45.2210
	N	0.266	0.274	0.312
First Order	R^2 Value	0.9806	0.9827	0.9839
	AIC	49.9157	48.6396	48.1059
Hixson Crowell	R^2 Value	0.9603	0.9637	0.9795
	AIC	0.8496	0.9482	1.5709

6.8.4   SLNs loaded gel characterization

6.8.4.1 Physical appearance, pH determination and spreadability

The BBD18 SLNs gel formulation, as shown in Figure 6.10, exhibited an off-white color with a smooth, homogeneous texture and excellent consistency. It is crucial for topical formulations to maintain a pH that is compatible with the skin's natural pH, as changes in pH can lead to skin irritation or disruption. To ensure compatibility, the formulation's pH was adjusted to 5.5 ± 0.1 using a 1% NaOH solution. The optimized SLNs gel formulation and placebo had similar spreadability values of 1.17 ± 0.035 cm^2.g^{-1} and 1.19 ± 0.051 cm^2.g^{-1}, respectively, with no significant differences observed between the drug-loaded formulation and the placebo gel.
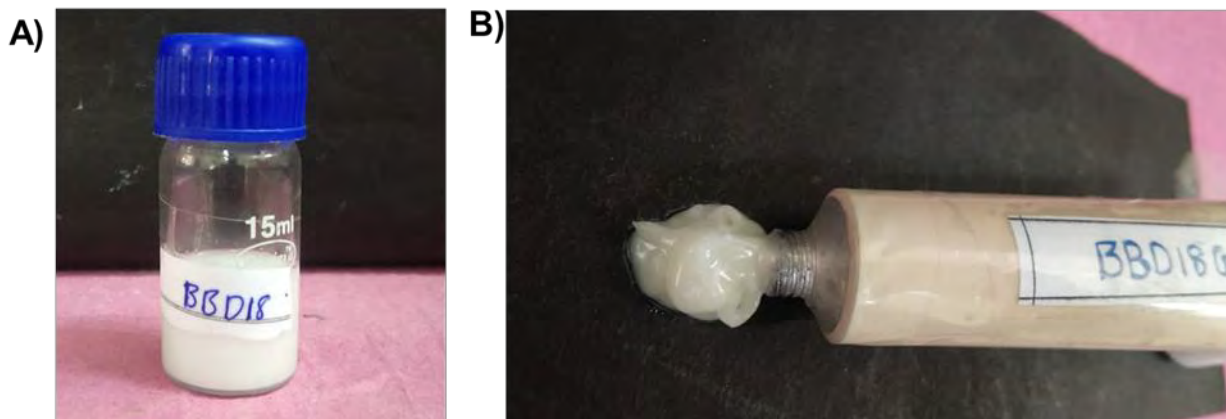
Figure 6.10 Physical appearance of (A) BBD18 SLNs; (B) BBD18 SLNs gel.

6.8.4.2 Particle integrity in hydrogel matrix

The BBD18 SLNs gel was prepared and characterized for PS, revealing a similarity in PS to that of the SLNs, measuring at 143.27 ± 22.35 nm. Further analysis of the SLNs gel using FESEM demonstrated a resemblance to the BBD18 SLNs, as depicted in Figure 6.11. Therefore, the data indicated that the nanocarriers remained intact even after being loaded into the Carbopol ETD 2020 hydrogel matrix.
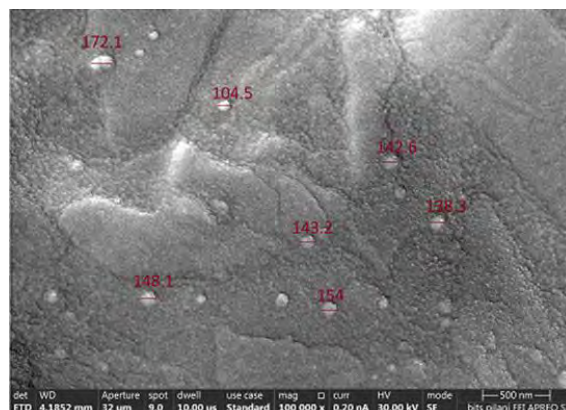

Figure 6.11 FESEM image of BBD18 SLNs loaded gels formulation.

6.8.4.3 Rheological behaviour

Viscosity

The optimized formulation exhibited an average viscosity of 5632.03 ± 99.69 mPa.s at a constant shear rate, and the viscosity did not significantly change with time during the constant shear rate. This is indicative of the gel's Newtonian behaviour, which can be seen in Figure 6.12.
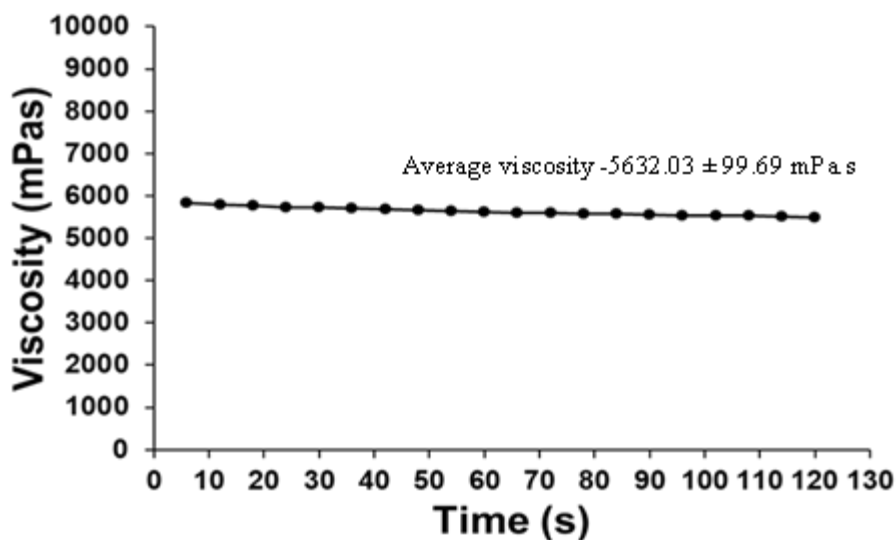

Figure 6.12 Viscosity plot of BBD18 SLNs gel formulation.

Shear flow

The flow characteristics of the BBD18 SLNs gel was conducted, and the results were shown in Figure 6.13. Here, the viscosity and shear stress varied with the function of shear rate. As a result, the formulation demonstrated non-Newtonian behaviour that corresponded to the Herschel-Bulkley model, equation (7).

$$\sigma = \sigma_0 + K \cdot \gamma^n \qquad\qquad\qquad eq.(7)$$

where σ_0 represents yield stress, K represents consistency index, and n represents power index; n < 1. The viscosity decreased as the shear rate increased, indicating shear thinning and pseudo plastic behaviour of the BBD18 SLNs gel.
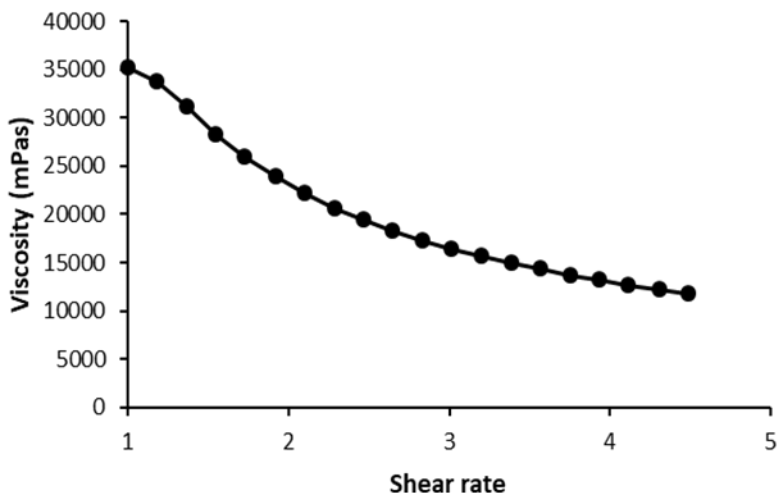

Figure 6.13 Shear flow of BBD18 SLNs gel formulation.

Strain sweep test

The linear viscoelastic region (LVR) was determined using an oscillation strain sweep (OSS) test, which allowed for the measurement of the viscoelastic moduli as a function of time or frequency. The LVR was found to end with a 10% decrease (1.24%) in the storage modulus (G′) plateau value, followed by an increase in the loss modulus (G″). This suggested that the viscoelastic properties of the sample may not be entirely independent of the strain amplitude, indicating a loss of the original structure upon the application of oscillation strain (OS). The flexible long straight chain polymers present in the sample were found to coil upon OS, potentially leading to some degree of interlocking and energy minimization. Additionally, hydrogen bonding between neighbouring molecules resulted in complete cross-linking. Under OS, the polymeric chains uncoiled and aligned with the flow, transitioning from a disorderly to an orderly arrangement that was

reversible. The values of log G′ and log G″ versus the logarithm of % strain, shown in Figure 6.14, demonstrated that the LVR exhibited predominantly elastic behaviour, indicating a strong gel structure [13]**.**
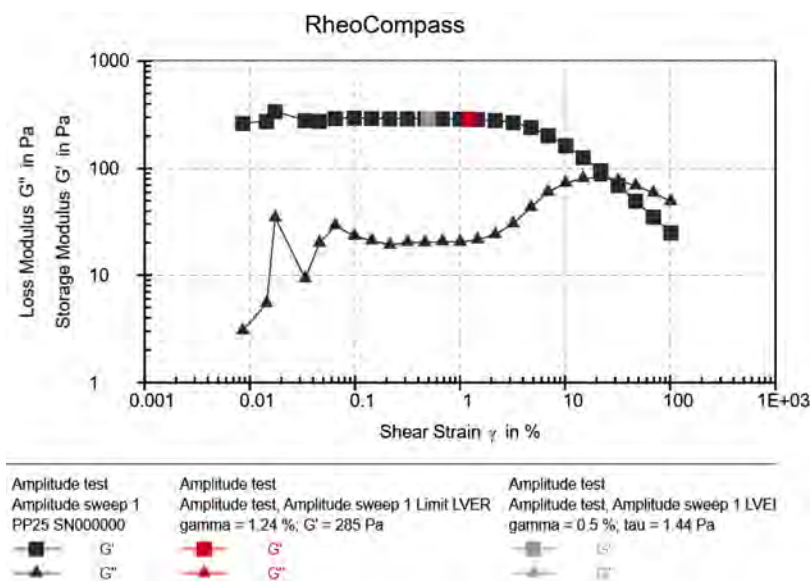

Figure 6.14 Amplitude sweep test of BBD18 SLNs gel formulation employing angular frequency.

Frequency sweep test

When the structural integrity of the gel is preserved, variations in frequency have no impact on G′ and G″ [14]. Figure 6.15 A & B presents the frequency distribution plotted on a logarithmic scale. The elastic and viscous moduli of the BBD18 SLNs gel remained constant regardless of frequency, suggesting a frequency-independent gel structure. Moreover, G′ consistently exceeded G″ across the frequency range, indicating a robust gel structure.
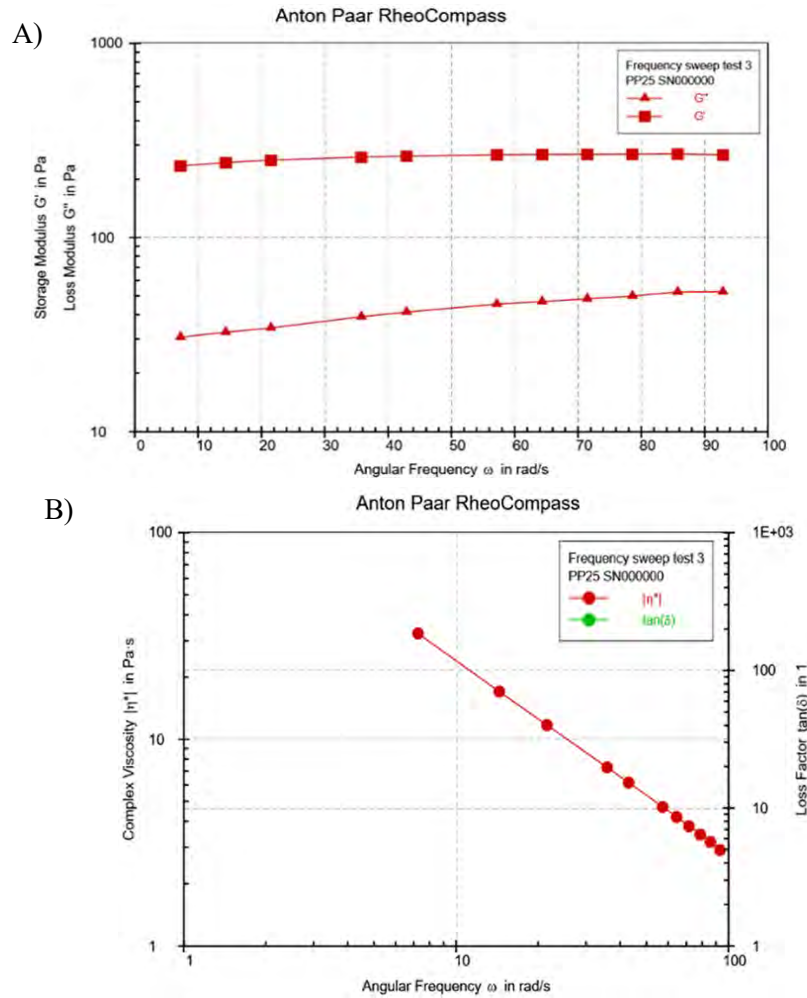
Figure 6.15 Frequency sweep test of (A) loss modulus and storage modulus of BBD18 SLNs gel formulation; (B) Complex viscosity of BBD18 SLNs gel formulation.

In summary, the rheology of the BBD18 SLNs gel was evaluated through viscosity and frequency tests. The results showed that the gel has a strong structure with excellent consistency and the ability to transform from a solid to a flowable state under increased shear stress (shear thinning behaviour), which enhances its spreadability during topical application. The gel's structural integrity was confirmed by the frequency strain and frequency sweep tests. This desirable spreadability results in a thin layer on the skin with improved bio-adhesive properties and sustained

release, leading to an enhanced therapeutic effect. Overall, the BBD18 SLNs gel is a promising option for patients [15][16].

6.8.5 *In-vitro* cell line study

6.8.5.1 Cytotoxicity studies

In the cytotoxicity test on HaCaT cell lines for both free DTB and BBD18 SLNs gel were evaluated. HaCaT cell lines were selected for the test because they represent 95% of the epidermal skin cells. Figure 6.16 depicts the cytotoxic effects of free DTB and BBD18 SLNs gel dispersion on HaCaT cell lines. The results showed that DTB did not have a significant impact on the keratinocyte cells, and more than 50% cell viability was observed at a 1000 nM concentration of both free DTB and BBD18 SLNs gel. Thus, it was concluded that the excipients used in the formulations are not toxic to keratinocyte cells**.**
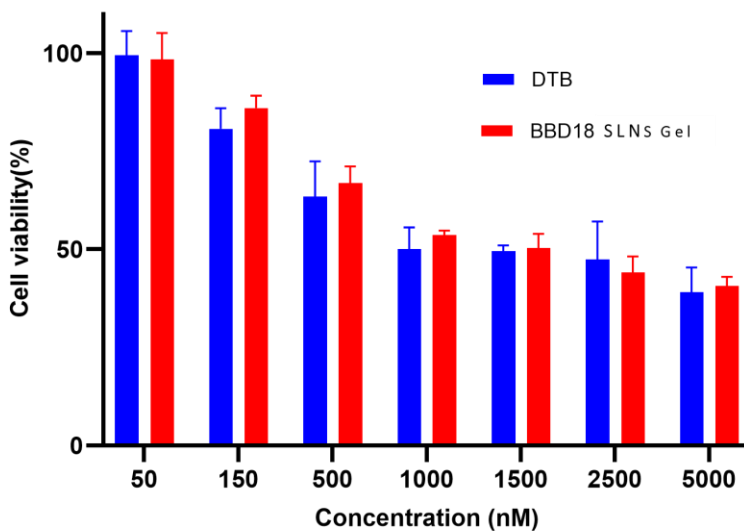

Figure 6.16 *In-vitro* comparative cell viability study of dasatinib (DTB) and BBD18 SLNs gel on HaCaT cell lines.

6.8.5.2 Effect on the production of TNF-α and IL-6

TNF-α and IL-6 are critical factors in fibroblast growth and pro-inflammatory mediator induction, such as PGE2 and IL-1, leading to synovitis, bone and cartilage destruction during RA

pathogenesis. Figure 6.17 shows that compared to free DTB, treatment with BBD18 SLNs gel significantly reduced LPS-induced TNF-α production from RAW 264.7 cells. These results suggest that the BBD18 SLNs gel anti-arthritic properties may inhibit inflammatory cytokines, including TNF-α. Inhibition of TNF-α production is linked to decreased inflammation and cartilage deterioration, which can effectively halt the progression of arthritis. Similarly, IL-6 production was decreased with BBD18 SLNs gels compared to free DTB Figure 6.18.
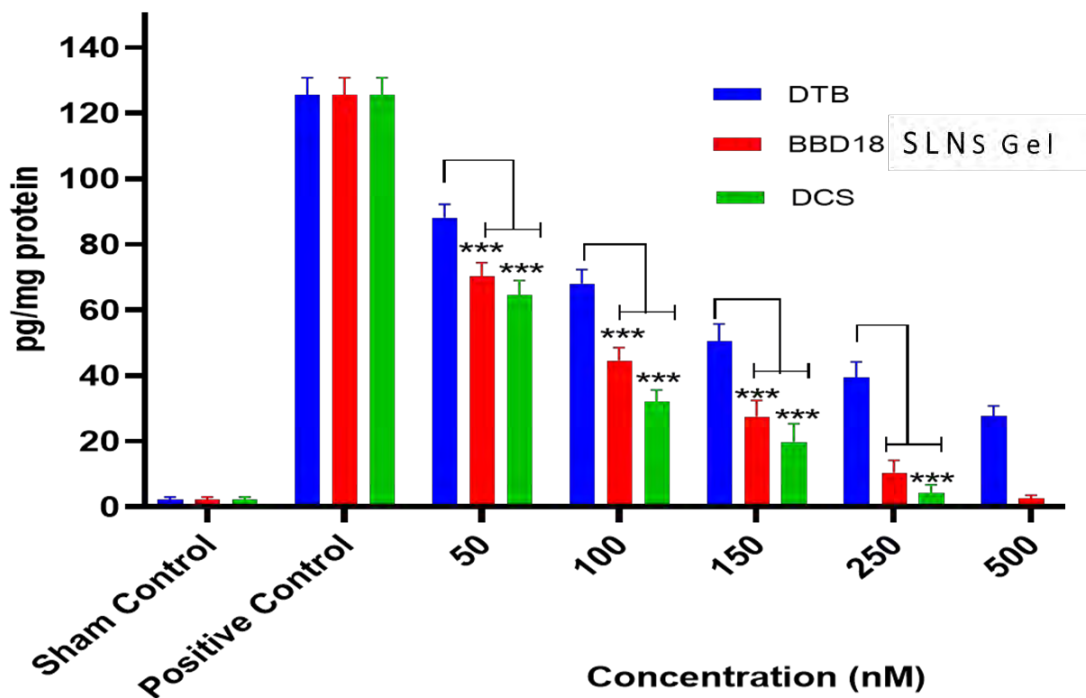

Figure 6.17 TNF-α expression level in RAW 264.7 cells treated with dasatinib (DTB), BBD18 SLNs gel and marketed diclofenac sodium (DCS) formulation.
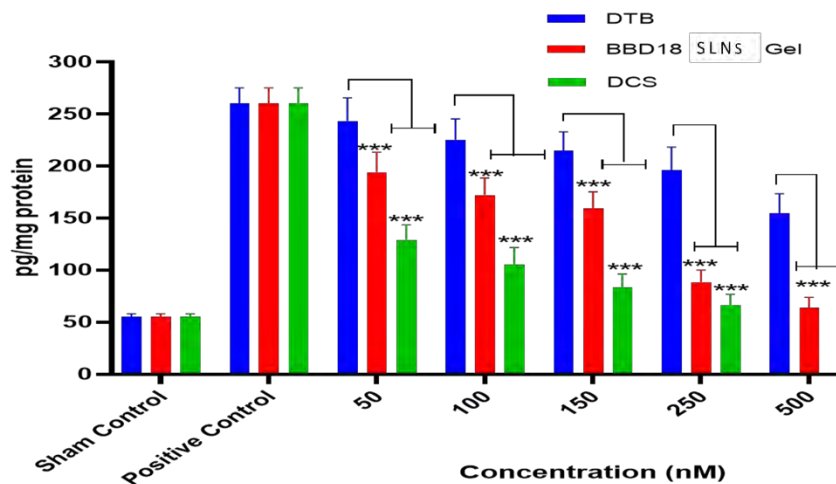
Figure 6.18 IL-6 expression level in RAW 264.7 cells treated dasatinib (DTB), BBD18 SLNs gel and marketed diclofenac sodium (DCS) formulation.

6.8.6 *Ex-Vivo* studies

6.8.6.1 *Ex-Vivo* skin permeation study

Ex-vivo permeation studies on rat abdominal skin were performed using pH 5.5 PB containing 1% Triton X100 as release media to evaluate the optimized BBD18 SLNs gel and FDG formulations. Figure 6.19 shows the total amount of drug permeation over a 24-hour period, with 33.72 ± 2.05 $\mu g/cm^2$ and 4.31 ± 1.07 $\mu g/cm^2$ of drug permeated through the skin after 12 h for BBD18 SLNs gel and FDG formulations, respectively. After 24 h, the amounts were 36.17 ± 3.5 $\mu g/cm^2$ and 6.86 ± 1.98 $\mu g/cm^2$. The flux across the skin was 0.58 ± 0.06 $\mu g /cm^2 /h$ for BBD18 SLNs gel and 0.1 ± 0.04 $\mu g /cm^2 /h$ for FDG formulations. Significantly higher drug permeation ($p < 0.001$) and flux across the skin were observed for BBD18 SLNs gel compared to FDG, demonstrating higher permeation efficiency of the BBD18 SLNs gel. In conclusion, the study found that the BBD18 SLNs gel has a greater drug permeation and flux across the skin than FDG [17].
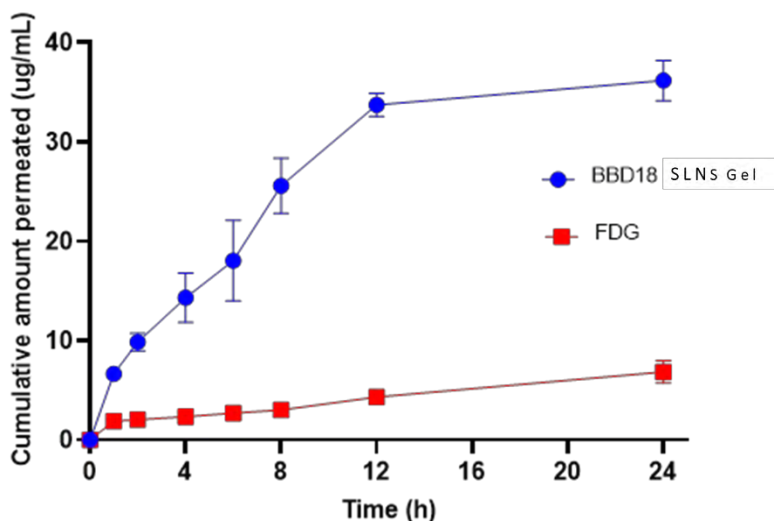
Figure 6.19. *Ex-vivo* permeation study of BBD18 SLNs gel and free drug loaded gel (FDG).

6.8.6.2 Skin deposition study

The results shown in Figure 6.20 indicate that, after 24 h, the BBD18 SLNs gel deposited 277.50 ± 9.63 ng/cm^2 of drug, while the FDG formulation deposited only 17.49 ± 3.28 ng/cm^2. The deposition with the BBD18 SLNs gel was found to be 20 times higher ($p < 0.05$) than with the FDG formulation, indicating that the BBD18 SLNs gel has superior drug deposition capacity and can sustain drug delivery to deeper layers [18].

Figure 6.20 *Ex-vivo* skin deposition study BBD18 SLNs gel and free drug loaded gel. (FDG) *** $p < 0.001$ vs. FDG.

6.8.6.3 Bio adhesion studies

The adhesive strength of BBD18 SLNs gel, BBD18Placebo SLNs gel, and 0.5% carbopol plain gel were measured and presented in Figure 6.21. The results indicated that the adhesiveness of BBD18 SLNs gel was comparable to the placebo gel, while a slight variation (non-significant) was observed with 0.5% carbopol gel. Th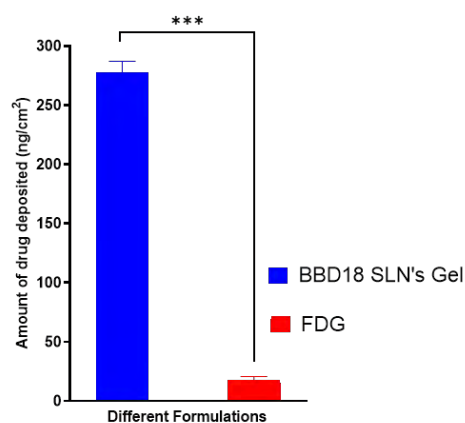e values obtained were 7.16 ± 0.211, 7.29 ± 0.32, and 7.36 ± 0.31 for BBD18 SLNs gel, BBD18 Placebo SLNs gel, and 0.5% carbopol plain gel, respectively. This finding suggests that the uniform dispersion of lipid nanoparticles in the aqueous gel base did not interfere with the swelling mechanism of the carbopol gel, as shown in Figure 6.21 [19].
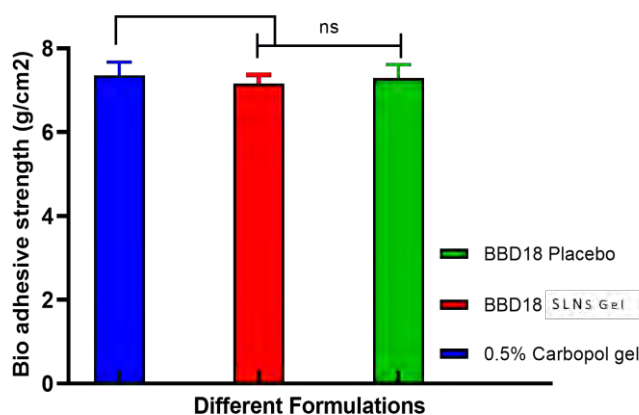
Figure 6.21 *Ex-vivo* comparative bio-adhesion strength of BBD18 placebo, BBD18 SLNs gel and 0.5% carbopol gel.

6.8.7   In-vivo studies

6.8.7.1 Skin irritation studies

The scores for erythema, atonia, and fissuring of the five groups were recorded in Table 6.7 after 72 h of observations. All formulations, except for the 5% SLS gel, behaved similarly to the non-treated (negative control) group, indicating that the developed topical formulation is safe for the skin. The study images are represented in Figure 6.22

After 72 h, the animals were sacrificed, and the treated skin patches were examined for histopathology, as shown in Figure 6.23. The epidermis layer of the untreated skin was thin, with no necrosis observed, and this was also observed in the BBD18 SLNs gel, BBD18 Placebo SLNs gel, and FDG. However, increased thickness (hyperkeratosis) of the epidermis layer with necrosis was observed in the case of the 5% SLS gel compared to other formulations. Binding of the SLS-loaded gel to the keratin in the subcutaneous layer causes ionic and hydrophobic interactions, resulting in subcutaneous swelling. Lipid removal from the subcutaneous exposes more keratin binding sites, causing protein denaturation. Surfactants also interact with horny layer proteins, causing reversible skin damage [20].In contrast, BBD18 SLNs gel uses non-ionic lipids and surfactants, which do not interact ionically with skin ionic proteins, reducing irritancy. Therefore, the topical BBD18 SLNs gel is a non-irritant.

Table 6.7 Grading for skin reaction for erythema and oedema.

Time (h)	BBD18Placebo SLNs gel	BBD18 SLNs gel	FDG	5% SLS GEL	Normal group
Erythema and Oedema					
0	0	0	0	0	0
1	0	0	0	0	0
6	0	0	0	0	0
12	0	0	0	1	0
24	0	0	0	2	0
48	0	0	0	3	0
72	0	0	1	3	0
Atonia- A decrease in normal elasticity of the skin					
0	1	1	1	1	1
1	1	1	1	1	1
6	1	1	1	2	1
12	1	1	1	2	1
24	1	1	1	3	1
48	1	1	1	3	1
72	1	1	2	3	1
Fissuring- Cracks on skin					

0	1	1	1	1	1
1	1	1	1	1	1
6	1	1	1	1	1
12	1	1	1	1	1
24	1	1	1	2	1
48	1	1	1	2	1
72	1	1	1	2	1

*Note; Grading for skin reaction for Erythema and Oedema (0- None, 1- Slight, 2- Moderate, 3- Severe), Atonia - A decrease in normal elasticity of the skin [1- Slight (slight impairment of elasticity), 2- Moderate (slow return to normal), 3- Marked (No elasticity)], Fissuring - Cracks on skin (1- Slight (Definite cracks in epidermis), 2- Moderate (Cracks on dermis), 3- Marked (Cracks and bleeding).
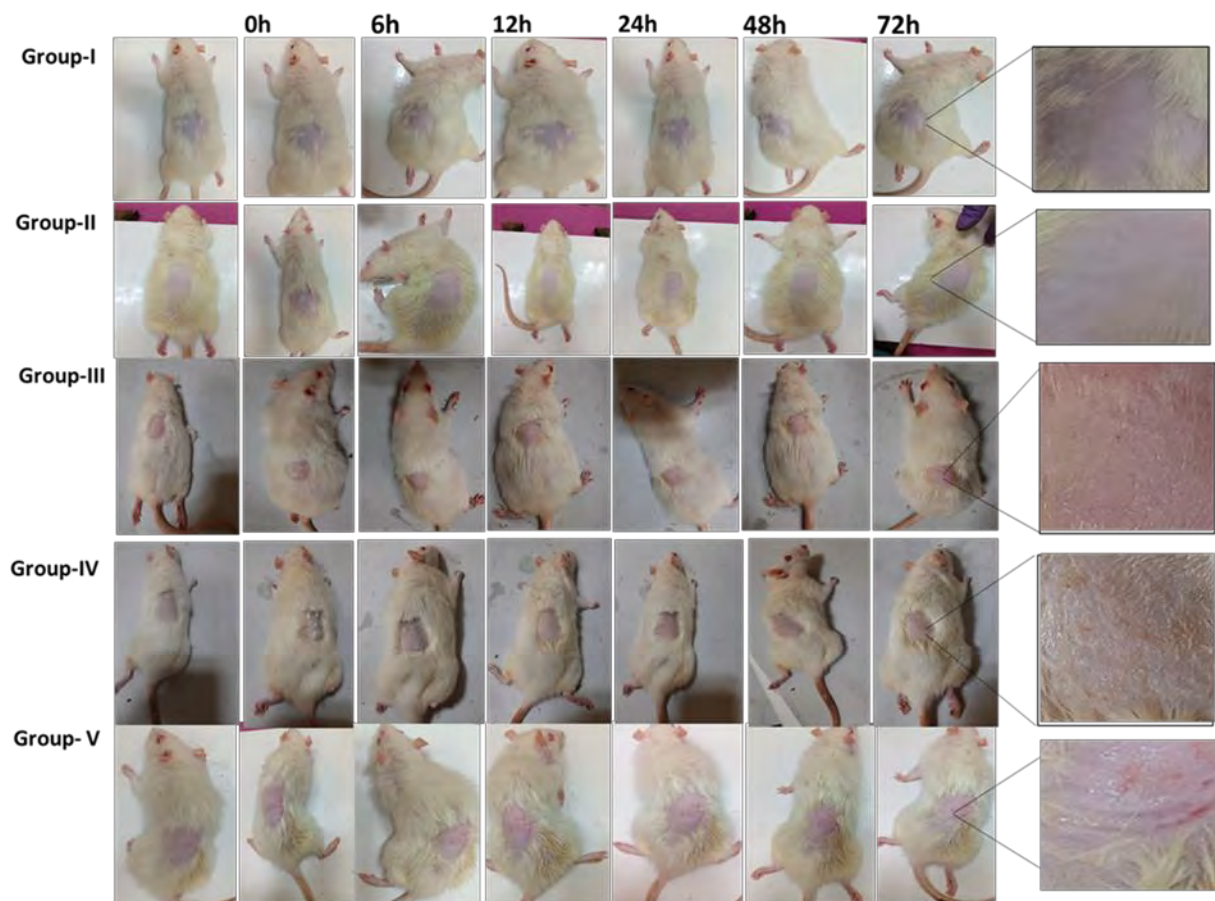

Figure 6.22 *In-vivo* skin irritation study.

Note *Group I—untreated group; Group II—FDG (200 mg from 0.05% gel); Group III— BBD18 SLNs gel (200 mg from 0.05% gel); Group IV— BBD18 Placebo SLNs gel (200 mg from 0.05% gel); Group V—received 5% SLS gel.

Figure 6.23 Histopathology of skin sample after skin irritation studies.

Note *Group I—untreated group; Group II—FDG (200 mg from 0.05% gel); Group III— BBD18 SLNs gel (200 mg from 0.05% gel); Group IV— BBD18 Placebo SLNs gel (200 mg from 0.05% gel); Group V—received 5% SLS gel.
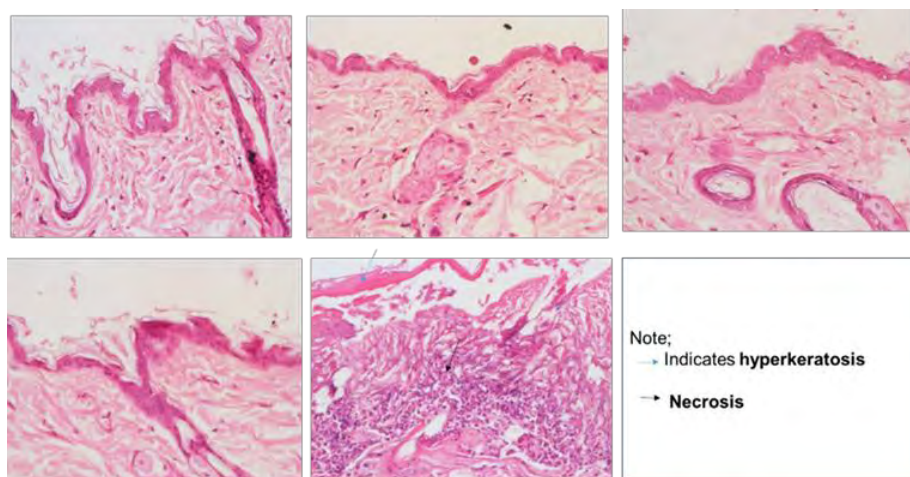
6.8.7.2 FCA-induced arthritis model (chronic inflammatory model)

6.8.7.2.1 Assessment of arthritis from physical parameters

During the CFA immunization experiment, rats experienced significant weight loss, as illustrated in Figure 6.24. Conversely, animals treated with MFD, BBD18 SLNs gel, and FDG displayed notable weight gain ($p < 0.001$) after day 27. Among the treatments, the BBD18 SLNs gel resulted in a significant ($p < 0.5$) improvement in body weight compared to topical FDG administration, although a similar difference was observed in the MFD-treated group. The study demonstrated that the BBD18 SLNs gel formulation was particularly effective, producing a significant weight gain from day 12 ($p < 0.05$).

The first phase of arthritis induction occurred on the 5th day when CFA -injected hind paws swelled to a maximum and turned red. This was followed by subsiding swelling until the 10th day, after which the paw swelled again in the second phase, worse than the first. However, topical administration of BBD18 SLNs gel and MFD from the fifth day of arthritis induction significantly

suppressed (p < 0.01) the second phase Figure 6.25 and reduced hind paw edema /redness in the arthritis groups. The arthritic clinical score also showed a significant decrease from day 15–27 (p < 0.05), indicating anti-arthritic activity Figures 6.26 & 6.27. The blank formulation, in comparison to the AIA control group, did not affect body weight change, paw swelling, or arthritic score.

Figure 6.24 Body weight comparative assessment after treatment with different formulation for BBD18 placebo gel, BBD18 SLNs loaded gel, free drug loaded gel (FDG), marketed formulation diclofenac (MFD) adjuvant induced arthritis (AIA), and normal groups.

*** $p < 0.001$. ** $p < 0.01$, *$p<0.5$ vs. normal group; $^{+++}p < 0.001$. $^{++}p < 0.01$, $^{+}p < 0.5$ vs. AIA control.
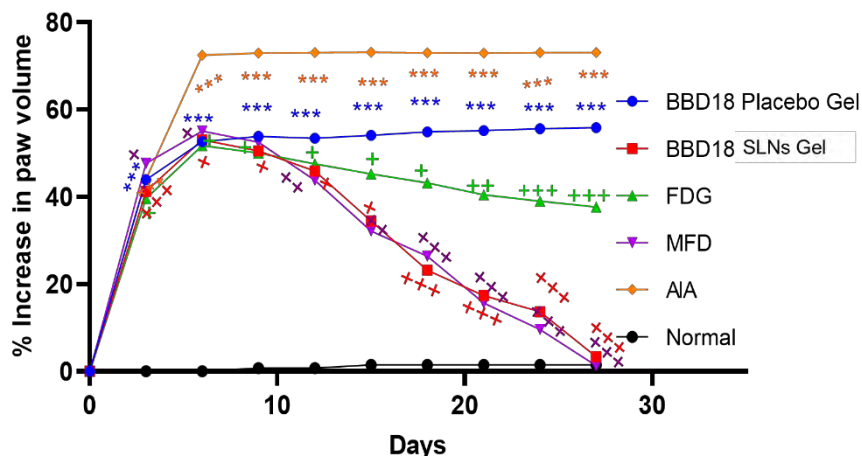
Figure 6.25 Comparative assessment of paw volume of the rat after treatment with different formulation for BBD18 placebo gel, BBD18 SLNs loaded gel, free drug loaded gel (FDG), marketed formulation diclofenac (MFD) adjuvant induced arthritis (AIA), and normal groups.

*** $p < 0.001$. ** $p < 0.01$, *$p<0.5$ vs. normal group; $^{+++}p < 0.001$. $^{++}p < 0.01$, $^{+}p < 0.5$ vs. AIA control.

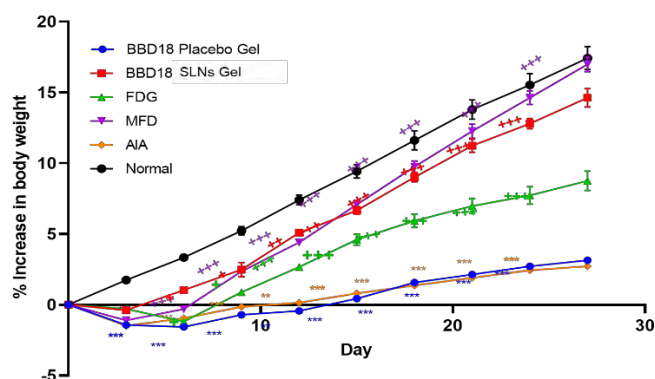**Figure 6. 26** Comparative assessment of arthritis score of the rat after treatment with different formulation for BBD18 placebo gel, BBD18 SLNs loaded gel, free drug loaded gel (FDG), marketed formulation diclofenac (MFD) adjuvant induced arthritis (AIA), and normal groups.

*** $p < 0.001$. ** $p < 0.01$, *$p<0.5$ vs. normal group; +++ $p < 0.001$. ++ $p < 0.01$, + $p < 0.5$ vs. AIA control.
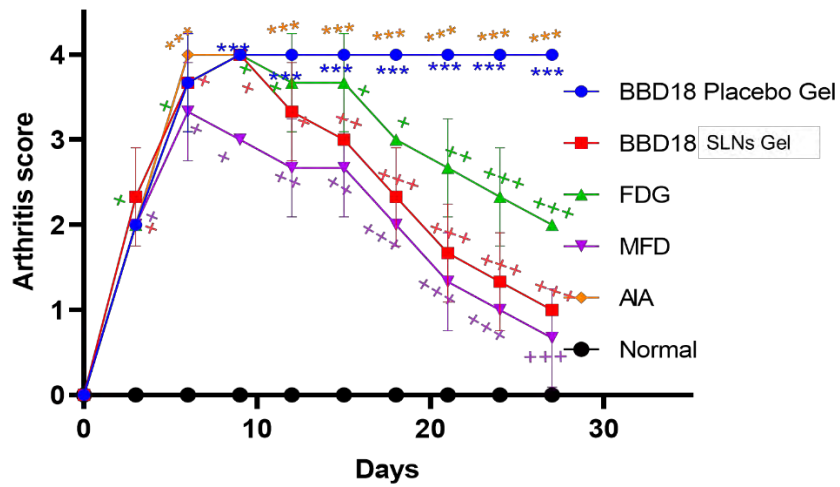

Figure 6.27 Representative images of FCA injected hind paws after 28 days of treatment with various formulations.

Note* (A) normal; (B) AIA; (C) FDG; (D) BBD18Placebo SLNs gel; (E) BBD18 SLNs gel; (F) MFD.

6.8.7.2.2 Nociceptive threshold

FCA-induced arthritis is a reliable model for evaluating chronic pain in rats due to its ability to induce chronic hypersensitivity to nociceptive stimulation [21]. Rats treated with FCA exhibited lower paw withdrawal thresholds than the normal control group, with the pain threshold being the lowest on day 5 Figure 6.28. However, BBD18 SLNs gel and MFG treatment resulted in a reduction of withdrawal latency from the 1st to the 5th day and an increase in paw withdrawal threshold from the 10th day when compared to the FCA-treated control group. Moreover, the hot plate test indicated an increased reaction time, suggesting that BBD18 SLNs gel has an anti-nociceptive effect.

Figure 6.28 Comparative assessment of nociceptive threshold in rats after treatment with different formulation for BBD18 placebo gel, BBD18 SLNs loaded gel, free drug loaded gel (FDG), marketed formulation diclofenac (MFD) adjuvant induced arthritis (AIA), and normal groups.

*** $p < 0.001$. ** $p < 0.01$, * $p < 0.5$ vs. normal group; $^{+++}p < 0.001$. $^{++}p < 0.01$, $^{+}p < 0.5$ vs. AIA control.

6.8.7.2.3 Motor incoordination test

The AIA model causes both pain and motor dysfunction, which ultimately results in hyperalgesia. [22], Motor incoordination is a sign of functional impairment and nervous system inflammation

[23]. Motor incoordination was assessed by the mean fall-off time in the rota rod test. FCA sub-plantar injection diminished fall-off time compared to the normal control group. Compared to the FCA control group, rats treated with BBD18 SLNs gel and MFD had a significantly longer fall off time from day 5 to day 28 Figure 6.29. These findings suggest that DTB-induced counter-regulation of spinal-glial activation improved motor coordination in BBD18 SLNs' gel. Therefore, DTB-loaded SLNs applied topically may treat arthritis-induced motor incoordination.
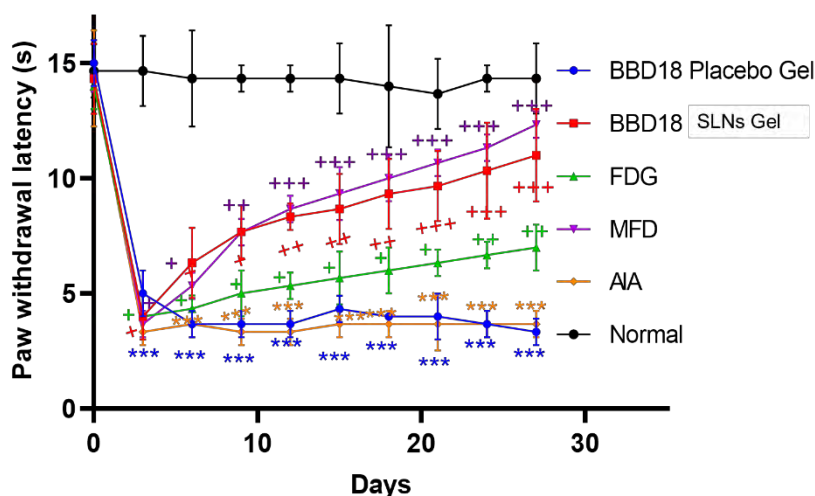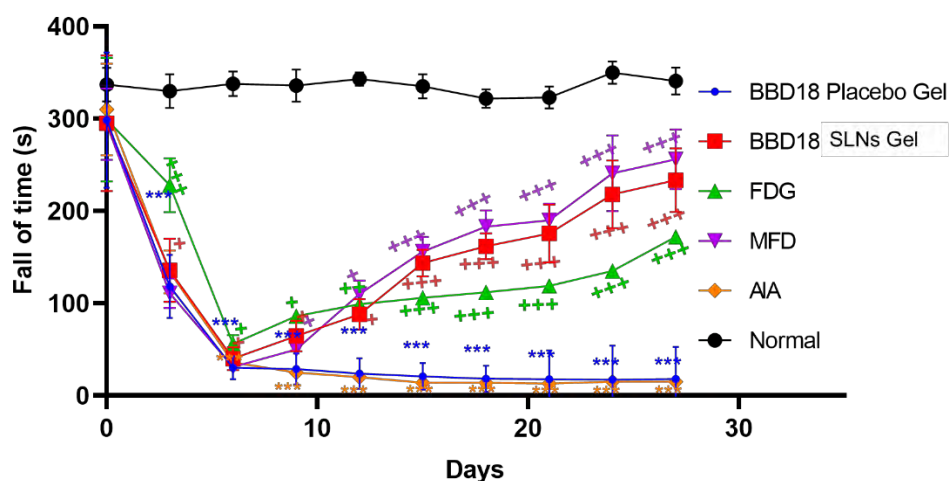

Figure 6.29 Comparative assessment of motor incoordination in rats after treatment with different formulation for BBD18 placebo gel, BBD18 SLNs loaded gel, free drug loaded gel (FDG), marketed formulation diclofenac (MFD) adjuvant induced arthritis (AIA), and normal groups.

*** $p < 0.001$. ** $p < 0.01$, *$p<0.5$ vs. normal group; $^{+++}p < 0.001$. $^{++}p < 0.01$, $^{+}p < 0.5$ vs. AIA control.

6.8.7.2.4 Storage stability of dasatinib loaded SLNs gel

The DTB loaded SLNs gel depicted particles integrity using Malvern zeta sizer without any aggregation. The assay results depicted no substantial change as represented in Table 6.8, indicating the stability of DTB loaded SLNs gel.

Table 6.8. Stability data of dasatinib loaded SLNs gel.

Stability data of dasatinib loaded SLNs gel at 25°C				
Parameter	**0 Month**	**15 days**	**1st month**	**2nd month**
Assay of gel (%)	99.00 ± 1.60	98.91 ± 1.51	98.12 ± 0.35	99.38 ± 2.64
Size (nm)	157.0 ± 19.4	156.25 ± 7.31	165.9 ± 19.91	172.5 ± 7.90
PDI	0.263 ± 0.1	0.25 ± 0.02	0.35 ± 0.029	0.36 ± 0.07

6.9 Outcomes of the research

In this research, SLNs gel was used to improve permeation while minimizing the systemic absorption of DTB, resulting in enhanced efficacy in RA treatment. The QbD method was used to examine the effect of different factors and their interactions in order to achieve the desired product. The higher drug solubility in lipid increased the % EE while decreasing drug leakage from the formulation. The optimal concentration of S_{mix} in the formulation favoured low PS with even distribution by stabilizing the oil-in-water interface. Carbopol ETD 2020 exhibited excellent spreadability and consistency during storage. The prepared BBD18 SLNs gel spread as a thin layer on the skin's surface, hydrating it by reducing trans-epidermal water loss. This hydration promotes skin lipid swelling and helps to improve permeation. *Ex-vivo* studies revealed that the BBD18 SLNs gel had better permeation than FDG. Further, *in-vivo* studies revealed that the BBD18 SLNs gel exhibited better efficacy in FCA induced rat model. The study demonstrated the ease of developing SLNs gel formulations from a wide range of materials, with improved safety and efficacy.

6.10   Conclusions

In this study, the improvement in skin permeation and deposition of a DTB-loaded SLNs gel was determined using a QbD-based approach. Using BBD, the effect of lipid, gelucire 48/16 concentration, and homogenization time on PS and % EE was investigated. The results revealed that topical DTB-loaded SLNs gel increased skin permeation and deposition, as expected, due to the occlusive effect of forming a very thin layer on the skin's surface. The SLNs *in-vitro* drug release demonstrated sustained release. The cell culture results illustrated the safety of the excipients, and the decrease in TNF-α levels expressed the efficacy of the BBD18 SLNs gel formulation. As a result, we conclude that topical delivery of DTB-loaded SLNs gel is a viable approach for the treatment of RA. However, more studies are required to improve the DTB loading to simulate the clinical dose for humans in the treatment of RA.
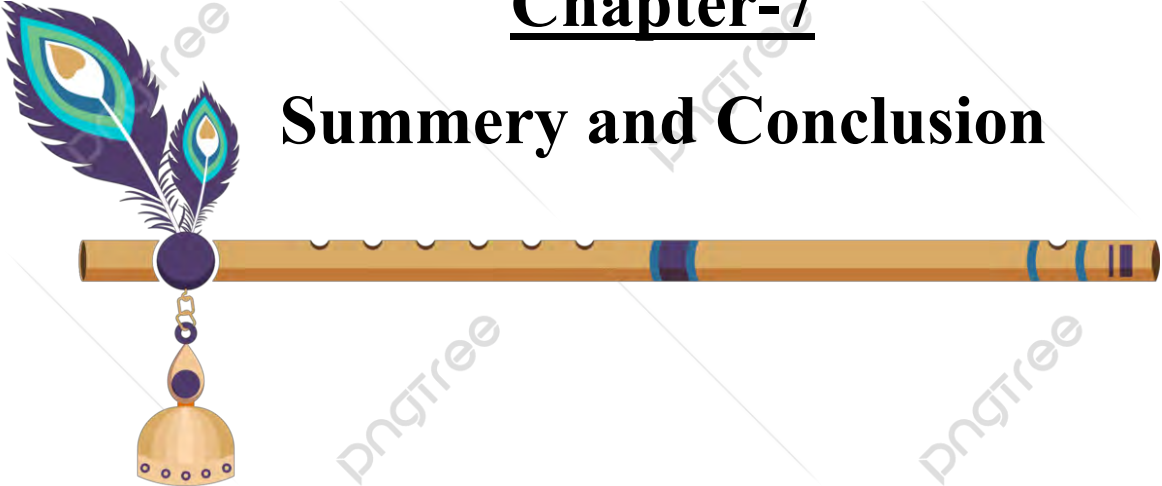
References:

1. Proksch, E. *et al.* (2008) The skin: An indispensable barrier. *Exp Dermatol* 17, 1063–1072

2. National Academies of Sciences, E. and M.H. and M.D.B. on H.S.P.C. on the A. of the A.S.D.R. the S. and E. of I.U. in C.T.P.C. *et al.* (2020) Commissioned Paper: Topical Dosage Form Development and Evaluation. *Compounded Topical Pain Creams* DOI: 10.17226/25689

3. Schäfer-Korting, M. *et al.* (2007) Lipid nanoparticles for improved topical application of drugs for skin diseases*Advanced Drug Delivery Reviews*, 59427–443

4. Müller, R.H. *et al.* (2002) Solid lipid nanoparticles (SLN) and nanostructured lipid carriers (NLC) in cosmetic and dermatological preparations. *Adv Drug Deliv Rev* 54

5. Zhou, H. *et al.* (2021) Current Advances of Nanocarrier Technology-Based Active Cosmetic Ingredients for Beauty Applications. *Clin Cosmet Investig Dermatol* 14, 867

6. Duong, V.A. *et al.* (2020) Preparation of Solid Lipid Nanoparticles and Nanostructured Lipid Carriers for Drug Delivery and the Effects of Preparation Parameters of Solvent Injection Method. *Molecules* 25, 4781

7. Rapalli, V.K. *et al.* (2020) Curcumin loaded nanostructured lipid carriers for enhanced skin retained topical delivery: optimization, scale-up, in-vitro characterization and assessment of ex-vivo skin deposition. *Eur J Pharm Sci* 152, 105438

8. Ghasemiyeh, P. and Mohammadi-Samani, S. (2018) Solid lipid nanoparticles and nanostructured lipid carriers as novel drug delivery systems: applications, advantages and disadvantages. *Res Pharm Sci* 13, 288

9.   Mahmood, A. *et al.* (2021) Luliconazole loaded lyotropic liquid crystalline nanoparticles for topical delivery: QbD driven optimization, in-vitro characterization and dermatokinetic assessment. *Chem Phys Lipids* 234, 105028

10.   Waghule, T. *et al.* (2019) Voriconazole loaded nanostructured lipid carriers based topical delivery system: QbD based designing, characterization, in-vitro and ex-vivo evaluation. *J Drug Deliv Sci Technol* 52, 303–315

11.   Waghule, T. *et al.* (2020) Nanostructured Lipid Carriers as Potential Drug Delivery Systems for Skin Disorders. *Curr Pharm Des* 26, 4569–4579

12.   Mohamed Rizwan, I. and Damodharan, N. (2020) Mathematical Modelling of Dissolution Kinetics in Dosage forms. *Res J Pharm Technol* 13, 1339–1345

13.   Ying, L.Q. and Misran, M. (2017) Rheological and physicochemical characterization of alpha-tocopherol loaded lipid nanoparticles in thermoresponsive gel for topical application. *Malaysian Journal of Fundamental and Applied Sciences* 13, 248–252

14.   Carlfors, J. *et al.* (1998) Rheological evaluation of Gelrite® in situ gels for ophthalmic use. *European Journal of Pharmaceutical Sciences* 6, 113–119

15.   Dantas, M.G.B. *et al.* (2016) Development and Evaluation of Stability of a Gel Formulation Containing the Monoterpene Borneol. *Scientific World Journal* 2016, 1–4

16.   Rapalli, V.K. *et al.* (2020) Curcumin loaded nanostructured lipid carriers for enhanced skin retained topical delivery: optimization, scale-up, in-vitro characterization and assessment of ex-vivo skin deposition. *European Journal of Pharmaceutical Sciences* 152, 105438

17. Guilherme, V.A. *et al.* (2019) Improved efficacy of naproxen-loaded NLC for temporomandibular joint administration. *Sci Rep* 9, 11160–11160

18. Garg, N.K. *et al.* (2017) Quality by Design (QbD)-enabled development of aceclofenac loaded-nano structured lipid carriers (NLCs): An improved dermatokinetic profile for inflammatory disorder(s). *Int J Pharm* 517, 413–431

19. Pal, R.R. *et al.* (2019) Tamanu oil potentiated novel sericin emulgel of levocetirizine: repurposing for topical delivery against DNCB-induced atopic dermatitis, QbD based development and in vivo evaluation. *J Microencapsul* 36, 432–446

20. Jibry, N. and Murdan, S. (2004) In vivo investigation, in mice and in man, into the irritation potential of novel amphiphilogels being studied as transdermal drug carriers. *European Journal of Pharmaceutics and Biopharmaceutics* 58, 107–119

21. Larson, A.A. *et al.* (1986) Pain threshold changes in adjuvant-induced inflammation: a possible model of chronic pain in the mouse. *Pharmacol Biochem Behav* 24, 49–53

22. Schaible, H.G. *et al.* (2005) Neurogenic aspects of inflammation. *Rheum Dis Clin North Am* 31, 77–101

23. Levine, J.D. *et al.* (2006) Neurogenic Inflammation and Arthritis. *Ann N Y Acad Sci* 1069, 155–167

Chapter-7

Summery and Conclusion

7. Summary and Conclusion

RA is an autoimmune disease, causes inflammation by targeting healthy cells. It is most common autoimmune disorders, affecting 1% of the world's population and mostly affecting joints. Tissue injury in the joint lining causes chronic pain, irregularities, and balance issues in the fingers, wrists, and knees. Various strategies for treating and managing RA have been developed, including topical, systemic, intra-articular, and biologics. Mild to moderate RA conditions are generally treated with topical therapies, while systemic therapies are reserved for severe cases. Immuno-suppressants, DMRDS, and biological agents are commonly used therapies for RA. However, with limitations of existing therapies and new discoveries in the pathogenesis of RA, newer molecules are being developed to target molecular-level mechanisms. Small molecules such as TKIs have shown promising results in treating RA by inhibiting several targets, including SRC family kinases, c-KIT, BCR/ABL, PDGFR, TNF-α, IL6, PI3K, and ERK.

Oral DTB (SPRYCEL tablet) exhibits severe side effects, including pulmonary hypertension, myelosuppression, gastrointestinal bleeding, and pleural effusions. Topical administration of DTB may be a feasible solution for mitigating these side effects. This approach can enhance therapeutic efficacy and produce localized effects while also reducing oral-related adverse effects. Regardless of these advantageous to achieve localized effects and increase penetration into underlying layers of skin, the conventional topical applications possess certain drawbacks like including the inability to deliver hydrophobic drugs and achieve the necessary drug concentration at the intended site, specifically the joint region. Additionally, it can be excessively greasiness and cause discomfort to the patient.

Lipid-based delivery systems are well explored for delivery of the drugs into targeting site by increasing skin permeation and deposition. The ease of preparation technique, low manufacturing cost, biocompatibility, protection of the drug from degradation, sustained

release, and increased skin deposition make the lipid nanoparticles a potential and ideal topical drug delivery. This can increase the efficacy of the drugs and reduce the systemic absorption of the drug.

To meet the objective in the present study, we have investigated topical delivery of DTB using lipid-based delivery systems (Emulgels and SLNs gel) for the treatment RA. The nano-emulgel and SLNs loaded gel were developed and characterized for *In-vitro, ex-vivo,* and *In-vivo* evaluation.

The developed formulation was evaluated for size, entrapment efficiency (EE), *in-vitro* drug release, *ex-vivo* permeation, skin deposition, skin adhesion, *in-vitro* viability study, inhibitory effect on TNF-α & IL-6, in-vivo irritation, skin samples histopathology and pharmacodynamic study for FCA induced arthritis.

Analytical development is the foremost step in drug product development. To meet the requirement, a sensitive, rapid, selective, accurate, and precise method was developed for routine analysis of DTB-loaded lipid-based nanoformulation for topical delivery. The method was developed on the Waters X-bridge™ C18 column (4.6*50mm) with 5μm particle size with a MP consisting of methanol and 10 mM phosphate buffer 50:50 ratio with a flow rate of 1 mL/min. The samples were analyzed at 315nm wavelength. The method was found linear in the range of 100 to 10000 ng/mL with 33 ng/mL as LOD and 100 ng/mL as LOQ, respectively. The developed method was tested for stability-indicating, and there was no interference of degradants with the RT of DTB. The developed method was found to be specific, and it was applicable for the determination of EE, assay, *in-vitro* release, and permeation study without any matrix effect of formulation and skin samples. The developed method chromatographic conditions were used for the bio analytical method with the small change in the MP composition used for quantification of DTB extracted from plasma samples.

For topical delivery of DTB, two types of lipid-based formulations, i.e., nano-emulgel, and

SLNs gel, were designed. Lipids were selected with the maximum solubility criteria. The peceol and geleol as oily vehicles was selected as oil phase for the development of emulsion, and Palmitic acid was selected as a solid lipid for the development of SLNs. To investigate how formulation and process variables impact the desired attributes of the final product, QbD was implemented. Central Composite design for emulsion and Box- Behnken design was employed was employed for SLNs formulation. In both designs with 17 runs (three levels) using design-expert software. The influence of independent variable including the amount of oil, percent of surfactant, homogenization speed, and homogenization time for emulsion. For SLNs formulation, solid lipid, surfactant (Gelucire), and homogenization time were investigated on response variables, i.e., PS and EE. For formulation optimization, the independent variables were analyzed at levels of low, medium, and high. Formulation was selected for further optimization based on desirability for PS< 200 nm with PDI < 0.300 and EE greater than 90%. The selected optimized formulation exhibited the EE as emulsion > SLNs. The complex structure of emulsion is expected for high EE compared to SLNs. The presence of a high concentration of liquid oil in emulsion enhanced EE compared to SLNs. The *in-vitro* drug release studies demonstrated the sustained-release up to 24h for both formulations.

The cell viability studies of optimized lipid formulations were performed on HaCaT cell lines demonstrated the formulation excipients were non-toxic. The in-vitro anti-inflammatory efficacy studies conducted in the RAW264.7 cell lines demonstrated the high efficacy in reducing the TNF-α and IL-6 levels with both formulations compared to the free drug.

The emulsions and SLNs was loaded into Carbopol ETD 2020 gel. The amplitude test and frequency sweep test performed on the prepared gel exhibited a high degree of crosslinking with significantly greater storage modulus (G') compared to loss modulus (G"). The skin permeation studies demonstrated the higher skin deposition of developed formulations compared to free drug-containing gel. The amount permeated and deposited was higher in SLNs loaded gel

compared to emulgel.

The *in-vivo* studies of designed formulations performed on Sprague Dawley (SD) rats demonstrated the formulation had no signs of irritation or erythema compared to SLS formulation. In histopathology data of the skin samples, revealed that no necrosis and hyperkeratosis was observed in DTB loaded different formulations and respective placebo formulations applied on rat skin. In FCA induced chronic inflammatory model, the body weight, paw withdrawal latency, and fall time decreased compared to before FCA injection and normal control group. Also, the paw volume and arthritis scores were increased compared to before FCA injection and normal control group. After treatment with different formulations, the increased weight gain, paw withdrawal latency, and fall of time. Also decrease in % paw volume and arthritis score, were observed with animals treated with emulgel, SLNs, and marketed formulation. That indicates the developed formulations have anti-arthritis activity. In developed formulations, the SLN gel formulation has shown better permeation, skin deposition in the *ex vivo* studies. In FCA-induced arthritis, it has shown almost similar effect to the marketed diclofenac gel.

Overall conclusion, the study found that the lipid-based nano formulations developed in this research are devoid of toxic solvents and exist in nano size (<200nm). These nano formulations demonstrate enhanced skin permeation, deposition, and sustained release compared to conventional topical preparations of Dasatinib. In vivo experiments revealed no skin toxicity in both nano formulation groups, when compared to the group treated with 5% SLS, indicating the non-toxic nature of the formulation. Furthermore, in an in vivo efficacy model of FCA-induced arthritis, both nano formulation groups exhibited a reduction in paw volume compared to the diseased control group and conventional DTB loaded formulation. Additionally, both nano formulations i.e., nano emulgel and SLN's, showed similar activity to the commercially available Diclofenac gel formulation. Overall, these findings highlight the potential of an

industrially feasible process for developing DTB-loaded lipid carriers for topical delivery.

Outcomes

Since the decade, lipid nanocarriers have attained great attention towards the delivery of topical therapeutics to improve permeation and skin deposition. The direct outcome of the present study emphasizes a large-scale feasible process for the development of DTB-loaded lipid carriers for topical delivery. The developed formulation has the potential to improve skin permeation and deposition, as well as demonstrating anti-arthritic activity in animal models. Additionally, the excipients utilized in the formulation remain within the inactive ingredient limits set by the FDA and have not displayed any cytotoxicity.

Future scope and directions

Further studies based on the present outcomes could include

- The surface modification of the formulation can be explored to estimate the dasatinib concentration in the synovial and joints region

- The prepared nanoparticles require further exploration in commercial scale-up studies

- The developed dasatinib loaded topical lipid nanocarriers can be explored for a clinical studies

- The scope of this work can be expanded to include other therapeutics that are intended for delivery into the joints, exhibiting similar physicochemical properties to dasatinib.

Appendix
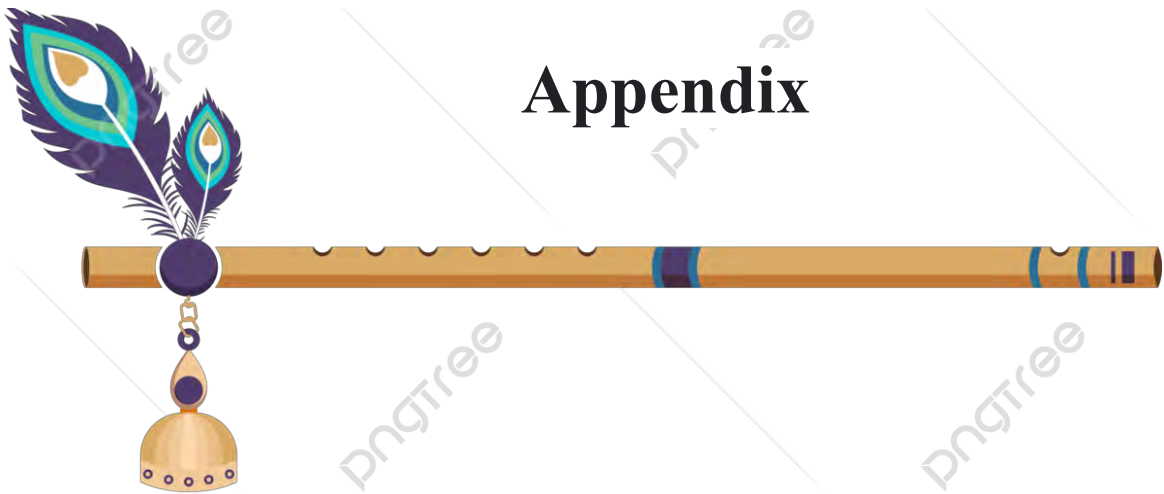
List of Publications and Presentations

Publications

1. **Donthi, Mahipal Reddy,** Ranendra Narayan Saha, Gautam Singhvi, and Sunil Kumar Dubey. " Dasatinib Loaded Topical Nano-emulgel for Rheumatoid Arthritis: Formulation Design and Optimization by QbD, In vitro, Ex vivo and In vivo Evaluation." Pharmaceutics 15.3 (2023): 736

2. **Donthi, Mahipal Reddy,** Siva Ram Munnangi, Kowthavarapu Venkata Krishna, Ranendra Narayan Saha, Gautam Singhvi, and Sunil Kumar Dubey. "Nanoemulgel: A Novel Nano Carrier as a Tool for Topical Drug Delivery." Pharmaceutics 15, no. 1 (2023): 164.

List of Patents

1. Donthi, Mahipal Reddy, Ranendra Narayan Saha, Gautam Singhvi, and Sunil Kumar Dubey. "A Lipid-based Foam Nanoemulgel Composition for Topical Application" (IN patent number: 448589; dated 31 August 2023.

Poster Presentations

1. Participated #RSCPoster and #RSCPoster pitch -2023 conferences Design and Optimization of Topical Dasatinib Nano-Emulgel for Rheumatoid Arthritis by QbD: In Vitro, Ex Vivo, and In Vivo Evaluation. organized by Royal society of chemistry 28th February 2023

Prof. Ranendra Narayan Saha

Prof. Ranendra Narayan Saha is Senior Professor at Department of Pharmacy BITS-Pilani, Pilani campus, Rajasthan. He worked as acting Vice Chancellor of BITS-Pilani. Additionally, he served as Director of the Dubai Campus of BITS-Pilani for seven years. He has completed his Bachelor and Master of Pharmacy from Jadavpur University, Kolkata and was awarded Doctor of Philosophy from BITS-Pilani. He has over 35 years of experience in teaching, research, and administration and has assisted several doctoral, graduate, and undergraduate students. He has an extensive background in research and is skilled in pharmacokinetics, novel drug delivery systems and nanomedicine. He has published books, various book chapters, and over one hundred research papers in prestigious national and international journals. In addition, he has presented multiple invited lectures at seminars and conferences organized by various colleges, pharmaceutical companies, and institutions in India and abroad. He is also a member of the advisory board and selection committees of several universities in India and overseas. Throughout the years, he has completed several government-sponsored initiatives and worked closely with the pharmaceutical industry, earning several patents and commercial products. He received *'Pharmacy Professional of the Year 2013'* an award given by Indian Association of Pharmaceutical Scientists and Technologists (IAPST). In 2011, he has been awarded *Shri B. K. Birla and Shrimati Sarala Birla Chair Professorship* at BITS Pilani for his contributions in teaching and research. He is also a recipient of '*The Best Pharmacy Teacher Award'* for the year 2005, awarded by Association of Pharmaceuticals Teachers of India (APTI), in recognition of his contribution in teaching and research in the field of Pharmacy.

Prof. Gautam Singhvi

Prof. Gautam Singhvi is an Associate Professor in the Department of Pharmacy, BITS, Pilani. He obtained his Ph.D. from BITS Pilani. He has 3 years of industrial research and 10 years of academic teaching and research experience. During his industrial tenure, he worked on solid oral, pellets, and complex pharmaceutical product development for the regulated market. Currently, he is involved in industrially feasible nanocarrier-based formulation development and optimization for various therapeutic agents. His team is extensively working on QbD-driven design of topical drug delivery systems for rheumatoid arthritis, psoriasis, and fungal infections. He has published several research/review articles and book chapters in reputed international peer-reviewed journals and international publishers. He is actively involved in sponsored research projects from government funding agencies and pharmaceutical industries. As an inventor, he has filed 10 formulation patents. He is also a peer reviewer of several international journals. Prof. Singhvi was listed in the "World Top 2% Scientists" in 2021 and 2022. He is very passionate about practicing the newer teaching pedagogy in his classroom teaching and motivating students to face the challenges of the new era.

Dr. Sunil Kumar Dubey

Dr. Sunil Kumar Dubey is currently working as General Manager, Medical Research, R&D Healthcare Division at Emami Ltd, Kolkata. He worked as an Assistant Professor in the Department of Pharmacy, BITS-Pilani, Pilani campus, Rajasthan. He awarded Doctor of Philosophy from BITS-Pilani, Pilani campus also he has more than 16 years of industrial, teaching, research, and administrative experience. He was also a visiting Assistant Research Professor in the Department of Chemical and Biomolecular Engineering at the University of Maryland, USA. Currently, he also serves as a guest faculty at various leading institutes including NIPER Guwahati, NIPER Raebareli, Jamia Hamdard, etc. He has an extensive research experience in the area of pharmacokinetic pharmacodynamic modelling and

simulations, development of phytopharmaceuticals and numerous nano-technology-based platforms. His expertise involves in validating the effectiveness of a vast range of healthcare products and providing business development-related insights. He is responsible for developing product concept notes, technical notes, monographs, and dossiers. He has published numerous research articles and book chapters in prestigious international peer-reviewed journals. He is included in the list of 'World's Top 2% Most-Cited Scientists' as per the Elsevier-Stanford University report.

Mr. Mahipal Reddy Donthi

Mahipal Reddy Donthi is a Research Scholar in the Department of Pharmacy, BITS-Pilani, Pilani campus, Rajasthan. He completed his post-graduation degree from University College of Pharmaceutical Sciences (Kakatiya University), Warangal. He has industrial research experience of 4 years in the area of orals as well as topical formulations development. The key area of research includes designing novel lipid-based nanocarriers for the treatment of rheumatoid arthritis, tissue engineering, nanotherapeutics, in-vitro cell-based studies, bioanalysis, animal model development, pharmacokinetic pharmacodynamic modelling and simulation studies.